# THE DEVELOPMENT OF CATALYTIC PROCESSES FOR THE ALTERNATING RING-OPENING COPOLYMERIZATION OF EPOXIDES WITH CYCLIC ANHYDRIDES: CONTROL OF POLYESTER REGIOCHEMISTRY, STEREOCHEMISTRY, AND MOLECULAR WEIGHT

A Dissertation

Presented to the Faculty of the Graduate School

Of Cornell University

In Partial Fulfillment of the Requirements for the Degree of

Doctor of Philosophy

By

Angela Marie DiCiccio

January 2014

# THE DEVELOPMENT OF CATALYTIC PROCESSES FOR THE ALTERNATING RING-OPENING COPOLYMERIZATION OF EPOXIDES WITH CYCLIC ANHYDRIDES: CONTROL OF POLYESTER REGIOCHEMISTRY, STEREOCHEMISTRY AND MOLECULAR WEIGHT

Angela Marie DiCiccio

Cornell University 2014

Sustainable growth initiatives have stimulated a revolution in the manufacturing and disposal of commodity materials. Original efforts to replace all persistent plastics with biodegradable alternatives were challenged by poor performance in common applications. Furthermore, redesigning processing methods to accommodate these new materials required more resources than continued use of traditional petrochemical plastics. Recognizing the need for both durable and biodegradable polymers, the updated concept of "bioplastics" encompasses the lifecycle of resources invested in synthetic materials. The frontier of plastics technology now focused on the discovery of efficient methods to transform commodity feedstocks into useful bioplastics.

Structurally diverse polyesters are attractive compliments to polyolefin based thermoplastics in applications that would benefit from their functionality and degradability. Several promising features include readily accessible and bio-derived monomers, biomedical and environmental compatibility, as well as green degradation pathways. This dissertation details the development of catalytic methods for the synthesis of new polyesters using commodity feedstocks with control over microstructure and size.

## BIOGRAPHICAL SKETCH

Angela Marie DiCiccio was born and raised a Red Sox fan in Leominster, Massachusetts (home of Jonny Appleseed and once the “Plastics Capital of the World’). Her aptitude for construction began at a young age, inspired by her father Tony. However, her mother Lisa’s passion for health care, medicine, and science instilled Angela's fascination with these fields as well. At Leominster High School, Angela excelled in biology but stumbled through a few minor laboratory disasters in chemistry, an experience that sparked her fascination with the field.

Angela matriculated to Mount Holyoke College to study biochemistry (with a focus in Biology since that was her strength) and was intent on pursuing a M.D. until she met Professor Geoff Coates during a summer research experience in 2006. With the help of Professor Coates and her advisor at Mount Holyoke, Professor Wei Chen, Angela discovered that the chemistry lab is a special place where construction and medicine/science can be combined, with a sprinkle of passion and creativity. After four wonderful years working under the direction of Professor Wei Chen at Mount Holyoke College, Angela joined Professor Coates' lab as a graduate student in 2008 and pursued the construction of new polyesters. Angela was particularly passionate about polyesters because of the environmental and biomedical implications of this class of polymer.

Angela graduated in 2014 and moved on to Professor Robert Langers' lab at the Massachusetts Institute of Technology where she is currently applying her synthetic background to the development of biomedical devices. Angela is unsure of where she will end up next, but invites anyone reading her thesis to send an email to check in!

This is dedicated to everyone who returns a smile. Thank you for taking a moment to make the world a little bit brighter ☺

ACKNOWLEDGEMENTS

An endless amount of appreciation is due to Professor Geoffrey Coates for his endless support. It is an incredible experience to work with such a generous, kind and intelligent advisor/mentor/friend. Since 2006, I have admired Geoff's ability to offer clarity, encouragement, criticism and support at the same time, truly efficient. Every time I make a presentation or give a talk I invoke "Geoff standards" and I produce a product that is more crisp and clear than I could have ever done on my own. I look forward to many years of friendship and collaboration.

Thank you to Professor David Collum and Professor William Dichtel for serving on my committee and as role models during my time at Cornell. I appreciate the honesty, candidness, and keen insight that you both provide in academic and social settings. I will miss hearing Professor Collum's stories and insights to the workings of the world, but I am comforted knowing that I can count on a yearly report as summary. It has been a unique pleasure to start my journey at Cornell at the same time as Professor Dichtel and it has been a thrill to watch him develop as an instructor in the classroom, advisor in the lab and mentor in life. As committee members, you are an elegantly balanced pair that has made my experience holistic and well-rounded.

A special thank you to Kelly Case for five+ years of friendship and support. I have learned so much from you about keeping life balanced, how to communicate, how to organize, and how to stay true to my values. I can't thank you enough for always keeping the Coates group functioning and knowing what we need. I look forward to many years of friendship. ☺

Dr. Anne Lapointe, thank you for being epic. Working with you is always fun, thought provoking and crazy efficient. Thank you for joining our group and sharing with us your laid-back, kind personality and delicious baked goods.

A giant thank you to my Coates group family! It is a great honor to be called a member of the Coates crew.

Special thanks to Dr. Ryan Jeske for showing me the ways of the polyester and teaching me how to do synthetic chemistry. I cherish your continued mentoring and friendship. I am incredibly lucky that you picked me as your REU student.

Dr. Joe Edson, Dr. Nick Robertson, Dr. Peter Widger and Dr. Amelia Anderson, thank you for being great 'upper classmates' and for leading by example. Your diligence, hard work and kindness set high standards to aspire to. Yuki, thank you for so many thoughtful discussions, smiles, espresso beans, and for always asking questions. Tam, Brandon, Kyle, Qi, Jessica, and Masato thank you for being wonderful co-workers, all of the smiles and shared snack-times.

I am delighted to have been around for the "bro crew" years of the Coates group. Tim, Bryan, Henry, Kevin "Noonie", Taz, PI, you are an incredible bunch. Thank you for including me in your antics, I look forward to more adventures! Draft trip?

To the post-doc/visiting scientist crew: Dr. Brian Long, Dr. Giang Vo, Dr. Hisashi Ohtaki, Dr. Jeung Gon Kim, Dr. Soumya Sarkar, Dr. Christopher Goh, Dr. Rocco Di Girolamo, Dr. Tulaza Vaidya, and Dr. Chad Ellis, thank you all for the life advice, chemistry guidance and simply for being wonderful people. I especially need to thank Chad and Blair for being my adopted "family unit" and letting me hangout with G, especially for the arrival of E! That is an incredibly special experience that I will never

forget. Tulaza thank you for being an incredible burst of fresh energy and ‘keepin it real’.

Erin Dunn, I cannot be happier to have had the opportunity to work and travel with you. You are my first wedding date, my first international travel buddy and bought me my first drink on a plane. Thank you for being an incredible friend and a thoughtful co-worker. I can't wait for our future adventures!

My ‘home’, the 565 office was a pleasure to work in, despite the temperature and music wars. I will forever crave a cup of coffee and peanut butter toast when I enter.

Thank you to Rachna and C for being great labmates and such hard workers! C, your endless enthusiasm for learning and life are infectious and bring about a mood of adventure and excitement that cannot be rivaled. Rachna, you are truly priceless. I am so happy to call you one of my best friends and learned so much from you. You gave me strength and support at all of the right times and I cannot thank you enough for being a part of my time at Cornell.

Ian, I need to thank you for taking the time to patiently explain the world to me and for always listening to me ramble when I just cannot contain myself. I am lucky to call you and Carolyn my friends!

Julie, I don't know what my life would be like without you! Thank you for choosing to do an REU at Cornell and then for returning to me. You and Sam are truly incredible and I am so lucky to have you in my life.

A special thank you to Kristina Hugar for being an awesome roommate, a rock-solid amazing friend, an incredible role model, the best cheerleader, and a wonderful

co-worker. I am really thankful that we were able to share so much of life and I look forward to continuing our friendship for a long long time!

And Nathan Van Zee, I have always looked forward to collaborating with you and learning from you. Your thirst for knowledge is incredible and your diligence in finding the answers is inspirational. Thank you for always looking up with a giant smile willing to help me or talk with me about anything. I look forward to seeing that smile for years to come.

Finally, Michael Mulzer, it's been quite an experience! I am so lucky to have had a batchmate that is so kind, humble and genius. You truly are a gifted visionary with *incredible* organization skills. I am lucky to have learned so much from you, but most of all, I am lucky to consider you a close friend. Thank you for being wonderful.

Megan and Erika, I could not have made it with you, thank you for being my rocks. I'm so lucky to have found such incredible people at Cornell and I think I won the lottery when I reflect on our friendship. It's incredible how much we've all grown.

A special thank you to Susan Langer for being my mentee/great friend for four years. No matter how overwhelmed I was with work I always looked forward to meeting with you. Although we were supposed to do schoolwork, and I was supposed to be teaching you, I learned so much from you that we definitely co-mentored our way through Cornell. Thank you for teaching me self-confidence and to be brave.

Anna Zimmerman, I still can't believe you moved to Cornell and were my local best friend for two years! I can never thank you enough for being my person in life. I still dream about our runs and all of our adventures with Margaux. You are awesome.

To the 2006 summer REU students and all of the other programs that year, thank you for making my first experience at Cornell/in Ithaca so magical that I had to return.

Thank you to my family for all of your patience, support and kindness. I know it seems strange that I went off to school forever, and came back unable to be your doctor, but I appreciate you listening to me ramble about my research and for all of your excitement and support for any opportunity that came my way. I am blessed to have such a dedicated and supportive crew.

A special acknowledgement to Nonno. I'm sad to think I was so far away for the last years of your life, but I want to thank you for always bragging and telling everyone about me. When I came back to honor and celebrate your life, strangers I never met knew I was "at Cornell doing amazing work". I love you and miss you.

Finally, Katie Vaillette, you have been my daily motivation and inspiration to pursue my dreams and make things happen. I find peace knowing that you are watching me everyday and I am thankful that you taught me to see the world as beautiful. Everyday I try to make the world a better place in your memory.

There are many people who have touched my life while at Cornell and in Ithaca, and I truly feel I was in the right place at the right time. I sincerely thank you for taking the time to make my world a happier place and to help me get to wherever it is that I am meant to be. ☺

Finally, thank you to the CCMR for use of their facilities and to IGERT and the NSF for funding.

TABLE OF CONTENTS

LIST OF FIGURES

CHAPTER ONE

CHAPTER TWO



CHAPTER THREE

LIST OF SCHEMES

CHAPTER ONE



CHAPTER TWO



CHAPTER THREE



CHAPTER FOUR

CHAPTER FIVE



CHAPTER SIX

LIST OF TABLES

CHAPTER TWO



CHAPTER THREE



CHAPTER FOUR



CHAPTER FIVE

CHAPTER ONE

# A REVIEW OF RECENT DEVELOPMENTS IN DISCRETE METAL CATALYSTS FOR THE RING-OPENING COPOLYMERIZATION OF EPOXIDES AND CYCLIC ANHYDRIDES

## 1.1 Introduction

The requirements for sustainable growth and limited environmental impact necessitates a revolution in manufacturing and consumption.[1,2] Increased support of biodegradable polymers between 1996 (14 million kg) and 2001 (68 million kg) reflects societies' changing priorities.[2a] Global efforts to address this paradigm shift attempt to make sustainable alternatives affordable but struggle to find competitive materials.[3,4,5] Meanwhile, manufacturers appeal to consumer demands with lifecycle assessments of commercial products and partnerships with producers of bio-derived chemicals.[3,5] Governments endorse programs dedicated to sustainable design and subsidize existing alternatives.[1a,3,5] Academic research maintains the forefront of discovery and understanding of sustainable technologies.[1,2]

The complexity of this issue inspired a reevaluation of the concept of sustainable materials. The exclusive association of "sustainable plastics" with biodegradability is flawed by the hidden environmental costs necessary for processing and specialized disposal.[4,5, 6] Redesigning industrial methods to exclusively accommodate known biodegradable materials would expend more resources than continued use of traditional petrochemical plastics. Recognizing the need for both durable and biodegradable polymers, the updated concept of "bioplastics" adopts a broader perspective that

encompasses the lifecycle of resources invested in synthetic materials. Contemporary sustainable bioplastics include polymers produced from renewable carbon sources, processed economically, and disposed of through recycling or composting: a life cycle with minimal environmental impact. Under this new definition, annual global demand for bioplastics is growing rapidly at an estimated rate greater than 20% and is expected to reach 1.9 million metric tons by 2017, the majority of which will be durable materials.[3,6]

Redesigning the synthesis of known commercial polymers is one approach to sustainable bioplastics. Bio-based high-density polyethylene (HDPE) exemplifies the advantages of this method.[3,6] Applications of HDPE are ubiquitous and no known biodegradable polymers compare in performance.[2b,3b] Braskem developed processes to produce ethylene from sugarcane sourced from Brazil, providing a biorenewable alternative to this irreplaceable resource. Bio-HDPE is responsible for the increase in durable bioplastic consumption; however, concerns about the ecological impact of crop-sourced polyolefins prevent their complete adoption.[2b,c] Diverse alternatives that do not rely on crop-based feedstocks are desired, and durable biodegradable options are yet to be discovered.[7]

Another approach to sustainable bioplastics is to utilize biodegradable polymers derived from known biorenewable resources. Several materials based on sugars such as starch, poly(lactide) (PLA), and poly(hydroxyalkanoates) (PHA) are valuable in niche markets[3] but are limited by costly processing and poor physical performance.[2,5,6] The properties of starch, PLA, and PHA can be improved by creating blends with polyolefins, however, the resulting materials can no longer be biodegraded or recycled.[4]

A complementary strategy is to discover new biodegradable high performance polymers from bio-derived resources.[1,7] Structurally diverse polyesters are attractive for this method because they can meet the requirements of green design and offer a range of properties.[1c,d] Several promising features include readily accessible and bio-derived monomers, biomedical and environmental compatibility, as well as green degradation pathways.[7] Before polyesters become commercially viable, processes are needed to efficiently produce high molecular weight polyesters with control over microstructures.

Industry synthesizes polyesters via the step-growth condensation copolymerization of diols and diesters (Scheme 1.1a).[8] Despite the advantage of widely available feedstocks, this process is energy intensive, and it is difficult to control polymer regiochemistry or molecular weight. Furthermore, utilizing enantiopure or reactive monomers in this process is often difficult or prohibitively expensive. These limitations restrict the use of step-growth as a viable method for the development of sustainable durable polyesters.

**Scheme 1.1** Polymerization routes for the synthesis of polyesters: a) Step-growth condensation copolymerization b) Chain-growth ring-opening copolymerization

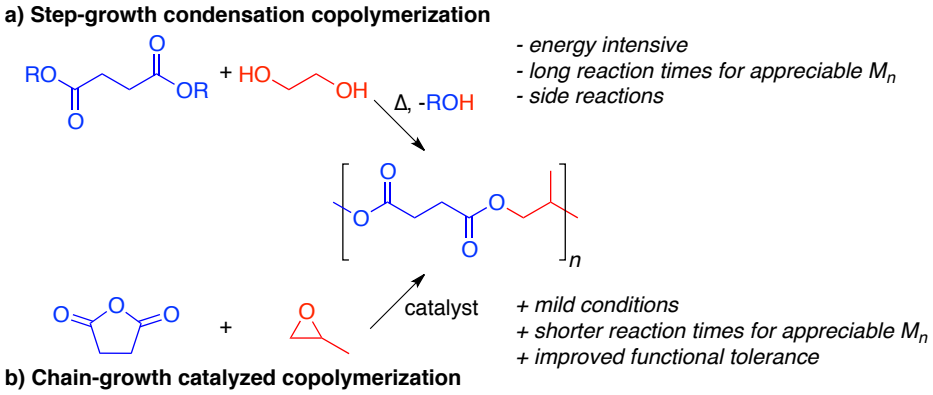


A parallel approach to structurally diverse polyesters is the chain-growth catalyzed perfectly alternating ring-opening alternating copolymerization (ROAC) of epoxides

and cyclic anhydrides (Scheme 1.1b). Discrete catalysts for this process can be employed to create polyesters with desired properties. Diverse monomers available for this route can be derived from diol, olefin, and diacid sources, many of which are renewable. Currently, catalyst technology for this transformation is in its infancy and polyesters made by this method have not found commercial use. However, encouraging advances in the development of polyolefin and polycarbonate processes foreshadow the potential of insightful catalyst design to achieve commercially valuable materials.

This review will summarize the evolution of homogenous metal complexes that catalyze the perfectly alternating ROAC of epoxides and cyclic anhydrides. Similar methods take advantage of the propensity of epoxides to homopolymerize to create polyester-ethers from the same feedstocks. While these related materials also meet the objectives of sustainable design and have interesting properties, their synthesis will not be discussed in this work.

## 1.2 First Catalysts for the ROAC of Epoxides and Cyclic Anhydrides

In 1985, Inoue and coworkers reported the first discrete metal complex to copolymerize epoxides and cyclic anhydrides.[9] (TPP)AlCl (tetraphenyl porphyrin aluminum chloride) (**1a**) paired with an [$EtPh_3P$][Br] (ethyl triphenyl phosphonium bromide) cocatalyst catalyzes the alternating copolymerization of phthalic anhydride (PA) and epoxides to yield polyesters without main-chain polyether linkages (Figure 1.1a). This process produces low molecular weight polyesters with narrow molecular weight distributions (PDI<1.2) over several days (4-16). Despite a linear increase in molecular weight, the observed molecular weights are much lower than the theoretical.

Identification of multiple end groups in the $^{13}C$ NMR spectrum suggests initiation from both sides of the Al center, partially accounting for this discrepancy (Figure 1.1b). The "living" nature of **1a** allows formation of block copolymers via: homopolymerization of epoxide (*b*-polyether), copolymerization of a different epoxide (*b*-polyester), or homopolymerization of cyclic esters like butyrolactone (*b*-polyester).

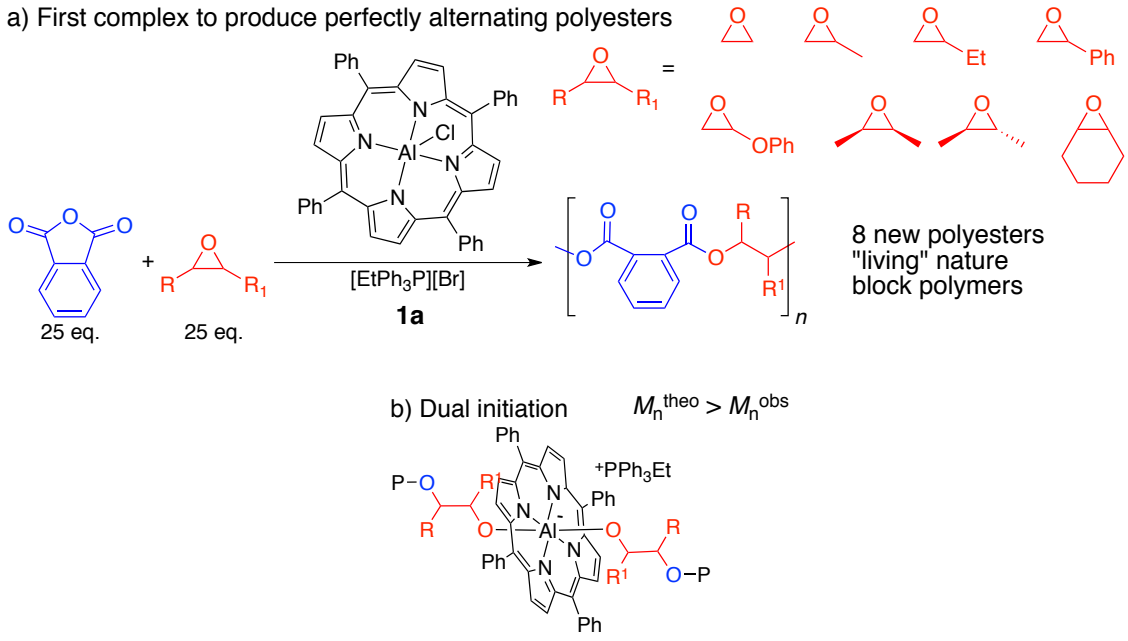


**Figure 1.1** (TPP)AlCl/[$EtPh_3P$][Br] catalyzed processes: a) copolymerization of PA/epoxides b) initiation of polymerization from both sides of the Al metal center.

Two decades later, our group reported a (BDI)ZnOAc (beta-diiminate Zn acetate) (**2a**) catalyst adapted for polyester formation (Figure 1.2a).[10] Initial trials concluded that the most active epoxide and $CO_2$ copolymerization catalyst (**2b**) is unstable under the conditions employed for the ROAC of epoxides and cyclic anhydrides. The crystal structure of a representative degradation product[11] corroborates literature reports that the BDI ligand is reactive towards electrophiles.[12] The proposed degradation occurs when the methine carbon of the BDI backbone ring-opens an anhydride to create a

neutral ligand that expels zinc (Figure 1.2b). Literature examples suggest that the reactivity of the methine carbon can be adjusted by substitution. Replacing the proton with an electron-withdrawing cyano group sufficiently deters degradation and results in the highly active epoxide and cyclic anhydride copolymerization catalyst, **2a** (Figure 1.2a).[13]

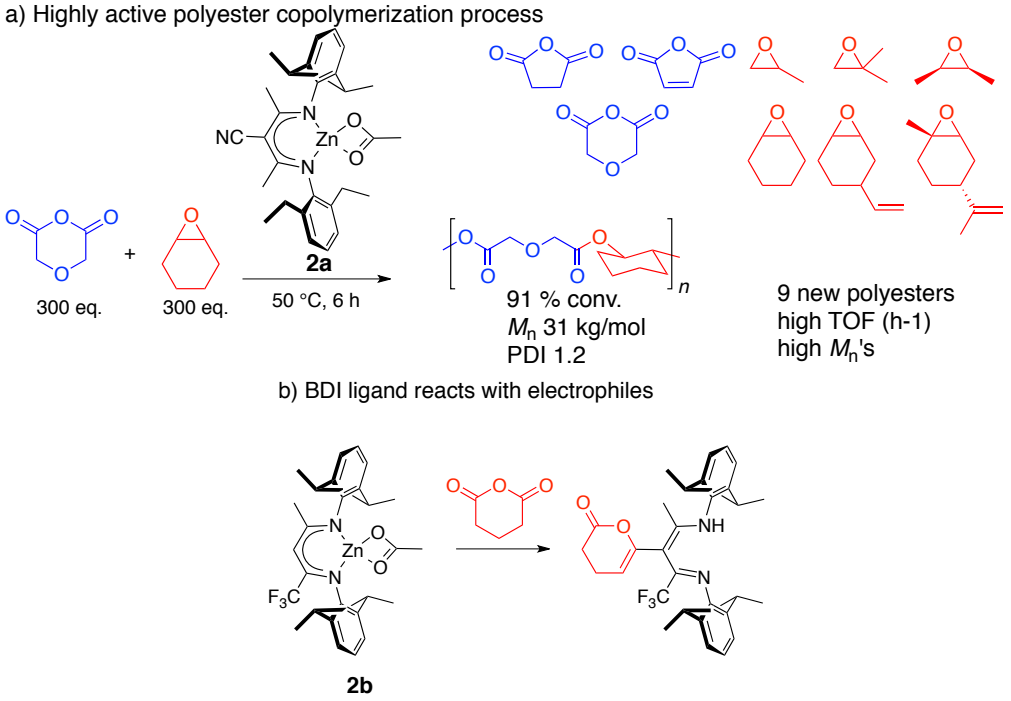


**Figure 1.2.** Ligand substitution affects (BDI)ZnOAc activity and stability: a) **2a** is highly active for the copolymerization of epoxides/cyclic anhydrides b) **2b** degrades in the presence of cyclic anhydrides.

Catalyst **2a** produces high molecular weight polyesters (>20 kDa) with narrow PDIs (1.2) in a few hours. Preliminary mechanistic studies suggest that **2a** operates through a monomer/dimer equilibrium, similar to that of **2b** in the copolymerization of epoxides and $CO_2$.[14] In 2009 our group exploited the versatility of this process in a one-pot terpolymerization to produce a poly(ester)-*b*-(carbonate).[15] In the presence of excess epoxide, cyclic anhydride, and $CO_2$, **2a** enchains cyclic anhydrides before $CO_2$ although, the rate of polymerization for polyester formation is slower than for

polycarbonate (Figure 1.3a). This indicates that the (BDI)zinc-alkoxide intermediate is more reactive towards anhydride than $CO_2$ (Figure 1.3b, $k_A >> k_{CO2}$). This system is an elegant example of a product-determining step that is pre-rate determining step.

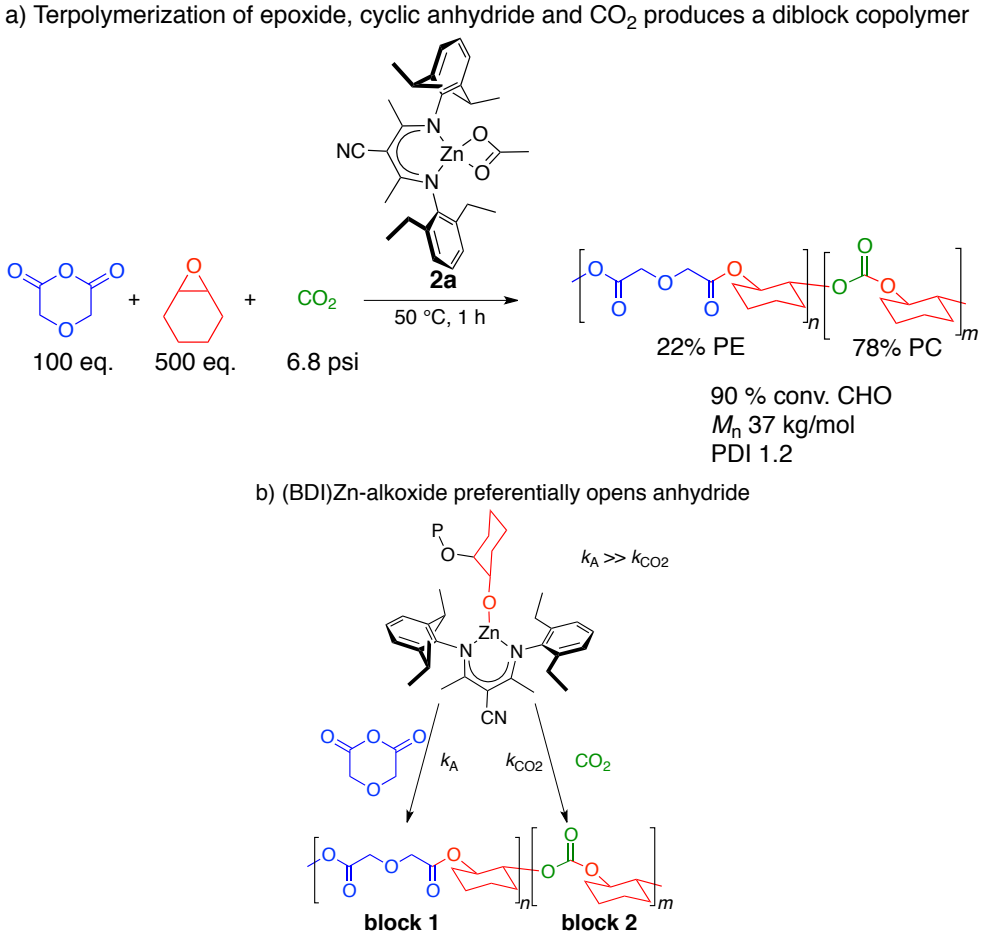


**Figure 1.3.** The reactivity of **2a** in the terpolymerization of epoxide, anhydride, and $CO_2$ proceeds to: a) form poly(ester)-*b*-(carbonate) b) ring-open anhydrides more quickly than inserting $CO_2$.

These reports highlight successful adaptations of polycarbonate systems for polyester synthesis and inspired the next generation of polyester processes based on the ROAC of epoxides with cyclic anhydrides.

### 1.3 Second Generation of ROAC Catalysts: Chromium and Aluminum

The chromium catalyzed ROAC of epoxides and cyclic anhydrides was introduced by three separate groups in 2011. Each report addressed different priorities and collectively exemplifies the versatility of this process. The following discussion summarizes the major achievements of each study, focusing on the development of highly active systems. For brevity, the details of catalyst optimization will be summarized and the reader should consult the primary literature for particulars about less active complexes. Overall, chromium catalyzed processes exhibit higher activity and produce more perfectly alternating polyesters, however, several aluminum systems excel when chromium is found to be less active.

Our group developed a (salcy)CrCl (**3a**) catalyzed process for the copolymerization of maleic anhydride (MA) with a variety of terminal epoxides to produce high molecular weight unsaturated polyesters (Figure 1.4a).[16] Quantitative isomerization with diethyl amine yields the fumarate analogues without side reactions (Figure 1.4b). Isomerization progress can be monitored using NMR spectroscopy and a desired maleate:fumarate ratio can be isolated by removal of diethyl amine, easily procuring polyesters with cis/trans isomer mixtures. The maleate and fumarate isomers have different $T_g$s, suggesting distinctive chain packing conformations (Figure 1.4b). NMR analysis of poly(propylene maleate) (PPM) is used to visualize the regioisomers of this regioirregular polyester.

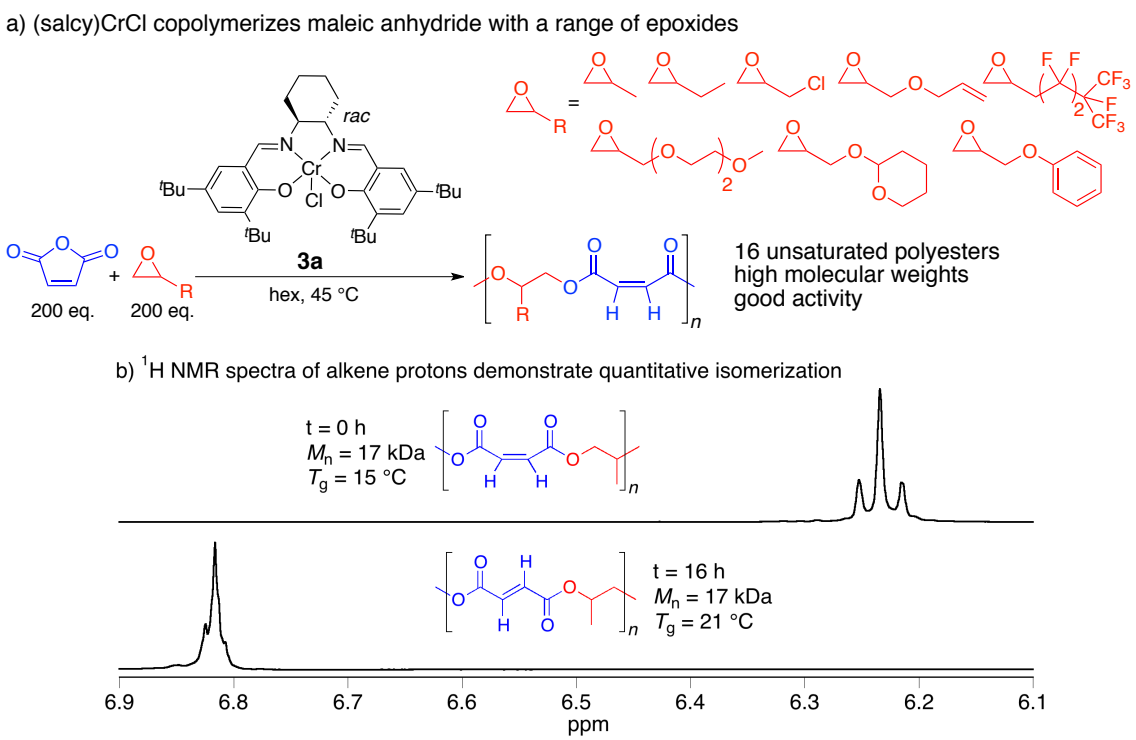


**Figure 1.4.** Polymerization of PPM and isomerization to PPF: a) **3a** catalyzed copolymerization of PO/MA to produce PPM b) alkene regions of the $^{1}$H NMR spectra of PPM and PPF demonstrating quantitative isomerization using catalytic $HNEt_2$.

**3a** initiates multiple chains per catalyst in the presence of chain transfer agents such as isopropanol (iPrOH) (Figure 1.5). Increases in the equivalents of [$^{i}$PrOH]:[**3a**] decreases polymer molecular weight while maintaining narrow PDIs, characteristic of immortal polymerization. Bifunctional chain transfer agents are applicable for the creation of telechelic polyester diols or diacids; valuable intermediates in the synthesis of polyurethanes, particularly for applications requiring cross-linking (i.e. coatings and resins).[1b,17,18]

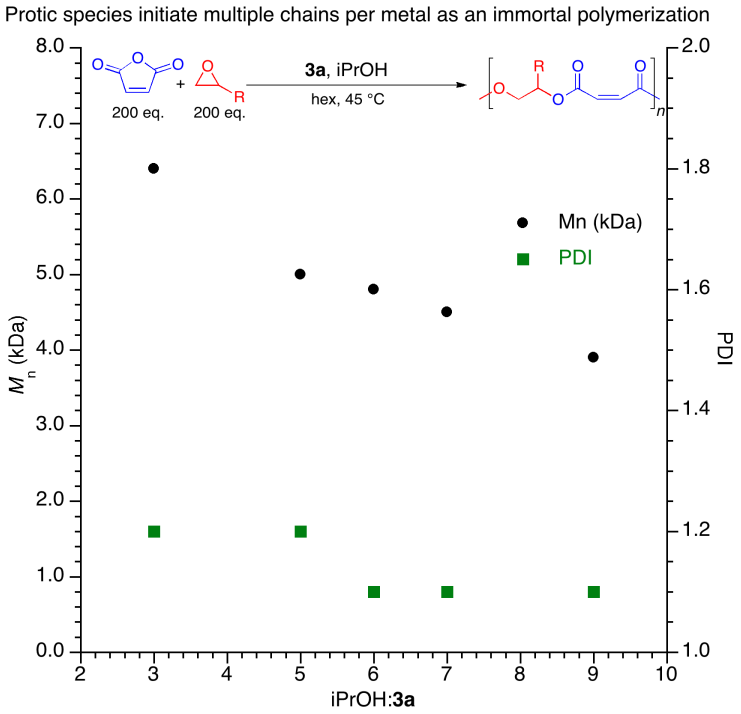


**Figure 1.5.** Changes in $M_n$ and PDI as a function of [$^i$PrOH]:[**3a**].

In contrast to most chromium-catalyzed polycarbonate and polyester systems,[1d,e,19] **3a** does not require a nucleophilic cocatalyst for activity. This condition is unique to MA processes and not applicable to other anhydrides. MA is known to form coordination complexes with transition metals, and perhaps acts as an internal cocatalyst during copolymerization by providing a trans axial ligand.[20]

Duchateau et al. tested two known poly(cyclohexene carbonate) catalysts[19] for the formation of aliphatic polyesters.[21] (TPP)CrCl (**3b**) and (salophen)CrCl (**3c**) both require one equivalent of DMAP to copolymerize cyclohexene oxide (CHO) with cyclic anhydrides (Figure 1.6). **3b**/DMAP yields perfectly alternating polyesters in all cases, while **3c**/DMAP sometimes incorporates polyether linkages. No correlation is observed between cyclic anhydride ring-strain and the copolymerization rate, supporting epoxide

ring-opening as the rate-determining step. There is a positive correlation between increased ring-strain and molecular weights; most reported polyesters are <10 kDa except for examples with the most strained phthalic anhydride (PA) (~20 kDa).

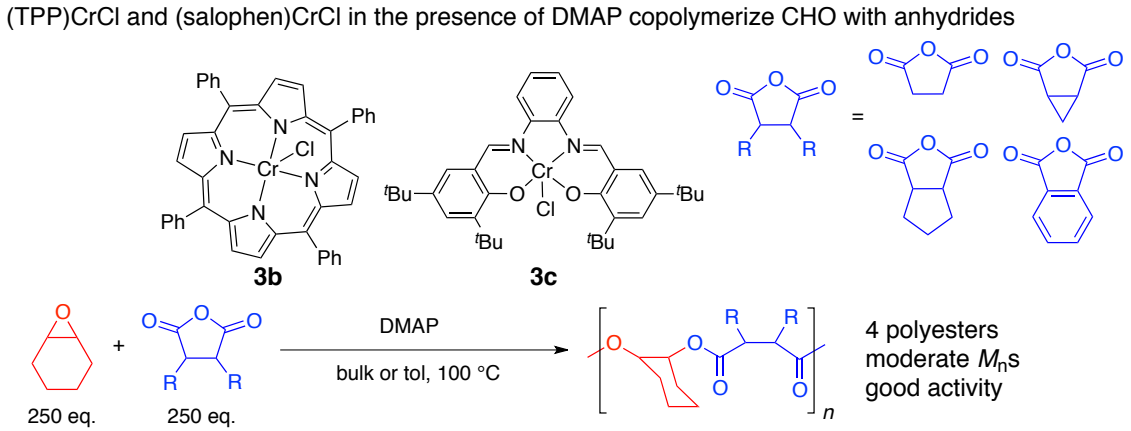


**Figure 1.6. 3b**/DMAP and **3c**/DMAP catalyzed ring-opening copolymerization of CHO with cyclic anhydrides of varying ring strain.

Addition of $CO_2$ to these processes can also yield terpolymers. Similar to the (BDI)ZnOAc[15] system, a stoichiometric ratio of anhydride:CHO in the presence of $CO_2$ produces predominately polyester (Figure 1.7a). Notably, the presence of $CO_2$ suppresses the formation of ether linkages for **3c**/DMAP. $CO_2$ also decreases polyester copolymerization rate in comparison to systems without it, which is attributed to competitive coordination. Unlike the (BDI)ZnOAc process, **3b**/DMAP and **3c**/DMAP catalyze polyester formation more quickly than polycarbonate. Finally, with excess epoxide, both **3b**/DMAP and **3c**/DMAP produce poly(ester)-*b*-(carbonate) structures with some cyclic carbonate byproduct attributed to backbiting (Figure 1.7b).

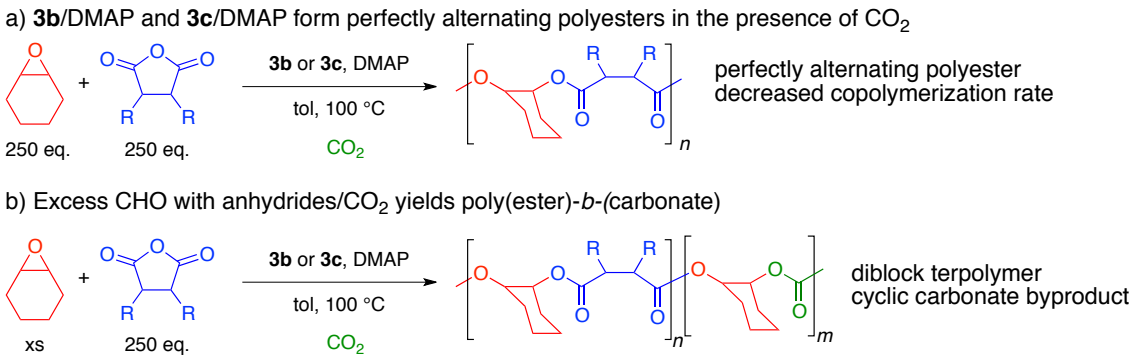


**Figure 1.7.** Terpolymerization products depend on reaction conditions: a) Stoichiometric CHO:anhydride forms polyester b) Excess CHO:anhydride yields a poly(ester)-*b*-(carbonate) terpolymer and cyclic carbonate byproducts.

MALDI spectrometry and GPC are used to analyze polyesters produced by **3b**/DMAP and **3c**/DMAP. Although signals for DMAP terminated polyesters dominate the spectra, dampening signals from other fragments, a hypothesis is generated from this analysis to explain the source of low molecular weight polyesters. The MALDI spectra of polyesters synthesized by **3b**/DMAP exhibit distributions for DMAP/hydroxyl and DMAP/Cl end groups. Spectra for polyesters from **3c**/DMAP show only DMAP/hydroxyl. Corresponding the MALDI distributions to GPC traces shows that the hydroxyl-terminated polyesters are twice the molecular weight of the other species and account for the bimodal appearance of the eluted GPC peaks. Water is implicated as a chain transfer agent and this hypothesis is tested by addition of water to a copolymerization which results in increased bimodal distributions.

Thomas et al. reported a process to directly utilize renewable, commercial resources for the tandem synthesis and copolymerization of cyclic anhydrides with epoxides.[22] (salcy)CrCl (**3a**) with 1 equivalent of [PPN][Cl] catalyzes the quantitative cyclization of dicarboxylic acids in the presence of dimethyl dicarbonate to a variety of cyclic

anhydrides under mild conditions (Figure 1.8). The volatile byproducts, MeOH and $CO_2$, are easily removed by vacuum to obtain pure cyclic anhydrides.

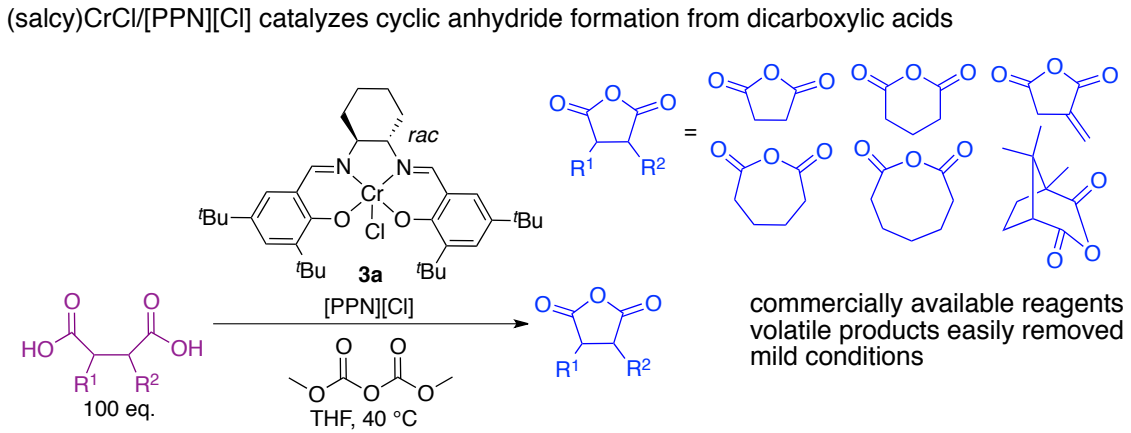


**Figure 1.8.** Tandem formation and copolymerization of cyclic anhydrides, catalyzed by **3a**/[PNN][Cl].

After removal of volatiles, copolymerization is initiated by addition of epoxide. **3a**/[PPN][Cl] copolymerizes several cyclic anhydrides and propylene oxide to perfectly alternating polyesters with moderate molecular weights (<16 kDa) and narrow PDIs (<1.3) (Figure 1.9a). For tandem reactions involving copolymerization with internal epoxides such as CHO, limonene oxide (LO), or pinene oxide (PiO), a (salcy)AlCl (**1a**)/[PPN][Cl] catalyzed process is more efficient (Figure 1.9b). Increased temperature, multiple equivalents of [PPN][Cl], and longer reaction times are required for activity but perfectly alternating polyesters are isolated with molecular weights up to 27 kDa and narrow PDIs (1.2).

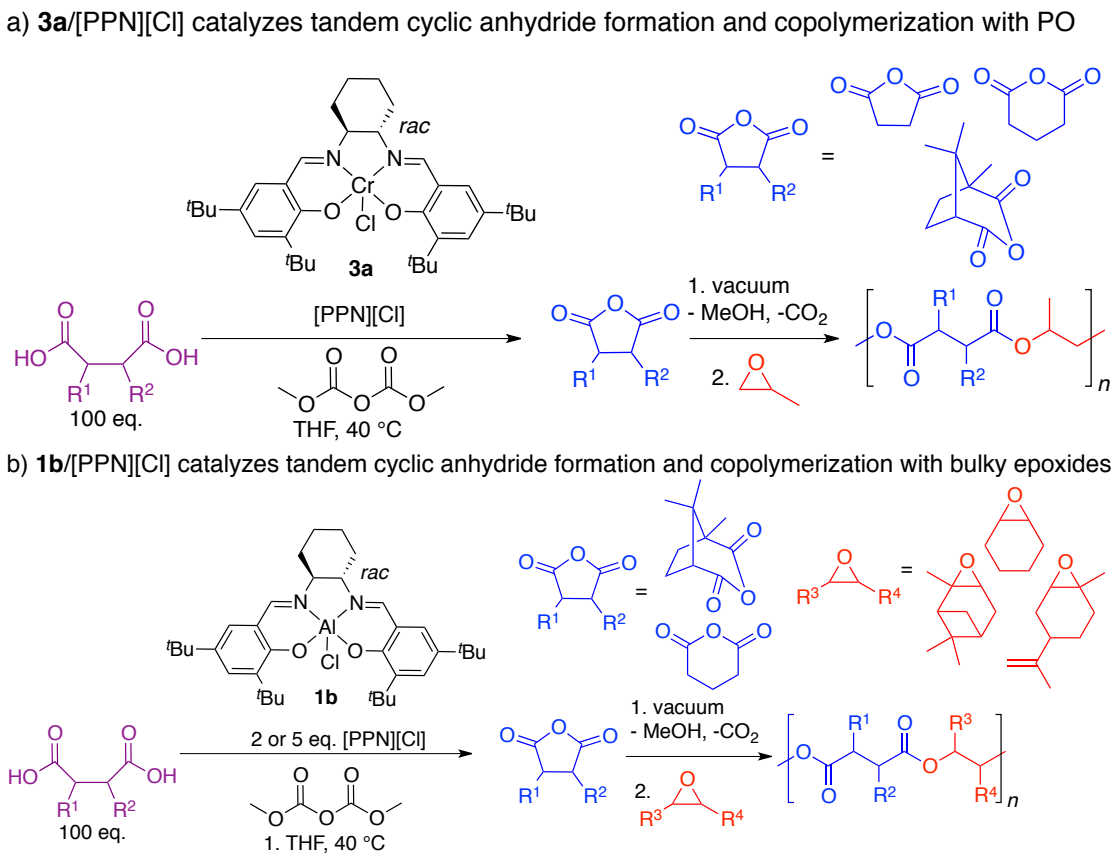


**Figure 1.9.** Two methods for the one pot tandem cyclic anhydride formation and copolymerization: a) **3a**/[PPN][Cl] catalyzes systems with PO b) **1b**/[PPN][Cl] catalyzes systems with bulky epoxides.

## 1.4 Mechanistic and Substrate Scope Investigations

Subsequent investigations seek to elucidate mechanistic details in pursuit of highly active and regioselective processes for the ROAC of epoxides and cyclic anhydrides. The following systematic studies analyze mechanistic impacts of variations to catalyst (ligand, metal), cocatalyst (identity, equivalents), and monomers (anhydride ring-strain, epoxide electronics/substitutions).

In 2012, Darensbourg and coworkers analyzed the kinetics of the ROAC of epoxides/cyclic anhydrides catalyzed by **3a**/[onium] salts.[23] Systems based on

**3a**/[PPN][X] are most active for the copolymerization of phthalic anhydride (PA) with cyclohexene oxide (CHO) and the identity of [X] does not impact rate (Figure 1.10). In the absence of [PPN][X], **3a** is essentially inactive for copolymerization. In the absence of **3a**, [PPN][Cl] copolymerizes PA and CHO at a slower rate than the combined system, but yields perfectly alternating polyester with a narrow molecular weight distribution (PDI 1.07). The reaction rate has a first order dependence on [CHO] and negligible dependence on [anhydride], in agreement with epoxide ring-opening as the rate-determining step.

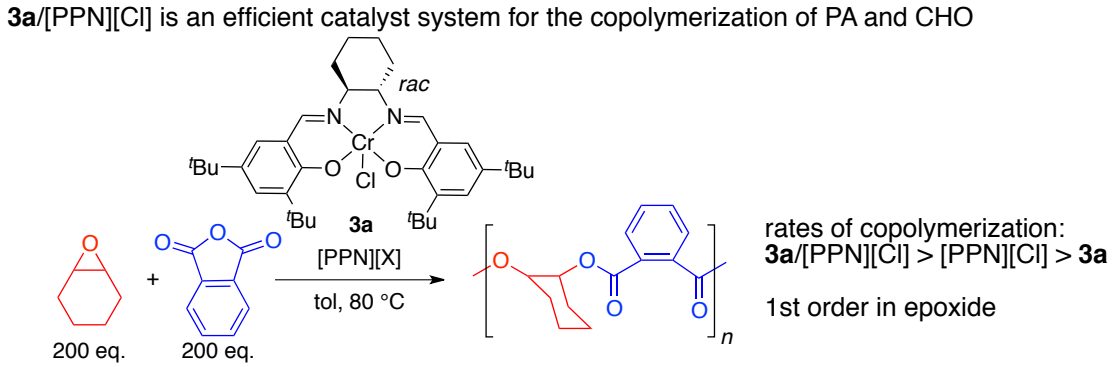


**Figure 1.10. 3a**/[PPN][Cl] catalyzed copolymerization of CHO/PA.

The rate of copolymerization depends on monomer structure, although no clear correlation with epoxide or anhydride structure is concluded (Figure 1.11). For 1,2-dicarboxylic cyclohexane anhydride (CHA) the copolymerization rate with epoxides decreases according to: propylene oxide (PO) > cyclohexene oxide (CHO) > styrene oxide (SO) (Figure 1.11a). Alternatively, for cyclohexene oxide (CHO) the copolymerization rate with cyclic anhydrides decreases according to: cyclohexene anhydride (CHE) > phthalic anhydride (PA) > cyclohexane anhydride (CHA) (Figure 1.11b). While the impact of monomer structure on polymerization rate is dubious, there is a positive correlation between the polymer $T_g$ and the steric bulk of the monomers;

CHE/CHO has the highest $T_g$ of 95 °C. Smaller anhydrides such as succinic (SA) and maleic (MA) are also active in this system and yield polymers with lower $T_g$s (SA/PO has a $T_g$ of -39 °C).

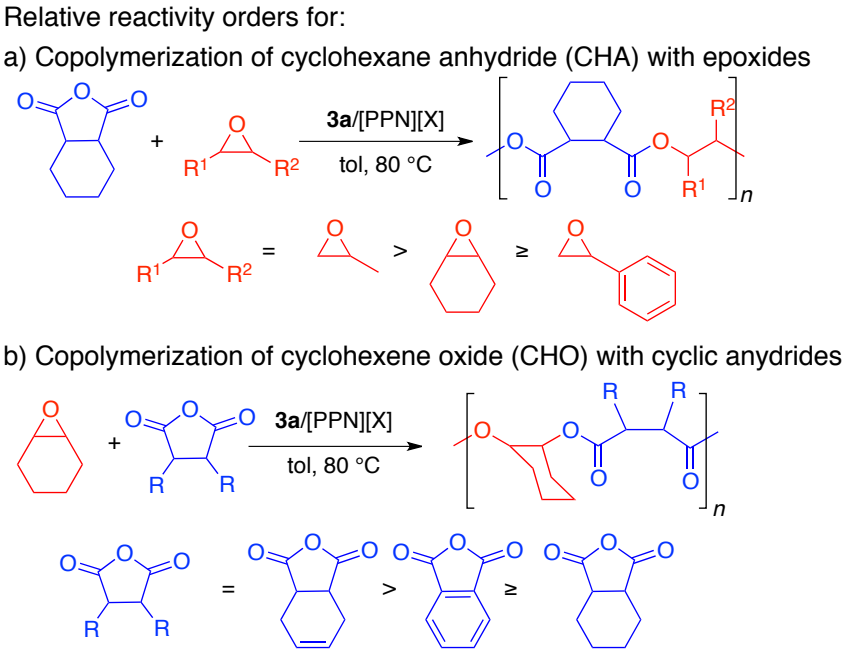


**Figure 1.11.** Copolymerization rate depends on monomer identity.

Finally, React-IR is used to monitor the terpolymerization of CHO, PA, and $CO_2$. The same pre-rate product-determining step is presumed to select for polyester formation before polycarbonate. Consistent with Duchateau's Cr catalyzed terpolymerization, the rate of polyester polymerization is faster than polycarbonate. Darensbourg and coworkers conclude that the slow polycarbonate rate is from the reversible insertion of $CO_2$ into the metal alkoxide and the competitive generation of cyclic carbonate. This is in constrast to the (BDI)ZnOAc system, where $CO_2$ insertion is irreversible.

Duchateau et al. also explored the kinetics of ROAC with systematic changes in catalyst, cocatalyst, and anhydride structure (Figure 1.12).[24] The impact of ligand and metal variations are evaluated for the copolymerization of several anhydrides (phthalic (PA), succinic (SA), and cyclopropane-1,2-dicarboxylic acid (CPrA)) with cyclohexene oxide (CHO). Increased steric bulk of the diamine ligand decreases copolymerization rate, consistent with CHO/$CO_2$ reactions (Figure 1.12a).[25] Cr creates the most active catalyst and produces the highest molecular weight polyesters. The (salophen)CrCl (**3c**) complex is tested with different cocatalysts for the copolymerization of PA and CHO. N-heterocyclic amines, phosphines, and bis(triphenylphophoranylidene)ammonium [PPN] salts are active cocatalysts in the ROAC process and [PPN] salts exhibit the highest activity.

(salophen)CrCl/[PPN][Cl] is the most active system for the ROC of epoxides/anhydrides

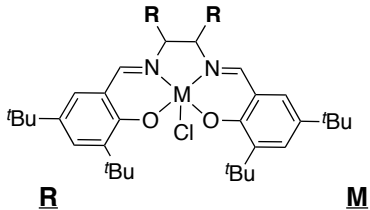


| R | | M |
|---|---|---|
| H | (salen) | Cr |
| -$(CH_2)_4$- | (salcy) | Co |
| -$(CH)_4$- | (salophen) | Al |
| $C_6H_6$ | (diphenyl salen) | |

relative copolymerization rates:
salophen > salen ~ salcy > diphenyl salen
Cr > Co > Al
[PPN] salts > N-heterocyclic nucleophiles > phosphines

**Figure 1.12.** Catalyst variations evaluated for the copolymerization of epoxides/cyclic anhydrides.

No clear correlation between anhydride ring-strain and copolymerization rate is observed, consistent with findings by Darensbourg et al. (Figure 1.13).[23] Of the three anhydrides studied, PA is most active and forms the highest molecular weight polyesters. Addition of diacids causes a decrease in molecular weight and is proposed to

act as chain transfer agents. Increasing equivalents of cocatalysts also decrease molecular weight; presumably by initiating chain transfer events.

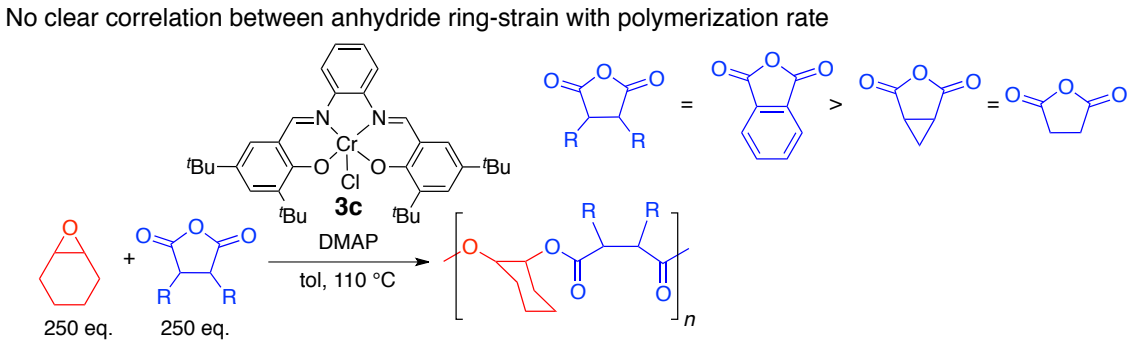


**Figure 1.13. 3c**/DMAP catalyzed ROAC of epoxides with anhydrides of different ring-strain.

In a subsequent investigation, Duchateau et al. reports **3c**/[PPN][Cl] as the most active system for the copolymerization of styrene oxide (SO) and cyclic anhydrides, although **3c**/phosphines produce higher molecular weight polyesters (Figure 1.14).[26] Lower catalyst concentrations decrease polymer molecular weight. This is explained by the increased isomerization of SO to phenylacetaldehyde, which tautomerizes to an enol that acts as a chain transfer agent. No correlation is found between anhydride ring-strain and copolymerization rate, but unsaturated anhydrides such as maleic (MA) and citraconic (CA) require lower temperatures and different solvent for activity.

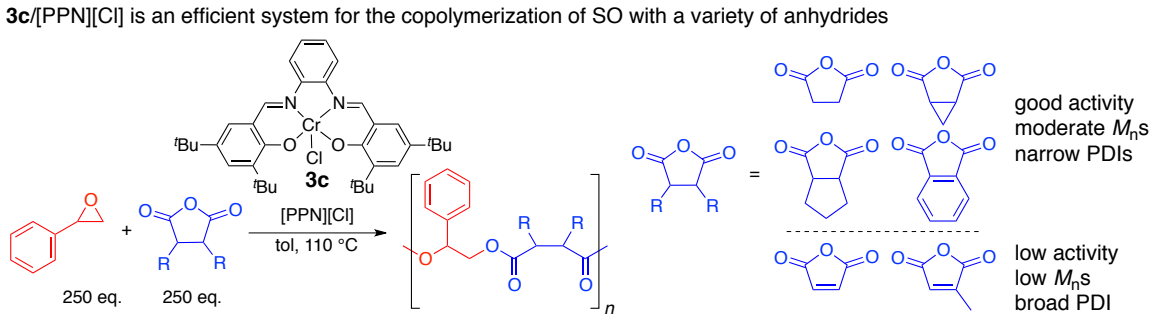


**Figure 1.14. 3c**/[PPN][Cl] catalyzed ROAC of SO/cyclic anhydrides.

Chisholm and coworkers also studied SO for copolymerization with succinic anhydride catalyzed by (TPP)CrCl (**3b**)/[PPN][Cl] (Figure 1.15).[27] NMR spectroscopy is used to confirm the isomerization of SO to phenylacetaldehyde and trace diacid from succinic anhydride is proposed to catalyze this transformation. Consequently, the highest molecular weight polyesters are achieved with a [SA]:[SO] ratio equal to 1 and as [SA]:[SO] increases, molecular weight decreases. NMR spectroscopy is also used to analyze the carbonyl and methylene carbons of SA to confirm the regioirregular structure of the poly(styrene succinate).

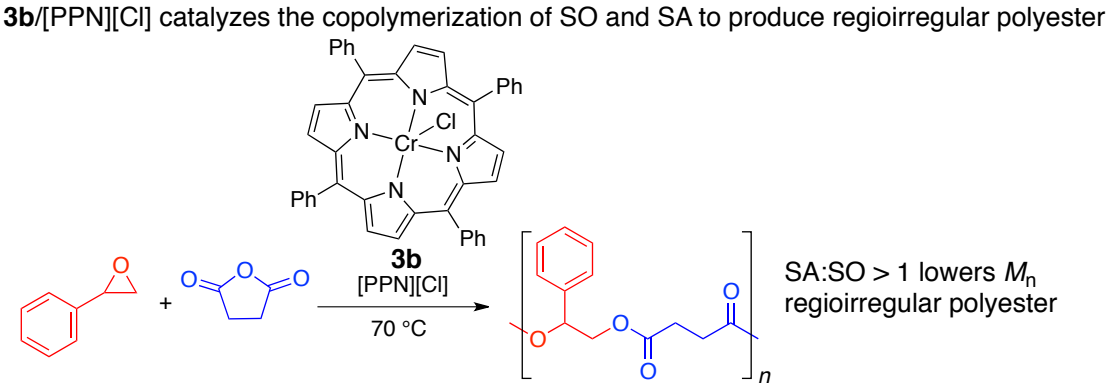


**Figure 1.15.** (TPP)CrCl/[PPN][Cl] catalyzed copolymerization of SO/SA.

More recently, Duchateau and coworkers reported **3c**/[PPN][Cl] for the copolymerization of limonene oxide (LO) and phthalic anhydride (PA) to create partially renewable polyesters (Figure 1.16).[28] In agreement with Thomas et al.,[22] the (salophen)AlCl (**1b**)/[PPN][Cl] analogue is also active for polymerizations containing LO. Diols, diacids, water, and diamines are used as chain transfer agents in these systems to modulate molecular weight. MALDI is used to analyze the poly(limonene phthalate) and confirms the perfectly alternating structure with a distribution of different chain ends including hydroxyls and chlorides. The same chain transfer agents

are effective in the copolymerization of PA/CHO and the MALDI spectra of the poly(cyclohexene phthalate) show hydroxyl, chloride, and acid end groups.

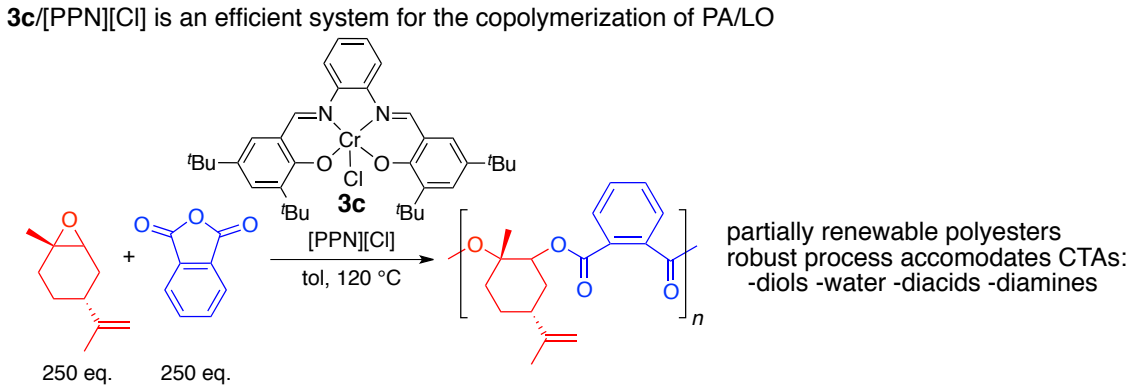


**Figure 1.16.** Copolymerization of PA/LO catalyzed by **3c**/[PPN][Cl].

Chisholm et al. screened different metal and ligand structures for copolymerizations of propylene oxide (PO) and methyl succinic anhydride (Me-SA) (Figure 1.18).[29] (TPP)CrCl (**3b**)/[PPN][Cl] is the most active system for this copolymerization. One equivalent of [PPN][Cl] is required to form perfectly alternating polyesters. Less than one equivalent results in significant incorporation of polyether stretches, yielding poly(ester-ether)s.

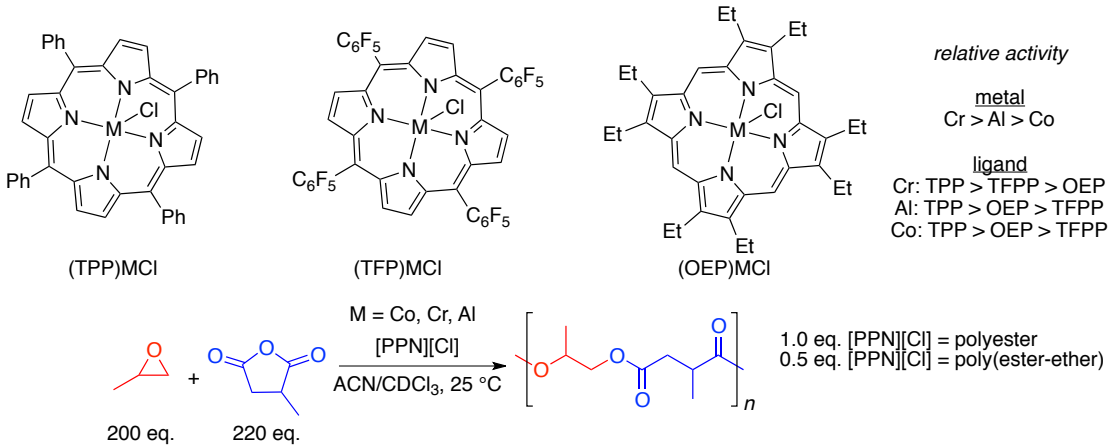


**Figure 1.17.** Three ligand/metal combinations evaluated for ROAC of PO/Me-SA.

**3b**/[PPN][Cl] and (TPP)AlCl (**1a**)/[PPN][Cl] are evaluated for copolymerization of PO and other anhydrides such as succinic (SA), maleic (MA), and phthalic (PA) to perfectly alternating polyesters (Figure 1.18). PA is the most active anhydride and produces the highest molecular weight polyesters (13.4 kDa for **1a** and 11.3 kDa for **3a**). End group analysis agrees with previous studies on polycarbonate mechanism,[30] which, suggest that Al initiates one chain per metal while Cr initiates two. In contrast to Inoue's report, Chisholm et al. concludes the same is true for polyester systems, accounting for the higher molecular weight polyesters produced by Al. For the terpolymerization of epoxide, cyclic anhydride, and $CO_2$, both systems first form polyester followed by polycarbonate.

$^{13}C$ NMR spectroscopy is used to analyze the methylene carbons of the succinate unit and quantify the regioisomers of poly(propylene succinate). At room temperature, (TPP)AlCl/[PPN][Cl] is the most regioregular system producing 86% HT linkages. At 60 °C, (TFPP)CrCl/[PPN][Cl] is the most regioregular producing 73% HT linkages.

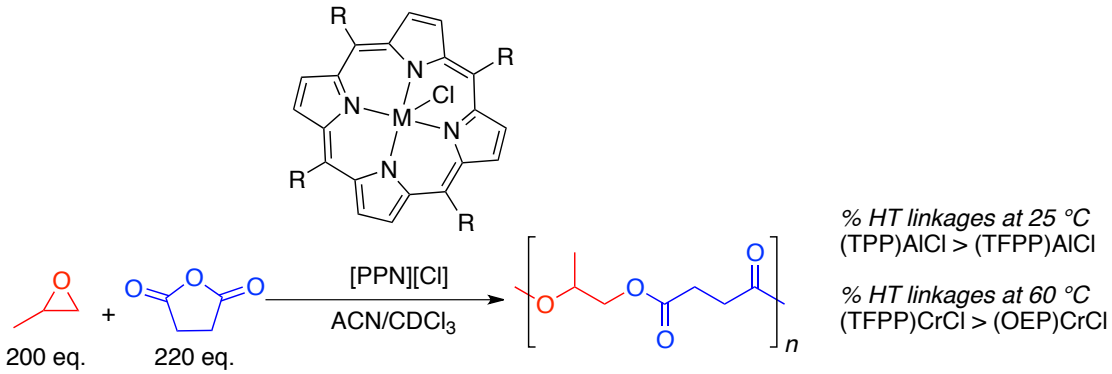


**Figure 1.18.** (TPP)AlCl/[PPN][Cl] catalyzed copolymerization of PO/SA.

Xiao-Bing Lu and coworkers explored salan ligands, encouraged by their high activity in polycarbonate polymerizations and the ease of creating bimetallic systems.[31]

Monomeric (salan)CrCl (**3d**) and bimetallic (binol-salan)CrCl (**3e**) are both active for the perfectly alternating copolymerization of maleic anhydride (MA) with epichlorohydrin (ECH) and phenyl glycidyl ether (PGE) (Figure 1.19).[32] For the copolymerization of MA/ECH, the activity of bimetallic **3e** is significantly higher than **3d**, however, neither catalyst compares in activity to (salen)CrCl **3a** (TOFs = 1, 7 and 33 $h^{-1}$ respectively). **3e** is used to catalyze the copolymerization of MA and *s*-PGE. Hydrolysis of this copolymer and analysis of the glycol products demonstrates >98% retention of stereochemistry, indicative of a regioselective process.

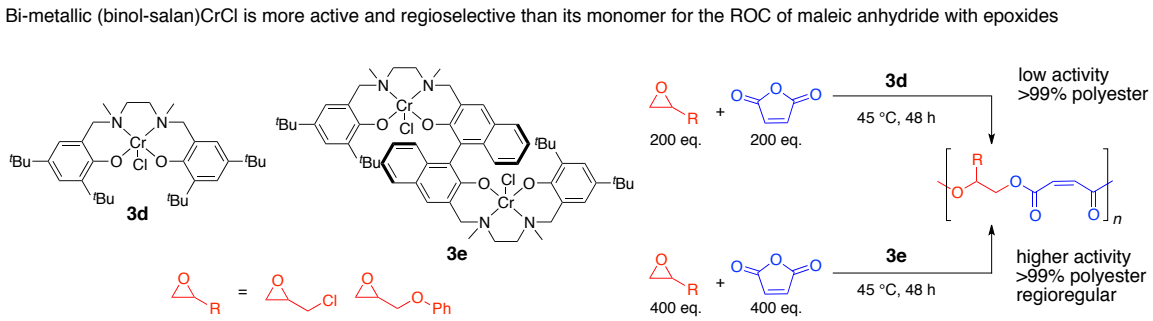


**Figure 1.19.** Salan catalysts tested for ROAC of MA/epoxides.

Bimetallic **3e** is also active for the copolymerization of SA/ECH, although this process requires higher temperatures and solvent (100 °C, toluene). The copolymerization of MA with CHO, affords mostly poly(cyclohexene oxide) with only 8% of ester linkages.

## 1.5 Summary and Outlook

Recent developments of highly active epoxide/cyclic anhydride copolymerization processes are advancing the potential of polyesters to become durable, biodegradable, thermoplastic alternatives. While no reported systems are able to produce high molecular weight polyesters with good control of regio- or stereochemistry, the progress

of discrete polyester catalysts and mechanistic knowledge is quickly advancing the frontier of this field. Aided by discoveries in polycarbonate systems, the production of poly(ester)-*b*-(carbonate)s will contribute to this new class of material.

The most studied ROAC systems are based on (salen)CrCl and (TPP)CrCl frameworks. The Cr metal center is surrounded by a square-planar ligand with two trans-axial coordination sites. A chloride counterion or a propagating polymer chain occupies one axial site. The other is open for coordination of a monomer, cocatalyst, or solvent molecule (Scheme 1.1a). There is evidence that initiation occurs with both counter-anions of the catalyst and cocatalyst, suggesting close association of the cocatalyst with the metal center. Scheme 1.1 presents a proposed mechanism based on the studies discussed above.

**Scheme 1.1.** Proposed Mechanism for the ROAC of Epoxides and Cyclic Anhydrides

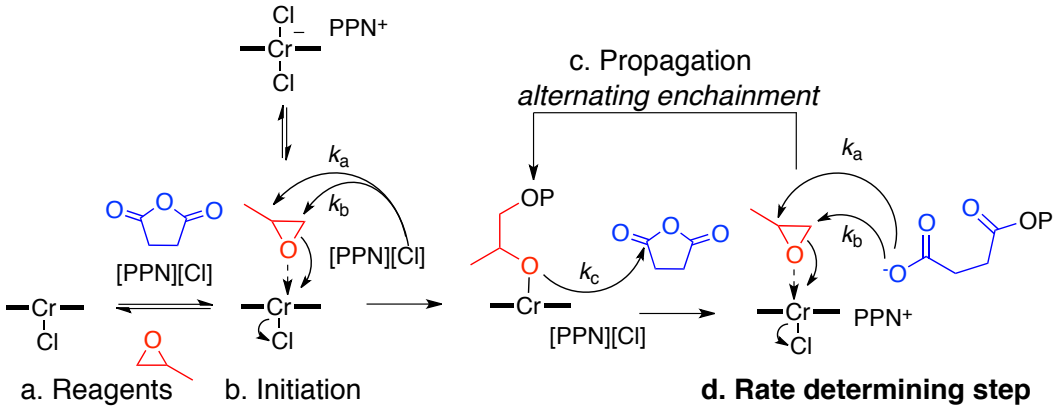


a. Initial reaction mixture
b. *Initiation*: ring-opening of coordinated epoxide
c. *Propagation*: alternating enchainment of anhydride and epoxide
d. *Rate-determining step*: carboxylate attack on coordinated epoxide
* Regiochemistry is dictated by epoxide ring-opening

One equivalent of [PPN][Cl] is generally required for high activity and alternating behavior, although maleic anhydride is an exception. MALDI analyses primarily detect

epoxide end groups, which, suggests that initiation is epoxide ring-opening. Nucleophilic attack at the methine ($k_a$) or methylene ($k_b$) carbon results in different regioisomers and is mostly random for Cr catalyzed processes (Scheme 1.1b).

Propagation proceeds via alternating metal-alkoxide ring-opening of anhydride (Scheme 1.1c) and metal-carboxylate ring-opening of epoxide (Scheme 1.1d). Copolymerization rate has a first order dependence on epoxide concentration, therefore excess epoxide is generally used. Epoxide ring-opening is the rate-determining step, but no correlation of rate with epoxide structure has been reported. However, differences in epoxide sterics and electronics impact copolymerization activity. There is no correlation between copolymerization rate and cyclic-anhydride ring-strain, although different anhydrides cause distinctive rates. The differences in rate associated with anhydride identity likely depend on the nucleophilicity of the propagating carboxylate.

Finally, chain transfer to protic species is reported as the source of lower molecular weights for these systems. It is significant to note that trace diacids in anhydrides are one source of protic impurities that lead to chain transfer and low molecular weight polymers. Anhydride purification and complete removal of diacid and water are suggested as methods to improve polyester molecular weight.

For terpolymerization with $CO_2$, parallels are consistently drawn between Cr and Zn catalyzed systems. It is assumed that the product-determining step depends on the rates of $k_c$ and $k_d$ (Scheme 1.2c) and for all systems $k_c >>> k_d$, causing production of polyester before polycarbonate. For (BDI)ZnOAc, the rate of polyester formation is unaffected by the presence of $CO_2$, indicating no competition between the monomers. However, in (salen)CrCl systems, the rate of polyester formation is much slower in the

presence of $CO_2$, attributed to reversible insertion of $CO_2$ to the metal alkoxide and potential formation of cyclics. Furthermore, for (BDI)ZnOAc the rate of polycarbonate formation is faster than polyester while for (salen)CrCl the opposite is true. These differences have not been addressed in detail but suggest fundamental distinctions for mechanism that should be probed.

**Scheme 1.2** The Product-Determining Step Forms Polyester Before Polycarbonate

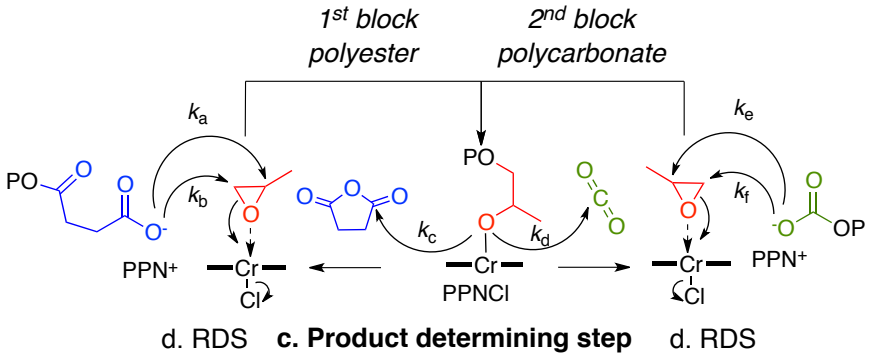


In general, the highest molecular weight polyesters are formed from the more active anhydrides (such as phthalic anhydride). Studies to probe why this anhydride is most active will be insightful for the design of new ligands that enhance the rate-determining step. Finally, except for the bimetallic copolymerization process presented by Xiao-Bing Lu, no systems have biased $k_a$ vs. $k_b$ to create perfectly regioregular polyester. Literature suggests that temperature, ligand, and metal will be key parameters for tuning the selectivity of this step.

## 1.6 Preface to this Dissertation

This body of work will detail new processes for the copolymerization of epoxides and cyclic anhydrides. Chapter two describes a (salcy)CrCl catalyzed process for the copolymerization of maleic anhydride and terminal epoxides. Chapter three discusses

the development of a regioselective (salcy)$CoNO_3$/[PPN][$NO_3$] process for the copolymerization of epoxides and cyclic anhydrides. Chapter four presents a modified (salcy)$CoNO_3$/[PPN][$NO_3$] complex for the living copolymerization of phthalic anhydride with terminal epoxides to high molecular weight polymers and block copolymers. Chapter five introduces chiral (salcy)$CoNO_3$ catalysts able to produce semi-crystalline polyesters. Chapter six summarizes mechanistic studies on (BDI)ZnOAc and (salcy)$CoNO_3$ processes and discusses similarities and differences between the systems. Finally chapter 7 will present extensions of each system and preliminary work that has been done in these areas. And now I thank you for reading ☺

REFERENCES

(1) (a) Miller, S. A. *ACS Macro Lett.* **2013**, *2*, 550. (b) Kreye, O.; Mutlu, H.; Meier, M. A. R. *Green Chem.* **2013**, *15*, 1431. (c) Lebarbé, T.; Maisonneuve, L.; Nguyen, T. H. N.; Gadenne, B.; Alfos, C.; Cramail, H. *Polym. Chem.* **2012**, *3*, 2842. (d) Jeske, R. C.; Coates, G. W. Homogenous Catalyst Design for the Synthesis of Aliphatic Polycarbonates and Polyesters. In *Handbook of Green Chemistry;* Crabtree, R. H., Ed.; Wiley-VCH: Weinheim, Germany, 2009; Vol. 1, pp 343. (e) Coates, G. W.; Moore, D. R. *Angew. Chem. Int. Ed.* **2004**, *43*, 6618. (f) Noordover, B. A. J.; Jasinka-Walc, L.; Meulen, I. v. d.; Duchateau, R.; Koning, C. E. Novel Biomass-Based Polymers: Synthesis, Characterization, and Application. In *Biobased Monomers, Polymers, and Materials*; Smith, P., et al. Ed.; ACS Symposium Series: Washington DC, 2012; pp 281.

(2) (a) Gross, R. A.; Kalra, B. *Science* **2002**, *297*, 803. (b) Harracksingh, R. Bioplastics surge towards commercialization. *ICIS Chem. Bus.* [Online] June 29, 2012. (accessed Sept 1, 2013). (c) Philp, J. C.; Bartsev, A.; Ritchie, R. J.; Baucher, M. A.; Guy, K. *New Biotechnol.* **2012**, http://dx.doi.org/10.1016/j.nbt.2012.11.021. (d) Ribeiro, I.; Peças, P.; Henriques, E. *Materials and Design* **2013**, *51*, 300.

(3) Bioplastics Market Update. *Compounding World* [Online] June 20, 2012. www.chem.umn.edu/csp/pdfs/CWJune2012%20article.pdf (accessed Aug 30, 2013).

(4) (a) Soroudi, A.; Jakubowicz, I. Recycling of bioplastics, their blends and biocomposites: A review. *Eur. Polym. J.* **2013**, http://dx.doi.org/10.1016/europolymj.2013.07.025. (b) Webb, H. K.; Arnott, J.; Crawford, R. J.; Ivanova, E. P. *Polymers* **2013**, *5*, 1.

(5) Gerngross, R. A.; Slater, S. C. *Sci. Am.* **2000**, *283*, 37.

(6) (a) Industry Experts. Bioplastics- A global market overview. *Industrial Biotechnology* **2012**, *8*, 62. (b) Reineck, P. *Bioplastics go mainstream* [Online]; Society of Chemical Industry www.scoi.org/News/Bioresources/Bioresource-bioplastics (accessed Sept 3, 2013).

(7) (a) Tsui, A.; Wright, Z. C.; Frank, C. W. *Annu. Rev. Chem. Biomol. Eng.* **2013**, *4* 143. (b) Webb, H. K.; Arnott, J.; Crawford, R. J.; Ivanova, E. P. *Polymers* **2013**, *5*, 1.

(8) (a) Nava, H. **2004**. Polyesters, Unsaturated. Kirk-Othmer Encyclopedia of Chemical Technology [Online]. (b) East, A. J. **2006**. Polyesters, Thermoplastic. Kirk-Othmer Encyclopedia of Chemical Technology.

(9) Aida, T.; Sanuki, K.; Inoue, S. *Macromolecules* **1985**, *18*, 1049.

(10) (a) Cheng, M.; Moore, D. R.; Reczek, J. J.; Chamberlain, B. M.; Lobkovsky, E. B.; Coates, G. W. *J. Am. Chem. Soc.* **2001**, *123*, 8738. (b) Allen, S. D.; Moore, D. R.;

Lobkovsky, E. B.; Coates, G. W. *J. Am. Chem. Soc.* **2002**, *124*, 14284. (c) Moore, D. R.; Cheng, M.; Lobkovsky, E. B.; Coates, G. W. *Angew. Chem. Int. Ed.* **2002**, *41*, 2599. (d) Allen, S. D.; Moore, D. R.; Lobkovsky, E. B.; Coates, G. W. *J. Org. Chem.* **2003**, *683*, 137. (e) Moore, D. R.; Cheng, M.; Lobkovsky, E. B.; Coates, G. W. *J. Am. Chem. Soc.* **2003**, *125*, 11911.

(11) Jeske, R. C. Ph.D. Thesis, Cornell University, June 2009.

(12) (a) Radzewich, C. E.; Coles, M. P.; Jordan, R. F.; *J. Am. Chem. Soc.* **1998**, *120*, 9384. (b) Yokota, S.; Tachi, Y.; Itoh, S. *Inorg. Chem.* **2002**, *41*, 1342. (c) Carey, D. T.; Cope-Eatough, E. K.; Vilaplana-Mafé, E.; Mair, F. S.; Pritchard, R. G.; Warren, J. E.; Woods, R. J. *Dalton Trans.* **2003**, 1083. (d) Basuli, F.; Huffman, J. C.; Mindiola, D. J. *Inorg. Chem.* **2003**, *42*, 8003.

(13) Jeske, R. C.; DiCiccio, A. M.; Coates, G. W. *J. Am. Chem. Soc.* **2007**, *129*, 11330.

(14) Unpublished results, please refer to Chapter 6.

(15) Jeske, R. C.; Rowley, J. M.; Coates, G. W. *Angew. Chem. Int. Ed.* **2008**, *47*, 6041.

(16) DiCiccio, A. M.; Coates, G. W. *J. Am. Chem. Soc.* **2011**, *133*, 10724.

(17) Engels, H. W.; Pirkl, H. G.; Albers, R.; Albach, R. W.; Krause, J.; Hoffmann, A.; Casselman, H.; Dormish, J. *Angew. Chem. Int. Ed.* **2013**, *52*, 2.

(18) Unpublished results, please refer to Chapter 7.

(19) (a) Kember, M. R.; Buchard, A.; Williams, C. K. *Chem. Commun.* **2011**, *47*, 141. (b) Darensbourg, D. J. *Chem. Rev.* **2007**, *107*, 2388.

(20) For a review on the properties, chemistry and applications of MA: *Kirk-Othmer Encyclopedia of Chemical Technology*, 5th ed.; Wiley: New York, 2004; Vol. 15, pp 481-523.

(21) Huijser, S.; Nejad, E. H.; Sablong, R.; de Jong, C.; Koning, C. E.; Duchateau, R. *Macromolecules*, **2011**, *44*, 1132.

(22) Robert, C.; de Montigny, F.; Thomas, C. M. *Nat. Comm.* **2011**, *2*, 586.

(23) Darensbourg, D. J.; Poland, R. R.; Escobedo, C. *Macromolecules* **2012**, *45*, 2242.

(24) Nejad, E. H.; van Melis, C. G. W.; Vermeer, T. J.; Koning, C. E.; Duchateau, R. *Macromolecules* **2012**, *45*, 1770.

(25) Darensbourg, D. J.; Mackiewicz, R. M.; Rodgers, J. L.; Fang, C. C.; Billodeaux, D. R.; Reibenspies, J. H. *Inorg. Chem*. **2004**, *43*, 6024.

(26) Nejad, E. H.; Paoniasari, A.; Koning, C. E.; Duchateau, R. *Polym. Chem.* **2012**, *3*, 1308.

(27) Harrold, N. D.; Li, Y.; Chisholm, M. H. *Macromolecules* **2013**, *46*, 692.

(28) Nejad, E. H.; Paoniasari, A.; van Melis, C. G. W.; Koning, C. E.; Duchateau, R. *Macromolecules* **2013**, *46*, 631.

(29) Bernard, A.; Chatterjee, C.; Chisholm, M. H. *Polymer* **2013**, *54*, 2639.

(30) (a) Chatterjee, C.; Chisholm, M. H. *Inorg. Chem*. **2011**, *50*, 4481. (b) Chatterjee, C.; Chisholm, M. H. *Inorg. Chem.* **2012**, *51*, 12041.

(31) (a) Li, B.; Wu, G. P.; Ren, W. M.; Wang, Y. M.; Lu, X. B. *J. Polym. Sci., Part A: Polym. Chem.* **2008**, *46*, 6102. (b) Rao, D. Y.; Li, B.; Zhang, R.; Wang, H.; Lu, X. B. *Inorg. Chem.* **2009**, *48*, 2830. (c) Darensbourg, D. J.; Ulusoy, M.; Karroonnirum, O.; Poland, R. R.; Reibenspies, J. H.; Cetinkaya, B. *Macromolecules* **2009**, *42*, 6992.

(32) Liu, J.; Bao, Y.-Y.; Liu, Y.; Ren, W.-M.; Lu, X.-B. *Polym. Chem.* **2013**, *4*, 1439.

CHAPTER TWO

# RING-OPENING COPOLYMERIZATION OF MALEIC ANHYDRIDE WITH EPOXIDES: A CHAIN GROWTH APPROACH TO UNSATURATED POLYESTERS

## 2.1 Abstract

In this report, we present the ring-opening copolymerization of maleic anhydride with a variety of epoxides catalyzed by a chromium(III) salen complex. Quantitative isomerization of the *cis*-maleate form of all polymers affords the *trans*-fumarate analogues. Addition of chain transfer reagents yields low $M_n$, narrow PDI polymer samples. This method provides access to a range of new unsaturated polyesters with versatile functionality, as well as the first synthesis of high molecular weight poly(propylene fumarate).

## 2.2 Introduction

Approximately 1.7 million metric tons of maleic anhydride (MA)[1] were produced and consumed in 2009, over 40% of which was used for the production of unsaturated polyesters (UPs).[2,3] Utilization of UPs in resins,[4] composite materials,[5] biomedical devices,[6] and drug delivery[7] applications benefits from the ability to enhance polymer properties through post polymerization modifications of the maleate or fumarate units provided by MA. For example, easily cured UPs excel in lightweight, sustainable coatings and materials technology, namely in applications such as wind turbines and high performance housing and marine materials.[8] Biodegradable UPs, such as

poly(propylene fumarate) (PPF),[9] can be used in orthopedic implants and tissue repair systems as they provide easy formation of robust, noncytotoxic tissue/bone scaffolds[6] that degrade to benign metabolic products.[10]

While UPs are a well-established material, their applications are currently limited by the inability to incorporate diverse functionality into the polymer chain, difficulty achieving high molecular weight, and formation of undesired ether linkages.[4a] The common method for polyester synthesis, step-growth copolymerization (Scheme 2.1a), requires high energy input, long reaction times, and often affords low molecular weight polymers with uncontrolled isomerization.[11] Other frequent problems include conjugate addition side-reactions and unwanted crosslinking.[4b] The development of a versatile, mild synthetic route to functionalized, unsaturated polyesters will advance the properties and expand the applications of this important class of materials.

**Scheme 2.1.** Polymerization Routes for the Synthesis of Poly(propylene fumarate): a) Reported Step-Growth; b) Proposed Chain-Growth

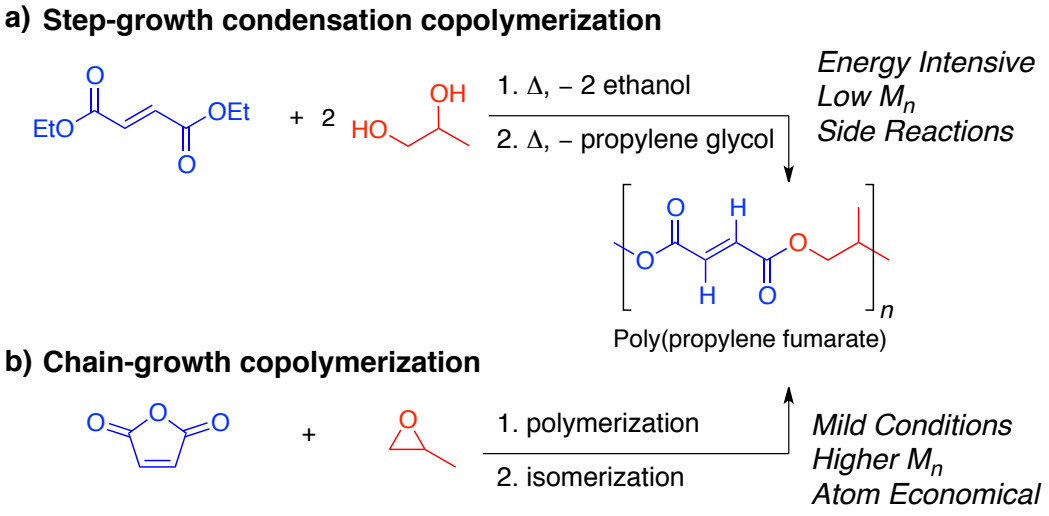

## 2.3 Catalyst Screening for the Chain-growth Copolymerization of Epoxides/MA

A mild catalytic chain-growth copolymerization (Scheme 2.1b) could circumvent many of the disadvantages of step-growth routes.[12] To our knowledge, no literature reports demonstrate catalytic, highly alternating copolymerization of maleic anhydride (MA) with a broad range of epoxides.[13,14] Systems reported for MA/epoxide copolymerizations generally suffer from harsh conditions, low reactivity, low molecular weight, and/or ether formation (Table 2.1, entries 1-2).[14] In this communication, we report a chromium(III) salen catalyst capable of copolymerizing MA with a range of epoxides under mild conditions to afford a variety of new functionalized unsaturated polyesters. We also present the first synthesis of highly alternating PPF with number average molecular weight ($M_n$) above 15 kDa.

Initially, we focused on catalyzing the ring-opening copolymerization of MA with propylene oxide (PO), to produce poly(propylene maleate) (PPM). We hypothesized that *cis-trans* isomerization of the backbone in isolated PPM would provide access to PPF.

**Table 2.1.** Recent Catalysts Applied for Copolymerization of Maleic Anhydride with Propylene Oxide from Literature (1-2) and this Work (4-6)

**Literature:**

$Mg(OEt)_2$ **1**

$Zn_3[Co(CN)_6]_2$ **2**

**This Work:**

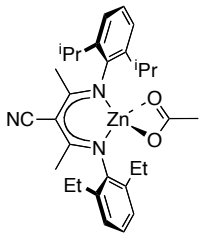


**3**

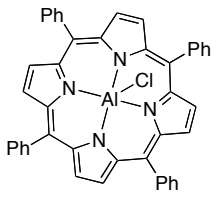


**4**

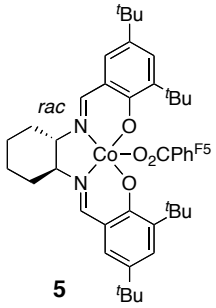


**5**

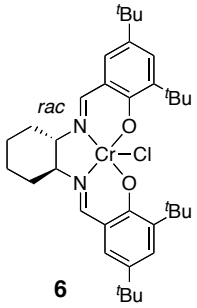


**6**

| entry | catalyst | temp (°C) | time (h) | conv (%)[a] | ether (%)[a] | $M_n$ (kDa)[b] | PDI[b] | ref. |
|---|---|---|---|---|---|---|---|---|
| 1 | **1** | 80 | 48 | 42 | 5[c] | 4 | 1.2 | 14a |
| 2 | **2** | 100 | 16 | 97 | 20[c] | 3 | 1.4 | 14b |
| 3[d] | **3** | 45 | 15 | 5 | 86 | 5 | 1.2 | - |
| 4[d] | **4** | 45 | 15 | 7 | 50 | 14 | 1.1 | - |
| 5[d] | **5** | 45 | 15 | 12 | <1[e] | 5 | 1.1 | - |
| 6[d] | **6** | 45 | 15 | 47 | <1[e] | 6 | 1.3 | - |
| 7[f] | **6** | 45 | 15 | >99 | <1[e] | 17 | 1.6 | - |

[a] $^1$H NMR spectra of crude reaction mixture was used to determine conversion and ether linkage percents (consecutive epoxide enchainment). [b] Determined by gel-permeation chromatography (GPC) calibrated with polystyrene standards in $CHCl_3$ at 40 °C. [c] Estimated on the basis of shifts due to ether linkages in the $^1$H NMR spectrum. [d] Reaction conditions: [MA]:[PO]:[cat] = 200:200:1, [MA] and [PO] = 4 mM in toluene. [e] No evidence of ether linkages detected in $^1$H NMR spectrum. [f] Reaction conditions the same as *d* except hexanes are used as a solvent. The reaction mixture is homogenous at the beginning of the reaction and solidifies upon consumption of all monomers.

We previously reported a highly active (BDI)ZnOAc[15] (BDI = β-diiminate) (**3**) catalyst for the copolymerization of saturated anhydrides with epoxides. However, with the unsaturated anhydride MA, the (BDI)ZnOAc system displayed low activity and

significant amounts of ether linkages (Table 2.1, entry 3). These results were similar to earlier reports using other zinc-based catalysts for this reaction (entry 2).[14b-14d]

Given the catalytic role of **3** in both $CO_2$/epoxide and anhydride/epoxide copolymerizations, we investigated other complexes which can catalyze $CO_2$/epoxide copolymerization.[16] The aluminum porphyrin complex (**4**, entry 4) exhibited low activity and produced a large percent of ether linkages while the cobalt salen complex (**5**, entry 5) demonstrated moderate activity with no detectable ether formation. The chromium(III) salen complex (**6**, entry 6) exhibited the highest activity and selectivity for the preparation of PPM. Using hexanes as a solvent afforded quantitative conversion (99%) and a relatively high $M_n$ (17 kDa) (entry 7). Polyester purity was confirmed by $^1$H and $^{13}$C NMR spectroscopy.

### 2.4 Cis-trans Isomerization of Poly(propylene maleate)

With an efficient synthesis of PPM in hand, we investigated the controlled *cis-trans* isomerization to form PPF.[14a] Catalytic isomerization of PPM with diethylamine[17,18] in chloroform at room temperature afforded PPF quantitatively as shown by $^1$H NMR spectroscopy (Figure 2.1). After reaction with diethylamine, the signal at 6.21 ppm of the *cis*-alkene of PPM was no longer present and a new signal at 6.84 ppm was observed, corresponding to the *trans*-alkene of PPF. The isomerization was performed as a one-pot procedure or with an isolated polymer sample. The molecular weight and PDI of the polymer remains consistent throughout the isomerization and the $T_g$ of the fumarate containing polyesters increases (Figure 2.1). To the best of our knowledge, this is the highest $T_g$ reported to date for these polymers.

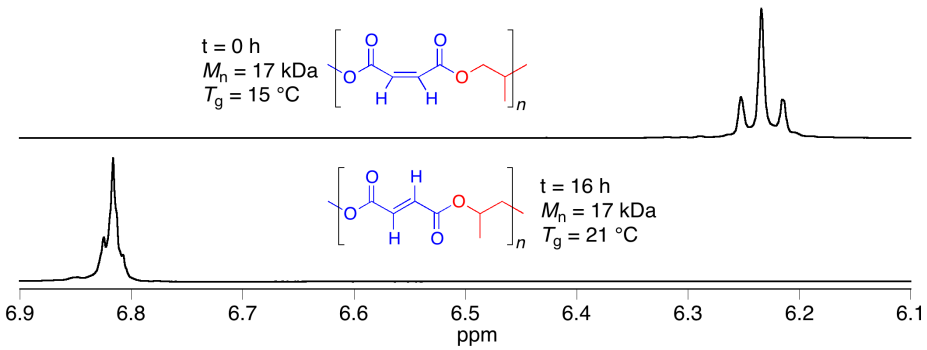


**Figure 2.1.** Alkene regions of the $^1$H NMR spectra of PPM and PPF demonstrating the clean *cis* to *trans* conversion by catalytic $HNEt_2$.[19]

## 2.5 Expansion of Substrate Scope

To explore the substrate scope of this copolymerization, we screened a variety of epoxides with MA (Table 2.2, entries 1-7). 1-Butene oxide (**8**, entry 1) exhibited comparable reactivity to PO. The functionalized epoxides epichlorohydrin (**9**, entry 2) and allyl glydicyl ether (**10**, entry 3) were polymerized with high conversions (99 and 98% respectively) and showed no evidence of ether linkages by $^1$H NMR spectroscopy. The resulting pendant functionalities provide an opportunity to tune the properties of these polyesters: for example, nucleophilic displacement of the alkyl halide can be envisioned for the epichlorohydrin derived polymer. Other types of functionality can also be incorporated to alter the bulk properties of the unsaturated polyesters. Epoxide **11** bearing a diethylene glycol (PEG) unit (entry 4) polymerized with high conversion (90%) and no detectable ether linkages. Recent efforts to incorporate PEG units into unsaturated polyesters couple maleate or fumarate units to oligo-PEG diols for applications ranging from biomedical to commodity materials.[5g,7a,20] Our method provides a simple polymerization approach to appending PEG units off of an

unsaturated polyester core while maintaining the biocompatible monomers. Perfluoro alkyl chain appended epoxide **12** (entry 5) copolymerized cleanly and in high conversion (90%) with MA. Fluorinated functionality offers distinctive properties such as low coefficients of friction, good chemical resistance, and low surface energies, which are excellent for unsaturated polyesters used in material coatings and biomedical applications.[21] Furthermore, epoxides with greater steric bulk near the reactive epoxide base such as acetal protected epoxide **13** (entry 6) and phenyl glycidyl ether **14** (entry 7) polymerized to high molecular weight (22 and 31 kDa respectively) with no evidence of ether linkages. Deprotection of THP from **13** would yield unsaturated polyester appended with a glycol per repeat unit. Finally, isomerization of all *cis*-polyesters from terminal epoxides (entries 1-7) quantitatively yielded the *trans*-fumarate analogues using the route described above.

**Table 2.2.** MA Copolymers with Other Epoxides Using Catalyst 6[a]

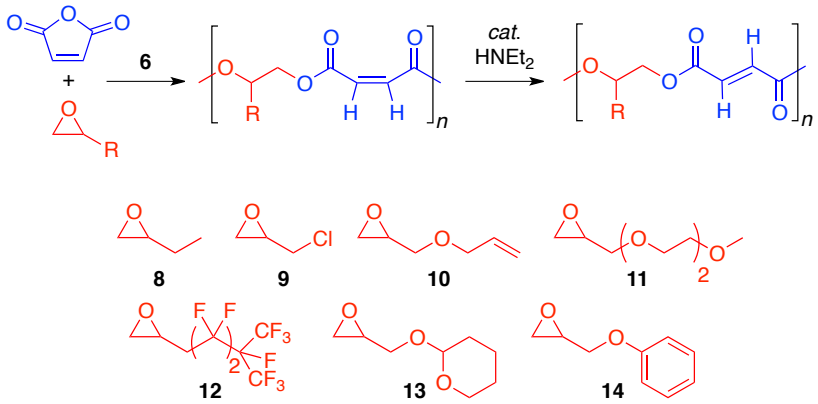


| entry | epoxide | time (h) | conv[b] (%) | ether[b] (%) | $M_n$ (kDa)[c] | $M_w/M_n$[c] | $T_g$ m[d] (°C) | $T_g$ f[d] (°C) |
|---|---|---|---|---|---|---|---|---|
| 1 | **8** | 14 | 90 | <1 | 21 | 1.5 | 11 | -14 |
| 2 | **9** | 6 | 99 | <1 | 25 | 1.7 | 33 | 45 |
| 3 | **10** | 15 | 98 | <1 | 25 | 1.3 | -10 | -6 |
| 4 | **11** | 4 | 99 | <1[22] | 33 | 1.1 | -26 | -29 |
| 5 | **12** | 16 | 90 | <1 | 25 | 1.7 | 40 | 53 |
| 6 | **13** | 15 | 99 | <1 | 21 | 1.4 | 35 | 36 |
| 7 | **14** | 12 | 99 | <1 | 31 | 1.4 | 41 | 50 |

[a]Reaction conditions: [MA]:[epoxide]:[**6**] = 200:200:1, [MA] and [epoxide] = 4 mmol in 1 mL hexanes, $T_{rxn}$ = 45 °C. [b]Determined by $^1$H NMR spectroscopy of crude reaction. [c]Molecular weight data was determined on GPC calibrated with polystyrene standards in $CHCl_3$ at 40 °C. $M_n$ data collected for isomerized polymers were within +/- 10% of the values reported for their maleate analogues and within the error of the GPC instrument used. The $M_w/M_n$ of the isomerized polymers changed by +/- 0.2. [d]Determined by DSC analysis, m = maleate and f = fumarate forms of the polymer.

## 2.6 Chain-Transfer Agents for Tailored Molecular Weights

Given the industrial importance of unsaturated polyester resins, we investigated whether low molecular unsaturated polyesters could be produced with our system without increasing catalyst loading. By using the same reaction conditions and adding

isopropanol as a chain transfer reagent, we were able to control the relative number of polymer chains produced and thus $M_n$ without a decrease in activity (Table 2.3).

**Table 2.3.** $M_n$ Changes as a Function of $^i$PrOH Addition[a]

| entry | [MA]:[$^i$PrOH] | conv[b] (%) | ether[b] (%) | $M_n$ (kDa)[c] | $M_w/M_n$[c] |
|---|---|---|---|---|---|
| 1 | 200:3 | 87 | <1 | 6.4 | 1.2 |
| 2 | 200:5 | 94 | <1 | 5.0 | 1.2 |
| 3 | 200:6 | 92 | <1 | 4.8 | 1.1 |
| 4 | 200:7 | 94 | <1 | 4.5 | 1.1 |
| 5 | 200:9 | 93 | <1 | 3.9 | 1.1 |

[a]Reaction conditions: [MA]:[epoxide]:[**6**] = 200:200:1, [MA] and [epoxide] = 4 mmol in 1 mL hexanes, $T_{rxn}$ = 45 °C, $t_{rxn}$ = 20 h, quenched with addition of glacial AcOH. [b]Determined by $^1$H NMR spectroscopy of crude reaction. [c]Determined by GPC calibrated with polystyrene standards in $CHCl_3$ at 40 °C.

As the molar ratio of isopropanol increases, the measured $M_n$ of the polymer sample decreases while maintaining a narrow polydispersity. This process can be tuned using a variety of chain transfer agents to achieve polymer samples of desired molecular weight and end group.

## 2.7 Conclusion and Outlook

In conclusion, we report the alternating ring-opening copolymerization of MA with terminal epoxides catalyzed by a chromium(III) salen complex. This method followed by isomerization allowed the quantitative formation of PPF with $M_n$ above 15 kDa under mild conditions. This system also copolymerizes epoxides containing new biocompatible and multi-functional substituents. Additionally, chain transfer was demonstrated with this system to afford low molecular weight unsaturated resin precursors under mild conditions, with low catalyst loading, and narrow polydispersity.

Post-polymerization modification, mechanistic studies, and expanding the substrate scope to include additional biorelevant, renewable monomers are currently in progress.

## 2.8 Acknowledgements

This work is adapted from a manuscript published in the *Journal of the American Chemical Society* in 2011, volume 133, page 10724 with coauthor Geoffrey W. Coates. We gratefully acknowledge the NSF (CHE-0809778) and Eastman Chemicals for financial support. A. M. D. acknowledges the NSF IGERT program for a graduate fellowship. We thank Rachna Khurana for the synthesis of **11** and **13**. We also thank Ivan Keresztes for help with $^{1}H$, $^{13}C$, and heteronuclear NMR spectroscopic data collection and analysis.

REFERENCES

(1) For a review on the properties, chemistry, and applications of maleic anhydride: Maleic Anhydride, Maleic Acid, and Fumaric Acid. *Kirk-Othmer Encyclopedia of Chemical Technology*, 5th ed.; Wiley: New York, 2004, Vol. 15, pp 481-523.

(2) *Maleic Anhydride*; World Petrochemicals Program Report; SRI Consulting. Menlo Park, CA, January 2010; abstract. http://www.sriconsulting.com/WP/Public/Reports/ma/ (accessed March 16, 2011).

(3) For a general review on unsaturated polyesters: Nava, H. Polyesters, Unsaturated. *Kirk-Othmer Encyclopedia of Chemical Technology*, 5th ed.; Wiley: New York, 2004, Vol. 20, pp 95-119.

(4) (a) Unsaturated Polyester Resins Chemistry and Technology. *Advances in Polymer Science: Crosslinking in Materials Science*; Springer-Verlag: Berlin, 2005, Vol. 184, pp 1-95. (b) Unsaturated Polyesters. *Comprehensive Polymer Science*. 1st ed.; Pergamon Press: New York, 1989, Vol. 5, pp 331-344. (c) Worzakowska, M. *J. Therm. Anal. Calorim.* **2010**, *102*, 745-750. (d) Jasinka, L.; Koning, C. E. *J. Polym. Sci. Part A: Polym. Chem*. **2010**, *48*, 2885-2895.

(5) (a) Lukaszczyk, J.; Smiga-Matuszowicz, M. *Polimery* **2010**, *55*, 83-92. (b) Aldemar, N.; Karagoz, B.; Erciyes, A. T.; Bicak, N. *J. Appl. Polym. Sci.* **2010**, *116*, 165-171. (c) Yu, J.-G.; Huang, K.-L.; Liu, S.-Q.; Tang, J.-C. *Chin. J. Chem.* **2008**, *26*, 560-563. (d) Aldemar, N.; Erciyes, A. T.; Bicak, N. *Polymer* **2010**, *51*, 5044-5050. (e) Kempen, D. H. R.; Lu, L. C.; Hefferan, T. E.; Creemers, L. B.; Heijink, A.; Maran, A.; Dhert, W. J. A.; Yaszemski, M. J. *Tissue Engineering Part A* **2010**, *16*, 3769-3777. (f) Ranganathan, S. I.; Yoon, D. M.; Henslee, A. M.; Nair, M. B.; Smid, C.; Kasper, F. K.; Tasciotti, E.; Mikos, A. G.; Decuzzi, P.; Ferrari, M. *Acta Biomat.* **2010**, *6,* 3448-3456. (g) Li, W.-L.; Xu, L.-X.; Luo, D.; Yuan, M.-Y.; Yang, M. *J. Appl. Polym. Sci.* **2008**, *108*, 39-46.

(6) For a review on biomedical polymer scaffolds: (a) Kim, M. S.; Kim, J. H.; Min, B. H.; Chun, H. J.; Han, D. K.; Lee, H. *Polymer Reviews* **2011**, *51*, 23-52. For recent developments in biomedical devices: (b) Cai, L.; Wang, S. *Biomaterials* **2010**, *31*, 7423-7434. (c) Wang, S.; Lu, L.; Yaszemski, M. J. *Biomacromolecules* **2006**, *7*, 1976-1982. (d) Cicotte, K. N.; Hedberg-Dirk, E. L.; Dirk, S. M. *J. Appl. Polym. Sci.* **2010**, *117*, 1984-1991. (e) Jayabalan, M.; Shalumon, K. T.; Mitha, M. K.; Ganesan, K.; Epple, M. *Biomed. Mater.* **2010**, *5*, 1-12. (f) Kamel, N. A.; Abou-Aiaad, T. H.; Iskander, B. A.; Khalil, S. K. H.; Mansour, S. H.; Abd-El-Messieh, S. L.; Abd-El-Nour, K. N. *J. Appl. Polym. Sci.* **2010**, *116*, 876-885. (g) Fisher, J. P.; Timmer, M. D.; Holland, T. A.; Dean, D.; Engel, P. S.; Mikos, A. G. *Biomacromolecules* **2003**, *4*, 1327-1334. (h) Wang, K.; Cai, L.; Hao, F.; Xu, X.; Cui, M.; Wang, S. *Biomacromolecules* **2010**, *11*, 2748-2759. (i) Yan, J.; Li, J. M.; Runge M. B.; Dadsetan, M.; Chen, Q. S.; Lu, L. C.; Yaszemski, M. J. *J. Biomater. Sci., Polym. Ed.* **2011**, *22*, 489-504. (j) Nguyen, C.; Young, S.; Kretlow, J. D.; Mikos, A. G.; Wong, M. *J. Oral Maxillofac. Surg.* **2011**, *69*, 11-18. (k) Wang, S.; Lu, L.; Gruetzmacher, J. A.; Currier, B. L.; Yaszemski, M. J.

*Macromolecules* **2005**, *38*, 7358-7370. (l) Timmer, M. D.; Carter, C.; Ambrose, C. G.; Mikos, A. G. *Biomaterials* **2003**, *24*, 4707-4714.

(7) (a) Dadsetan, M.; Liu, Z.; Pumberger, M.; Giraldo, C. V.; Ruesink, T.; Lu, L.; Yaszemski, M. J. *Biomaterials* **2010**, *31*, 8051-8062. (b) Hacker, M. C.; Haesslein, A.; Ueda, H.; Foster, W. J.; Garcia, C. A.; Ammon, D. M.; Borazjani, R. N.; Kunzler, J. F.; Salamone, J. C.; Mikos, A. G. *J. Biomed. Mater. Res., Part A* **2008**, 976-999. (c) Peng, D.; Huang, K.; Liu, Y.; Liu, S. *Int. J. Pharm.* **2007**, *342*, 82-86. (d) Lee, J. W.; Kang, K. S.; Lee, S. H.; Kim, J. Y.; Lee, B. K.; Cho, D. W. *Biomaterials* **2011**, *32*, 744-752.

(8) (a) Boswell, C.; Victory, M.; Yeen, C.-S.; Balboa, B. Maleic Anhydride on the Up; ICIS Chemical Business Report, New York, October 2010. (b) Burridge, E. Maleic Anhydride; European Chemical Profile; ICIS Chemical Business Report, England, August 2010. (c) Maleic Anhydride; *Chemical Week*, May 2009, *171*, pp 29.

(9) Recent representative synthesis of PPF: Kasper, F. K.; Tanahashi, K.; Fisher, J. P.; Mikos, A. G. *Nat. Protoc.* **2009**, *4*, 518-525.

(10) Poly(propylene fumarate) degrades to fumaric acid and propylene glycol. Fumaric acid is a metabolic intermediate in the citric acid cycle and thus readily metabolized. Propylene glycol is easily broken down in the body and FDA approved.[9]

(11) Luston, J.; Vass, F. *Adv. Polym. Sci*. **1984**, *56*, 92-131.

(12) (a) Huijser, S.; Nejad, E. H.; Sablong, R.; de Jong, C.; Koning, C. E.; Duchateau, R. *Macromolecules* **2011**, *44*, 1132-1139. (b) Jeske, R. C. Synthesis of Aliphatic Polyesters and Block Copolymers: New Routes to New Materials via the Highly Alternating Ring-Opening Copolymerization of Epoxides and Cyclic Anhydrides, Ph.D. Dissertation, Cornell University, Ithaca, NY, 2009. (c) Huijser, S. Synthesis and Characterization of Biodegradable Polyesters: Polymerization Mechanisms and Polymer Microstructures Revealed by MALDI-ToF-MS, Ph.D. Dissertation, Technische Universiteit Eindhoven, Eindhoven, The Netherlands, 2009.

(13) (a) Fischer, R. F. *J. Polym. Sci.* **1960**, *64*, 155-172. (b) Schaefer, J.; Katnik, R. J.; Kern, R. J. *J. Am. Chem. Soc.* **1968**, *90*, 2476-2480.

(14) (a) Takenouchi, S.; Takasu, A.; Inai, Y.; Hirabayashi, T. *Polym. J.* **2002**, *34*, 36-42. (b) Hua, Z.; Qi, G.; Chen, S. *J. Appl. Polym. Sci.* **2004**, *93,* 1788-1792. (c) Suh, H. S.; Ha, J. Y.; Yoon, J. H.; Ha, C.-S.; Suh, H.; Kim, I. *React. Funct. Polym.* **2010**, *70*, 288-293. (d) Kuran, W.; Nieslochowski, A. *J. Macromol. Sci.-Chem.* **1981**, *A51*, 1567-1575. (e) Nieslochowski, A.; Kuran, W. *Polym. Bull.* **1980**, *2*, 411-416.

(15) (a) Jeske, R. C.; DiCiccio, A. M.; Coates, G. W. *J. Am. Chem. Soc.* **2007**, *129*, 11330-11331. (b) Jeske, R. C.; Rowley, J. M.; Coates, G. W. *Angew. Chem. Int. Ed.* **2008**, *47*, 6041-6044.

(16) (a) Kember, M. R.; Buchard, A.; Williams, C. K. *Chem. Comm.* **2011**, *47*, 141-163. (b) Coates, G. W.; Moore, D. M. *Angew. Chem. Int. Ed.* **2004**, *126*, 16326-16327. (c) Darensbourg, D. J. *Inorg. Chem*. **2010**, *49*, 10765-10780.

(17) Catalytic diethylamine ([alkene]/[amine] = 10) was used for the standard isomerizations described in this paper. Lower catalyst loading could be used with longer reaction times.

(18) Fryhle, C. B.; Rybak, C. M.; Pulley, K. E. *J. Chem. Ed*. **1991**, *68*, 1050-1053.

(19) For an analysis of the peak shapes in the alkene region of the $^{1}$H NMR spectrum of the cis isomer please see supporting information.

(20) Sharma, A. K.; Kumar, R.; Canteenwala, T. C.; Parmar, V. S.; Patkar, S.; Jumar, J.; Watterson, A. C. *J. Macromol. Sci. Part A., Pure Appl. Chem.* **2005**, *42*, 1515-1521.

(21) (a) Imae, T. *Curr. Opin. Colloid Interface Sci.* **2003**, *8*, 307-314. (b) Pilati, F.; Toselli, M.; Messori, M.; Credali, U.; Tonelli, C.; Berti, C. *J. Appl. Polym. Sci.* **1998**, *67*, 1679-1691.

(22) Note that in the $^{1}$H NMR spectrum of monomer 11, protons from the ether linkages of the pendant chain overlap the region where homopolymer ether linkages would appear. Thus, $^{13}$C NMR spectroscopy was used to confirm absence of ether stretches in the polymer. The methine from the epoxide homopolymer appears at 78 ppm and is absent in the copolymer spectrum, confirming pure polyester linkages for the polymer reported in Table 2, entry 4.

APPENDIX ONE

# RING-OPENING COPOLYMERIZATION OF MALEIC ANHYDRIDE WITH EPOXIDES: A CHAIN-GROWTH APPROACH TO UNSATURATED POLYESTERS

**Contents**

### A1.1 General Considerations

All manipulations of air and water sensitive compounds were carried out under dry nitrogen using a Braun Labmaster Glovebox or standard Schlenk line techniques. $^{1}$H NMR spectra were recorded on a Varian INOVA 400 ($^{1}$H, 400 MHz), Varian INOVA 500 ($^{1}$H, 500 MHz), or Varian INOVA 600 ($^{1}$H, 600 MHz) spectrometer. $^{1}$H NMR spectra were referenced with residual non-deuterated solvent shifts ($CHCl_3$ = 7.26 ppm), $^{19}$F NMR spectra were referenced with internal standard monofluorobenzene ($C_6H_5F$ = 130.15 ppm), and $^{13}$C NMR spectra were referenced by solvent shifts ($CDCl_3$ = 77.16 ppm).

Gel permeation chromatography (GPC) analyses were carried out using a Waters instrument, (M515 pump, 717+ Autosampler) equipped with a Waters UV486 and Waters 2410 differential refractive index detectors, and three 5 μm PSS SDV columns (Polymer Standards Service; 50 Å, 500 Å, and Linear M porosities) in series. The GPC columns were eluted with chloroform at 40 °C at 1 mL/min and were calibrated with monodisperse polystyrene standards.

Differential scanning calorimetry of polymer samples was performed on a Mettler-Toledo Polymer DSC instrument equipped with liquid nitrogen cooling system and automated sampler. Typical DSC experiments were made in aluminum pans under nitrogen with a heating rate of 10 °C/min from -70 °C to +200 °C. Data was processed using StarE software. Polymers incorporating **9**, **10**, and **13** were difficult to dissolve in chloroform after DSC analysis, suggesting potential crosslinking.

### A1.2 Materials

HPLC grade toluene, tetrahydrofuran, and hexanes were purchased from Fisher Scientific and purified over solvent columns. Dichloromethane and anhydrous ether were used as received from Sigma Aldrich and stored over 3 Å activated molecular sieves. 2-[2-(2-methoxyethoxy)ethoxy]methyl oxirane [i] (**11**) and 2-(oxiran-2-ylmethoxy)tetrahydro-2*H*-pyran) [ii] (**13**) were synthesized according to literature procedures. All other epoxides were obtained from commercial sources. All epoxides were stirred over $CaH_2$ for three days, degassed through 3 freeze-pump-thaw cycles, vacuum transferred under $N_2$, and stored in the glovebox until use. Maleic anhydride (>99% purity, Bartek) was sublimed under dry nitrogen and stored in a glovebox. (BDI)ZnOAc **3**,[iii] aluminum porphyrin **4**,[iv] and cobalt salen **5**,[v] were prepared according to literature procedures. All other reagents were purchased from commercial sources and used as received.

### A1.3 Complex Synthesis

Chromium salen, **6,** was prepared according to a modified literature procedure:[vi] In a glovebox, anhydrous $CrCl_2$ (0.640 g, 5.20 mmol) and N,N'-bis(3,5-di-*tert*-butyl salicylidene)-1,2-cyclohexene diamine ligand[6a] (2.45 g, 4.75 mmol) were added to a flame dried schlenk flask equipped with a stir bar and were diluted with ~50 mL anhydrous THF. The slurry was allowed to stir for at least 3 h under dry $N_2$. After 3 h, the stopper of the flask was removed and replaced with a drying tube charged with a dri-rite agent. The brown solution was allowed to stir for an additional 3 h while oxidizing under dry air. Subsequently, the reaction mixture was diluted with

diethyl ether (100 mL) and washed with saturated ammonium chloride (3 x 100 mL) and brine (3 x 100 mL). The organic layer was collected and dried over anhydrous sodium sulfate, filtered, and evacuated to dryness, yielding a dark brown powder. The powder was rinsed with pentane until the filtrate appeared clear and dried under vacuum at 80 °C. (2.20 g, 74% yield).

### A1.4 Representative Copolymerization Procedure

In a glovebox, 0.020 mmol catalyst and 4.0 mmol anhydride were placed in a flame dried vial equipped with a stir bar. The appropriate solvent (hexanes, 0.50 mL) was added, followed by 4.0 mmol epoxide. The vial was sealed with a Teflon lined cap, removed from the glovebox, and placed in an aluminum heat block preheated to the desired temperature (45 °C). After the reaction became viscous, the vial was removed from the heat block and a small aliquot was removed for $^{1}$H NMR spectrum analysis to determine monomer conversion. The viscous reaction mixture was then dissolved in a minimum amount of dichloromethane and precipitated into an excess of hexanes. This process was repeated (diethyl ether was used as the non-solvent in the case of PPM) until all residual monomer was removed. For epoxide **10**, a 1.0% solution of BHT was added to stabilize the polymer. After polymer washes, the material was collected and dried *in vacuo*.

### A1.5 Representative Isomerization Procedure

For a one-pot procedure, 0.1 equivalent of diethyl amine was added directly to the polymer mixture at the end of the polymerization and the polymer was dissolved in

$CDCl_3$. For a two-step procedure, an isolated polymer sample was dissolved in $CDCl_3$ and 0.1 equivalent of diethyl amine was added. For both procedures, the solution was allowed to stir and isomerization progress was checked by $^1H$ NMR spectroscopy. Upon completion of reaction, all volatiles were removed under vacuum. The polymer was subsequently redissolved in $CH_2Cl_2$ and precipitated into hexanes. The polymers were then dried under vacuum and isomerization completion was confirmed by $^1H$ NMR spectroscopy. Note that one-pot procedures produced polymer with a more narrow polydispersity for PPF than the two-pot (1.2 vs. 1.7 respectively).

**A1.6 Representative Chain Transfer Copolymerization Procedure**

In a glovebox, 0.020 mmol catalyst and 4.0 mmol anhydride were placed in a flame dried vial equipped with a stir bar. The appropriate solvent (hexanes, 0.50 mL) was added, followed by 4.0 mmol epoxide. The vial was sealed with a Teflon lined reactor vial cap, removed from the glovebox, and injected with the appropriate equivalents of iPrOH. The vial was then placed in an aluminum heat block preheated to the desired temperature (45 °C). After the reaction became viscous, the vial was removed from the heat block, quenched with 0.1 mL glacial AcOH and a small aliquot was removed for $^1H$ NMR spectroscopy analysis to determine monomer conversion. The viscous reaction mixture was then dissolved in a minimum amount of $CH_2Cl_2$ and precipitated into an excess of hexanes. This process was repeated until all residual monomer was removed.

## A1.7 NMR Spectra and Peak Assignments for Maleate Containing Polyesters ($CDCl_3$)

All polymers were prepared following the representative copolymerization procedure. A center spike artifact appears at 110 ppm in several $^{13}C$ NMR spectra. Multiple signals may be reported for the same carbon due to the regioirregularity.

Poly(propylene maleate), (Table 2.1, entry 8). $^{1}H$ NMR spectrum ($CDCl_3$, 400 MHz): δ 6.29-6.24 (m, 2H); 5.28-5.22 (m, 2H); 4.31-4.19 (m, 1H); 1.32 (d, $J$ = 6.8 Hz, 3H). $^{13}C$ NMR spectrum ($CDCl_3$, 100 MHz): δ 164.68, 164.39; 130.44, 130.39, 129.93, 129.79, 129.33, 129.29; 69.10; 66.37; 16.19.

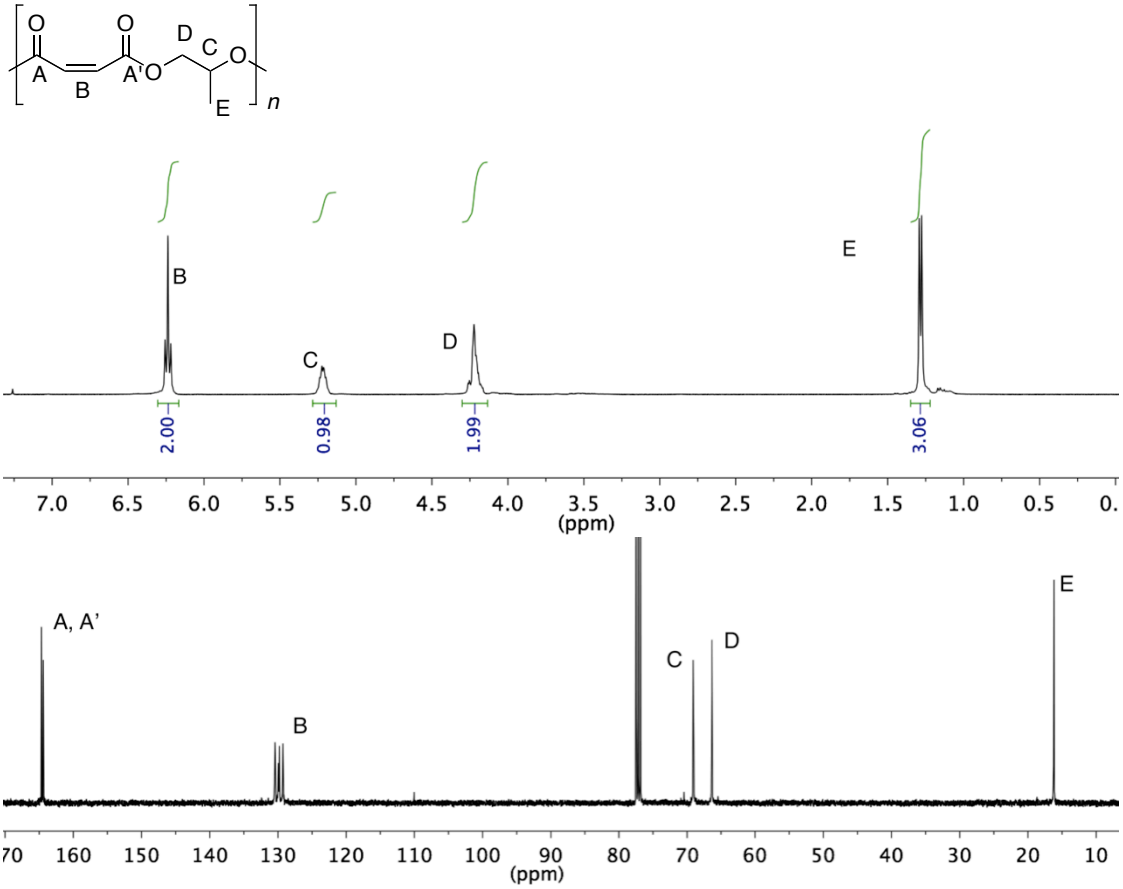


**Figure A1.1.** Poly(propylene maleate), Table 1, in $CDCl_3$. Top: $^{1}H$ NMR spectrum. Bottom: $^{13}C$ NMR spectrum.

Poly(1-butene-*alt*-maleate), (Table 2.2, entry 1). $^{1}$H NMR spectrum ($CDCl_3$, 400 MHz): δ 6.27-6.23 (m, 2H); 5.15-5.07 (m, 1H); 4.35-4.18 (m, 2H); 1.72-1.64 (m, 2H); 0.94 (t, $J$ = 7.3 Hz, 3H). $^{13}$C NMR spectrum ($CDCl_3$, 100 MHz): δ 164.87, 164.70; 130.17, 129.86, 129.45 (bm); 73.56, 73.49; 64.84, 64.94; 23.72; 9.53.

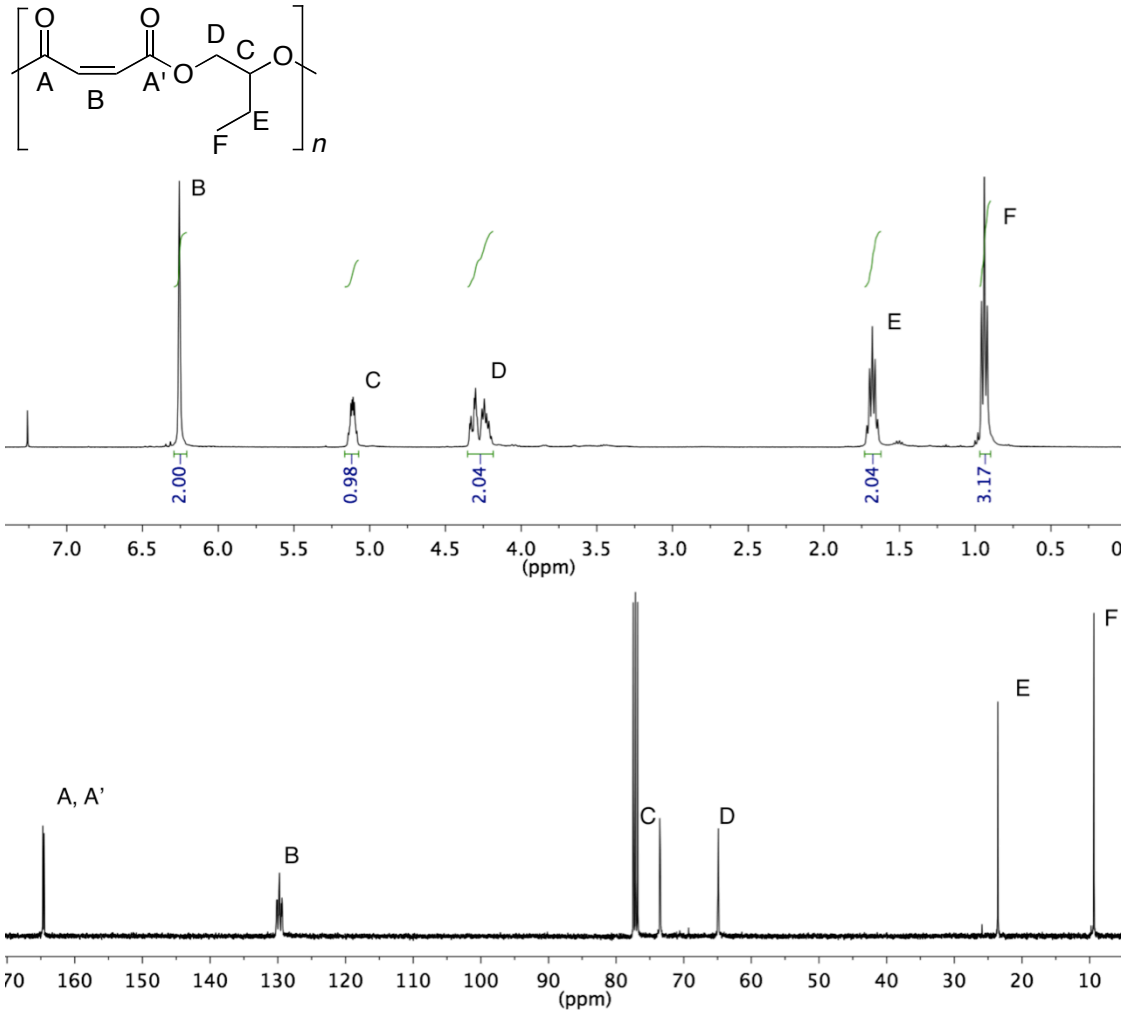


**Figure A1.2.** Poly(1-butene-*alt*-maleate) in $CDCl_3$. Top: $^{1}$H NMR spectrum. Bottom: $^{13}$C NMR spectrum.

Poly(3-chloroprop-1-ene-*alt*-maleate), (Table 2.2, entry 2). $^{1}$H NMR spectrum ($CDCl_3$, 400 MHz): δ 6.35-6.29 (m, 2H); 5.37-5.31 (m, 1H); 4.50-4.38 (m, 2H); 3.73 (d, $J$ = 5.5 Hz, 2H). $^{13}$C NMR spectrum ($CDCl_3$, 100 MHz): δ 164.41, 164.12; 130.02, 129.87; 71.07; 62.87; 41.78.

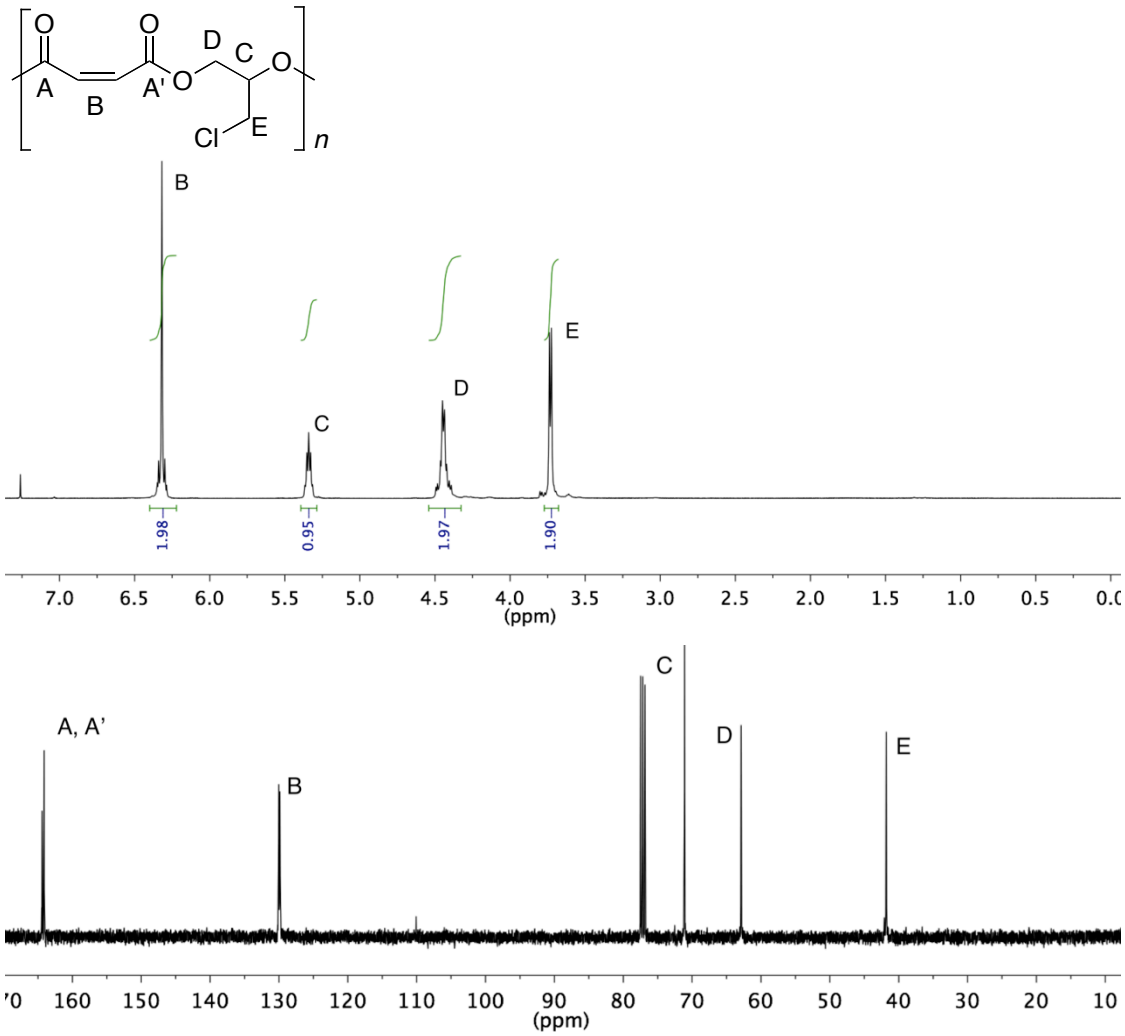


**Figure A1.3.** Poly(3-chloroprop-1-ene-*alt*-maleate) in $CDCl_3$. Top: $^{1}$H NMR spectrum. Bottom: $^{13}$C NMR spectrum.

Poly(3-(allyloxy)prop-1-ene-*alt*-maleate), (Table 2.2, entry 3). $^{1}$H NMR spectrum ($CDCl_3$, 400 MHz): δ 6.31-6.23 (m, 2H); 5.84 (ddt, *J* = 16.3, 10.6, 5.3 Hz, 1H); 5.33-5.27 (m, 1H); 5.25 (dd, *J* = 17.6, 1.0 Hz, 1H); 5.17 (dd, *J* = 10.0, 1.0 Hz, 1H); 4.47-4.33 (m, 2H); 4.04-3.93 (m, 2H); 3.67-3.53 (m, 2H). $^{13}$C NMR spectrum ($CDCl_3$, 100 MHz): δ 164.68, 164.48; 134.26; 130.26, 129.69; 117.59; 72.40; 71.13; 67.82; 63.43. *Trace BHT and hexanes are present in spectra. Assignments confirmed by HMBC and HSQC spectra.

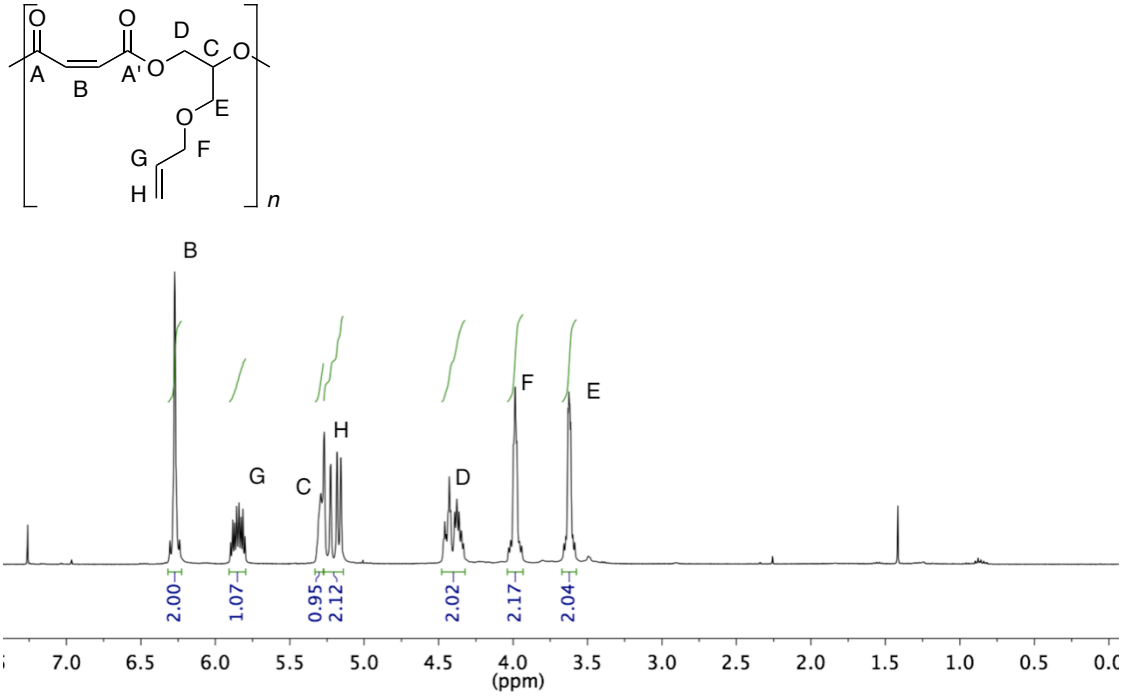

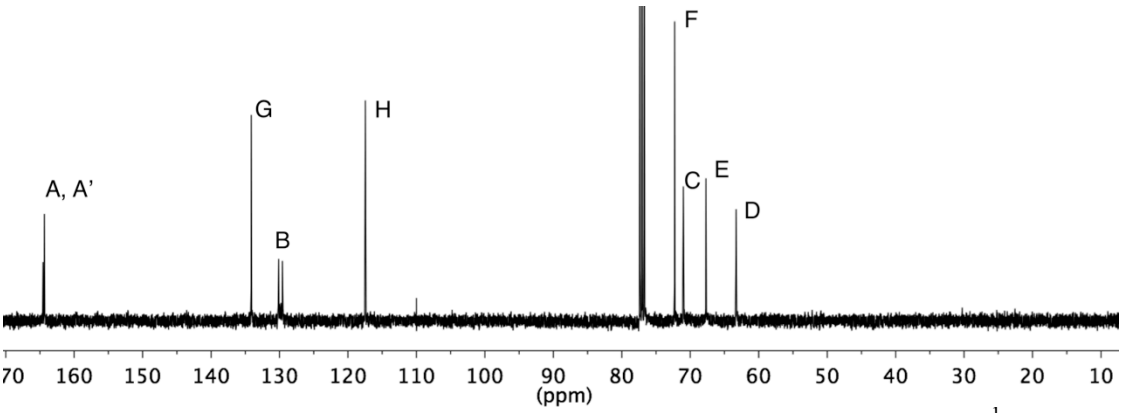


**Figure A1.4.** Poly(3-(allyloxy)prop-1-ene-*alt*-maleate) in $CDCl_3$. Top: $^{1}H$ NMR spectrum. Bottom: $^{13}C$ NMR spectrum.

Poly(3-[2-(2-methoxyethoxy)ethoxy]prop-1-ene-*alt*-maleate), (Table 2.2, entry 4). $^{1}$H NMR spectrum ($CDCl_3$, 400 MHz): δ 6.30-6.23 (m, 2H); 5.33-5.26 (m, 2H); 4.47-4.32 (m, 2H); 3.71-3.49 (m, 10H); 3.34 (s, 3H). $^{13}$C NMR spectrum ($CDCl_3$, 100 MHz): δ 164.62, 164.43; 130.30, 129.65; 71.95; 71.01 (2C); 70.60; 70.52; 68.97; 63.38; 59.08.

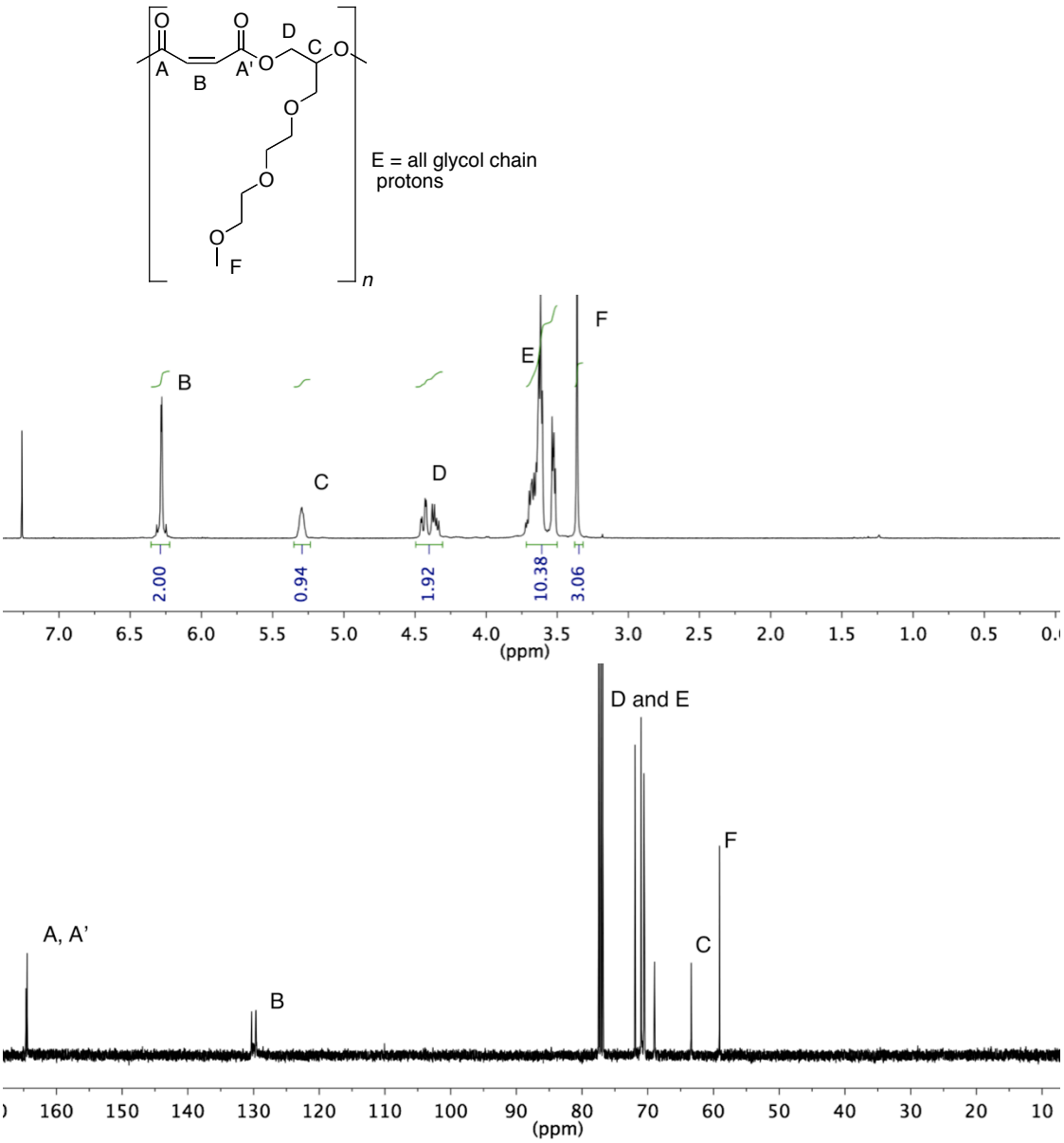


**Figure A1.5.** Poly(3-[2-(2-methoxyethoxy)ethoxy]prop-1-ene-*alt*-maleate) in $CDCl_3$. Top: $^{1}$H NMR spectrum. Bottom: $^{13}$C NMR spectrum.

Poly(4,4,5,5,6,7,7,7-octafluoro-6-(trifluoromethyl)hept-1-ene-*alt*-maleate), (Table 2.2, entry 5). $^{1}$H NMR spectrum ($CDCl_3$, 400 MHz): δ 6.32-6.24 (m, 2H); 5.63-5.52 (m, 1H); 4.48-4.22 (m, 2H); 2.67-2.39 (m, 2H). $^{19}$F NMR spectrum ($CDCl_3$, 376 MHz): δ -72.58 (6F); -113.54 (m, 2F); -116.68 (2F); -186.42 (1F). $^{13}$C NMR spectrum ($CDCl_3$, 150 MHz): δ 164.45, 163.74; 130.55-129.27 (m); 121.9-115.8 (qd, $J$ = 291, 26 Hz); 119.54-115.56 (tt, $J$ = 258, 33 Hz); 114.55-110.15 (ttd, $J$ = 268, 36, 26 Hz); 91.31-88.79 (m); 64.78 (m); 65.69; 31.98 (t, $J$ = 21 Hz).

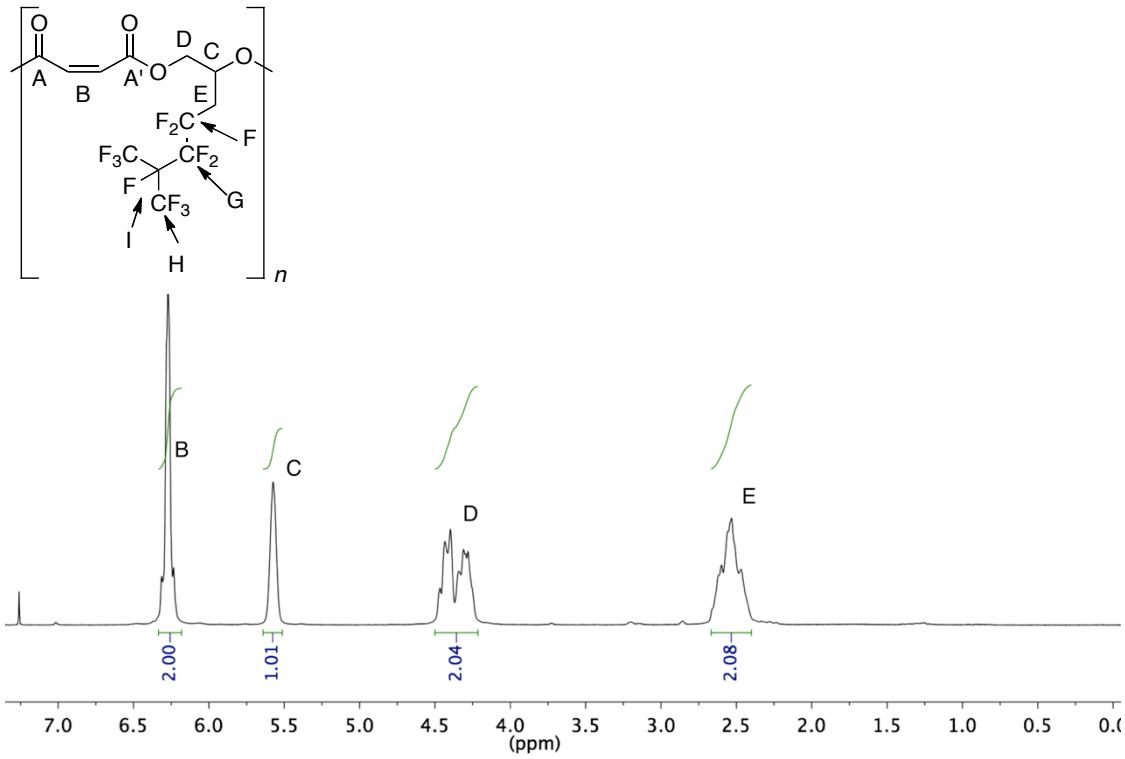

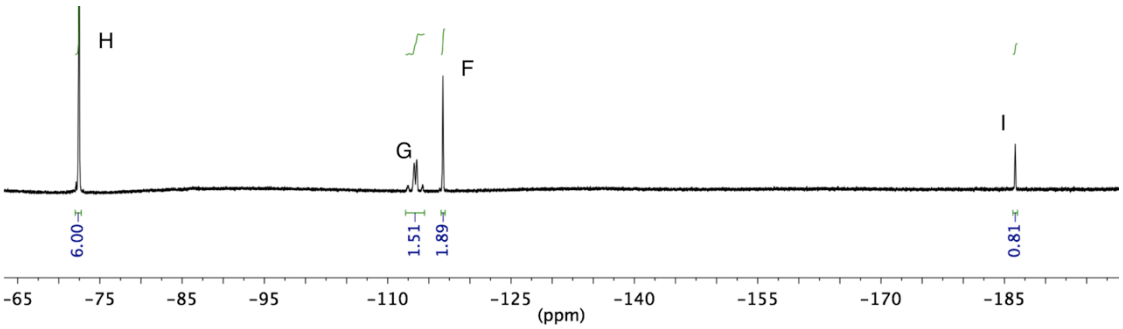


**Figure A1.6.** Poly(4,4,5,5,6,7,7,7-octafluoro-6-(trifluoromethyl)hept-1-ene-*alt*-maleate) in $CDCl_3$. Top: $^{1}H$ NMR spectrum. Bottom: $^{19}F$ NMR spectrum.

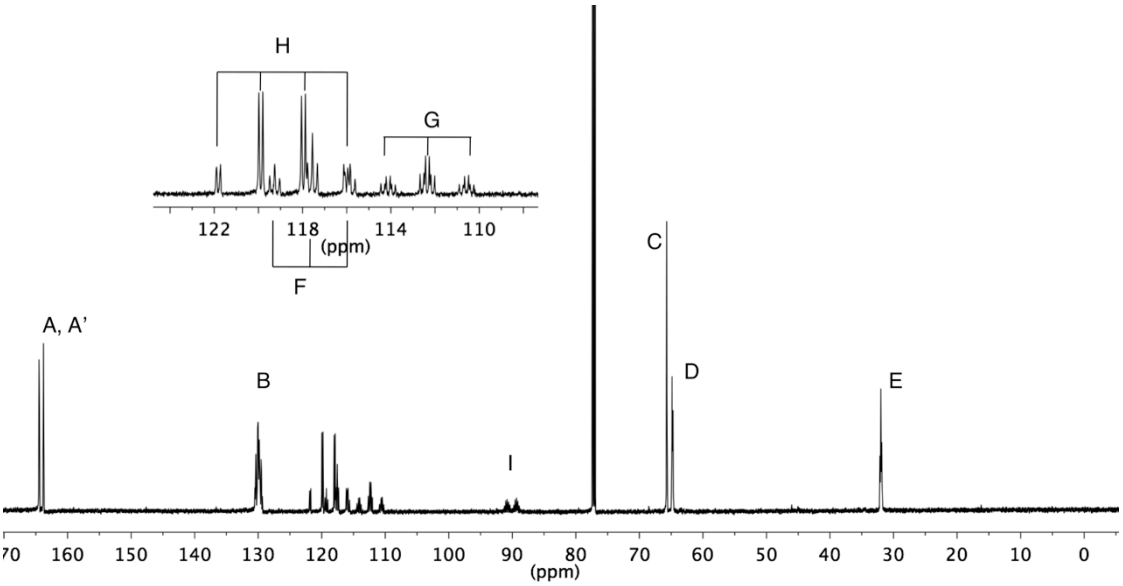


**Figure A1.7.** Poly(4,4,5,5,6,7,7,7-octafluoro-6-(trifluoromethyl)hept-1-ene-*alt*-maleate) in $CDCl_3$. $^{13}C$ NMR spectrum.

Poly([2-(allyloxy)tetrahydro-2*H*-pyran]-*alt*-maleate), (Table 2.2, entry 6). $^{1}$H NMR spectrum ($CDCl_3$, 400 MHz): δ 6.27-6.20 (m, 2H); 5.33-5.27 (m, 1H); 4.58-4.53 (m, 1H); 4.46-4.28 (m, 2H); 3.87-3.78 (td, $J$ = 11.4, 5.3 Hz, 1H); 3.77-3.70 (t, $J$ = 9.4 Hz, 1H); 3.60-3.54 (dd, $J$ = 10.9, 4.38 Hz, 1H); 3.48-3.40 (m, 1H); 1.79-1.40 (m, 6H). $^{13}$C NMR spectrum ($CDCl_3$, 100 MHz): δ 164.51, 164.27; 130.15, 129.51; 98.73; 71.04; 65.01; 63.29; 61.86; 30.19; 25.25; 19.00. Assignments confirmed by HMBC and HSQC spectra.

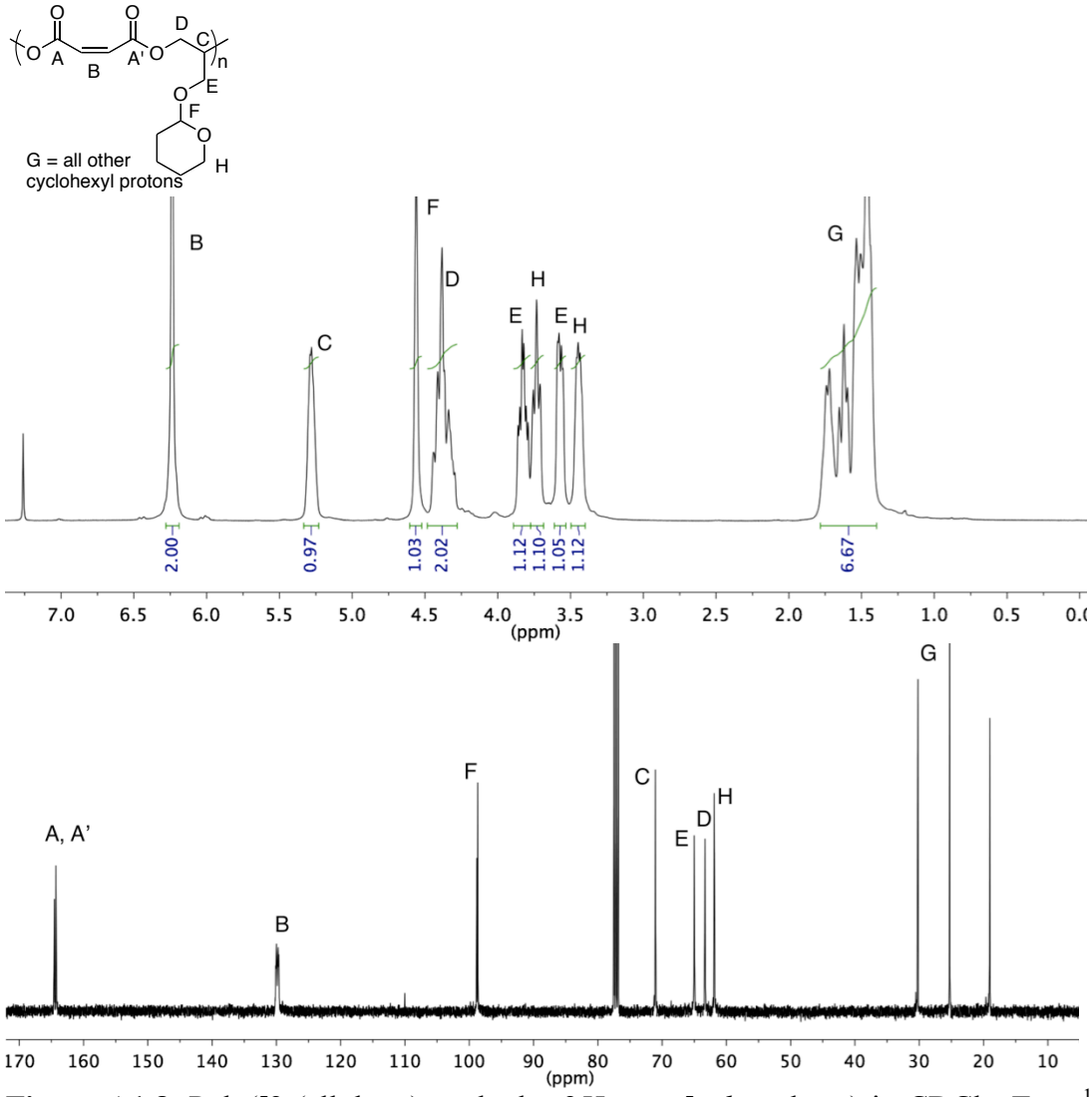


**Figure A1.8.** Poly([2-(allyloxy)tetrahydro-2*H*-pyran]-*alt*-maleate) in $CDCl_3$. Top: $^{1}$H NMR spectrum. Bottom: $^{13}$C NMR spectrum.

Poly([allyloxy]benzene-*alt*-maleate), (Table 2.2, entry 7). $^{1}$H NMR spectrum ($CDCl_3$, 400 MHz): δ 7.24 (t, *J* = 7.9 Hz, 2H); 6.92 (t, *J* = 7.9 Hz, 1H); 6.87 (d, *J* = 7.9 Hz, 2H); 6.27-6.20 (m, 2H); 5.45-5.40 (m, 1H); 4.51-4.40 (m, 2H); 4.10 (d, *J* = 4.9 Hz, 2H). $^{13}$C NMR spectrum ($CDCl_3$, 100 MHz): δ 164.52, 164.30; 158.09; 129.93, 129.75; 129.51; 121.33; 114.51; 70.39; 65.44; 62.91. Assignments confirmed by HMBC and HSQC spectra.

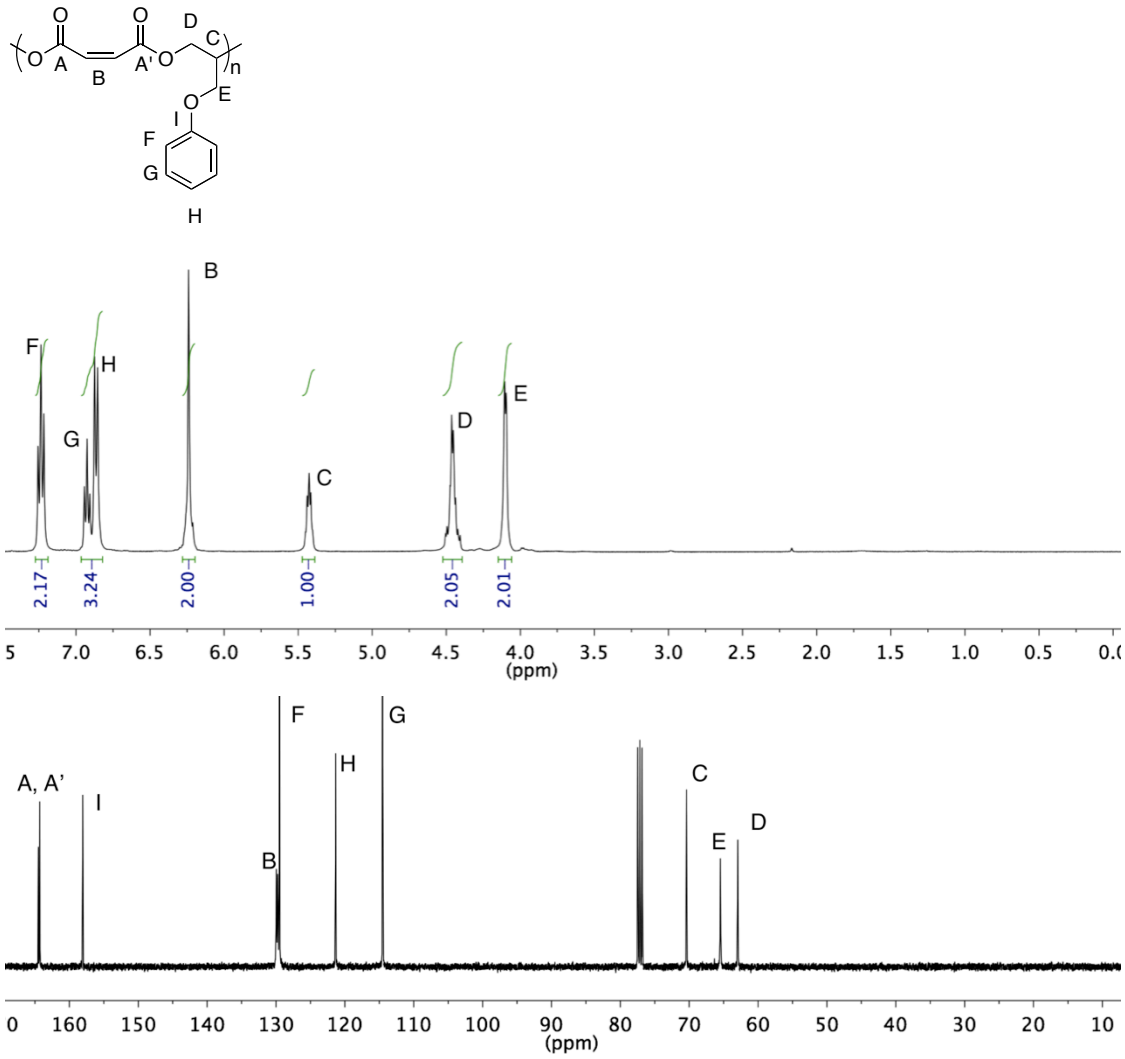


**Figure A1.9.** Poly([allyloxy]benzene-*alt*-maleate) in $CDCl_3$. Top: $^{1}$H NMR spectrum. Bottom: $^{13}$C NMR spectrum.

### A1.8 NMR Spectra and Peaks Assignments for Fumarate Polyesters ($CDCl_3$)

The fumarate forms of the polymers were formed *via* isomerization procedure.

Poly(propylene fumarate), (Figure 2.1). $^{1}H$ NMR spectrum ($CDCl_3$, 400 MHz): δ 6.87-6.80 (m, 2H); 5.31-5.24 (m, 1H); 4.36-4.20 (m, 2H); 1.33 (d, $J$ = 6.8 Hz, 3H). $^{13}C$ NMR spectrum ($CDCl_3$, 100 MHz): δ 164.50, 164.44, 164.18, 164.13; 134.13, 133.90, 133.65, 133.40; 69.37; 66.69; 16.46.

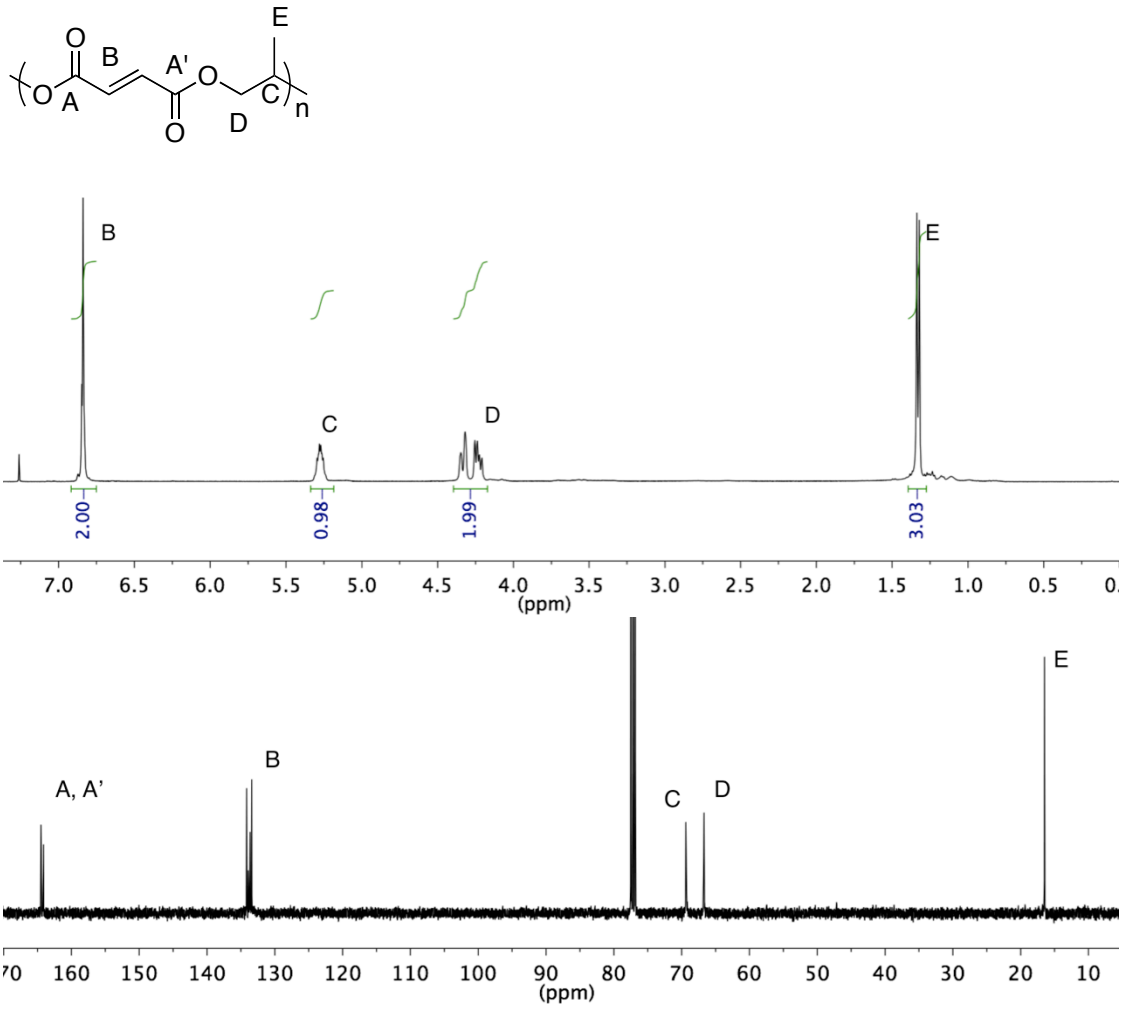


**Figure A1.10.** Poly(propylene fumarate), in $CDCl_3$. Top: $^{1}$ H NMR spectrum. Bottom: $^{13}C$ NMR spectrum.

Poly(1-butene-*alt*-fumarate). $^{1}$H NMR spectrum ($CDCl_3$, 400 MHz): δ 6.88-6.81 (m, 2H); 5.19-5.11 (m, 1H); 4.41-4.19 (m, 2H); 1.75-1.65 (m, 2H); 0.94 (t, $J$ = 7.3 Hz, 3H). $^{13}$C NMR spectrum ($CDCl_3$, 100 MHz): 164.54, 164.48, 164.40, 164.33; 134.05, 133.86, 133.62, 133.42; 73.87, 73.76; 65.41; 23.83; 9.54.

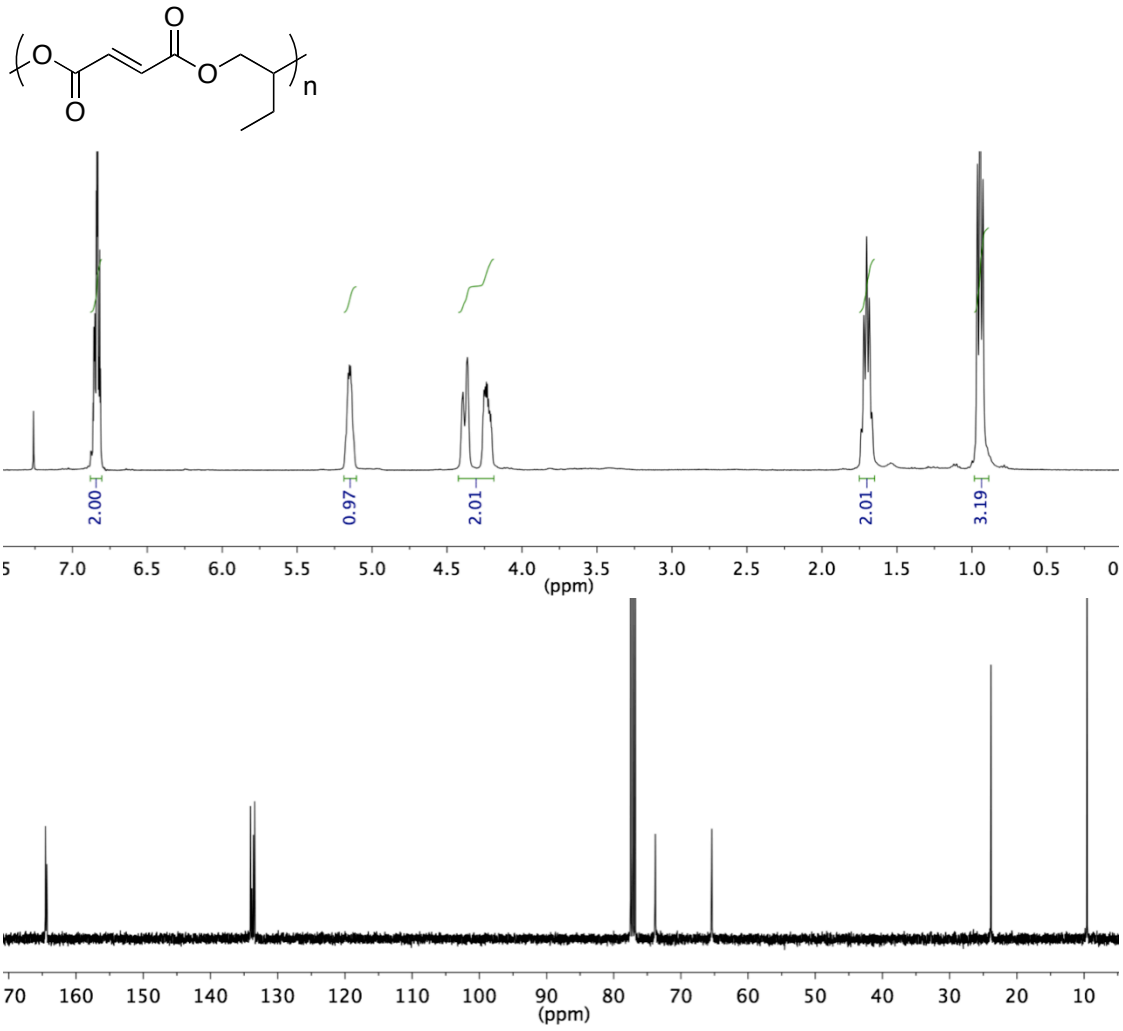


**Figure A1.11.** Poly(1-butene-*alt*-fumarate) in $CDCl_3$. Top: $^{1}$H NMR spectrum. Bottom: $^{13}$C NMR spectrum.

Poly(3-chloroprop-1-ene-*alt*-fumarate). $^{1}$H NMR spectrum ($CDCl_3$, 400 MHz): δ 6.94-6.84 (m, 2H); 5.41-5.35 (m, 1H); 4.57-4.40 (m, 2H); 3.75, 3.74 (d, $J$ = 5.5 Hz, 2H). $^{13}$C NMR spectrum ($CDCl_3$, 100 MHz): δ 164.04, 163.66; 133.94, 133.56; 71.43; 63.29; 41.84. *Note: Trace ethanol and acetone from the solvent are present.

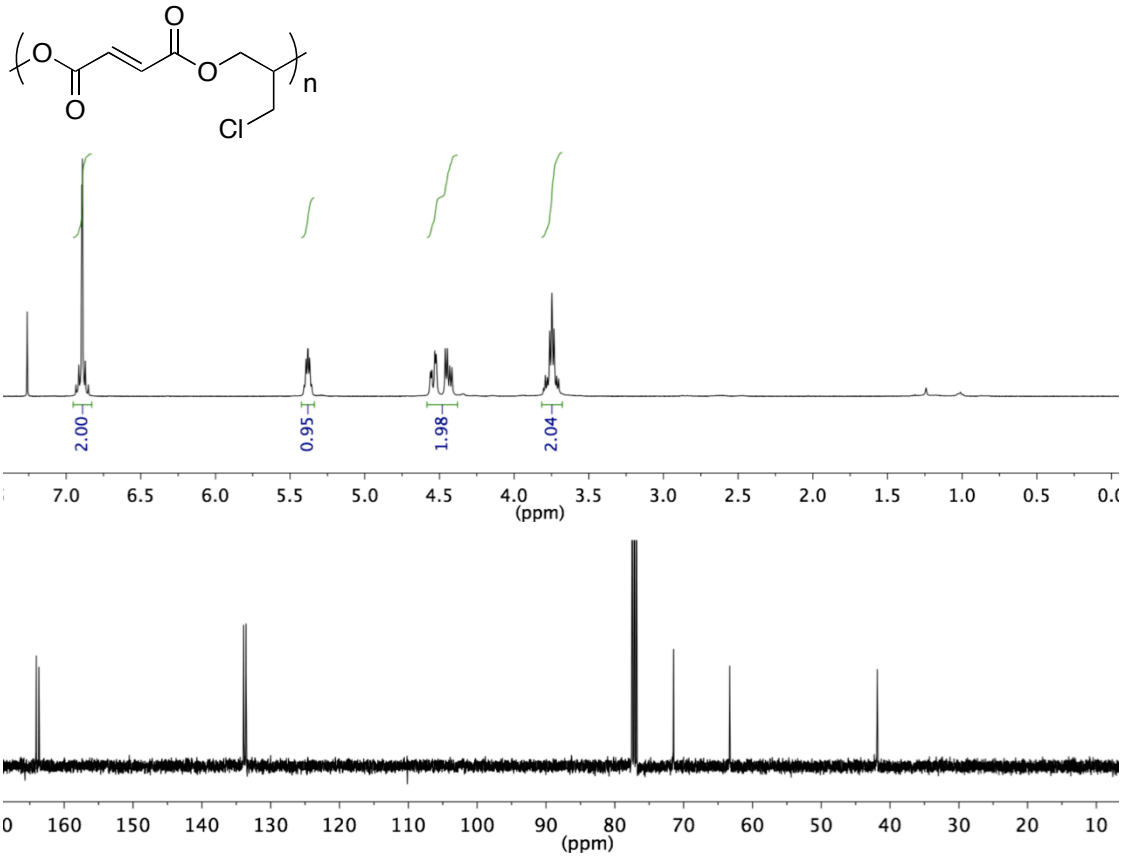


**Figure A1.12.** Poly(3-chloroprop-1-ene-*alt*-fumarate) in $CDCl_3$. Top: $^{1}$H NMR spectrum. Bottom: $^{13}$C NMR spectrum.

Poly(3-(allyloxy)prop-1-ene-*alt*-fumarate). $^{1}$H NMR spectrum ($CDCl_3$, 400 MHz): δ 6.90-6.83 (m, 2H); 5.85 (ddt, $J$ = 16.3, 10.6, 5.3 Hz, 1H); 5.37-5.30 (m, 1H); 5.26 (dd, $J$ = 17.12, 1 Hz, 1H); 5.20 (dd, $J$ = 10, 1 Hz, 1H); 4.54-4.34 (m, 2H); 4.05-3.95 (m, 2H); 3.63 (d, $J$ = 5.21 Hz, 2H). $^{13}$C NMR spectrum ($CDCl_3$, 100 MHz): δ 164.38, 164.09; 134.07; 133.83, 133.75; 117.87; 72.51; 71.38; 67.89; 63.66. *Note: Trace hexanes and BHT are seen in the spectra.

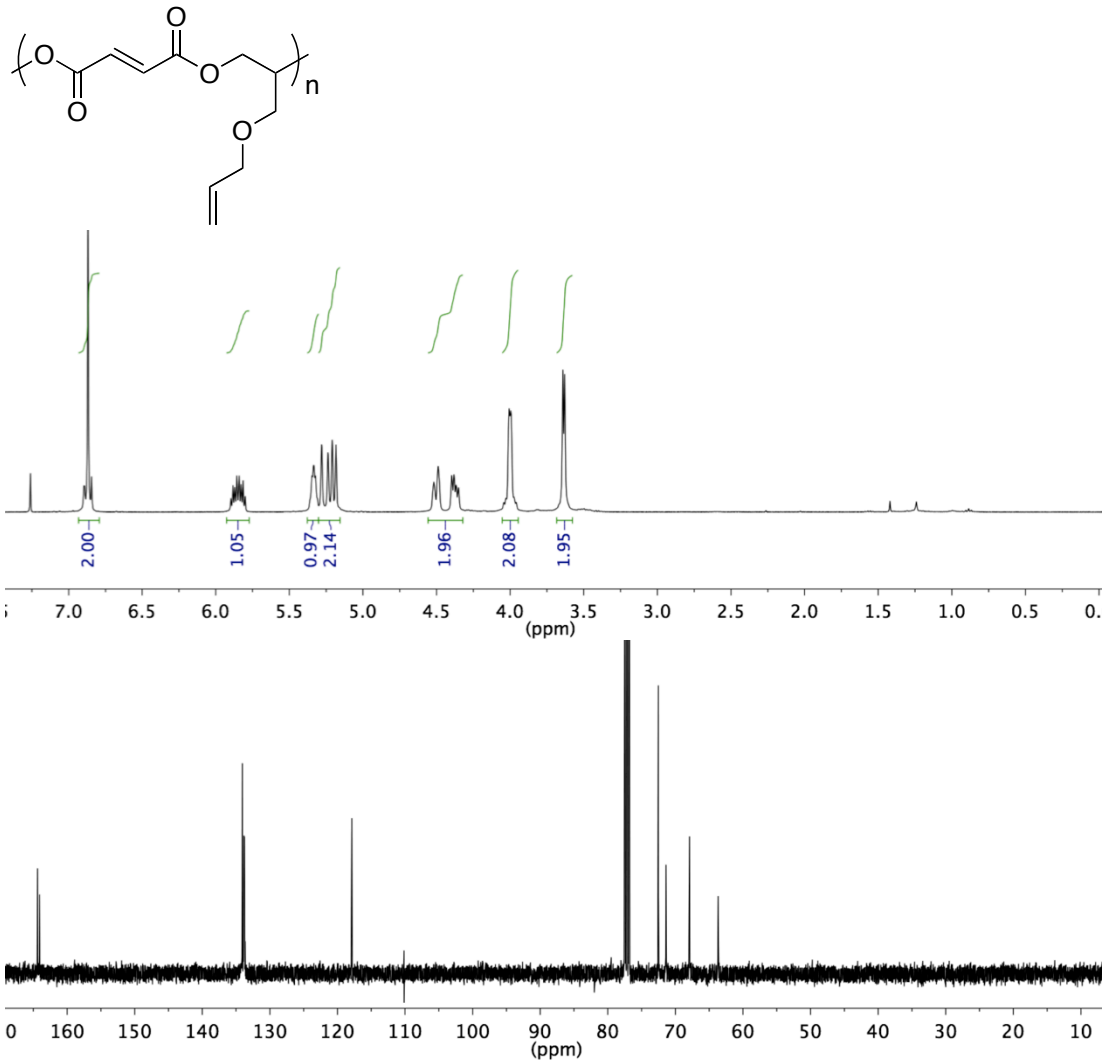


**Figure A1.13.** Poly(3-(allyloxy)prop1-ene-*alt*-fumarate) in $CDCl_3$. Top: $^{1}$H NMR spectrum. Bottom: $^{13}$C NMR spectrum.

Poly(3-[2-(2-methoxyethoxy)ethoxy]prop-1-ene-*alt*-fumarate). $^{1}$H NMR spectrum ($CDCl_3$, 400 MHz): δ 6.88-6.83 (m, 2H); 5.35-5.29 (m, 1H); 4.52-4.31 (m, 2H); 3.71-3.50 (m, 10H); 3.35 (s, 3H). $^{13}$C NMR spectrum ($CDCl_3$, 100 MHz): δ 164.35, 164.04; 133.81, 133.70; 71.99; 71.33; 71.15; 70.70; 70.64; 69.21; 63.63; 59.13.

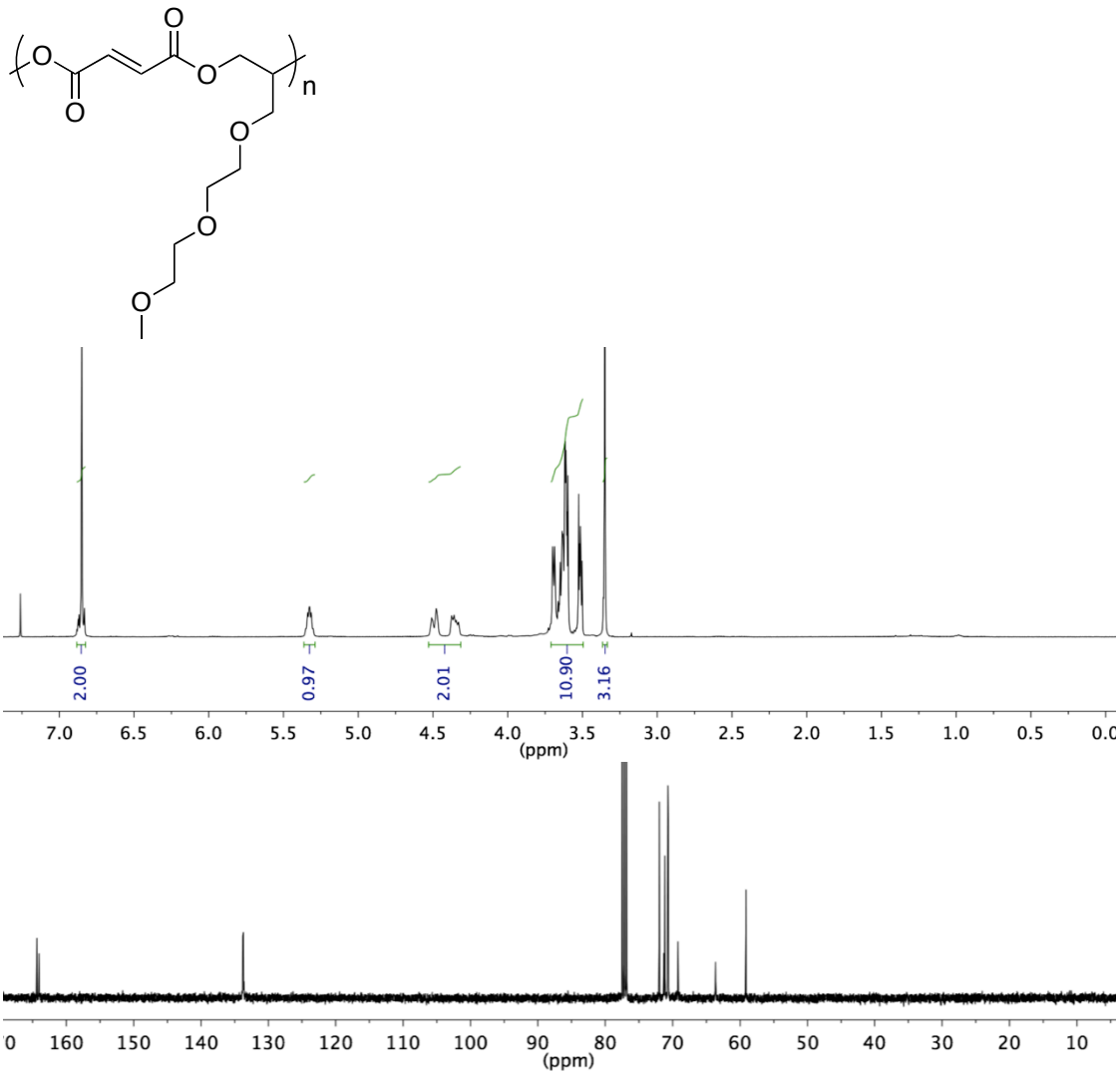


**Figure A1.14.** Poly(3-[2-(2-methoxyethoxy)ethoxy]prop-1-ene-*alt*-fumarate) in $CDCl_3$. Top: $^{1}$H NMR spectrum. Bottom: $^{13}$C NMR spectrum.

Poly(4,4,5,5,6,7,7,7-octafluoro-6-(trifluoromethyl)hept-1-ene-*alt*-fumarate). $^{1}$H NMR spectrum ($CDCl_3$, 400 MHz): δ 6.95-6.82 (m, 2H); 5.74-5.62 (m, 1H); 4.61-4.27 (m, 2H); 2.73-2.43 (m, 2H). $^{13}$C NMR spectrum ($CDCl_3$, 125 MHz): δ 164.00, 163.97, 163.33, 163.30; 133.73, 133.60; 122.58-115.20 (qd, $J$ = 291, 26 Hz); 119.74-115.01 (tt, $J$ = 258, 33 Hz); 115.01-109.56 (ttd, $J$ = 268, 36, 26 Hz); 91.53-88.51 (m); 65.88; 65.18; 32.24 (t, $J$ = 21 Hz). *Note: Trace pentane is present in the $^{1}$H and $^{13}$C NMR spectra.

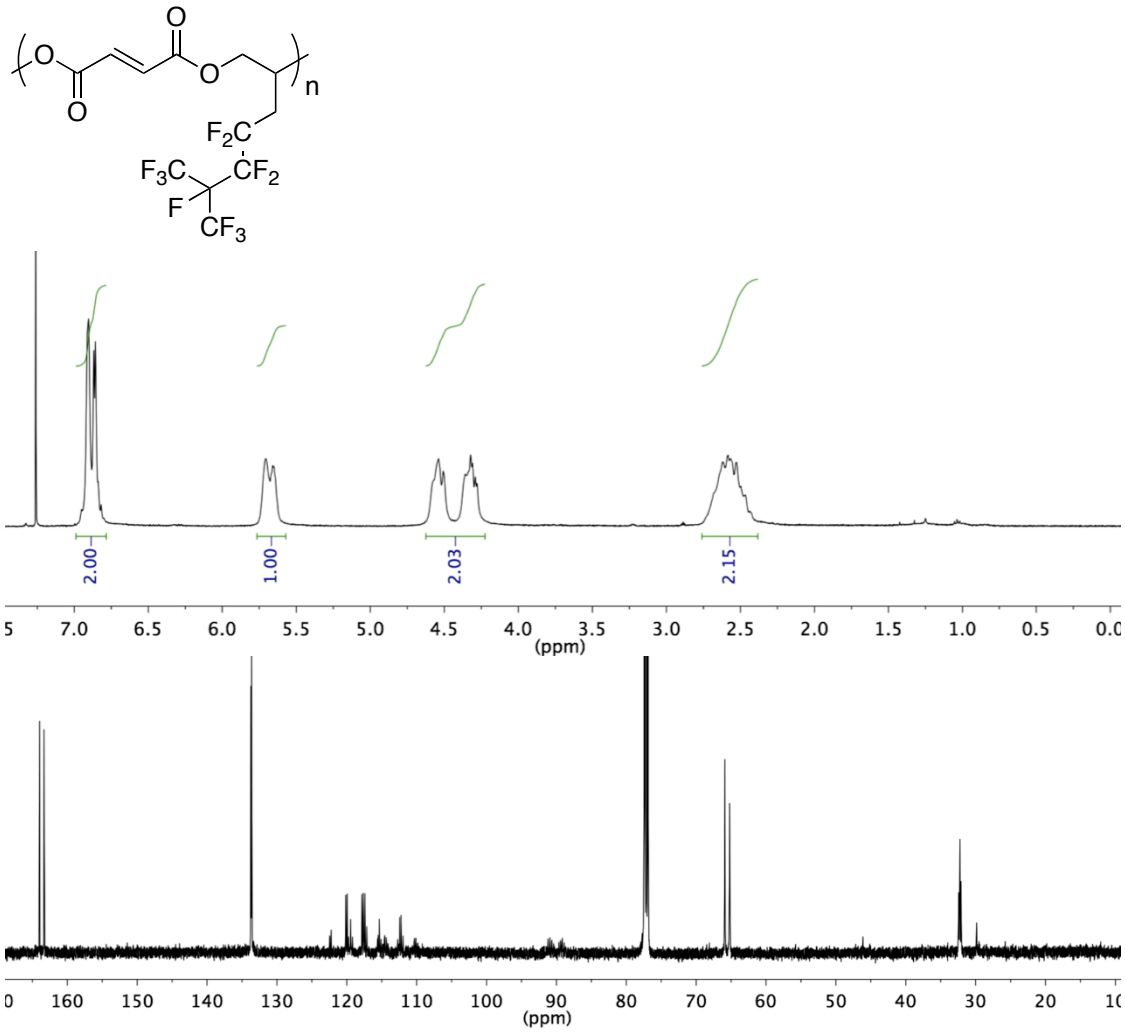


**Figure A1.15.** Poly(4,4,5,5,6,7,7,7-octafluoro-6-(trifluoromethyl)hept-1-ene-*alt*-fumarate) in $CDCl_3$. Top: $^{1}$H NMR spectrum. Bottom: $^{13}$C NMR spectrum.

Poly(2-(allyloxy)tetrahydro-2*H*-pyran)-*alt*-fumarate). $^{1}$H NMR spectrum ($CDCl_3$, 400 MHz): δ 6.90-6.84 (m, 2H); 5.40-5.31 (m, 1H); 4.61-4.58 (m, 1H); 4.54-4.34 (m, 2H); 3.91-3.84 (m, 1H); 3.80-3.71 (m, 1H); 3.64-3.56 (m, 1H); 3.51-3.43 (m, 1H); 1.79-1.43 (m, 6H). $^{13}$C NMR spectrum ($CDCl_3$, 125 MHz): δ 164.37, 164.02; 133.84, 133.67; 99.06, 98.82; 71.47, 71.35; 65.20; 63.66; 62.15; 30.34; 25.33; 19.16. Note, diastereomer peaks are reported in the $^{13}$C NMR spectrum due to THP.

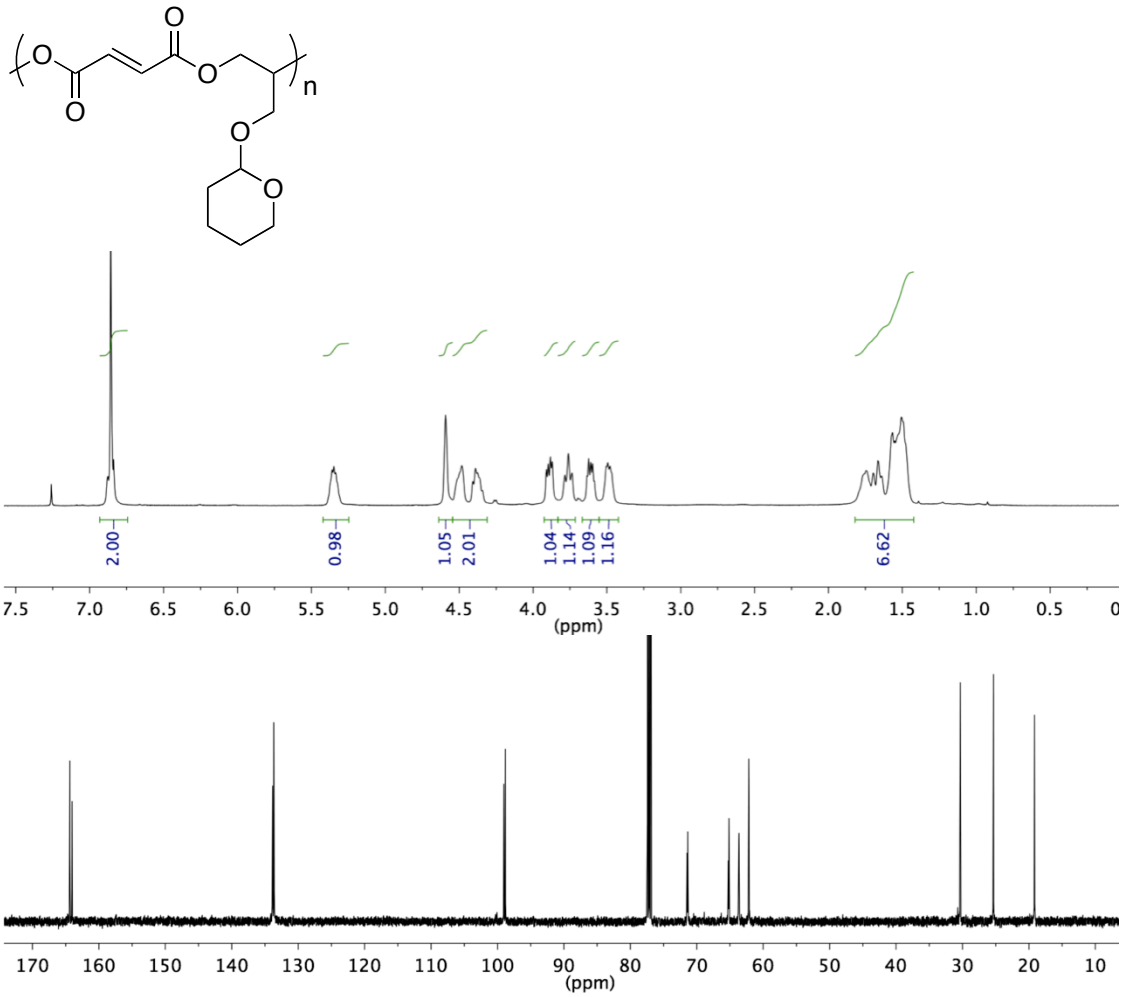


**Figure A1.16.** Poly(2-(allyloxy)tetrahydro-2*H*-pyran)-*alt*-fumarate in $CDCl_3$. Top: $^{1}$H NMR spectrum. Bottom: $^{13}$C NMR spectrum.

Poly([allyloxy]benzene-*alt*-fumarate). $^{1}$H NMR spectrum ($CDCl_3$, 400 MHz): δ 7.28 (t, *J* = 7.9 Hz, 2H); 6.97 (t, *J* = 7.9 Hz, 1H); 6.89 (d, *J* = 7.9 Hz, 2H); 6.89-6.85 (m, 2H); 5.55-5.48 (m, 1H); 4.63-4.46 (m, 2H); 4.18 (d, *J* = 4.9 Hz, 2H). $^{13}$C NMR spectrum ($CDCl_3$, 100 MHz): δ 164.26, 163.97; 158.09; 133.84, 133.71; 129.74; 121.71; 114.69; 70.80; 65.75; 63.38.

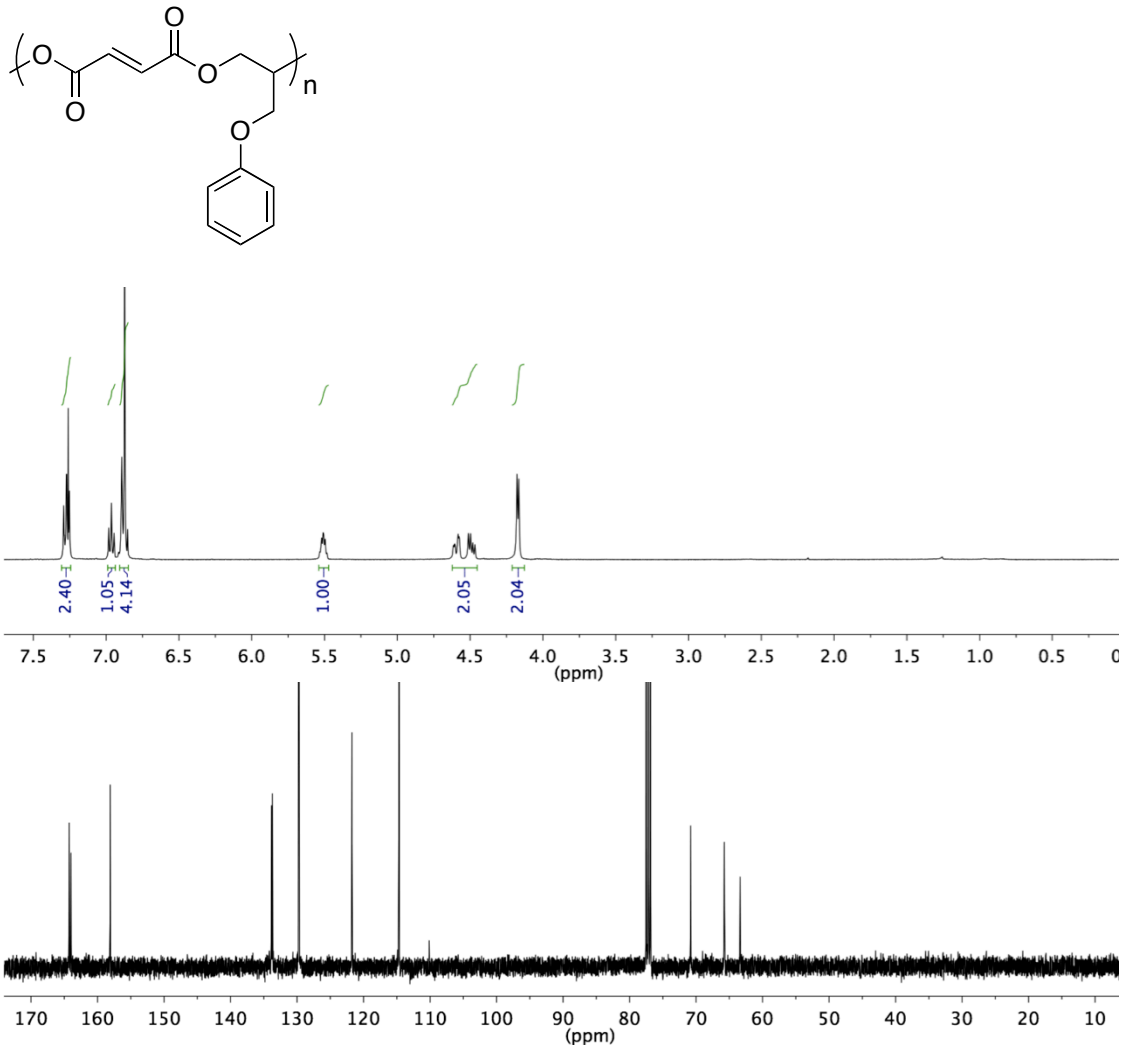


**Figure A1.17.** Poly([allyloxy]benzene-*alt*-fumarate) in $CDCl_3$. Top: $^{1}$H NMR spectrum. Bottom: $^{13}$C NMR spectrum.

### A1.9 Analysis of Hydrogenated PPM and PPF

To ensure that the PPM and PPF polymers were isomers of one another without additional side reactions, the resulting polymers were hydrogenated and characterized. The polymers were hydrogenated using (1,5-Cyclooctadiene)(pyridine)(tricyclohexylphosphine)-iridium(I)hexafluorophosphate) (Crabtree's catalyst) in $CH_2Cl_2$ under 800 psi $H_2$ for 13 h at 23 °C to yield identical polymers as determined by $^1H$ and $^{13}C$ NMR spectroscopy (Figure A1.18).

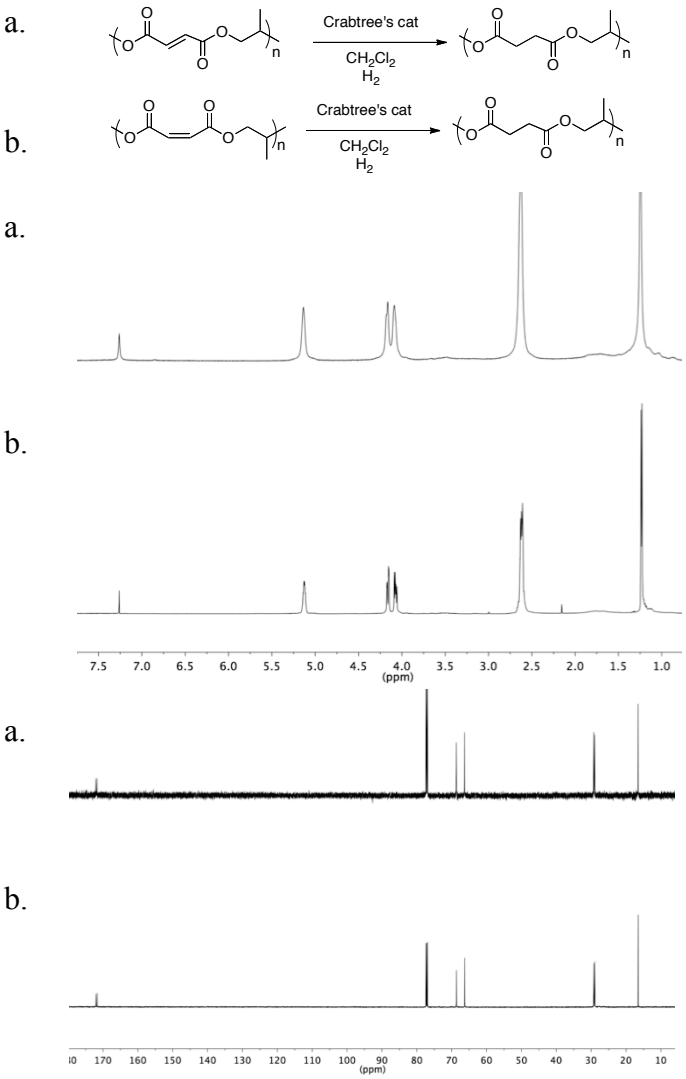


**Figure A1.18.** $^1H$ NMR spectra (top) and $^{13}C$ spectra (bottom) of hydrogenated (a) PPF and (b) PPM.

### A1.10 Analysis of $^{1}$H NMR Spectroscopy of cis-alkene in PPM ($CDCl_3$)

The *cis*-alkene region of the $^{1}$H NMR spectrum of PPM was analyzed in detail. The alkene peaks in the $^{1}$H NMR spectrum of PPM appear in a pattern similar to a 1:3:1 "triplet" (Figure A1.19), that experiments showed is actually due to a mixture of regioisomers.

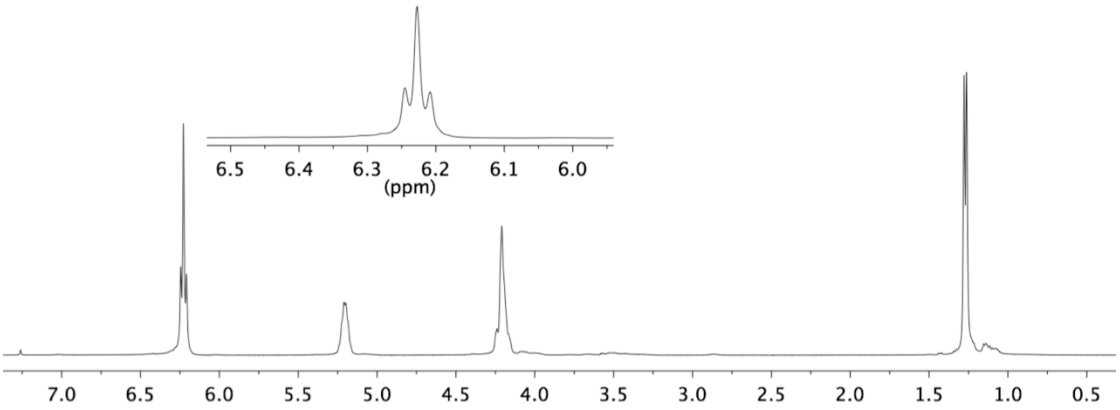


**Figure A1.19.** $^{1}$H NMR spectrum of PPM featuring an inset of the peaks in the alkene region.

We first investigated whether the multiple alkene peaks are a result of the stereochemistry introduced to the polymer chain from the chiral PO units. To explore the influence of stereochemistry, a PPM analogue was synthesized using *S*-PO instead of the *rac*-PO. The $^{1}$H NMR spectra of the two polymers appear identical (Figure A1.20). The $^{13}$C NMR shows differences in the intensities of some peaks, particularly in the alkene region. Notably, the two outer groups of peaks of the four present in the $^{13}$C alkene region (~130 ppm) (c.) increase in intensity. While stereochemistry changed some peak intensities, the number of resonances does not change.

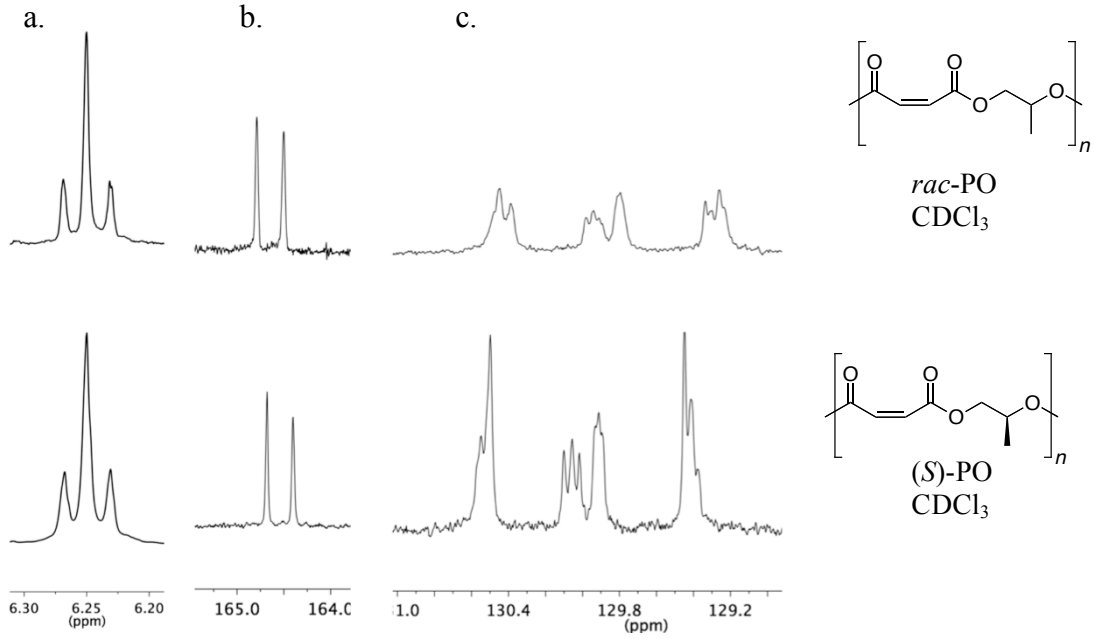


**Figure A1.20.** a. Alkene region of the $^{1}$H NMR spectrum of *rac*-PPM (top) and *S*-PPM (bottom). b. Carbonyl region and c. alkene region of the $^{13}$C NMR spectrum of *rac*-PPM (top) and *S*-PPM (bottom).

Next the regiochemistry of the polymer chain was considered. Four distinct proton environments are possible due to tail-to-tail (T,T), tail-to-head (T,H), and head-to-head (H,H) arrangements of the PO units (Figure A1.21).

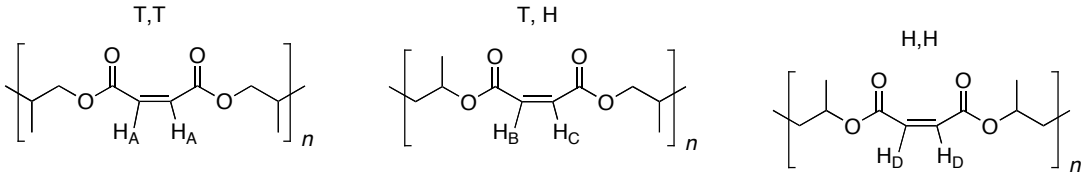


**Figure A1.21.** Possible polymer regioisomers due to different regiochemistry of insertion of PO into the growing polymer chain.

The four alkene signals in the $^{13}C$ NMR spectrum of PPM supports the presence of the three regioisomers proposed above. Each carbon attached to a proton of a different letter would have a different signal, thus we could expect to see: $C_A$, $C_B$, $C_C$, and $C_D$. Analysis of a gbsHMBC spectrum ($CDCl_3$, 600 $^1H$ NMR) optimized for the carbonyl region of the polymer suggests two distinct carbonyl carbons, one adjacent to a methine and one adjacent to a methylene (Figure A1.22). The carbonyl carbons are clearly influenced by the 3J coupling of the adjacent methine/methylene carbons, however, are unable to distinguish differences from the adjacent alkene. Thus we can assign the top carbonyl peak in Figure A1.22 as $CO_A$, $CO_B$, or $CO_C$ (where $CO_A$ = carbonyl next to $H_A$) and the bottom carbonyl peak as $CO_D$, $CO_B$, or $CO_C$.

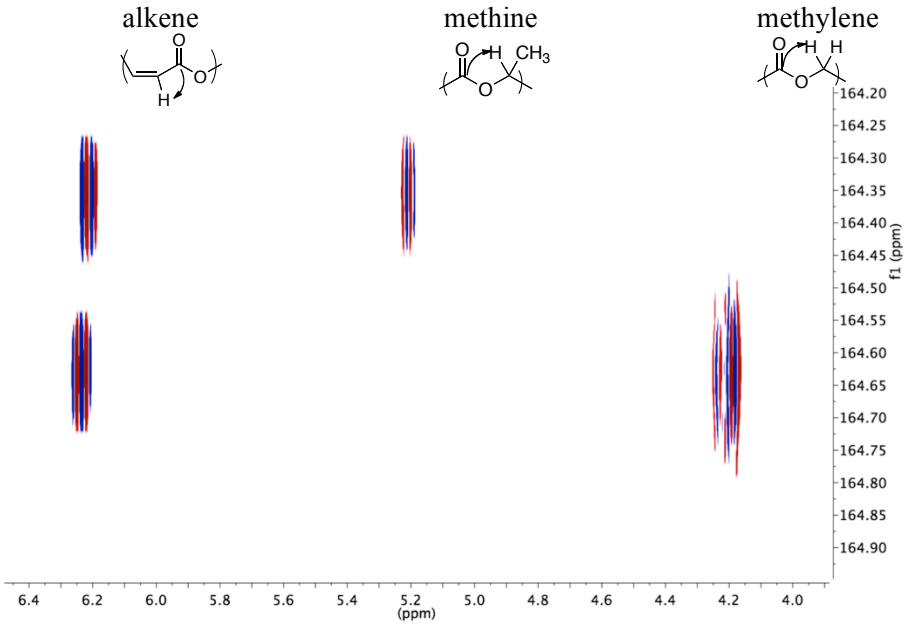


**Figure A1.22.** Band-selective gbsHMBC spectrum optimized for 155-170 ppm, used to elucidate the fine structure of protons coupling to carbonyl carbons.

Analysis of a band-selective HSQCAD spectrum ($CDCl_3$, 600 $^1H$ NMR) optimized for the alkene $^{13}C$ region of the polymer shows four distinct alkene proton-carbon

environments (Figure A1.23). The two singlet peaks at δ (6.23, 129.9) ppm and δ (6.27, 129.8) ppm represent protons from environments $H_A$ and $H_D$, in reference Figure A1.21. These environments are expected to be singlets due to the symmetry of the alkene. From the HMBCAD, we can assign 6.23 to $H_A$ and 6.27 to $H_D$. Strongly leaning doublets at δ (6.24, 129.2) ppm and δ (6.26,130.4) ppm represent protons from environments $H_B$ and $H_C$ in reference to Figure S 21. Each of these protons has one coupling partner due to the asymmetry of the alkene and thus should appear as doublets with strong roofing caused by their chemical shift separation being comparable to their coupling constant.

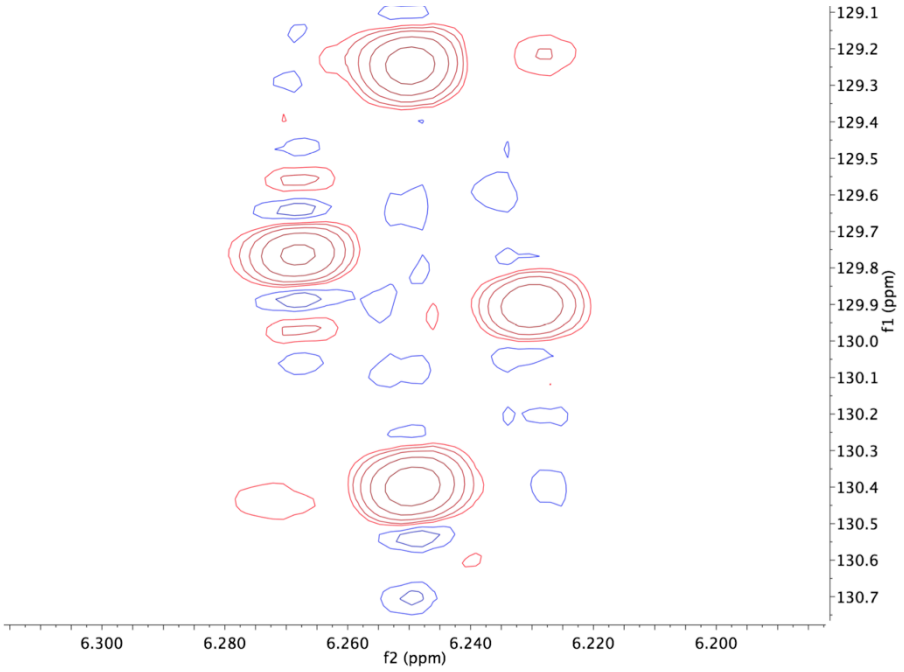


**Figure A1.23.** HSQCAD spectrum specific to the $^{1}H$ and $^{13}C$ alkene regions of PPM.

To better illustrate the apparent peaks from the original $^{1}H$ NMR spectrum, MNOVA software was used to extract slices corresponding to the $^{1}H$ NMR spectrum of individual signals in the HSQC spectrum (Figure A1.24). The center of the doublets

for $H_B$ and $H_C$ are at 6.24 and 6.26 ppm and the doublet signals appear at 6.23, 6.25 and 6.25, 6.27 ppm respectively. As a result of roofing, the doublet signals at 6.25 ppm are the largest. The signals at 6.23 and 6.27 ppm directly overlap with the singlets for $H_A$ and $H_D$ and contribute a small amount to those peaks. An overlaid array of the spectra suggests that these two roofing doublets and two singlets are the four signals that make up the apparent peaks in the $^1$H NMR spectrum (Figure A1.25).

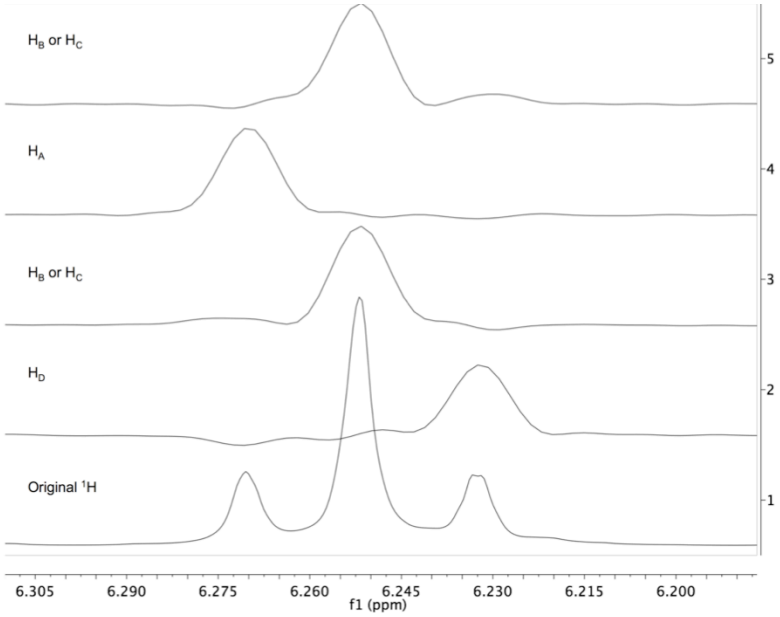


**Figure A1.24.** Extracted $^1$H NMR spectrum profiles of individual protons in the HSQC spectrum of PPM.

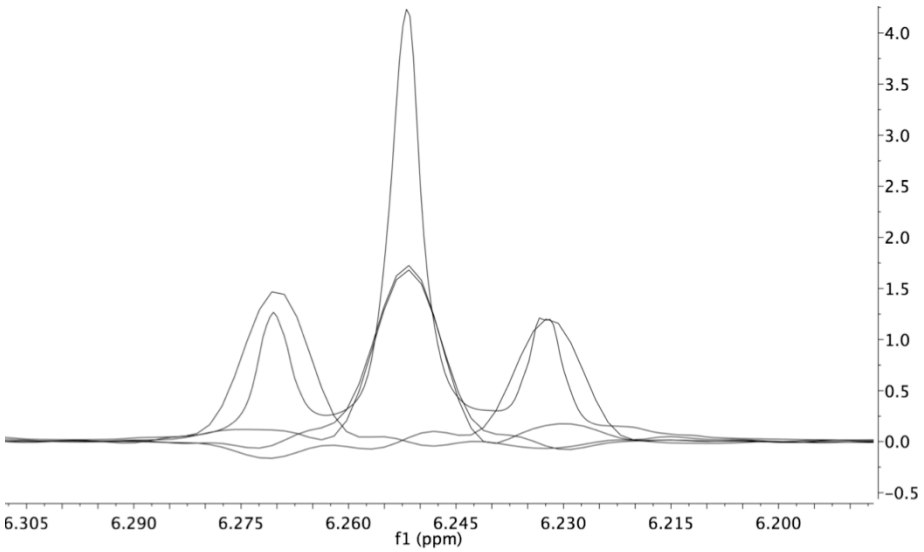


**Figure A1.25.** Superimposed $^{1}$H NMR spectral profiles from Figure A1.24 demonstrating the origin of the apparent peaks of the original $^{1}$H NMR spectrum of PPM.

REFERENCES

(1) Jungk, S. J.; Moore, J. A.; Gandour, R. D. *J. Org. Chem.* **1983**, *48*, 1116-1120.

(2) Matsumo, K.; Fuwa, S.; Shimojo, M.; Kitajimo, H. *Bull. Chem. Soc. Jpn.* **1996**, *69*, 2977-2988.

(3) Jeske, R. C.; DiCiccio, A. M. ; Coates, G. W. *J. Am. Chem. Soc.* **2007**, *129*, 11330-11331.

(4) Takeda, N.; Inoue, S. *Macromol. Chem. Phys.* **1978**, *179*, 1377-1381.

(5) Cohen, C. T.; Chu, T.; Coates, G. W. *J. Am. Chem. Soc.* **2005**, *127*, 10869-10878.

(6) (a) Darensbourg, D. J.; Yarbrough, J. C. *J. Am. Chem. Soc.* **2002**, *124*, 6335-6342. (b) Larrow, J. F.; Jacobsen, E. N. *J. Org. Chem.* **1994**, *59*, 1939-1942.

# CHAPTER THREE

# REGIOSELECTIVE COPOLYMERIZATION OF EPOXIDES WITH CYCLIC ANHYDRIDES: A NEW ROUTE TO SEMICRYSTALLINE POLYESTERS FROM COMMODITY FEEDSTOCKS

## 3.1 Abstract

Recent developments in polyester synthesis have led to several systems based on zinc, chromium, and aluminum catalysts for the ring-opening alternating copolymerization of epoxides with cyclic anhydrides. However, to date regioselective processes for this copolymerization have remained relatively unexplored. Herein we report the development of a highly active, regioselective system for the copolymerization of a variety of terminal epoxides and cyclic anhydrides. Using enantiopure propylene oxide, we synthesize the first examples of semi-crystalline polyesters *via* the copolymerization of readily available epoxide/anhydride monomer pairs.

## 3.2 Introduction

Polyethylene (PE) and isotactic polypropylene (iPP) are important industrial polymers because of their low cost and superior performance.[1] The thermal properties of PE and iPP can be tuned by adjusting percent crystallinity, facilitating the processing and utilization of these materials in a broad range of applications. For PE, semi-crystallinity results from a linear backbone structure, while for iPP, it results from high stereo- and regioregularity.[1b, 2] Synthesis of stereo- and regioregular

polymers requires processes that control polymer backbone microstructure, either by retaining inherent stereochemistry in regioselective processes or by performing stereoselective transformations.[3] Recent advances in catalyst design have enabled the development of new systems that can create polymers with precise control of stereo- and regiochemistry.[3] In some cases the development of living systems has been applied to the preparation of polymers with defined molecular weights and block morphologies.[3c-e]

One limitation to polyolefin synthesis, however, is the difficulty of incorporating polar monomers.[4]Functionally diverse polymers that retain the competitive properties of semicrystalline PE and iPP are necessary for many engineering applications. Polyesters are good candidates for a new class of functionally diverse semi-crystalline materials because of the many possible combinations of readily-available epoxides and cyclic anhydrides.[5,7] Most commodity polyesters are prepared industrially via the step-growth copolymerization of diols and diesters (Scheme 3.1a).[5b] Although a wide range of dialcohol and diacid/diester monomers are available, this process is energy intensive and it is difficult to control polymer composition and reach high molecular weight.[1a,5b, 6,8,8] Furthermore, unsymmetrically-substituted monomers are randomly enchained by step-growth mechanisms to create regioirregular, amorphous polymers.

**Scheme 3.1.** Copolymerization Routes for the Synthesis of Polyesters: a) Step-Growth Condensation, and b) Chain-Growth Ring-Opening

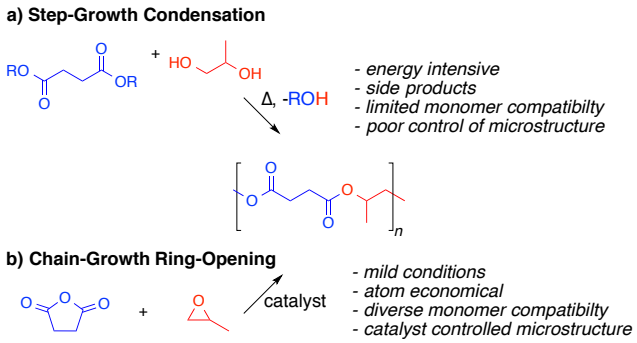


Alternatively, polyesters can be synthesized by the chain-growth ring-opening polymerization of lactides and lactones.[7] In this atom economical process, regiochemistry is inherent to the monomers. Poly(lactide) and poly(hydroxybutyrate) are examples of semi-crystalline polyesters prepared by this method; however, their utility is in some cases restricted by thermal properties and limited functional diversity.[8]

The ring-opening alternating copolymerization (ROAC) of epoxides and cyclic anhydrides is another promising route to structurally diverse polyesters (Scheme 3.1b).[7,9] Beta-diiminate (BDI) zinc(II)[9a,b] and N,N'-bis(salicylidene)ethylenediimine (salen) chromium(III) and related [9b-j] complexes can catalyze the formation of highly alternating polyesters from a variety of cyclic anhydrides and epoxides. All of these monometallic systems, however, give regioirregular polyesters. In contrast, Lu[7i] reported a bimetallic Cr complex that showed up to 99% regioregular head-to-tail linkages for the copolymerization of maleic anhydride with (*S*)-phenyl glycidyl ether. Based on this important lead, we hypothesized that other systems could be developed for the copolymerization of a wide range of other monomer pairs.

The copolymerization of epoxides with $CO_2$ is a good model for the reaction of epoxides with cyclic anhydrides since both are proposed to operate via similar mechanisms.[7] It has been demonstrated that (BDI)Zn[10] and (salen)Cr-type[11] catalysts exhibit low regioselectivity in the ring-opening copolymerization of terminal epoxides and $CO_2$. [12] However, we and others have observed that N,N'-bis(salicylidene)cyclohexanediimine (salcy) cobalt(III)-type catalysts[13] produce highly regioregular polycarbonates. For this reason, we initiated the investigation of epoxides and cyclic anhydride copolymerization catalyzed by (salcy)Co(III)-type complexes.[14]

Herein we report the effects of complex preparation, cocatalyst, and ligand electronics on the activity of (salcy)Co(III) catalysts for the copolymerization of various epoxides and anhydrides. We also show that epoxide electronics distinctly influence copolymerization rates with maleic anhydride, where the most electron poor epoxides produce the most active (TOF >100 $h^{-1}$) systems. Other anhydrides provide more robust copolymerization systems, producing high molecular weights and maintaining good activity at low catalyst concentrations. Finally, the high regioselectivity of this system allows the creation of semicrystalline stereoregular polyesters *via* the copolymerization of enantiopure propylene oxide with several cyclic anhydrides.

### 3.3 Results and Discussion

Several studies report low activity for the cobalt-catalyzed copolymerization of epoxides with cyclic anhydrides.[9b,d,f,h,j] In agreement with these results, we observed lower yields for the reaction of propylene oxide and maleic anhydride catalyzed by

*rac*-(salcy)$CoO_2CC_6F_5$ compared to *rac*-(salcy)CrCl.[8b] However, the poly(propylene maleate) (PPM) synthesized by the cobalt catalyst is more regioregular than the PPM produced by the corresponding chromium catalyst (Figure 3.1).[9b] Intrigued by these results, we focused our efforts on improving the activity of the regioselective cobalt copolymerization system.

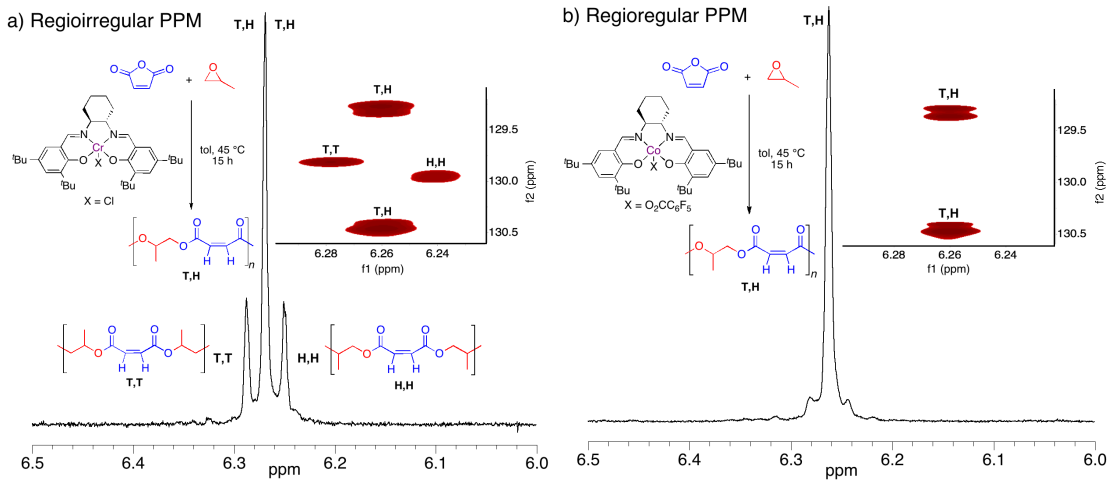


**Figure 3.1.** Analysis of regiochemistry using $^1$H and bsgHSQC NMR spectroscopy of PPM: a) alkene region of the spectrum of regioirregular poly(propylene maleate) produced by *rac*-(salcy)CrCl; b) alkene region of the spectrum of regioregular poly(propylene maleate) produced by *rac*-(salcy)$CoO_2CC_6F_5$.

Because salcy complexes are well known to affect enantioselective epoxide ring-opening,[15] we chose to study variations of (salcy)Co(III) catalysts. We initially screened complexes with initiators and cocatalysts previously unexplored in this context (Table 3.1). Two catalysts with different initiators were synthesized *via* distinctive methods. **Cat1** was prepared by metallation of *rac*-(salcy)$H_2$ with $Co(OAc)_2$ and subsequent oxidation of the isolated *rac*-(salcy)Co(II) complex with trifluoroacetic acid in air to give *rac*-(salcy)$CoO_2CCF_3$.[16] **Cat2** was prepared via a one-pot procedure by metallation of (salcy)$H_2$ with $Co(NO_3)_2$•$6H_2O$ and *in situ*

oxidization in air with the $HNO_3$ formed during the reaction to obtain *rac*-(salcy)$CoNO_3$.[17]

**Table 3.1.** Initiators and Cocatalysts Evaluated for the Regioselective Copolymerization of Propylene Oxide (**1a**)/Maleic Anhydride (**2a**) by (salcy)Co(III)-type Catalysts[a]

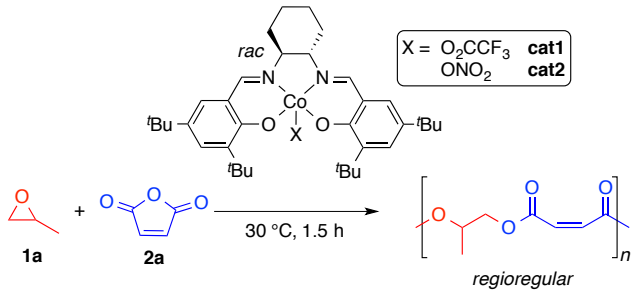


| entry | catalyst | cocatalyst | % conv. 2a[b] | % ether linkages[c] | $M_n^{theo}$ (kDa) | $M_n^{obs}$ (kDa)[d] | PDI[d] |
|---|---|---|---|---|---|---|---|
| 1 | **cat1** | - | 19 | 22 | 3.2 | 3.0 | 1.16 |
| 2 | **cat1** | [PPN][$O_2CCF_3$] | 25 | <1 | 2.0[e] | 1.8 | 1.10 |
| 3 | **cat2** | - | 42 | 16 | 6.9 | 3.4 | 1.22 |
| 4 | **cat2** | [PPN][$NO_3$] | 52 | <1 | 4.1[e] | 2.6 | 1.18 |

[a]General conditions: **1a**:**2a**:**cat**:cocat = 200:100:1:1. [b]Calculated using $^1$H NMR spectroscopy based on **2a** as the limiting reagent. [c]Determined by $^1$H NMR spectroscopy of crude reaction mixture. [d]Measured using gel-permeation chromatography relative to polystyrene standards eluted at 0.3 mL/min with THF at 30 °C. [e]Calculated based on the assumption of two initiating groups.

Due to the tendency of (salcy)Co(III) complexes to reduce *in situ*, reaction conditions were simplified to 30 °C in neat substrate.[14b,18] **Cat1** and **cat2** were screened with racemic propylene oxide (**1a**) and maleic anhydride (**2a**) (Table 3.1). In the absence of ionic cocatalysts, both systems formed polyester containing polyether linkages (formed *via* the consecutive enchainment of epoxide monomers, entries 1 and 3). This is in contrast to our previous results with *rac*-(salcy)$CoO_2CC_6F_5$ in which no measurable polyether linkages formed; however, the latter reaction was performed at higher temperatures under more dilute conditions and exhibited lower activity.[9c]

Activity and selectivity increases for (salcy)M(III) catalyzed epoxide/$CO_2$ and epoxide/anhydride copolymerizations are reported with the addition of nucleophilic cocatalysts like bis(triphenylphosphine)iminium salts ([PPN][X]).[9g,14b] In the presence of [PPN][X], both catalysts yielded exclusively alternating, regioregular polyesters (entries 2 and 4). **Cat2** showed higher activity than **cat1** under both conditions and exhibited less reduced *rac*-(salcy)Co(III) (a bright brick-red color *vs.* the green-brown color of the Co(III) species). For this reason, **cat2** (and derivatives thereof) with one equivalent of [PPN][$NO_3$] were selected for further study. Despite activity optimization, molecular weights of maleic anhydride copolymers are generally lower than predicted and are the subject of on-going investigations.

Next, the electronic effects of salcy ligand substituents were examined. We expected the electronic nature of the ligand to influence the Lewis acidity of the cobalt center and therefore to influence the reaction rate.[13,19] Additionally, phenolate ligands have been reported to influence the redox properties of coordinated metals, affecting activity according to redox stability.[20] Five additional *rac*-(salcy)Co$NO_3$ complexes with electron donating (OMe, Me) or electron withdrawing (F, Cl, $NO_2$) substituents in the 5-positions of the salicylidene moieties were prepared and tested for the copolymerization of **1a** with **2a** (Figure 3.2a). Electron withdrawing ligands resulted in more active catalysts as measured by average turnover frequency (TOF; [RPU]([**cat**]•h)$^{-1}$). Notably, **cat5** produced the highest TOF of 38 $h^{-1}$ (entry 4). However, activity did not improve linearly with increasingly electron-withdrawing ligands, suggesting that Lewis acidity is not the only contributor to overall activity.

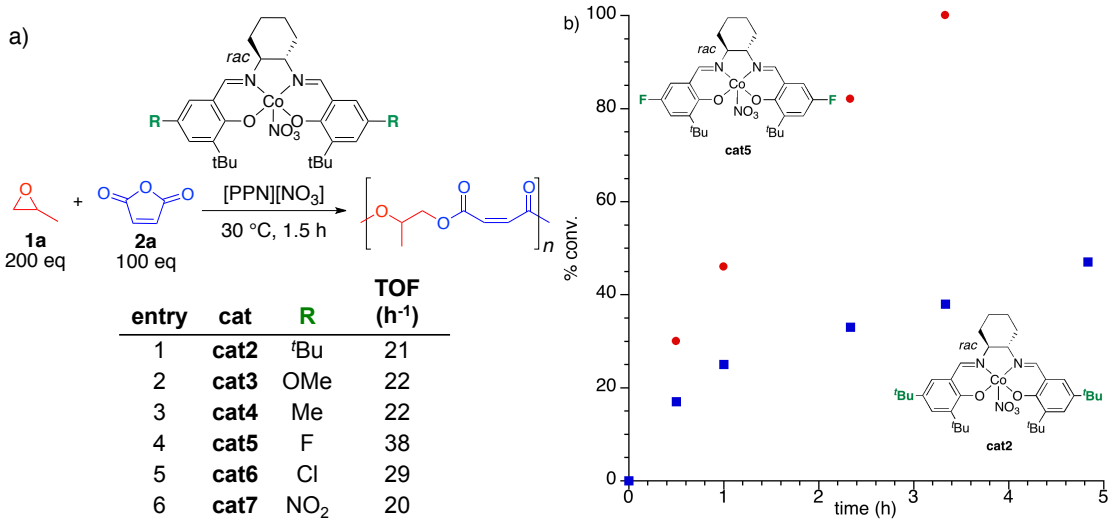


| entry | cat | R | TOF ($h^{-1}$) |
|---|---|---|---|
| 1 | **cat2** | $^t$Bu | 21 |
| 2 | **cat3** | OMe | 22 |
| 3 | **cat4** | Me | 22 |
| 4 | **cat5** | F | 38 |
| 5 | **cat6** | Cl | 29 |
| 6 | **cat7** | $NO_2$ | 20 |

**Figure 3.2.** The impact of ligand electronics on the copolymerization behavior of *rac*-(salcy)$CoNO_3$/[PPN][$NO_3$] catalyst systems: a) Average TOF ([RPU]([**cat**]•h)$^{-1}$) of each catalyst for the copolymerization of **1a**/**2a** measured at $t_{rxn}$ 1.5 h; b) Percent conversion *versus* time for the **cat2** and **cat 5** catalyzed copolymerization of **1a**/**2a**.

The effect of ligand electronics on the copolymerization behavior of **cat2** (R = $^t$Bu) and **cat5** (R = F) was first analyzed using *in situ* $^1$H NMR spectroscopy to evaluate catalyst activity and stability during the copolymerization of PO and MA.[21] Addition of **cat2**/[PPN][$NO_3$] to PO/MA immediately produced a paramagnetic mixture, preventing measurement of polymerization kinetics and suggesting the formation of Co(II) or a high spin Co(III) species. In contrast, **cat5**/[PPN][$NO_3$] remained diamagnetic, allowing direct monitoring of polymerization progress and suggesting the presence of a stable, octahedral (salcy)Co(III) species. Time-lapse aliquots of each polymerization reflected the activity/stability (or lack thereof) of each systems (Figure 3.2b). The overall productivity of **cat2** diminished, reaching only 40% conversion in 5 hours. This suggests that the paramagnetic species could be contributing to catalyst deactivation. Conversely, the productivity of **cat5** remained constant, achieving 100% conversion in 4 hours.

The electrochemical properties of each catalyst were studied using cyclic voltammetry (CV). The CV curves of **cat2** and **cat5** exhibited four redox events, one metal centered couple near -100 mV representing the Co(II)/Co(III) transition and three ligand centered couples at potentials >600 mV (Figure 3.3). These curves matched well with literature reports of similar compounds.[20a] Under representative copolymerization conditions, the catalysts retained all signature redox couples. Differences in the electrochemical behaviors of the metal centers were measured by changes in potential for the Co(II)/Co(III) transitions and were dependent on ligand identity.[21] Ultimately, the Nernst equation revealed a much larger ratio of [Co(III)]:[Co(II)] for **cat5** (58) than for **cat2** (18) (Figure 3.3). Additionally, the copolymerization mixture with **cat5** maintained a stable resting voltage, indicating that the ratio of [Co(III)]:[Co(II)] was consistent. However, the resting potential of the copolymerization with **cat2** continually decreased, signifying an increase in [Co(II)] over time. These results associate catalyst deactivation with high [Co(II)], suggesting that the low activity of **cat2** results from its low electrochemical stability under the copolymerization conditions.

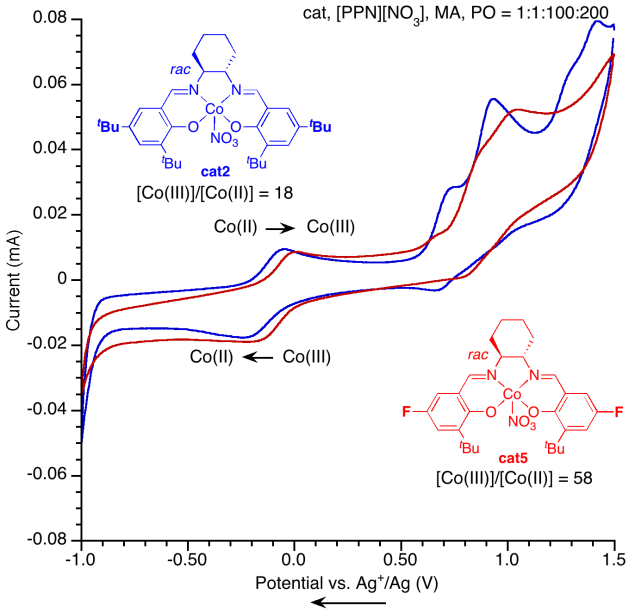


**Figure 3.3.** CV curves collected from 1.5 to -1.0 V for 1.0 mM solutions of **cat2** (blue) and **cat5** (red) in 0.1 M TBAP/ACN with 1 eq. [PPN][$NO_3$], 100 eq MA, and 200 eq PO.

With a more robust cobalt catalyst system in hand, we evaluated copolymerization scope and stereoselectivity. **Cat5**/[PPN][$NO_3$] was tested for the ROAC of maleic anhydride with a variety of epoxides (Table 3.2). NMR spectroscopic analysis of the polyester products revealed highly regioregular structures.[21] Electron-rich epoxides (entries 1-2) were slower to copolymerize, glycidyl ethers (entries 3-5) with electron-withdrawing substituents exhibited enhanced polymerization rates. Electron poor epoxides (entries 6 and 7) were faster and yielded polyesters with higher molecular weights and narrower polydispersity indices (PDIs). Epoxides with orthogonally reactive groups such as methylmethacrylates (MMA; **1d**) and primary alkyl chlorides (**1f**) (entries 4 and 6) readily polymerized without side reactions to afford eligible polyesters capable of facile post-polymerization modifications.

**Table 3.2.** ROAC of Maleic Anhydride (**2a**) with Terminal Epoxides (**1a-g**) using **cat5**/[PPN][$NO_3$][a]

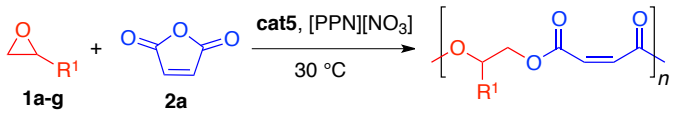


| entry | $R^1$ (1) | time (h) | % conv. 2a[b] | TOF ($h^{-1}$) | $M_n^{theo}$ (kDa)[c] | $M_n^{obs}$ (kDa)[d] | PDI[d] | $T_g$ (°C)[e] |
|---|---|---|---|---|---|---|---|---|
| 1 | Me (**1a**) | 1.5 | 65 | 43 | 5.1 | 3.4 | 1.21 | 21 |
| 2 | Et (**1b**) | 1.5 | 37 | 25 | 3.2 | 2.2 | 1.19 | 9 |
| 3 | $CH_2O^nBu$ (**1c**) | 1.5 | 40 | 27 | 4.6 | 3.3 | 1.26 | -18 |
| 4 | $CH_2OMMA$ (**1d**) | 0.83 | 91 | 109 | 10.9 | 6.3 | 1.24 | -6[f] |
| 5 | $CH_2OPh$ (**1e**) | 0.67 | 71 | 140 | 8.8 | 4.8 | 1.27 | 36 |
| 6 | $CH_2Cl$ (**1f**) | 0.25 | 77 | 308 | 7.3 | 5.5 | 1.17 | 26 |
| 7 | $CF_3$ (**1g**) | 0.67 | 88 | 131 | 9.2 | 5.2 | 1.13 | 25 |

[a]General conditions: **1**:**2**:**cat5**:[PPN][$NO_3$] = 200:100:1:1. [b]Calculated using $^1$H NMR spectroscopy based on **2a** as the limiting reagent. [c]Calculated based on the assumption of two initiating groups. [d]Measured using gel-permeation chromatography relative to polystyrene standards eluted with THF 30 °C. [e]Measured using differential scanning calorimetry, values reported are from second heat. [f]Upon rigorous drying this polymer cross-linked, thus the DSC measurement reflects the cross-linked product.

Next, the ROAC of different cyclic anhydrides (**2b-d**) with propylene oxide (**1a**) was evaluated using **cat2-cat7**/[PPN][$NO_3$].[21] In all examples, **cat5**/[PPN][$NO_3$] exhibited the highest activity and was further tested at lower catalyst concentration (Table 3.3). Catalyst degradation limited molecular weights for the ROAC of propylene oxide (**1a**) with maleic (**2a**) and succinic anhydride (**2b**) (entries 1 and 2). In contrast, **cat5**/[PPN][$NO_3$] was highly active for the copolymerization of propylene oxide with diglycolic (**2c**) and phthalic anhydrides (**2d**), producing high molecular weight polyesters (entries 3 and 4). The ROAC of any of these anhydrides with the electron-poor epoxide epichlorohydrin (**1f**), exhibited higher TOFs and were amenable to changes in reaction stoichiometry (entries 5-8).

**Table 3.3.** **cat5**/[PPN][$NO_3$] Catalyzed Copolymerization of a Variety of Cyclic Anhydrides (**2a-d**) with Propylene Oxide (**1a**) or Epichlorohydrin (**1f**)[a,22]

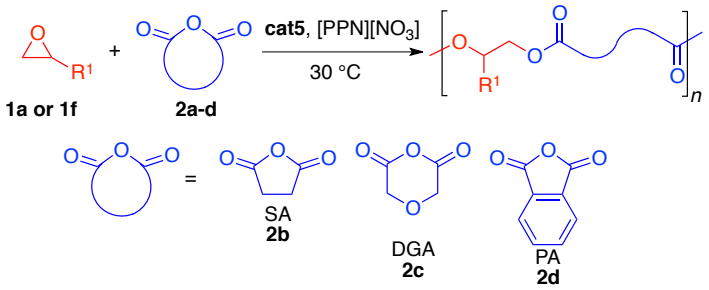


| entry | reagents | time (h) | % conv. 2[b] | % ether[c] | $M_n^{theo}$ (kDa)[d] | $M_n^{obs}$ (kDa)[e] | PDI[e] | $T_g$ (°C)[f] |
|---|---|---|---|---|---|---|---|---|
| 1[g] | **1a/2a** | 1.5 | 65 | <1 | 5.1 | 3.4 | 1.21 | 21 |
| 2[h] | **1a/2b** | 5.0 | 85 | <1 | 6.7 | 4.8 | 1.23 | -8 |
| 3 | **1a/2c** | 3.0 | 71 | <1 | 24.7 | 10.7 | 1.29 | 2 |
| 4 | **1a/2d** | 3.5 | 70 | <1 | 28.8 | 19.1 | 1.16 | 63 |
| 5 | **1f/2a** | 6.5 | 71 | <1 | 19.4 | 16.0 | 1.26 | 16 |
| 6 | **1f/2b** | 5.0 | 83 | <1 | 31.9 | 20.0 | 1.28 | 7 |
| 7 | **1f/2c** | 1.0 | 97 | <1 | 40.4 | 17.5 | 1.27 | 1 |
| 8[i] | **1f/2d** | 2.5 | 80 | <1 | 38.4 | 21.0 | 1.13 | 65 |

[a]General conditions: **1**:**2**:**cat5**:[PPN][$NO_3$] = 800:400:1:1. [b]Calculated using $^1$H NMR spectroscopy based on **2** as the limiting reagent. [c]Determined by $^1$H NMR spectroscopy of crude reaction mixture. [d]Calculated based on the assumption of two initiating groups. [e]Measured using gel-permeation chromatography relative to polystyrene standards eluted with THF at 30 °C. [f]Measured using differential scanning calorimetry, values reported are from second heat. [g]**1a**:**2a**:**cat5** = 200:100:1. [h]**1a**:**2b**:**cat5** = 200:200:1, [**cat5**] = 0.1 mM benzene. [i]**1g**:**2d**:**cat5** = 400:400:1, [**cat5**] = 0.05 mM THF.

Finally, the regioselectivity of this system was quantitatively measured by analyzing the retention of stereochemistry from copolymerizations using enantiopure (*S*)-PO (*S*-**1a**). Polyesters with anhydrides **2a-d** were synthesized using **cat5** and (*S*)-PO, and the percentage of regioerrors was determined by measuring the enantiomeric excess of the propylene glycol formed upon hydrolysis of the polyester (Figure 3.4). All anhydrides exhibited high levels of regioregularity (94-99 % ee) while DGA and

PA were almost exclusively regioregular. Importantly, polyesters formed with MA and PA and (*S*)-PO exhibited high melting points (134 and 150 °C respectively), giving the first examples of semi-crystalline polyesters synthesized via alternating copolymerization of readily available epoxides and cyclic anhydrides.

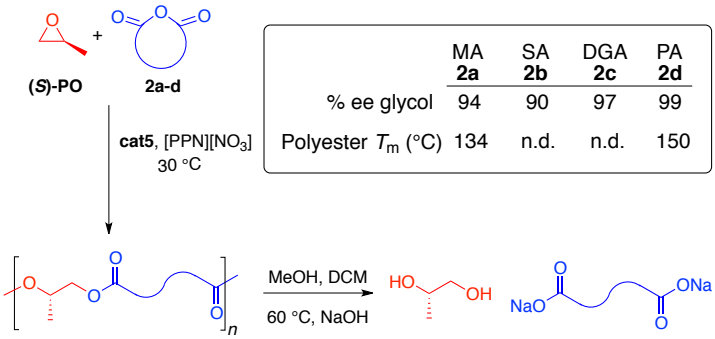


| | MA **2a** | SA **2b** | DGA **2c** | PA **2d** |
|---|---|---|---|---|
| % ee glycol | 94 | 90 | 97 | 99 |
| Polyester $T_m$ (°C) | 134 | n.d. | n.d. | 150 |

**Figure 3.4.** Quantitative analysis of regiochemistry for polyesters made with (*S*)-PO/anhydrides by **cat5**/[PPN][$NO_3$] via degradation and % ee analysis of isolated propylene glycol products.

### 3.4 Conclusions

We report here the first highly active and regioselective catalyst system for the ring-opening copolymerization of epoxides and cyclic anhydrides. Through detailed studies on ligand electronics and its impact on catalyst behavior, the fluorine substituted (salcy)$CoNO_3$ complex, **cat5**, was developed as a more stable and active copolymerization catalyst with good substrate scope. We are incorporating these findings into progressive ligand design with the goal of further improving activity and molecular weight capabilities of the (salcy)$CoNO_3$ system. The stable diamagnetic (salcy)Co(III) complex is being utilized to understand the mechanism of epoxide and cyclic anhydride enchainment to strategize methods to avoid chain termination. Semi-crystalline polyesters from racemic starting materials will be pursued using chiral derivatives of the redox stabilized ligand architectures.

REFERENCES

(1) (a) Leiz, J. R.; Asua, J. M. 2002. Copolymers. Kirk-Othmer Encyclopedia of Chemical Technology. (b) Kissin, Y. V. 2005. Olefin Polymers, Introduction. Kirk-Othmer Encyclopedia of Chemical Technology.

(2) (a) Rosen, S. L. 2000. Polymers. Kirk-Othmer Encyclopedia of Chemical Technology. (b) Deplace, F.; Wang, Z.; Lynd, N. A.; Hotta, A.; Rose, J. M.; Hustad, P. D.; Ian, J.; Ohtaki, H.; Coates, G. W.; Shimizu, F.; Hirokane, K.; Yamada, F.; Shin, Y.-W.; Rong, L.; Zhu, J.; Toki, S.; Hsiao, B. S.; Fredrickson, G. H.; Kramer, E. J. *J. Polym. Sci., Part B: Polym. Phys.* **2010**, *49*, 1428-1437.

(3) (a) Coates, G. W. *Chem. Rev.* **2000**, *100*, 1223-1252. (b) Resconi, L.; Cavallo, L.; Fait, A.; Piemontesi, F. *Chem. Rev.* **2000**, *100*, 1253-1345. (c) Domski, G. J.; Rose, J. M.; Coates, G. W.; Bolig, A. D.; Brookhart, M. *Prog. Polym. Sci.* **2007**, *32*, 30-92. (d) Anderson-Wile, Amelia M.; Edson, Joseph B.; Coates, Geoffrey W. Living Alkene Polymerization for Polyolefin Architectures. In *Complex Macromolecular Architectures*; Hadjichristidis, N., Ed.; John Wiley & Sons: Singapore, Singapore, 2011; pp. 267-316. (e) Coates, G. W.; Hustad, P. D.; Reinartz, S. *Angew. Chem. Int. Ed.* **2002**, *41*, 2236-2257.

(4) (a) Boffa, L. S.; Novak, B. M. *Chem. Rev.* **2000**, *100*, 1479-1493. (b) Chung, T. C. M. Functionalization of Polyolefins; Academic Press, London, 2002. (c) Nakamura, A.; Ito, S.; Nozaki, K. *Chem. Rev.* **2009**, *109*, 5215-5244.

(5) (a) Nava, H. 2004. Polyesters, Unsaturated. Kirk-Othmer Encyclopedia of Chemical Technology. (b) East, A. J. 2006. Polyesters, Thermoplastic. Kirk-Othmer Encyclopedia of Chemical Technology.

(6) Tabone, M. D.; Cregg, J. J.; Beckman, E. J.; Landis, A. E. *Environ. Sci. Technol.* **2010**, *44*, 8264-8269.

(7) (a) Jeske, R. C.; Coates, G. W. Homogenous Catalyst Design for the Synthesis of Aliphatic Polycarbonates and Polyesters. In *Handbook of Green Chemistry;* Crabtree, R. H., Ed.; Wiley-VCH: Weinheim, Germany, 2009; Vol. 1, pp 343-373. (b) Kamber, N. E.; Jeong, W.; Waymouth, R. M.; Pratt, R. C.; Lohnmeijer, B. G. G.; Hedrick, J. L. *Chem. Rev*. **2007**, *107*, 5813-5840. (c) Stanford, M. J.; Dove, A. P. *Chem. Soc. Rev.* **2010**, *39*, 486-494. (d) Dijkstra, P. J.; Du, H.; Feijen, J. *Polym. Chem.* **2011**, *2*, 520-527.

(8) (a) Tsui, A.; Wright, Z. C.; Frank, C. W. *Annu. Rev. Chem. Biomol. Eng.* **2013**, *4*, 143-170. (b) Jérôme, C.; Lecomte, P. *Adv. Drug Delivery Rev.* **2008**, *60*, 1056-1076.

(9) (a) Jeske, R. C.; DiCiccio, A. M.; Coates, G. W. *J. Am. Chem. Soc.* **2007**, *129*, 11330-11331. (b) Jeske, R. C.; Rowley, J. M.; Coates, G. W. *Angew. Chem., Int. Ed.* **2008**, *47*, 6041-6044. (c) DiCiccio, A. M.; Coates, G. W. *J. Am. Chem. Soc.* **2011**, *133*, 10724-10727. (d) Huijser, S.; Nejad, E. H.; Sablong, R.; de Jong, C.; Koning, C. E.; Duchateau, R. *Macromolecules* **2011**, *44*, 1132. (e) Robert, C.; de Montigny, F.; Thomas, C. M. *Nat. Comm.* **2011**, *2*, 586-592. (f) Nejad, E. H.; van Melis, C. G. W.; Vermeer, T. J.; Koning, C. E.; Duchateau, R. *Macromolecules* **2012**, *45*, 1770-1776. (g) Darensbourg, D. J.; Poland, R. R.; Escobedo, C. *Macromolecules* **2012**, *45*, 2242-2248. (h) Nejad, E. H.; Paoniasari, A.; Koning, C. E.; Duchateau, R. *Polym. Chem.* **2012**, *3*, 1308-1313. (i) Liu, J.; Bao, Y.-Y.; Liu, Y.; Ren, W.-M.; Lu, X.-B. *Polym. Chem.* **2013**, *4*, 1439-1444. (j) Nejad, E. H.; Paoniasari, A.; van Melis, C. G. W.; Koning, C. E.; Duchateau, R. *Macromolecules* **2013**, *46*, 631-637. (k) Bernard, A.; Chatterjee, C.; Chisholm, M. H. *Polymer* **2013**, *54*, 2639-2646. (l) Harrold, N. D.; Li, Y.; Chisholm, M. H. *Macromolecules* **2013**, *46*, 692-698.

(10) Allen, S. D.; Moore, D. R.; Lobkovsky, E. B.; Coates, G. W. *J. Am. Chem. Soc.* **2002**, *124*, 14284-14285.

(11) (a) Darensbourg, D. J.; Yarbrough, J. C. *J. Am. Chem. Soc.* **2002**, *124*, 6335-6342. (b) Eberhardt, R.; Allmendiner, M.; Rieger, B. *Macromol. Rapid Commun.* **2003**, *24*, 194-196.

(12) (a) Coates, G. W.; Moore, D. R. *Angew. Chem. Int. Ed.* **2004**, *43*, 6618-6639. (b) Darensbourg, D. J. *Chem. Rev.* **2007**, *107*, 2388-2410. (c) Kember, M. R.; Buchard, A.; Williams, C. K. *Chem. Comm.* **2010**, *47*, 141-163.

(13) Qin, Z. Q.; Thomas, C. M.; Lee, S.; Coates, G. W. *Angew. Chem. Int. Ed.* **2003**, *42*, 5484-5487.

(14) (a) Lu, X. B.; Wang, Y. *Angew. Chem. Int. Ed.* **2004**, *43*, 3574-3577. (b) Cohen, C. T.; Chu, T.; Coates, G. W. *J. Am. Chem. Soc.* **2005**, *127*, 10869-10878. (c) Nakano, K.; Kamada, T.; Nozaki, K. *Angew. Chem. Int. Ed.* **2006**, *45*, 7274-7277. (d) Noh, E. K.; Na, S. J.; Sujith, S.; Kim, S. W.; Lee, B. Y. *J. Am. Chem. Soc.* **2007**, *129*, 8082-8083. (e) Nakano, K.; Hashimoto, S.; Nakamura, M.; Kamasa, T.; Nozaki, K. *Angew. Chem. Int. Ed.* **2011**, *50*, 4868-4871.

(15) For a review on this topic please see: Jacobsen, E. N. *Acc. Chem. Res.* **2000**, *33*, 421-431.

(16) (a) Lu, X. B.; Liang, B.; Zhang, Y. J.; Tian, Y. Z.; Wang, Y. M.; Bai, C. X.; Wang, H.; Zhang, R. *J. Am. Chem. Soc.* **2004**, *126*, 3732-3733. (b) Tokunaga, M.; Larrow, J. F.; Kakiuchi, F.; Jacobsen, E. N. *Science*, **1997**, *277*, 936-938.

(17) This is a modified procedure different from literature routes that use $AgNO_3$ for oxidation. An example of (salen)$CoNO_3$ complexes synthesized by other routes: Paddock, R. L.; Nguyen, S. T. *Macromolecules* **2005**, *38*, 6251-6253.

(18) (a) Ren, W. M.; Wang, Y. M.; Zhang, R.; Jiang, J. Y.; Lu, X. B. *J. Org. Chem.* **2013**, *78*, 4801-4810. (b) Schaus, S. E.; Brandes, B. D.; Larrow, J. F.; Tokunaga, M.; Hansen, K. B.; Fould, A. E.; Furrow, M. E.; Jacobsen, E. N. *J. Am. Chem. Soc.* **2002**, *124*, 1307-1315.

(19) Darensbourg, D. J.; Fitch, S. B. *Inorg. Chem.* **2008**, *47*, 11868-11878.

(20) Selected papers that discuss these phenomena: (a) Kochem, A.; Kanso, H.; Baptiste, B.; Arora, H.; Philouze, C.; Jarjayes, O.; Vezin, H.; Luneau, D.; Orio, M.; Thomas, F. *Inorg. Chem.* **2012**, *51*, 10557-10571. (b) Kurahashi, T.; Fujii, H. *Inorg. Chem.* **2013**, *52*, 3903-3910. (c) Kochem, A.; Chiang, L.; Baptiste, B.; Philouze, C.; Leconte, N.; Jarjayes, O.; Storr, T.; Thomas, F. *Chem. Eur. J.* **2012**, *18*, 14590-14593. (d) Zhuang, X.; Oyaizu, K.; Niu, Y.; Koshika, K.; Chen, X.; Nishide, H. *Macromol. Chem. Phys.* **2010**, *211*, 669-676. (e) Thomas, F.; Arora, H.; Philouse, C.; Jarjayes, O. *Inorganic Chimica Acta* **2010**, *363*, 3122-3130. (f) Schenk, K. J.; Meghdadi, S.; Amirnasr, M.; Habibi, M. H.; Amiri, A.; Salehi, M.; Kashi, A. *Polyhedron* **2007**, *26*, 5448-5457. (g) Nishinaga, A.; Tajima, K.; Speiser, B.; Eichhorn, E.; Rieker, A.; Ohya-Nishiguchi, H.; Ishizu, K. *Chem. Lett.* **1991**, 1403-1407. (h) Chiang, L.; Allan, L. E. N.; Alcantara, J.; Wang, M. C. P.; Storr, T.; Shaver, M. P. *Dalton Trans.* doi: 10.1039/c3dt51846a.

(21) Please refer to supporting information for more detail.

(22) The regiochemistry of all polyesters generated by **cat5**/[PPN][$NO_3$] were analyzed by $^{1}H$ and $^{13}C$ NMR spectroscopy and appear to have high levels of regioregularity. Regiochemistry was quantitatively measured for polymers with (*S*)-PO as described above.

APPENDIX TWO

# REGIOSELECTIVE COPOLYMERIZATION OF EPOXIDES WITH CYCLIC ANHYDRIDES: A NEW ROUTE TO SEMICRYSTALLINE POLYESTERS FROM COMMODITY FEEDSTOCKS

**Contents**

### A2.1. General Considerations

All manipulations of air and water sensitive compounds were performed under dry nitrogen using a Braun Labmaster Glovebox or standard Schlenk line techniques. NMR spectra were recorded on a Mercury 300 ($^{1}$H, 300 MHz), Varian INOVA 400 ($^{1}$H, 400 MHz; $^{13}$C, 100 MHz; $^{19}$F 376 MHz), Varian INOVA 500 ($^{1}$H, 500 MHz; $^{13}$C, 125 MHz), or Varian INOVA 600 ($^{1}$H, 600 MHz; $^{13}$C, 150 MHz) spectrometer. $^{1}$H NMR spectra were referenced with residual non-deuterated solvent shifts ($CHCl_3$ = 7.26 ppm or $C_5D_4HN$ = 7.22 ppm), $^{13}$C NMR spectra were referenced by solvent shifts ($CDCl_3$ = 77.16 ppm or $C_5D_5N$ = 123.87 ppm) and $^{19}$F NMR spectra were referenced to fluorobenzene added as an internal standard ($C_6H_5F$ = -131.15 ppm).

Gel permeation chromatography (GPC) analyses were conducted using an Agilent PL-GPC 50 integrated system, (2 x PLgel Mini-MIX C columns, 5 micron, 4.6 mmID) equipped with UV and refractive index detectors. The GPC columns were eluted at a rate of 0.3 mL/min with tetrahydrofuran (30 °C) and were calibrated relative to monodisperse polystyrene standards.

Differential scanning calorimetry of polymer samples was performed on a Mettler-Toledo Polymer DSC instrument equipped with a Julabo chiller and autosampler. Typical DSC experiments were made in crimped aluminum pans and experiments were conducted with a heating rate of 10 °C/min from -70 °C to +200 °C. Data were processed using StarE software.

HR/MS analysis was performed at Cornell University by direct-inject on a JEOL GCMate.

## A2.2. Materials

### 2.1. General materials

$CaH_2$ pellets (90%) used for drying epoxides were purchased from Strem and used as received. All solvents were used as received unless otherwise noted. Butylated hydroxytoluene (BHT) was purchased from Sigma Aldrich (>99% purity). [PPN][Cl] was purchased from Sigma Aldrich (98% purity) and recrystallized by layering $CH_2Cl_2/Et_2O$. Trifluoroacetic acid was purchased from Oakwood Products (99% purity). Hexamine (>99% purity) was purchased from Sigma Aldrich. HPLC grade dichloromethane used for metallation was purchased from Fisher Scientific and purified through a solvent purification system under inert atmosphere and degassed for 1 h prior to use. Ethanol used for metallation was purchased from Kroptec, stored over 3 Å sieves and degassed for 1 h prior to use. All NMR solvents were purchased from Cambridge Isotopes and stored over 3 Å molecular sieves. Fluorobenzene was purchased from Sigma Aldrich (99% purity) and used as received. All other reagents were purchased from Aldrich, Alfa-Aesar, Acros, or TCI and were used as received unless otherwise noted.

### 2.2. Polymerization monomers

Propylene oxide (**1a**), 1-butene oxide (**1b**), butyl glycidyl ether (**1c**), phenyl glycidyl ether (**1e**) and epichlorohydrin (**1f**) were purchased from Sigma Aldrich, dried over $CaH_2$ for 3 days under inert atmosphere, vacuum transferred to a flame dried thick walled Schlenk adapted flask and stored in the glove box. Glycidyl methacrylate (**1d**) was purchased from Sigma Aldrich, transferred to a flame dried

Schlenk adapted flask, vigorously degassed with dry nitrogen for 2 h and stored in the glovebox freezer at -17 °C. 1,1,1-trifluoro-2,3-epoxypropane (**1g**) was purchased from Oakwood Products, dried over $CaH_2$ for 3 days under inert atmosphere, vacuum transferred to a flame dried thick walled Schlenk adapted flask and stored in the glove box.

Maleic anhydride (**2a**) (>99% purity, Bartek) was stored under inert atmosphere and sublimed before use. Succinic anhydride (**2b**) (>97% purity, Sigma Aldrich) and phthalic anhydride (**2d**) (>99% purity**,** Sigma Aldrich) were boiled in $CHCl_3$ at 60 °C (10 g anhydride in 100 mL solvent) for 1 h followed by hot filtration to remove insoluble diacids. The organic filtrates were concentrated to white solids via roto-evaporation and washed with diethyl ether. The resulting white powders were collected, dried under vacuum for 12 h in the presence of drierite to remove residual moisture, and sublimed under reduced pressure (80 °C). The purified anhydrides were collected under inert atmosphere and stored in the glovebox until use. Diglycolic anhydride (**2c**) (>95% purity, TCI) was dried under vacuum in the presence of drierite and sublimed under reduced pressure (85 °CThe purity of all anhydrides were confirmed by $^1$H NMR in DMSO-$d_6$.

### 2.3. Metal precursors

$Co(OAc)_2$•$4H_2O$ (>99.8% purity) and $Co(NO)_3$•$6H_2O$ (>99% purity) were purchased from Strem and stored in a dessicator until use.

## A2.3. Synthesis of starting materials

### 3.1. Salicylaldehyde syntheses

For previously reported compounds, $^1$H NMR assignments are included. Full assignments for the unreported **salcy5** are included. All yields represent average isolated yields.

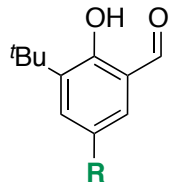


| R = | | |
|---|---|---|
| | $^t$Bu | **aldehyde2** |
| | OMe | **aldehyde3** |
| | Me | **aldehyde4** |
| | F | **aldehyde5** |
| | Cl | **aldehyde6** |
| | $NO_2$ | **aldehyde7** |

**aldehyde2**: 3,5-di-tert-butylsalicylaldehyde was purchased from Combi-Blocks (>98%) and used as received.

**aldehyde3**: 3-*tert*-butyl-4-hydroxyanisole (>98% purity, Sigma Aldrich) was formylated according to a modified Duff reaction as reported by Jacobsen et al.[1] 3-*tert*-butyl-4-hydroxyanisole (2.00 g, 11.1 mmol) and hexamine (2.80 g, 22.2 mmol) were refluxed in trifluoroacetic acid (20 mL) overnight. After cooling, the solution was hydrolyzed in 1M HCl (50 mL) for 1 h and subsequently neutralized with $Na_2CO_3$ (aq). The product was extracted into diethyl ether, dried over $Na_2SO_4$ and concentrated. The yellow oil was purified via column chromatography to yield an orange oil (90:10, hex:EtOAc) (50% isolated yield). $^1$H NMR spectrum ($CDCl_3$, 300 MHz): δ 11.51 (s, 1H); 9.84 (s, 1H); 7.17 (d, $J$ = 3.1 Hz, 1H); 6.81 (d, $J$ = 3.1 Hz, 1H); 3.81 (s, 3H); 1.41 (s, 9H).

**aldehyde4**: 2-*tert*-butyl-4-methylphenol (99%, Sigma Aldrich) was formylated according to a modified Duff reaction as reported by Jacobsen et al.[1] 2-*tert*-butyl-4-methylphenol (5.00 g, 30.44 mmol) and hexamine (8.54 g, 60.89 mmol) were refluxed in trifluoroacetic acid at 90 °C (30 mL) overnight. Upon cooling, the solution was hydrolyzed in 2M HCl overnight. A solid precipitated and was collected via vacuum filtration. This solid was dissolved in $CH_2Cl_2$, neutralized with $Na_2CO_3$ (aq), washed with brine and the organics were dried over $Na_2SO_4$. The product was purified by column chromatography (90:10, hex:$Et_2O$) and the white solid was dried under vacuum (27% isolated yield). $^1$H NMR spectrum ($CDCl_3$, 400 MHz): δ 11.60 (s, 1H); 9.83 (s, 1H); 7.33 (d, $J$ = 2.1 Hz, 1H); 7.18 (d, $J$ = 2.1 Hz, 1H); 2.32 (s, 3H); 1.41 (s, 9H).

**aldehyde5**: 2-*tert*-butyl-4-fluorophenol was synthesized according to a literature procedure.[2] 4-fluorophenol (Combi-Blocks, 5.00 g, 44.6 mmol) was dissolved in a solution of *tert*-butyl alcohol (Aldrich, 8.53 mL, 89.2 mmol), 4.0 mL of $H_2SO_4$ was slowly added, turning the solution from a pale yellow to a light orange. The solution was stirred for 16 h, diluted with $CH_2Cl_2$ and the acid layer was removed by draining out of a seperatory funnel. The remaining organic solution was neutralized with $Na_2CO_3$ (aq), washed with brine (2 times), extracted into diethyl ether and dried over $Na_2SO_4$. The concentrated product was purified using column chromatography (95:5, hex:EtOAc) to yield a light green oil (60% yield). $^1$H NMR spectrum ($CDCl_3$, 400 MHz): δ 6.97 (m, 1H); 6.74 (m, 1H); 6.60 (m, 1H); 4.81 (bs, 1H); 1.38 (s, 9H).

Next, 2-*tert*-butyl-4-fluorophenol (4.31 g, 25.6 mmol), 1.5 equivalents of 2,6-lutidine (4.4 mL, 38.4 mmol), and 5.0 equivalents of paraformaldehyde (5.76 g, 192.15 mmol) were measured into a side arm round bottom flask and evacuated. The round bottom was placed under an atmosphere of nitrogen and the solids were slurried by addition of dry, degassed toluene (40 mL). The mixture was cooled to 0 °C and 0.5 equivalents of anhydrous $SnCl_4$ (Aldrich, 1.49 mL, 12.8 mmol) were added via syringe. The reaction was allowed to warm to room temperature and was heated at 90 °C for 16 h. Note, that as the reaction comes to temperature there is a build up of pressure that needs to be relieved by either opening the flask to nitrogen or quickly to vacuum. After 16 h, the reaction was allowed to cool to room temperature and 60 mL of 2M HCl was added with vigorous stirring to break apart the solid cake formed at the bottom of the flask. After the solids were sufficiently masticated, the solution was filtered over a pad of celite to remove residual Sn and extracted with $Et_2O$ (3x 50 mL). The organic layers were collected, washed with brine and dried over $Na_2SO_4$. The solution was concentrated to a crunchy yellow solid that could be recrystallized from MeOH (30% isolated yield). $^1$H NMR spectrum in ppm ($CDCl_3$, 400 MHz): δ 11.59 (s, 1H); 9.82 (s, 1H); 7.29-7.26 (dd, *J* = 3.1, 10.5 Hz, 1H); 7.07 (dd, *J* = 3.1, 7.0 Hz, 1H); 1.41 (s, 9H). $^{13}$C NMR spectrum ($CDCl_3$, 125 MHz): 196.27-196.25 (d, *J* = 2.6 Hz); 157.70-157.69 (d, *J* = 1.4 Hz); 156.30-154.41 (d, *J* = 238.6 Hz); 141.20-141.16 (d, *J* = 5.5 Hz); 122.55-122.35 (d, *J* = 24.4 Hz); 119.97-119.92 (d, *J* = 6.5 Hz); 115.68-115.50 (d, *J* = 22.3 Hz); 35.23; 29.09. $^{19}$F NMR spectrum ($CDCl_3$, 376 MHz): δ -123.79 (d,d, *J* = 7.9, 10.6 Hz, 1F).

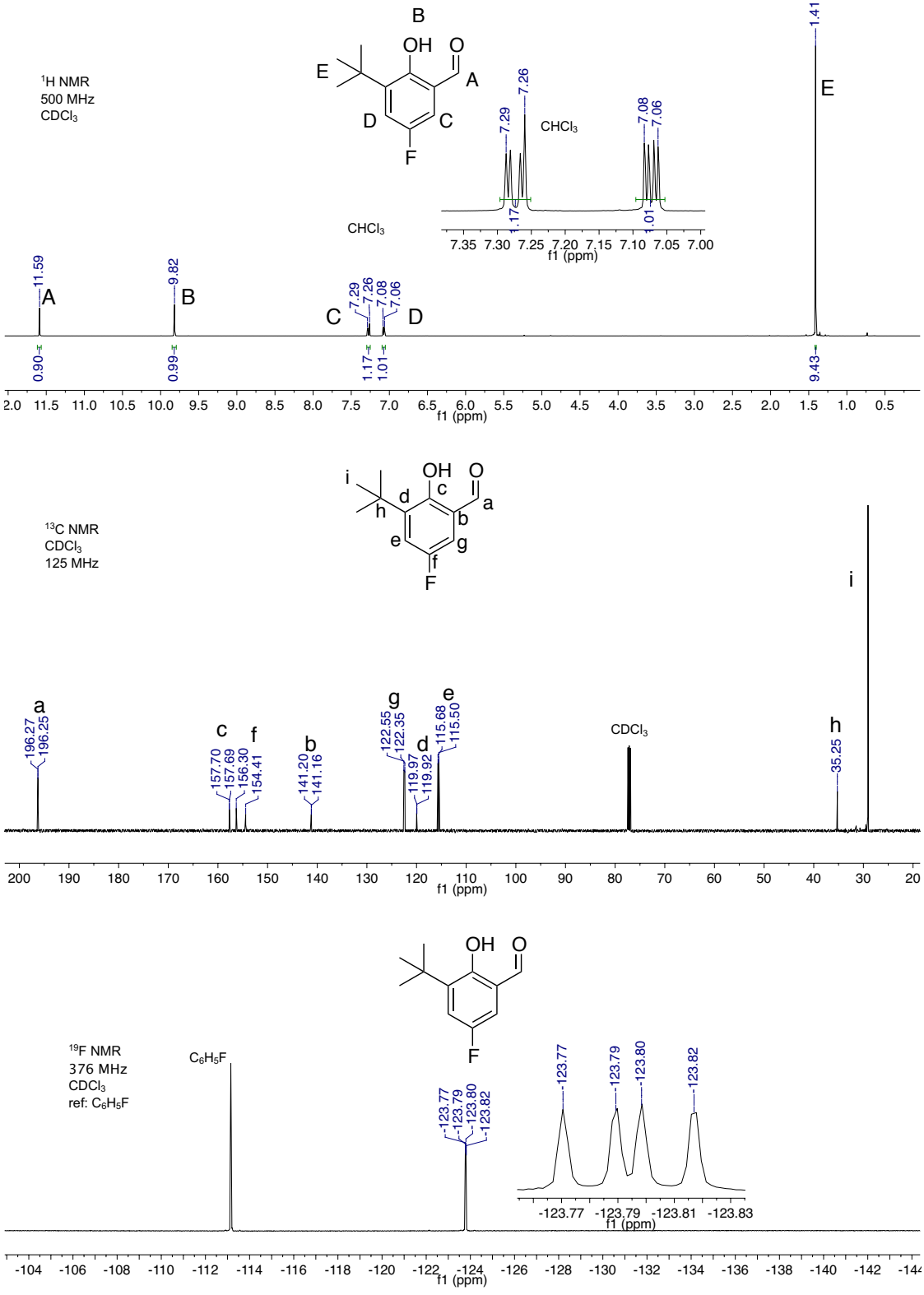


**Figure A2.1.** NMR spectra of **aldehyde5** in $CDCl_3$. Top: $^{1}H$ NMR spectrum. Middle: $^{13}C$ NMR spectrum. Bottom: $^{19}F$ NMR spectrum, referenced to fluorobenzene.

**aldehyde6**: 2-*tert*-butyl-4-chlorophenol was synthesized according to literature procedure.[3] 4-chlorophenol (Combi-Blocks, 8.00 g, 62.2 mmol) was dissolved in a solution of *tert*-butyl alcohol (Aldrich, 11.9 mL, 124.5 mmol), and 7.50 mL of concentrated $H_2SO_4$ was slowly added, turning the solution from a pale yellow to a light orange. The solution was stirred for 2 days, neutralized with $Na_2CO_3$ (aq), extracted into diethyl ether and dried over $Na_2SO_4$. The concentrated product was purified using column chromatography (95:5, hex:EtOAc) to yield a yellow oil (70% isolated yield). 2-tert-butyl-4-chlorophenol was formylated according to a modified Duff reaction as reported by Jacobsen et al.[1] The product was purified by column chromatography (90:10, hex:EtOAc) to yield a yellow crystalline solid (24% isolated yield). $^1$H NMR spectrum in ppm ($CDCl_3$, 400 MHz): δ 11.72 (s, 1H); 9.82 (s, 1H); 7.46 (d, $J$ = 2.6 Hz, 1H); 7.38 (d, $J$ = 2.6 Hz, 1H); 1.41 (s, 12H).

**aldehyde7**: 3-*tert*-butylsalicylaldehyde (96%, Aldrich) was nitrated according to literature procedure.[4] 3-*tert*-butylsalicylaldehyde (2.16 g, 12.1 mmol) was dissolved in acetic acid, a solution of $HNO_3$ (0.82 mL, 12.2 mmol) in 10 mL of acetic acid was added slowly. The solution changed to a deep orange. After stirring for 6 h, saturated $Na_2CO_3$ was carefully added and the product was extracted into dichloromethane. The product was purified by column chromatography (80:20, hex:EtOAc) to yield an orange crystalline solid (60% isolate yield). $^1$H NMR spectrum in ppm ($CDCl_3$, 400 MHz): δ 12.43 (s, 1H); 9.96 (s, 1H); 8.41 (s, 2H); 1.46 (s, 9H).

### 3.2. N,N'-bis(3-tertbutyl-5-R-salicylidine)-1,2-cyclohexadiimine Syntheses

For previously reported compounds, $^1$H NMR assignments are included. Full assignments for the unreported **salcy5** are included. All reported yields represent average isolated yields.

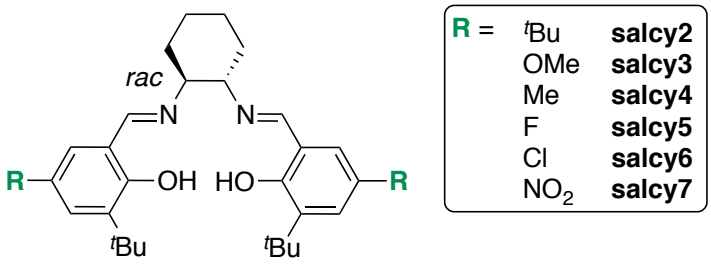


**General procedure for salcy2**: Salcy2 was prepared according to literature procedure and the $^1$H NMR spectrum of the product matched well with literature.[4] 3-5-di-*tert*-butylsalicylaldehyde (0.50 g, 0.91 mmol) was dissolved in ethanol (7 mL) at 80 °C. Trans-1,2-diaminocyclohexane (54.90 µL, 0.46 mmol) was added to the salicylaldehyde solution and the solution was refluxed at 80 °C overnight. Upon cooling and addition of minimal $dH_2O$, the ligand precipitated. The precipitate was collected by filtration and dried under vacuum (85% isolated yield). $^1$H NMR spectrum ($CDCl_3$, 400 MHz): δ 13.71 (s, 2H); 8.30 (s, 2H); 7.30 (d, $J$ = 2.5 Hz, 2H); 6.98 (d, $J$ = 2.5 Hz, 2H); 3.32 (bm, 2H); 1.95 (bm, 2H), 1.89 (bm, 2H); 1.73 (bm, 2H); 1.47 (bm, 2H); 1.41 (s, 18H); 1.23 (s, 18H).

**salcy3**: Synthesized according to the general procedure detailed above except this ligand was extracted from the crude reaction mixture into $CH_2Cl_2$, washed with saturated $NH_4Cl$ and brine, dried over $Na_2SO_4$ and concentrated to yield clean product. The $^1$H NMR spectrum of the product matched well with literature report. Yellow powder (83% isolated yield) matched well with lierature. $^1$H NMR spectrum ($CDCl_3$,

400 MHz): δ 13.46 (s, 2H); 8.23 (s, 2H); 6.89 (dd, *J* = 1.1, 2.9 Hz, 2H); 6.47 (dd, *J* = 1.1, 2.9 Hz); 2H); 3.68 (s, 6H); 1.98 (bm, 2H); 1.88 (bm, 2H); 1.75 (bm, 2H); 1.47 (bm, 2H); 1.39 (s, 18H).

**salcy4**: Synthesized according to the general procedure detailed above. 1H NMR spectrum of the light yellow powder (83% isolated yield) matched well with literature report.[1] $^{1}$H NMR spectrum ($CDCl_3$, 400 MHz): δ 13.63 (s, 2H); 8.22 (s, 2H); 7.04 (m, 2H); 6.78 (m, 2H); 3.30 (m, 2H); 2.19 (s, 6H); 1.97 (bm, 2H); 1.88 (bm, 2H); 1.74 (bm, 2H); 1.46 (bm, 2H); 1.40 (s, 18H) ppm. $^{13}$C NMR spectrum ($CDCl_3$, 100 MHz): 165.65; 158.09; 136.85; 130.36; 129.84; 126.55; 118.42; 72.55; 34.78; 33.26; 29.51; 24.28; 20.70.

**salcy5**: Synthesized according to the general procedure detailed above except this ligand was extracted from the crude reaction mixture in $CH_2Cl_2$, washed with saturated $NH_4Cl$ and brine, dried over $Na_2SO_4$ and concentrated to yield clean product. The $^{1}$H NMR spectrum of the product matched well with literature report.[1] Yellow powder (75% isolated yield). $^{1}$H NMR spectrum ($CDCl_3$, 500 MHz): δ 13.58 s, (2H); 8.20 (s, 2H); 6.99 (dd, *J* = 3.09, 10.81 Hz, 2H); 6.67 (dd, *J* = 3.09, 7.85 Hz, 2H); 3.33 (m, 2H); 1.99 (m, 2H); 1.90 (m, 2H); 1.75 (m, 2H); 1.48 (m, 2H); 1.38 (s, 18H). $^{13}$C NMR spectrum ($CDCl_3$, 125 MHz): δ 164.79-164.77 (d, *J* = 2.9 Hz); 156.50-156.49 (d, *J* = 1.4 Hz); 158.8-154.01 (d, *J* = 234.6 Hz); 139.50-139.46 (d, *J* = 5.8 Hz); 118.10-118.04 (d, *J* = 7.7 Hz); 117.21-117.02 (d, *J* = 24.2 Hz); 114.25-114.07 (d, *J* = 22.7 Hz); 72.54; 35.10; 33.06; 29.21; 24.36. $^{19}$F NMR spectrum ($CDCl_3$, 376 MHz): δ -126.51 (dd, *J* = 7.8, 10.7 Hz, 1F).

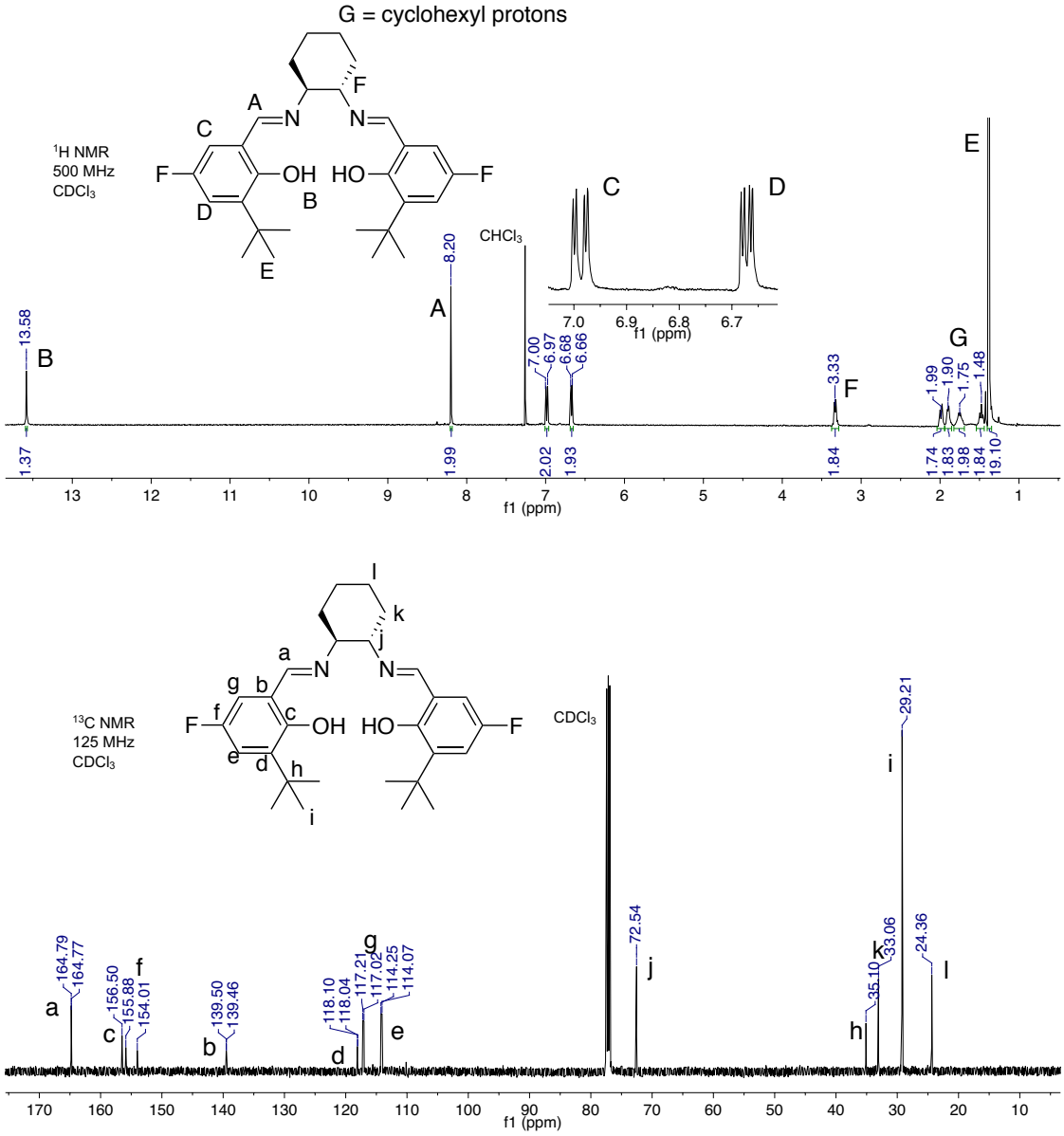
G = cyclohexyl protons
$^{1}$H NMR
500 MHz
$CDCl_3$
A
B
C
D
E
F
G
$CHCl_3$
13.58
8.20
7.00
6.97
6.68
6.66
3.33
1.99
1.90
1.75
1.48
1.37
1.99
2.02
1.93
1.84
1.74
1.83
1.98
1.84
19.10
f1 (ppm)
$^{13}$C NMR
125 MHz
$CDCl_3$
$CDCl_3$
164.79
164.77
156.50
155.88
154.01
139.50
139.46
118.10
118.04
117.21
117.02
114.25
114.07
72.54
35.10
33.06
29.21
24.36
f1 (ppm)

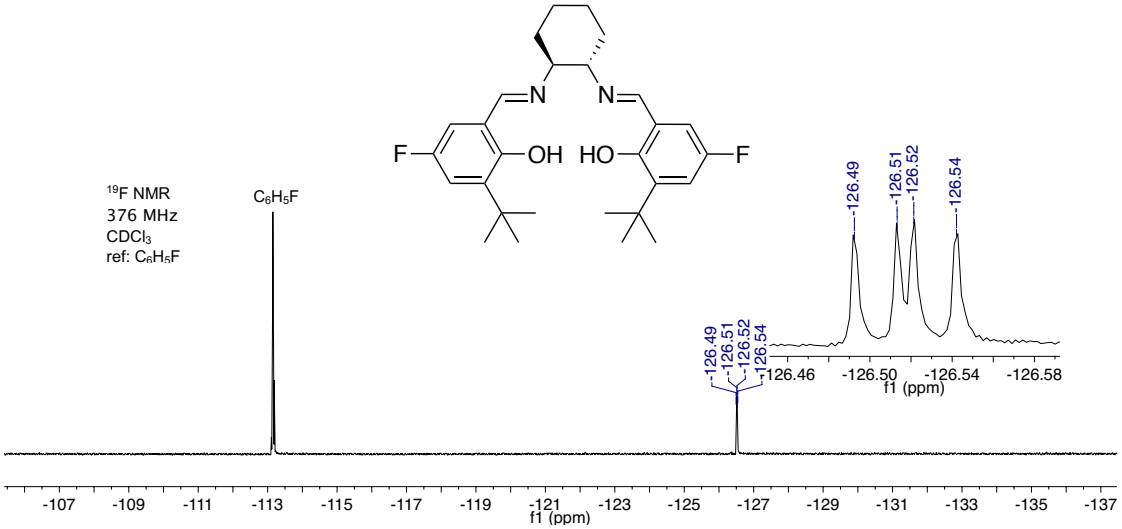


**Figure A2.2.** NMR spectra of **salcy5** in $CDCl_3$. Top: $^{1}H$ NMR spectrum. Middle: $^{13}C$ NMR spectrum. Bottom: $^{19}F$ NMR spectrum referenced to fluorobenzene as an internal standard.

**salcy6**: Synthesized according to the general procedure detailed above and the $^{1}H$ NMR spectrum of the product matched well with literature report.[1] Yellow powder (80% isolated yield). $^{1}H$ NMR spectrum ($CDCl_3$, 400 MHz): δ 13.81 (s, 2H); 8.18 (s, 2H); 7.18 (d, $J$ = 2.5 Hz, 2H); 6.95 (d, $J$ = 2.5 Hz, 2H); 3.31 (m, 2H); 1.99 (bm, 2H); 1.90 (bm, 2H); 1.75 (bm, 2H); 1.48 (bm, 2H); 1.39 (s, 18H).

**salcy7**: Synthesized according to the general procedure detailed above and the $^{1}H$ NMR spectrum of the product matched well with literature report.[1] Light orange/yellow solid (85% isolate yield). $^{1}H$ NMR spectrum ($CDCl_3$, 400 MHz): δ 15.02 (s, 2H); 8.35 (s, 2H); 8.16 (d, $J$ = 2.7 Hz, 2H); 8.00 (d, $J$ = 2.7 Hz, 2H); 3.46 (bm, 2H); 2.09 (bm, 2H); 1.97 (bm, 2H); 1.82 (bm, 2H); 1.54 (bm, 2H); 1.40 (s, 18H).

### 3.3. Cobalt Complexes

Note: In some spectra a molecule of ethanol is present which remained after drying under vacuum at 45 °C. Residual water is from the solvent. All catalyst NMRs are included and are consistent with reported known analogues. HR/MS values are reported for the (salcy)Co fragments without the $NO_3$ counterion which is lost during analysis.

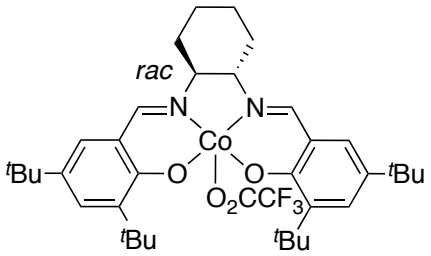


**cat1**: (salcy)$CoO_2CCF_3$ was synthesized according to a modified procedure adapted from the synthesis of (salcy)$CoO_2CCH_3$ reported by Jacobsen et al.[5] except that trifluoroacetic acid was used instead of acetic acid. The compound was rinsed thoroughly with pentane and isolated as a light brown powder (80% yield). $^1$H NMR spectrum ($C_5D_5N$, 400 MHz): δ 8.72 (2H), 7.76 (2H); 7.66 (2H); 3.92 (2H); 3.06 (2H); 2.03 (2H); 1.84 (2H); 1.67 (s, 18H); 1.47 (2H); 1.27 (s, 18H). $^{13}$C NMR spectrum ($C_5D_5N$, 125 MHz): 168.01; 162.60; 144.20; 138.10; 136.38; 132.21; 120.67; 124.36; 117.72; 71.52; 36.79; 34.61; 31.88; 31.11; 30.66; 25.36. HR/MS: calculated 603.34 g/mol; found 603.34 g/mol.

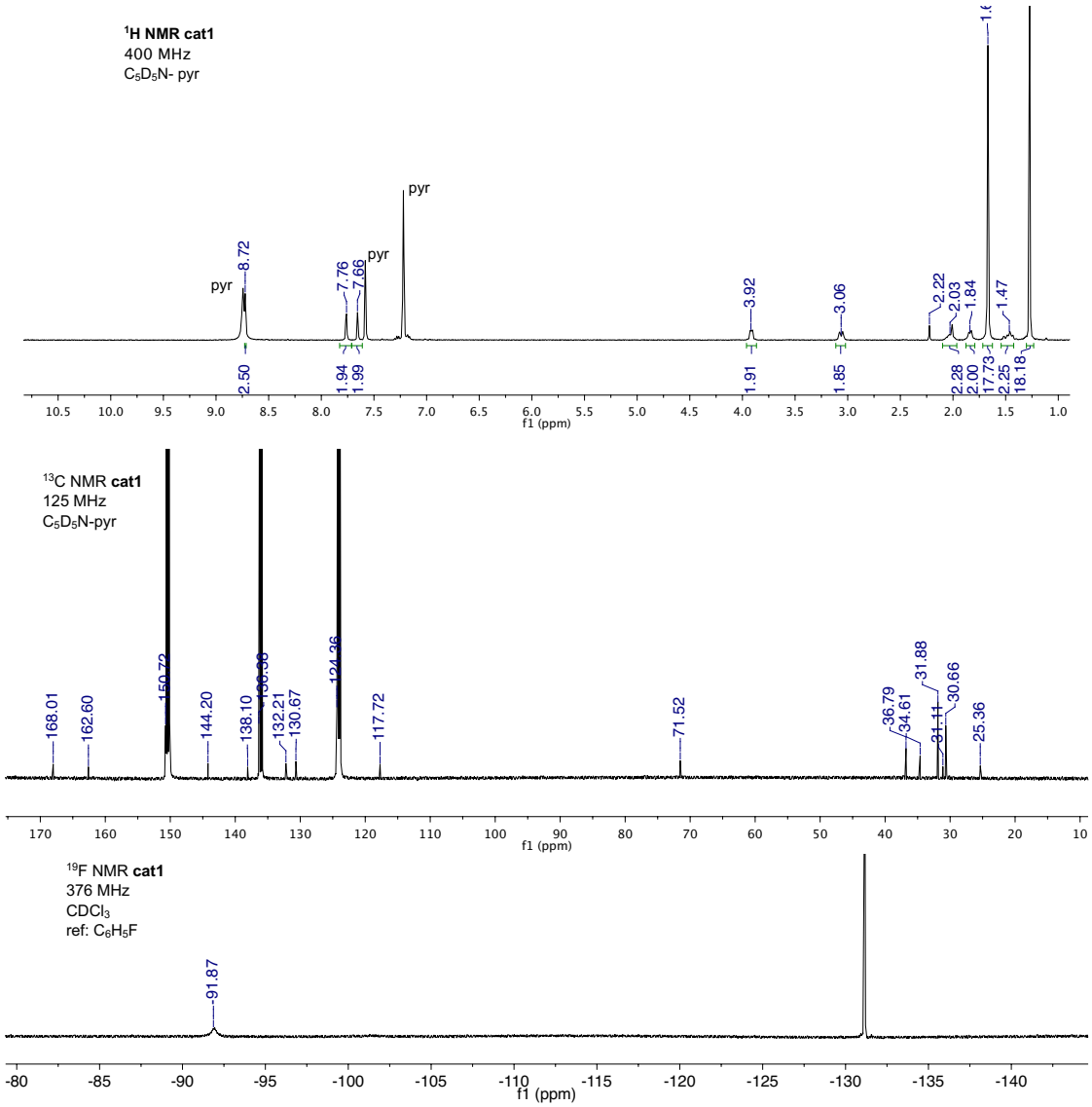


**Figure A2.3.** NMR spectra for **cat1** in pyridine-$d_5$. Top: $^{1}$H NMR spectrum. Middle: $^{13}$C NMR spectrum. Bottom: $^{19}$F NMR spectrum.

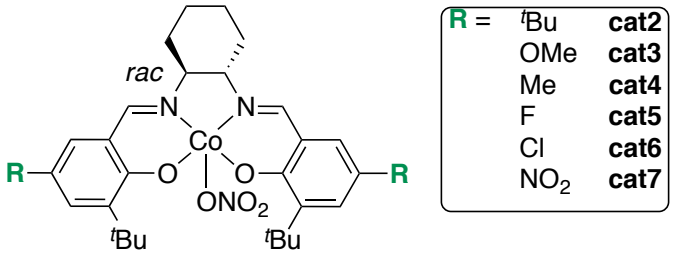


| R = | | |
|---|---|---|
| | $^{t}$Bu | **cat2** |
| | OMe | **cat3** |
| | Me | **cat4** |
| | F | **cat5** |
| | Cl | **cat6** |
| | $NO_2$ | **cat7** |

**Representative synthesis for cat2**: After rigorous drying, a solution of **salcy2** (0.30 mg, 0.55 mmol) was made in dry, degassed dichloromethane. 1.1 equivalents of

$Co(NO)_3 \bullet 6H_2O$ (99% purity Strem, 0.17 mg, 0.60 mmol) was desiccated in a flame dried Schlenk flask under vacuum at 60 °C while being crushed by a stir bar. When the red crystals turned to light pink powder, a solution was made in dry, degassed ethanol. The purple Co/EtOH solution was slowly added to the yellow ligand solution and turned red upon mixing. The red solution was allowed to stir for 1 h and then was opened to air that is diffused through a tube filled with desiccant on top to allow oxidation. After 12 h, the solution was filtered and solvent was removed under vacuum. The resulting powder was rinsed rigorously with pentane until the filtrate was clear, collected, and further dried under vacuum. (80% yield). $^{1}$H NMR spectrum ($C_5D_5N$, 500 MHz): δ 8.69 (2H); 7.73 (2H); 7.65 (2H); 3.88 (2H); 3.03 (2H); 2.02 (2H); 1.79 (2H); 1.64 (s, 18H); 1.48 (2H); 1.25 (s, 18H). $^{13}$C NMR spectrum ($C_5D_5N$, 125 MHz): δ 167.53; 162.01; 143.50; 137.45; 135.73; 131.54; 130.22; 117.25; 71.00; 36.20; 34.04; 31.34; 30.53; 30.13; 29.38; 24.83. HR/MS: calculated 603.34 g/mol; found 603.34 g/mol.

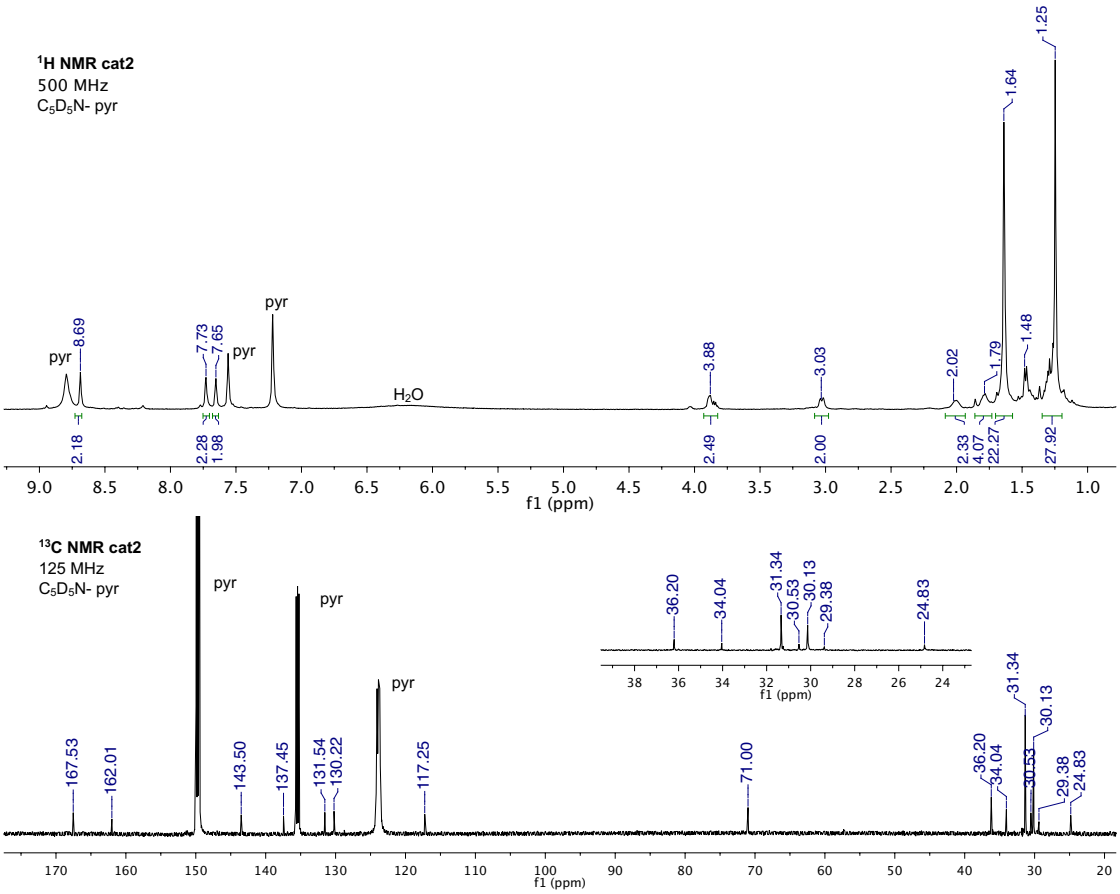


**Figure A2.4.** NMR spectra of **cat2** in pyridine-$d_5$. Top: $^{1}$H NMR spectrum. Bottom: $^{13}$C NMR spectrum with an inset to magnify the alkyl region.

**cat3**: Dark brown crystalline solid (75% isolated yield). $^{1}$H NMR spectrum ($C_5D_5N$, 500 MHz): δ 8.62 (2H); 7.30 (2H); 7.17 (2H); 3.82 (2H); 3.73 (6H); 3.03 (2H); 2.00 (2H); 1.76 (2H); 1.50 (18H); 1.40 (2H). $^{13}$C NMR spectrum ($C_5D_5N$, 125 MHz): δ 166.71; 158.89; 145.25; 135.70; 125.08; 116.41; 112.56; 70.89; 55.51; 35.94; 30.48; 29.76; 24.77. HR/MS: calculated 551.23 g/mol; found 551.23 g/mol.

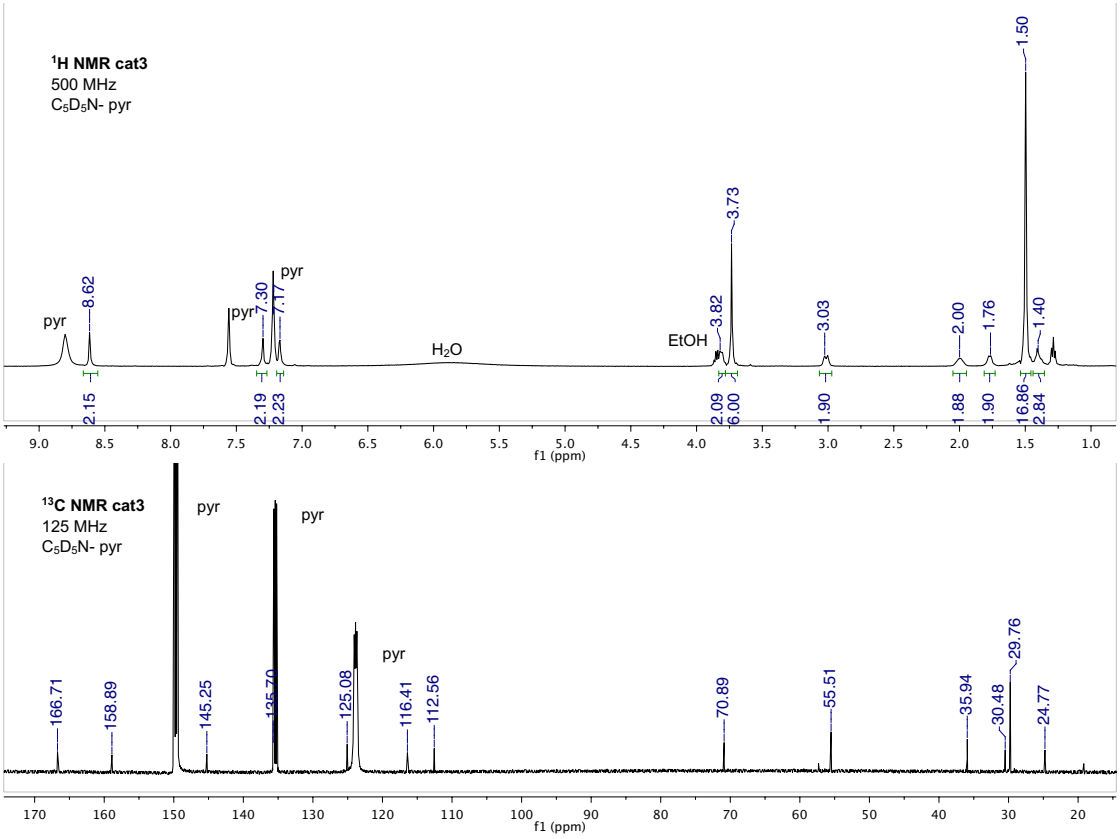


**Figure A2.5.** NMR spectra of **cat3** in pyridine-$d_5$. Top: $^{1}$H NMR spectrum. Bottom: $^{13}$C NMR spectrum.

**cat4**: Dark green powder (85% isolated yield). $^{1}$H NMR spectrum ($C_5D_5N$, 500 MHz): δ 8.47 (2H); 7.35 (2H); 7.26 (2H); 3.82 (2H); 3.00 (2H); 2.22 (6H); 2.03 (2H); 1.82 (2 H); 1.56 (18H); 1.45 (2H). $^{13}$C NMR spectrum ($C_5D_5N$, 125 MHz): δ 167.17; 162.22; 144.13; 124.35; 117.81; 71.10; 36.12; 30.54; 30.39; 30.22; 30.04; 25.12; 20.56. HR/MS: calculated 519.24 g/mol; found 519.24 g/mol.

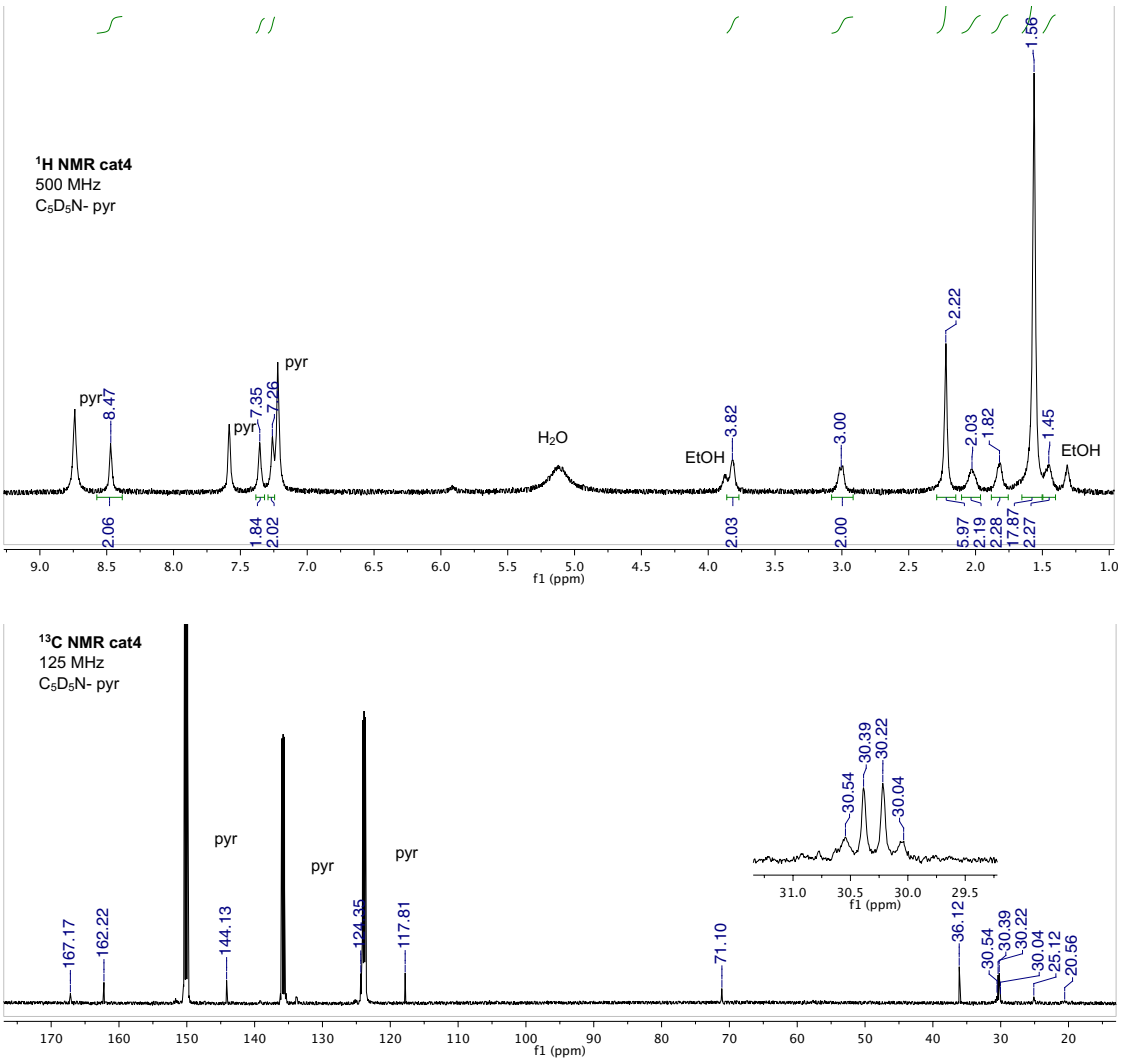


**Figure A2.6.** NMR spectra of **cat4** in pyridine-$d_5$. Top: $^{1}$H NMR spectrum. Bottom: $^{13}$C NMR spectrum with inset zoom of alkyl region.

**cat5**: Dark brown powder (82% isolated yield). $^{1}$H NMR spectrum ($C_5D_5N$, 500 MHz): δ 8.62 (2H); 7.45 (2H); 7.32 (2H); 3.86 (2H); 2.99 (2H); 2.04 (2H); 1.76 (2H); 1.47 (18H); 1.41 (2H). $^{13}$C NMR spectrum ($C_5D_5N$, 125 MHz): δ 167.14; 167.12; 160.23; 154.19; 152.35; 150.10; 145.93-145.88 (d, $J$ = 5.9 Hz); 135.76; 122.42-122.25 (d, $J$ = 24.9 Hz); 116.95-116.77 (d, $J$ = 22.1 Hz); 116.76-116.69 (d, $J$ = 8.6 Hz); 71.09;

57.37; 36.12; 30.44; 29.57; 24.75; 19.26. $^{19}$F NMR ($C_5D_5N$, 376 MHz): -129.1 (d,d, *J* = 8.6, 10.5 Hz, 2F). HR/MS: calculated 527.19 g/mol; found 527.19 g/mol.

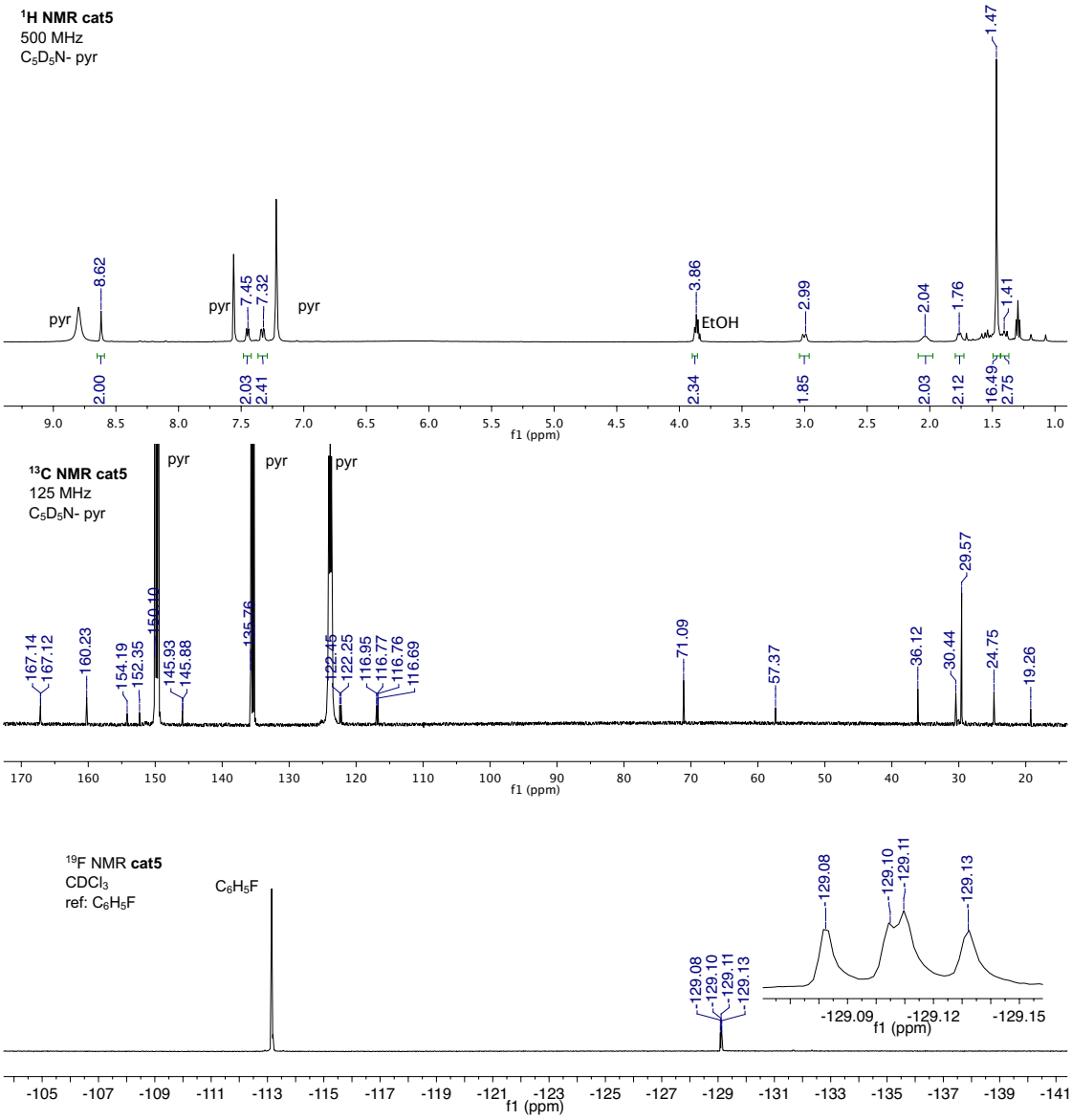


**Figure A2.7.** NMR spectra of **cat5** in pyridine-$d_5$. Top: $^{1}$H NMR spectrum. Middle: $^{13}$C NMR spectrum. Bottom: $^{19}$F NMR spectrum with internal reference fluorobenzene.

**cat6**: Dark brown/black powder (77% isolated yield). $^{1}$H NMR spectrum ($C_5D_5N$, 400 MHz): δ 8.60 (2H); 7.64 (2H); 7.39 (2H); 3.92 (2H); 3.03 (2H); 2.07 (2H); 1.74 (2H); 1.61 (2H); 1.45 (2H); 1.40 (18H). $^{13}$C NMR spectrum ($C_5D_5N$, 125 MHz): δ 166.72; 161.85; 145.48; 135.14; 132.87; 132.22; 119.37; 118.24; 70.73; 56.83; 35.52; 30.00; 29.04; 24.23; 18.70. HR/MS: calculated 559.13 g/mol; found 559.13 g/mol.

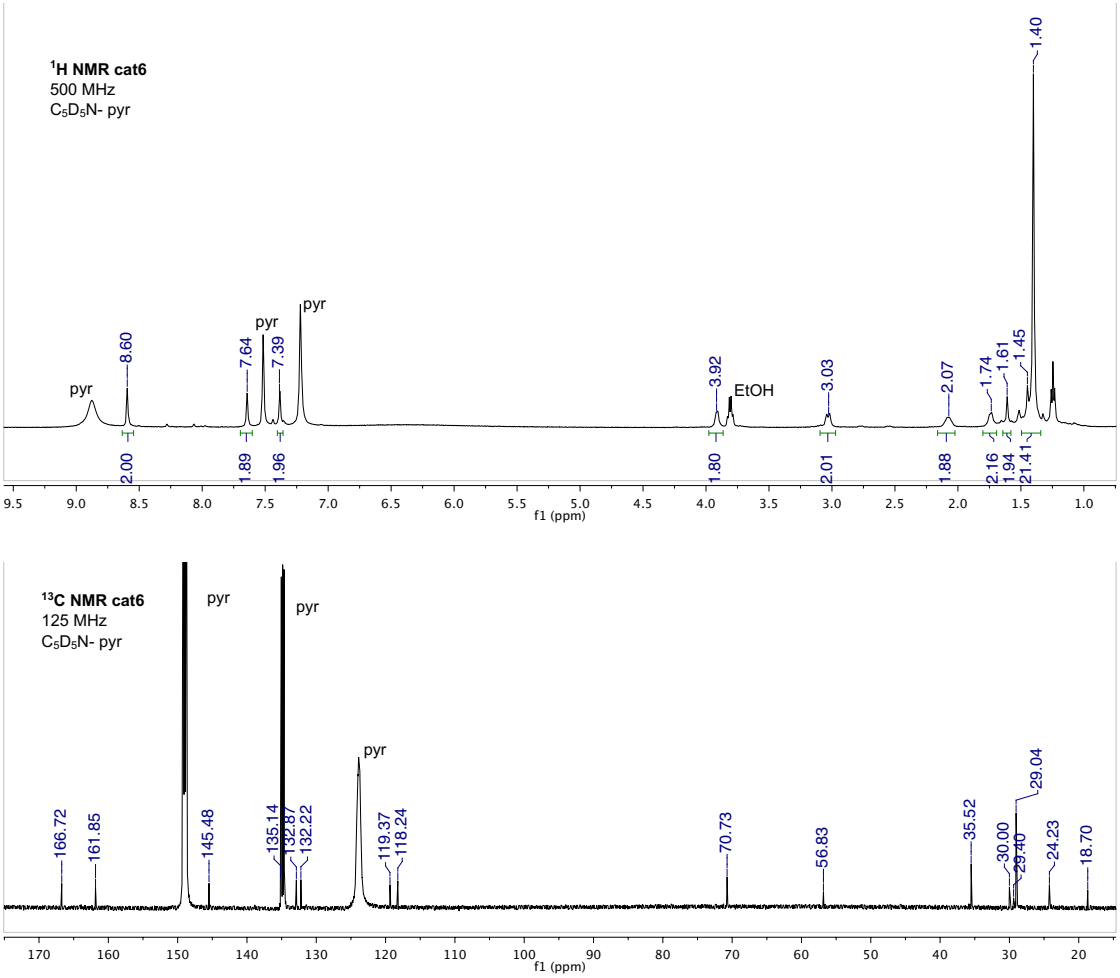


**Figure A2.8.** NMR spectra of **cat6** in pyridine-$d_5$. Top: $^{1}$H NMR spectrum. Bottom: $^{13}$C NMR spectrum.

**cat7**: Light brown/amber powder (70% isolated yield). $^{1}$H NMR spectrum ($C_5D_5N$, 400 MHz): δ 8.97 (2H); 8.76 (2H); 8.23 (2H); 4.16 (2H); 3.20 (2H); 2.25 (2H); 1.78

(2H); 1.61 (2H) 1.46 (18H). $^{13}$C NMR spectrum ($C_5D_5N$, 125 MHz): δ168.87; 168.73; 144.35; 137.24; 135.04; 132.49; 126.82; 117.60; 71.78; 57.26; 35.97; 30.54; 29.56; 29.26; 24.60; 19.15. HR/MS: calculated 581.18 g/mol; 581.18 g/mol.

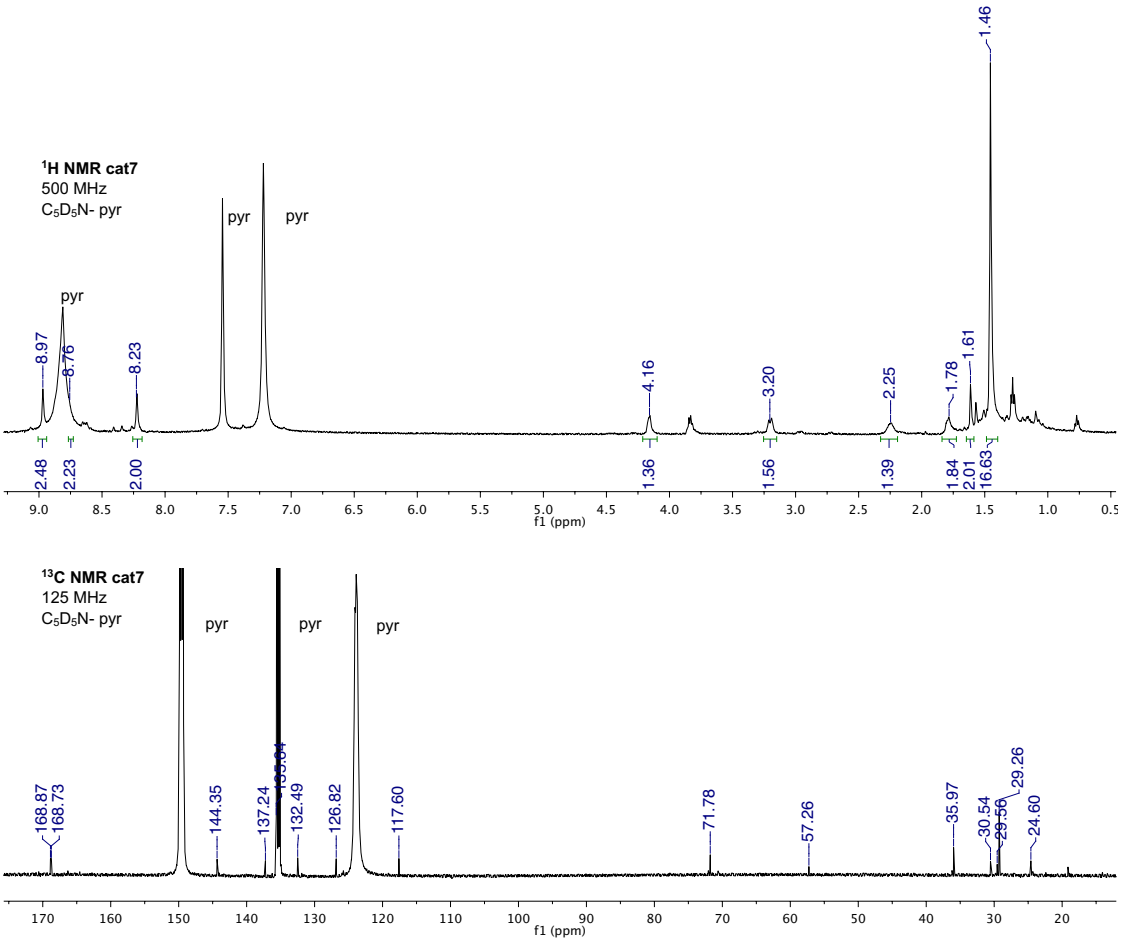


**Figure A2.9.** NMR spectra of **cat7** in pyridine-$d_5$. Top: $^{1}$H NMR spectrum. Bottom: $^{13}$C NMR spectrum.

### 3.4. [PPN][X] Salts

**[PPN][$NO_3$]**: [PPN]Cl (3.0 g, 5.2 mmol) was dissolved in 50 mL of $dH_2O$ at 50 °C. When completely dissolved, an excess of concentrated $HNO_3$ (0.3 mL) was added via syringe. A white precipitate immediately formed and the slurry was stirred for 1 h at

50 °C. The mixture was filtered using a fine frit to and the white solid was washed generously with warm water to remove any residual acid and [PPN]Cl. The precipitate was collected, dried under vacuum at 60 °C for 24 h (2.95 g, 95% isolated yield). Purity was determined by $^{1}$H NMR spectroscopy to detect removal of water and the presence of one set of aryl peaks. A melting point of 230 °C was measured using differential scanning calorimetry. This value matched well with the reported melting point from literature.[6]

**[PPN][$O_2CCF_3$]**: Synthesized according to literature procedure for [PPN][$O_2CC_6F_5$]. Trifluoroacetic acid (0.8 mL, 10 mmol) was stirred with NaOH (0.44 g, 10 mmol) in 10 mL of $dH_2O$ until homogenous. [PPN]Cl was heated in 60 mL of deionized $H_2O$ until dissolved. The solution of Na[$O_2CCF_3$] in $dH_2O$ was added to the dissolved solution of [PPN][Cl] and a white precipitate formed. The solution was stirred under heat for another 10 minutes, hot filtered, and the solid was collected. The white powder was dried under vacuum at 60 °C overnight. NMR spectropscopy was used to confirm purity based on diagnostic fluorine signals. $^{1}$H NMR ($CDCl_3$, 400 MHz): δ 7.66 (m, 6); 7.46 (m, 24). $^{19}$F NMR ($CDCl_3$, 376 MHz): δ 74.6 (s, 3F).

### A2.4. Representative Copolymerization Procedure

**Poly(propylene maleate)** (Figure 3.2). In a glovebox, catalyst (0.01 mmol), [PPN][$NO_3$] (6.0 mg, 0.01 mmol) and maleic anhydride (**2a**) (98.0 mg, 1.00 mmol) were measured into a flame dried 4.0 mL vial equipped with a Teflon coated stir bar. Propylene oxide (**1a**) (0.14 mL, 2.0 mmol) was added via syringe with care to wash all solids into the base of the vial. The vial was sealed with a Teflon lined cap, removed from the glovebox, and placed in an aluminum heat block preheated to the desired temperature (30 °C). After the reaction became viscous or all visible anhydride monomer disappeared, the vial was removed from the heat block, the mixture was dissolved in $CH_2Cl_2$, and a small aliquot was analyzed by $^1$H NMR spectroscopy for conversion. The mixture was then dissolved in dichloromethane and precipitated into an excess of hexanes. This process was repeated until all residual monomer was removed. For polyesters containing phthalic anhydride, methanol was used as a non-solvent. After several rounds of precipitation, the material was collected and dried *in vacuo*.

**4.1. NMR Spectra and Peak Assignments for Polyesters in Table 2**

**Poly(propylene maleate)**, (Table 2, entry 1). $^{1}$H NMR spectrum ($CDCl_3$, 400 MHz): δ 6.26 (leaning d, 2H); 5.24 (m, 1H); 4.24 (m, 2H); 1.31 (d, $J$ = 5.8 Hz, 3H). $^{13}$C NMR spectrum ($CDCl_3$, 125 MHz): δ 164.82, 164.54; 130.57-130.51 (d), 129.46-129.39 (d), 69.28; 66.49; 16.32.

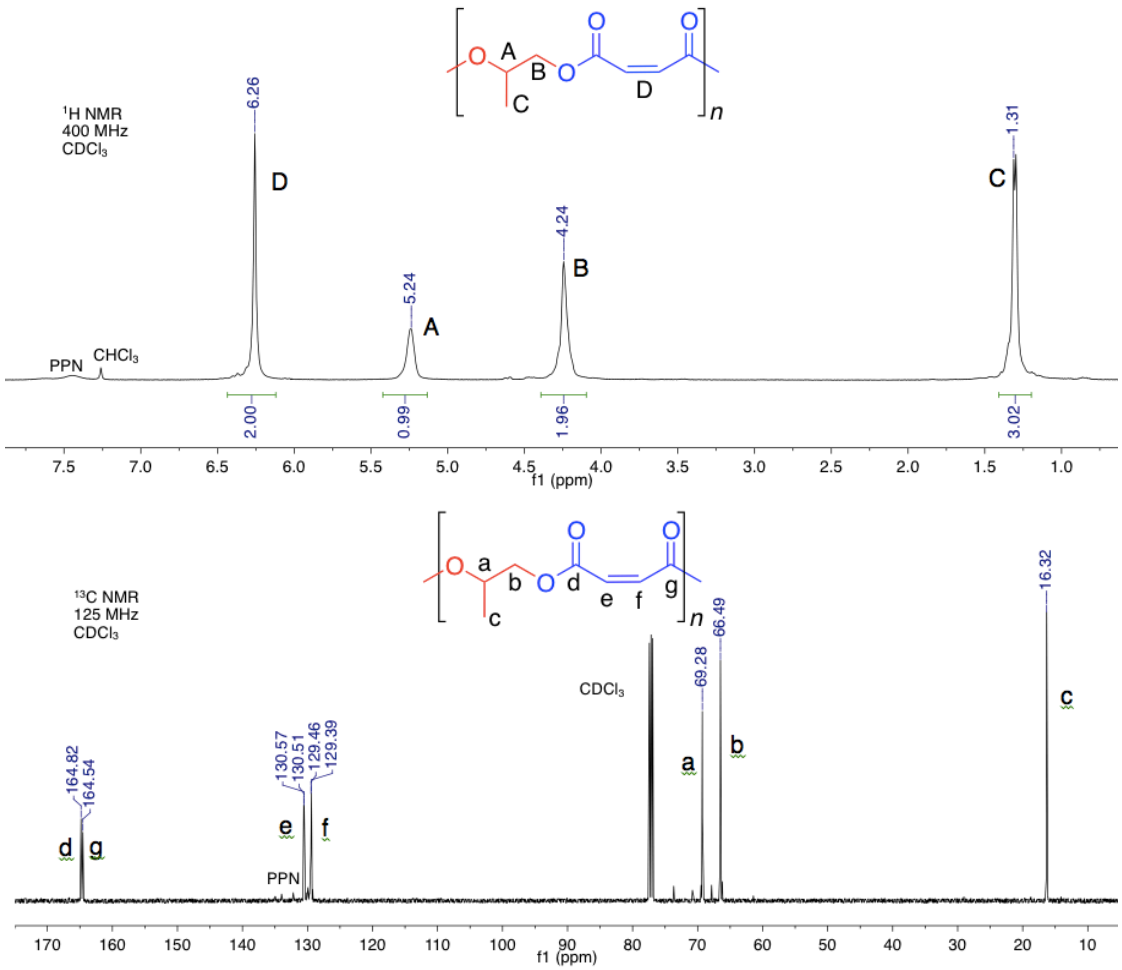


**Figure A2.10.** Poly(propylene-*alt*-maleate) in $CDCl_3$. Top: $^{1}$H NMR spectrum. Bottom: $^{13}$C NMR spectrum. Note: residual PPN salts and end groups are visible in both spectra.

**Poly(1-butene-*alt*-maleate)**, (Table 2, entry 2). $^{1}$H NMR spectrum ($CDCl_3$, 500 MHz): δ 6.26 (m, 2H); 5.11 (m, 1H); 4.31-4.25 (bm, 2H); 1.68 (m 2H); 0.94 (t, $J$ = 7.8 Hz, 3H). $^{13}$C NMR spectrum ($CDCl_3$, 125 MHz): δ 164.93; 164.73; 130.31; 129.68; 73.76; 65.07; 23.74; 9.52.

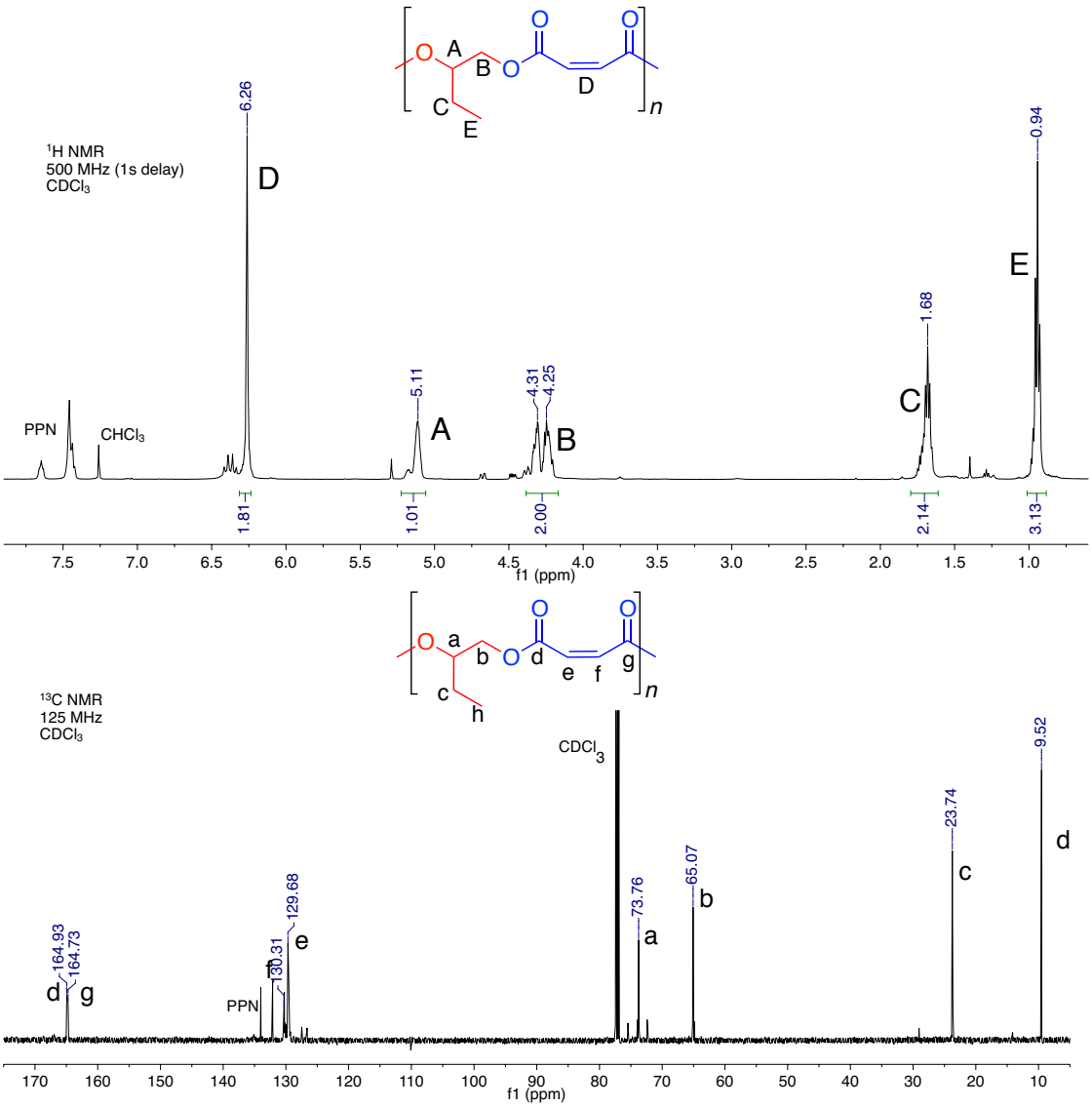


**Figure A2.10.** Poly(1-butene-*alt*-maleate) in $CDCl_3$. Top: $^{1}$H NMR spectrum. Bottom: $^{13}$C NMR spectrum. Note: residual PPN salts and end groups are visible in both spectra.

**Poly([allyloxy]butane-*alt*-maleate)**, (Table 3.2, entry 3). $^{1}$H NMR spectrum ($CDCl_3$, 500 MHz): δ 6.27 (m, 2H); 5.29 (m, 1H); 4.43-4.36 (bm, 2H); 3.60 (m, 2H); 3.44 (m, 2H); 1.52 (m, 2H); 1.34 (m, 2H); 0.89 (t, $J$ = 7.2 Hz, 3H). $^{13}$C NMR spectrum ($CDCl_3$, 125 MHz): δ 164.75; 164.54; 130.34; 129.71; 71.61; 71.25; 68.53; 63.58; 31.72; 19.34; 14.03.

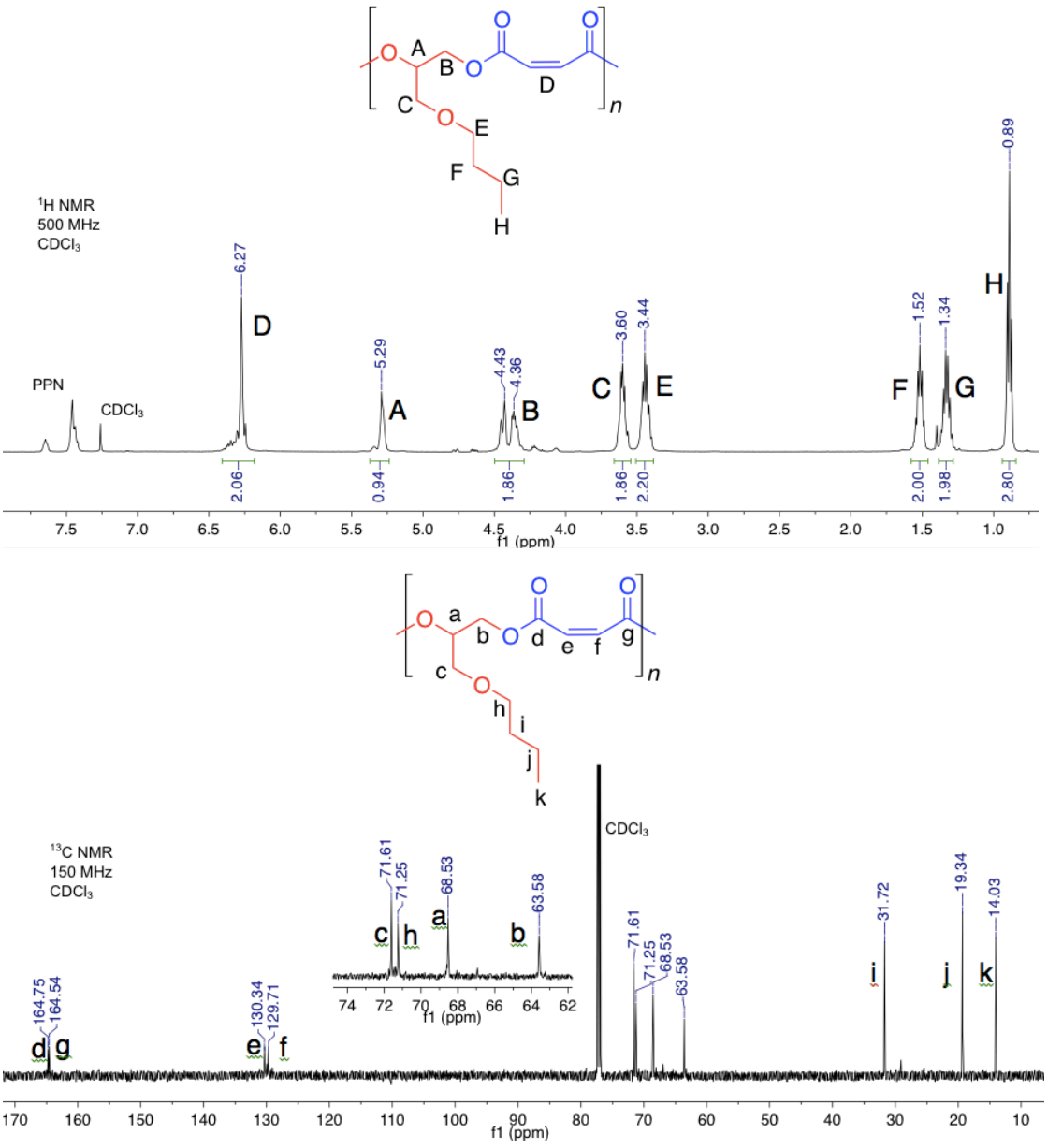


**Figure A2.12. Poly(**[allyloxy]butane-*alt*-maleate) in $CDCl_3$. Top: $^{1}$H NMR spectrum. Bottom: $^{13}$C NMR spectrum.

**Poly([allyloxy]methacrylate-*alt*-maleate)**, (Table 2, entry 4). $^{1}$H NMR spectrum ($CDCl_3$, 500 MHz): δ 6.11 (m, 2H); 5.99 (1H); 5.43 (1H); 5.31 (m, 1H); 4.23 (bm, 4H); 1.79 (s, 3H). $^{13}$C NMR spectrum ($CDCl_3$, 125 MHz): δ 166.51; 164.32; 164.01; 135.63; 129.81; 129.77; 126.27; 69.79; 62.66; 62.11; 18.10.

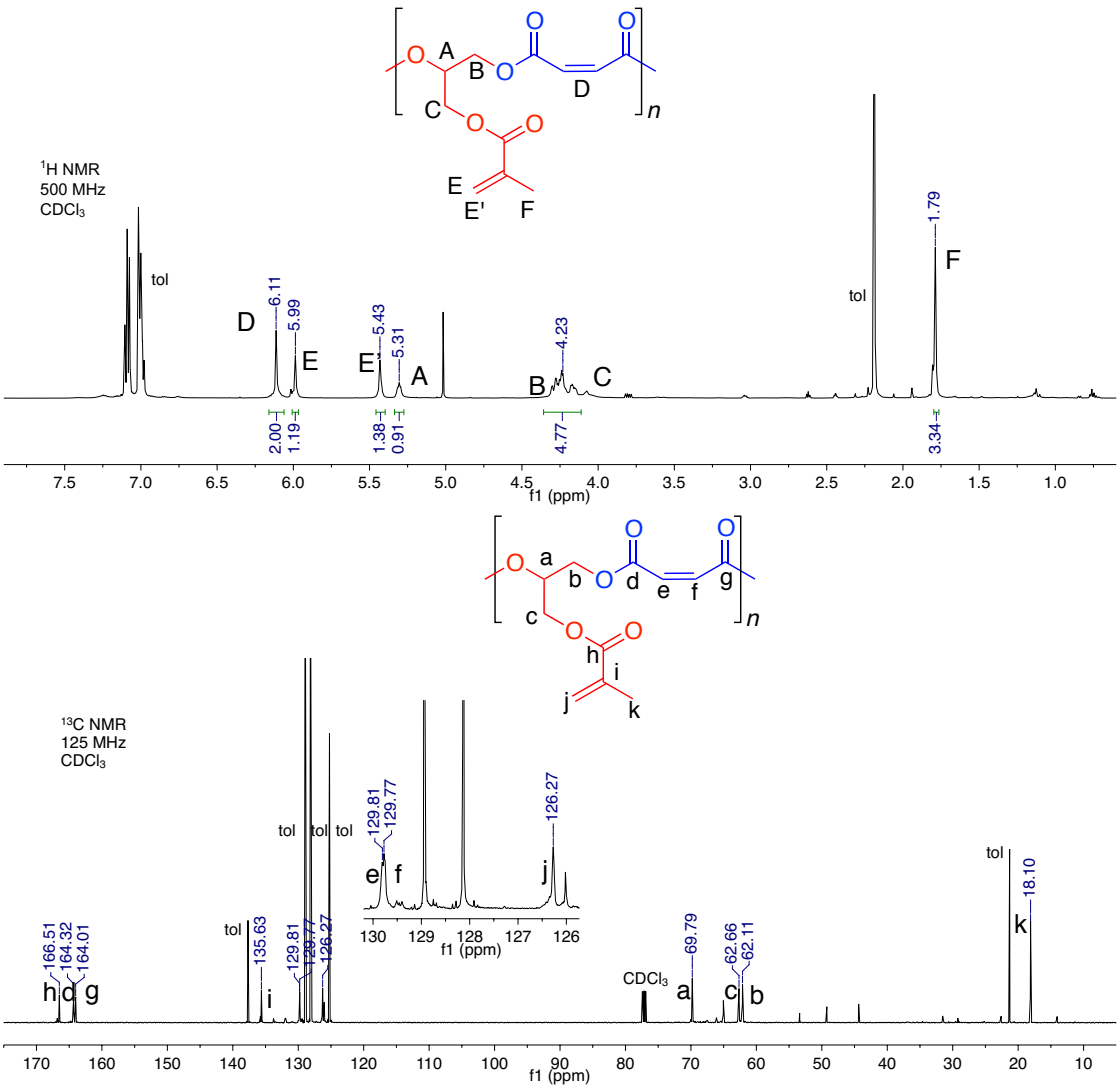


**Figure A2.11.** Poly([allyloxy]methacrylate-*alt*-maleate) in $CDCl_3$. Top: $^{1}$H NMR spectrum. Bottom: $^{13}$C NMR spectrum. Note: To prevent crosslinking, this polymer was stored dilute in toluene with BHT, visible in the spectra. Residual PPN salts (7.5 ppm), and end groups are apparent in both spectra.

**Poly([allyloxy]benzene-*alt*-maleate)**, (Table 2, entry 5). $^{1}$H NMR spectrum ($CDCl_3$, 500 MHz): δ 7.27 (bm, 2H); 6.96 (bm, 1H); 6.91 (bm, 2H); 6.28 (m, 2H); 5.47 (m, 1H); 4.50 (m, 2H); 4.14 (m, 2H). $^{13}$C NMR spectrum ($CDCl_3$, 150 MHz): δ 164.64; 164.43; 158.23; 130.10; 129.89; 129.65; 121.51; 114.70; 70.57; 65.65; 63.12.

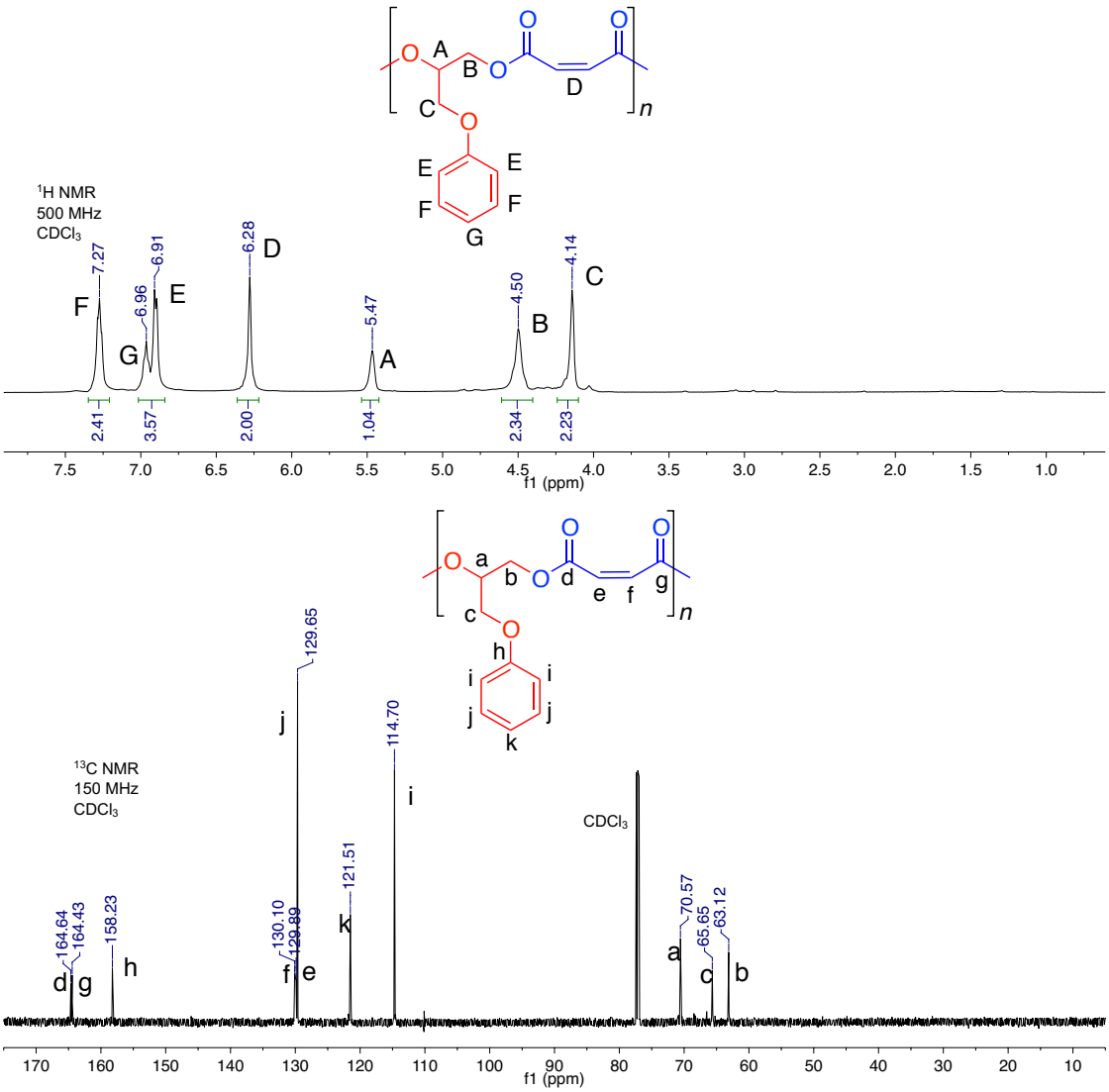


**Figure A2.12.** Poly([allyloxy]benzene-*alt*-maleate) in $CDCl_3$. Top: $^{1}$H NMR spectrum. Bottom: $^{13}$C NMR spectrum.

**Poly(3-chloroprop-1-ene-*alt*-maleate)**, (Table 2, entry 6). $^{1}$H NMR spectrum ($CDCl_3$, 500 MHz): δ 6.33 (m, 2H); 5.35 (m, 1H); 4.47 (m, 2H); 3.75 (m, 2H). $^{13}$C NMR spectrum ($CDCl_3$, 150 MHz): δ 164.45; 164.15; 130.09; 129.93; 71.19; 62.95; 41.85.

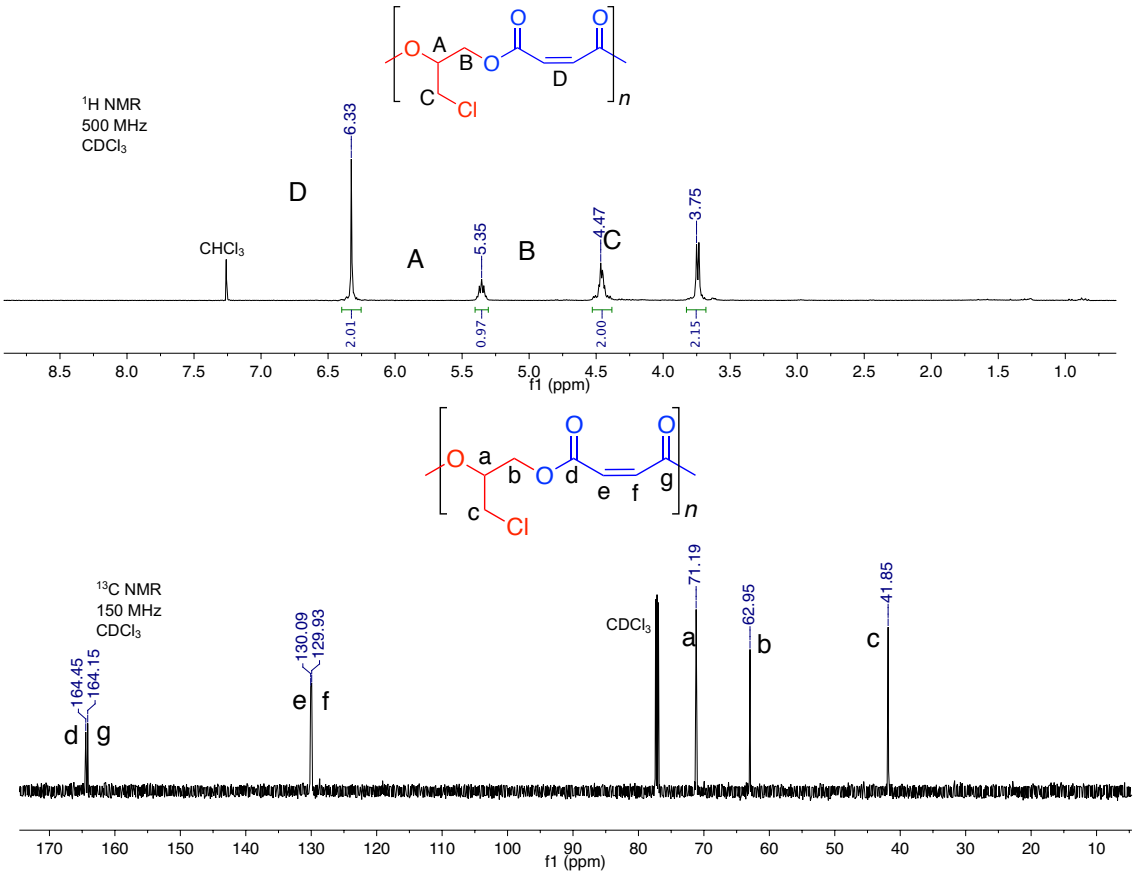


**Figure A2.13.** Poly(3-chloroprop-1-ene-*alt*-maleate) in $CDCl_3$. Top: $^{1}$H NMR spectrum. Note: residual hexanes are apparent at 0.88 and 1.26 ppm. Bottom: $^{13}$C

**Poly(1,1,1-trifluoroprop-2,3-ene-*alt*-maleate)**, (Table 2, entry 7). $^{1}$H NMR spectrum ($CDCl_3$, 500 MHz): 6.41-6.38 (d, $J$ =11.7 Hz, 1H); 6.33-6.31 (d, $J$ = 11.7 Hz, 1H); 5.63 (m, 1H); 4.61-4.40 (m, 2H). δ $^{13}$C NMR spectrum ($CDCl_3$, 125 MHz): δ 163.98; 162.85; 131.15-131.07 (d, $J$ = 9.7 Hz); 128.68; 125.87-119.17 (q, $J$ = 286.1 Hz); 68.73-67.95 (q, $J$ = 32.8 Hz); 60.44-60.37 (d, $J$ = 8.4 Hz).

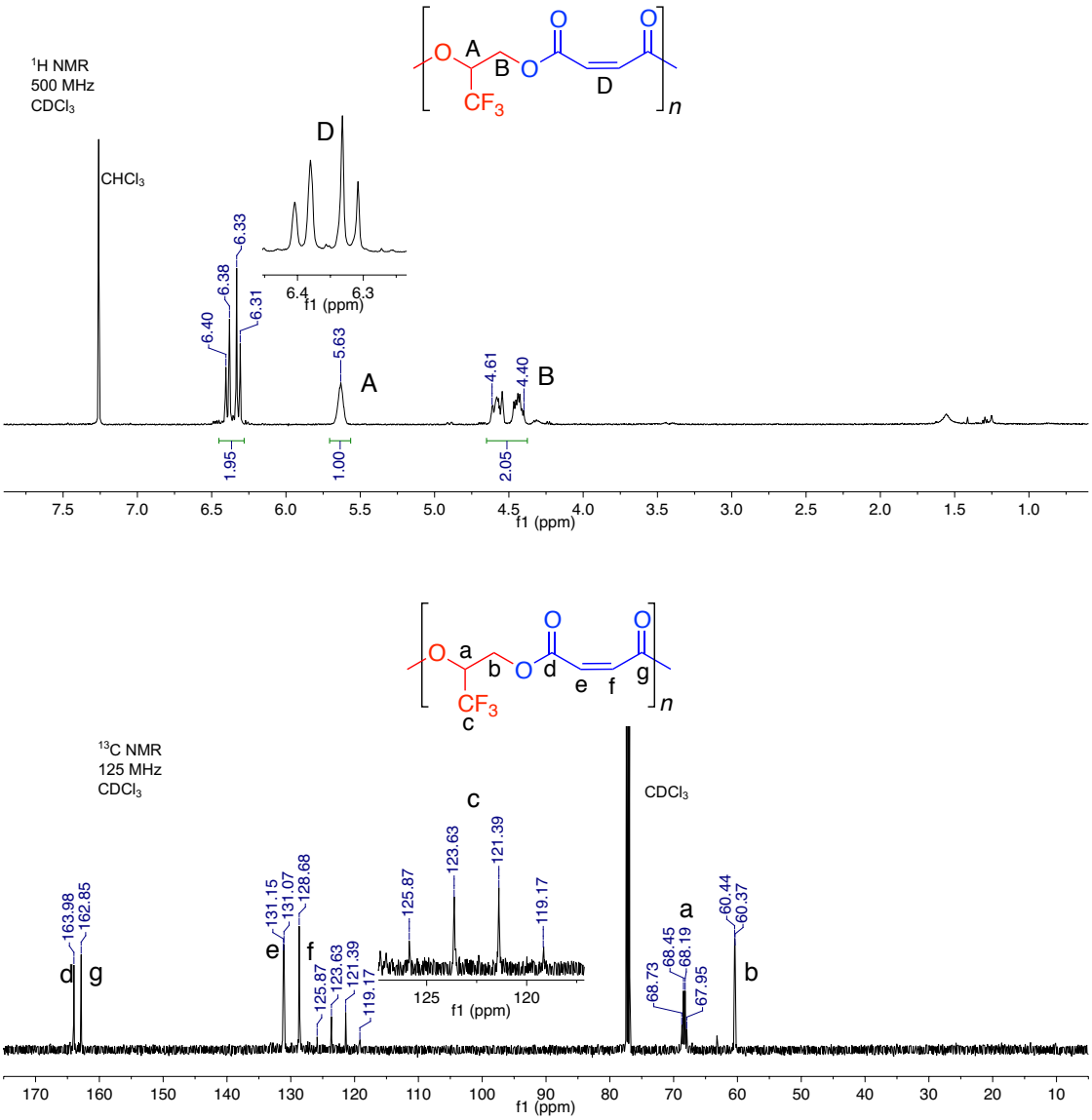


**Figure A2.14.** Poly(1,1,1-trifluoroprop-2,3-ene-*alt*-maleate) in $CDCl_3$. Top: $^{1}$H NMR spectrum. Note: water is present at 1.56 ppm. Bottom: $^{13}$C NMR spectrum.

### 4.2. NMR Spectra and Peak Assignments for Polyesters in Table 3

**Poly(propylene maleate)**, (Table 3, entry 1). Please refer to Figure A2.10.

**Poly(propylene succinate)**, (Table 3.3, entry 2). $^{1}$H NMR spectrum ($CDCl_3$, 500 MHz): δ 5.15 (m, 1H); 4.19-4.16 (dd, *J* = 2.4, 11.6 Hz, 1H); 4.10-4.06 (dd, *J* = 6.2, 11.6 Hz, 1H); 2.63 (bm, 4H); 1.25 (d, *J* = 6.2, 3H). $^{13}$C NMR spectrum ($CDCl_3$, 150 MHz): δ 172.03; 171.68; 68.60; 66.21; 29.17; 28.90; 16.45.

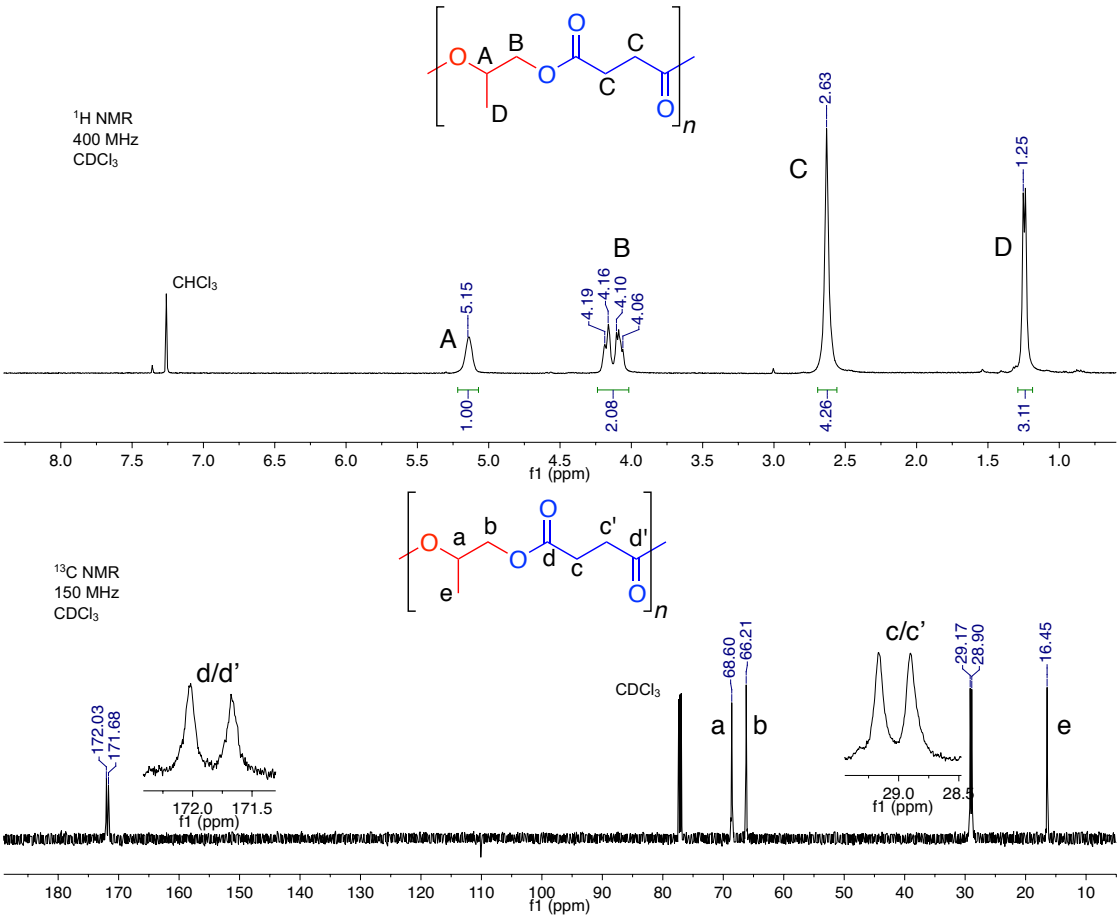


**Figure A2.15.** NMR spectra of poly(propylene succinate) in $CDCl_3$. Top: $^{1}$H NMR spectrum. Bottom: $^{13}$C NMR spectrum with insets of carbonyl and alkyl carbons of the

**Poly(propylene diglycolate)**, (Table 3.3, entry 3). $^{1}$H NMR spectrum ($CDCl_3$, 500 MHz): δ 5.24 (bm, 1H); 4.32 (bm, 1H); 4.22 (d, $J$ = 13.3 Hz, 4H); 4.12 (bm, 1H); 1.28 (d, $J$ = 6.6 Hz, 3H). $^{13}$C NMR spectrum ($CDCl_3$, 125 MHz): δ 169.59; 169.27; 69.08; 68.21; 68.02; 66.36; 16.52.

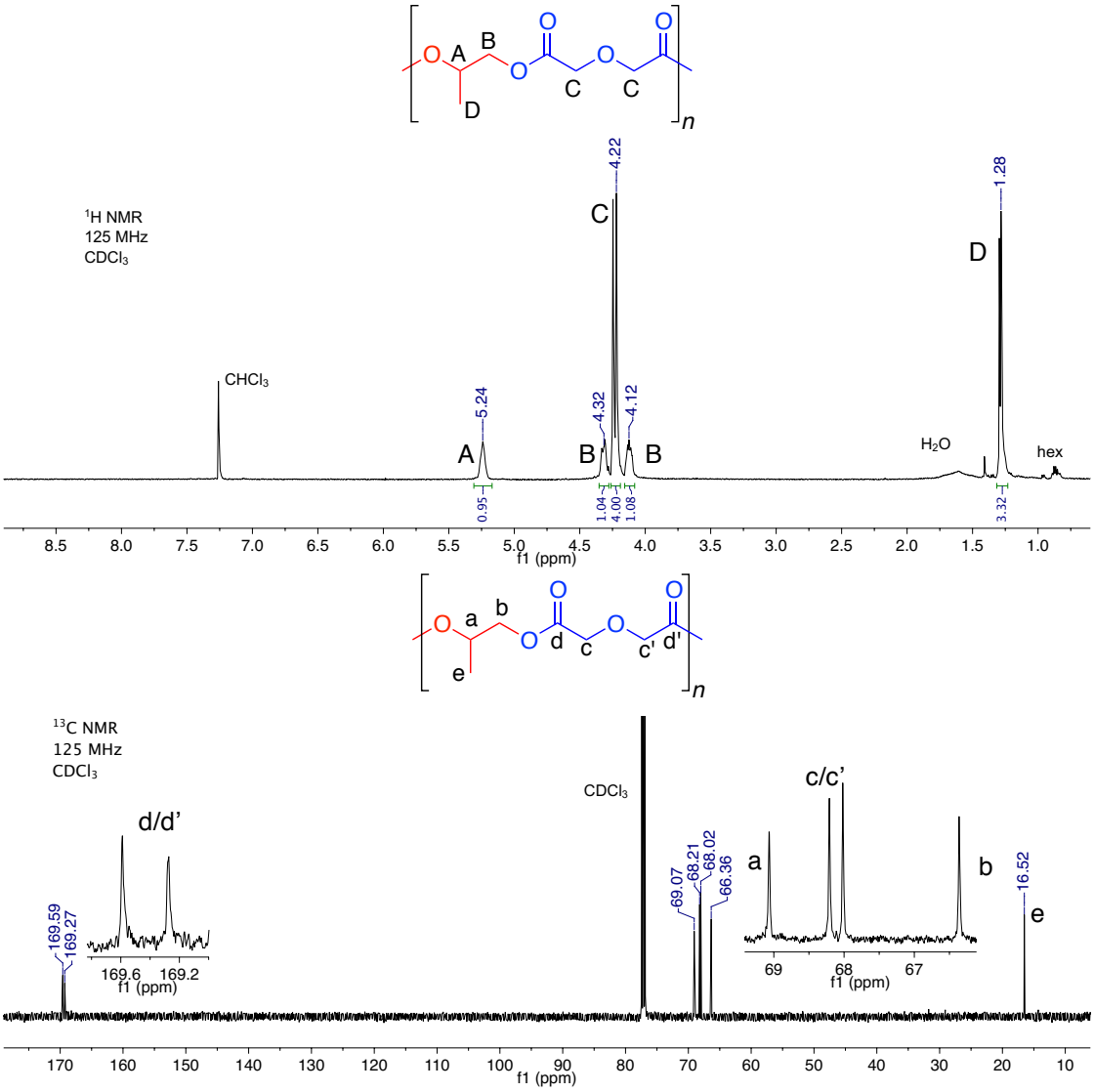


**Figure A2.16.** NMR spectra of poly(propylene diglycolate) in $CDCl_3$. Top: $^{1}$H NMR spectrum. Note: water (1.56 ppm) and hexanes (0.88 and 1.26 ppm) are evident. Bottom: $^{13}$C NMR spectrum.

**Poly(propylene phthalate),** (Table 3.3, entry 4). $^{1}$H NMR spectrum ($CDCl_3$, 500 MHz): δ 7.69 (bm, 2H); 7.48 (bm, 2H); 5.42 (bm, 1H); 4.44-4.32 (bm, 2H); 1.34 (d, *J* = 6.6 Hz, 3H). $^{13}$C NMR spectrum ($CDCl_3$, 125 MHz): δ 166.97 (m); 166.83 (m); 132.32-132.27 (m); 131.54-131.51 (bm); 131.38; 131.22; 129.11; 128.99; 69.71; 67.04; 16.43.

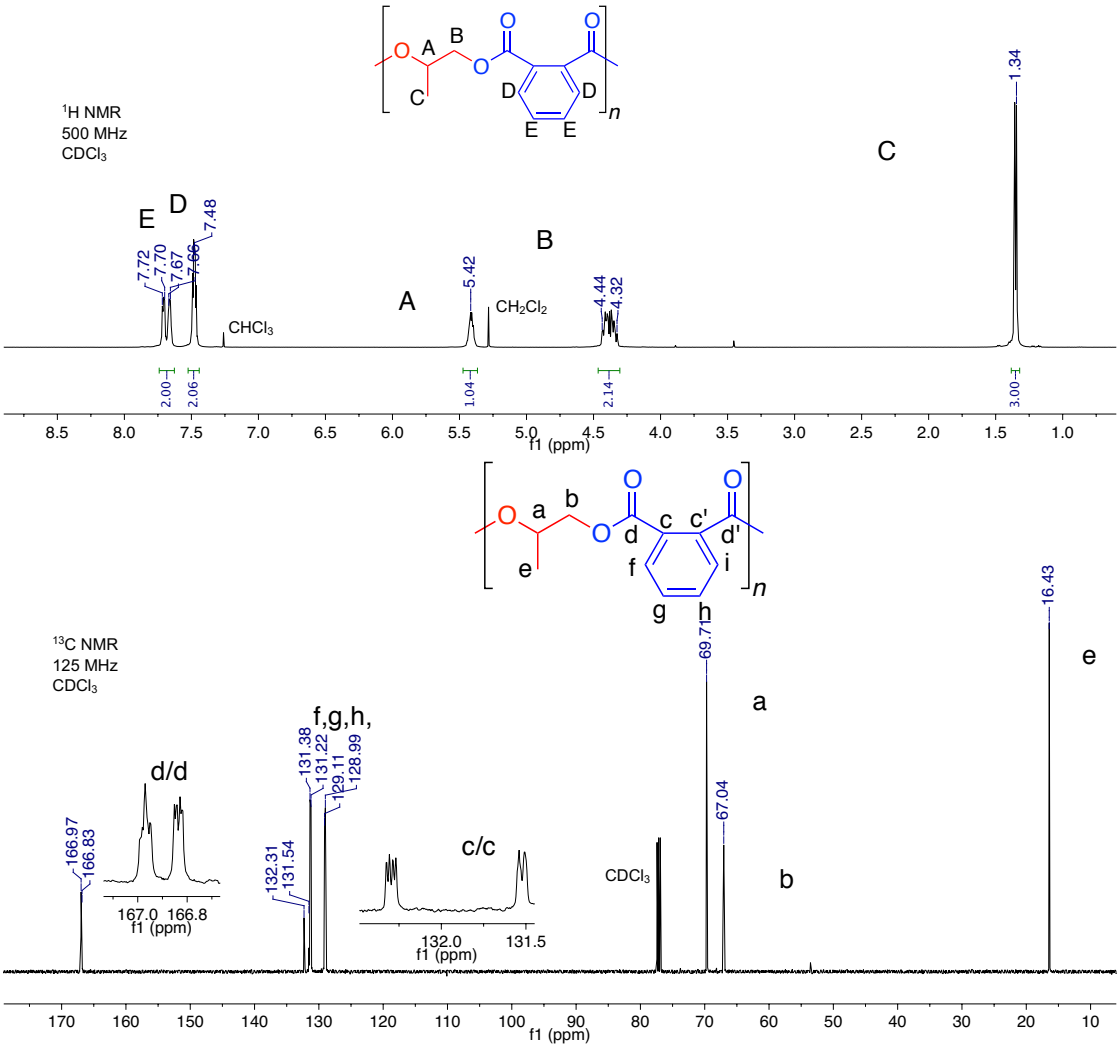


**Figure A2.17.** NMR spectra of poly(propylene phthalate) in $CDCl_3$. Top: $^{1}$H NMR spectrum. Note: residual dichloromethane is present at 5.30 ppm. Bottom: $^{13}$C NMR spectrum.

**Poly(3-chloroprop-1-ene-*alt*-maleate)**, (Table 3.3, entry 6). Please refer to Figure A2.15.

**Poly(3-chloroprop-1-ene-*alt*-succinate)**, (Table 3.3, entry 7). $^{1}$H NMR spectrum ($CDCl_3$, 400 MHz): δ 5.24 (m, 1H); 4.39-4.35 (dd, $J$ = 4.1, 11.9 Hz, 1H); 4.30-4.25 (dd, $J$ = 5.7, 11.9 Hz, 1H); 3.67 (m, 2H); 2.68 (4H). $^{13}$C NMR spectrum ($CDCl_3$, 150 MHz): δ 171.60; 171.26; 70.73; 62.59; 42.12; 28.88; 28.74.

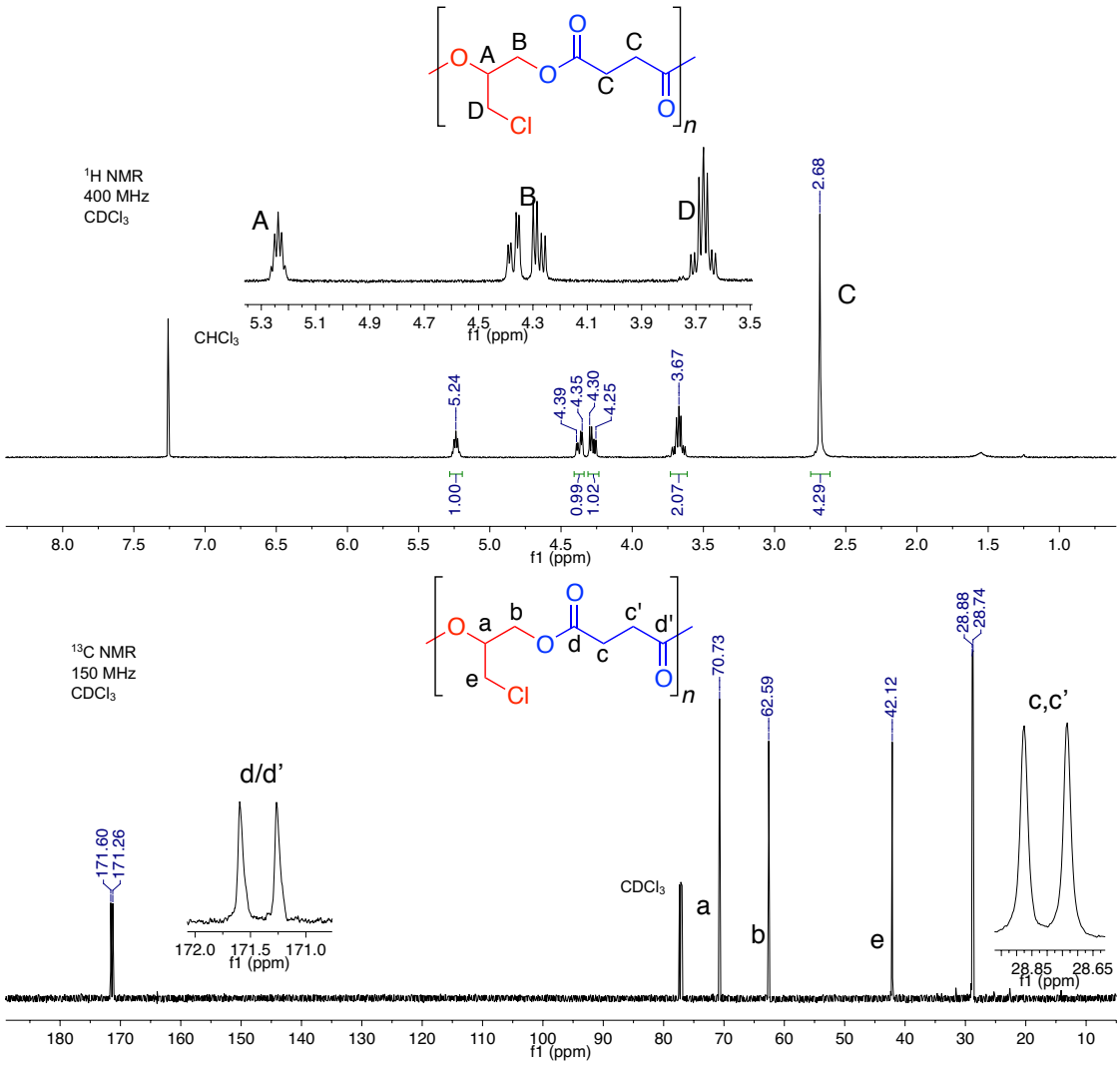


**Figure A2.18.** NMR spectra for poly(3-chloroprop-1-ene-*alt*-succinate) in $CDCl_3$. Top: $^{1}$H NMR spectrum. Note: residual water is evident at 1.56 ppm. Bottom: $^{13}$C NMR spectrum with insets of the carbonyl and alkyl regions of the succinate subunit.

**Poly(3-chloroprop-1-ene-*alt*-diglycolate)**, (Table 3.3, entry 8). $^{1}$H NMR spectrum ($CDCl_3$, 300 MHz): δ 5.33 (m, 1H); 4.53-4.48 (dd, $J$ = 3.1, 12.2 Hz, 1H); 4.34-4.28 (dd, $J$ = 5.8, 12.2 Hz, 1H); 4.28-4.27 (d, $J$ = 4.0 Hz, 4H); 3.70 (m, 2H). $^{13}$C NMR spectrum ($CDCl_3$, 150 MHz): δ 169.23; 168.90; 70.97; 67.79; 62.72; 41.96.

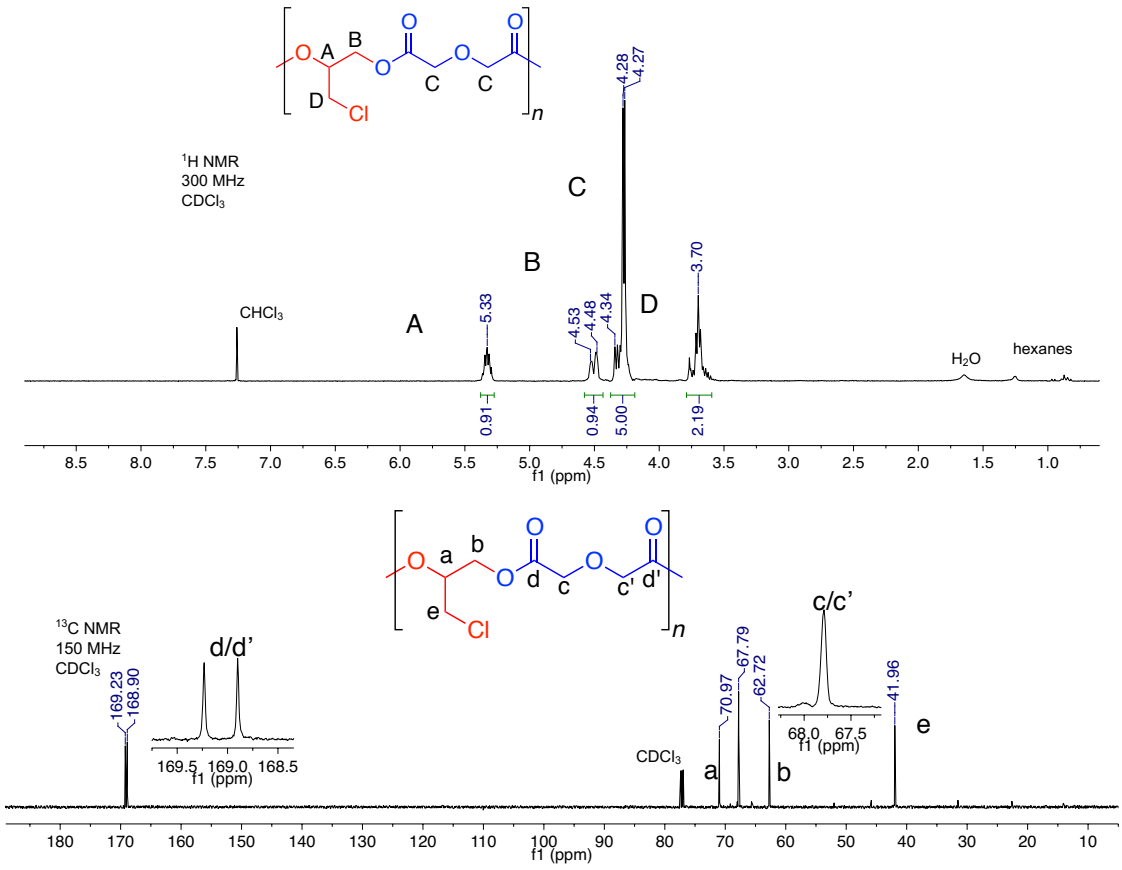


**Figure A2.19.** NMR spectra for poly(3-chloroprop-1-ene-*alt*-diglycolate) in $CDCl_3$. Top: $^{1}$H NMR spectrum. Note: water (1.56 ppm) and hexanes (0.88, 1.26 ppm) are present. Bottom: $^{13}$C NMR spectrum. Note: residual hexanes are present (14.14, 22.70, 31.64 ppm). Other baseline peaks match with expected end groups.

**Poly(3-chloroprop-1-ene-*alt*-phthalate)**, (Table 3.3, entry 9). $^{1}$H NMR spectrum ($CDCl_3$, 500 MHz): δ 7.71 (m, 2H); 7.53 (m, 2H); 5.51 (m, 1H); 4.58 (m, 2H); 3.79 (m, 2H). $^{13}$C NMR spectrum ($CDCl_3$, 150 MHz): δ 166.55; 131.77; 131.64; 131.16; 129.30; 129.18; 71.58; 63.54; 42.17.

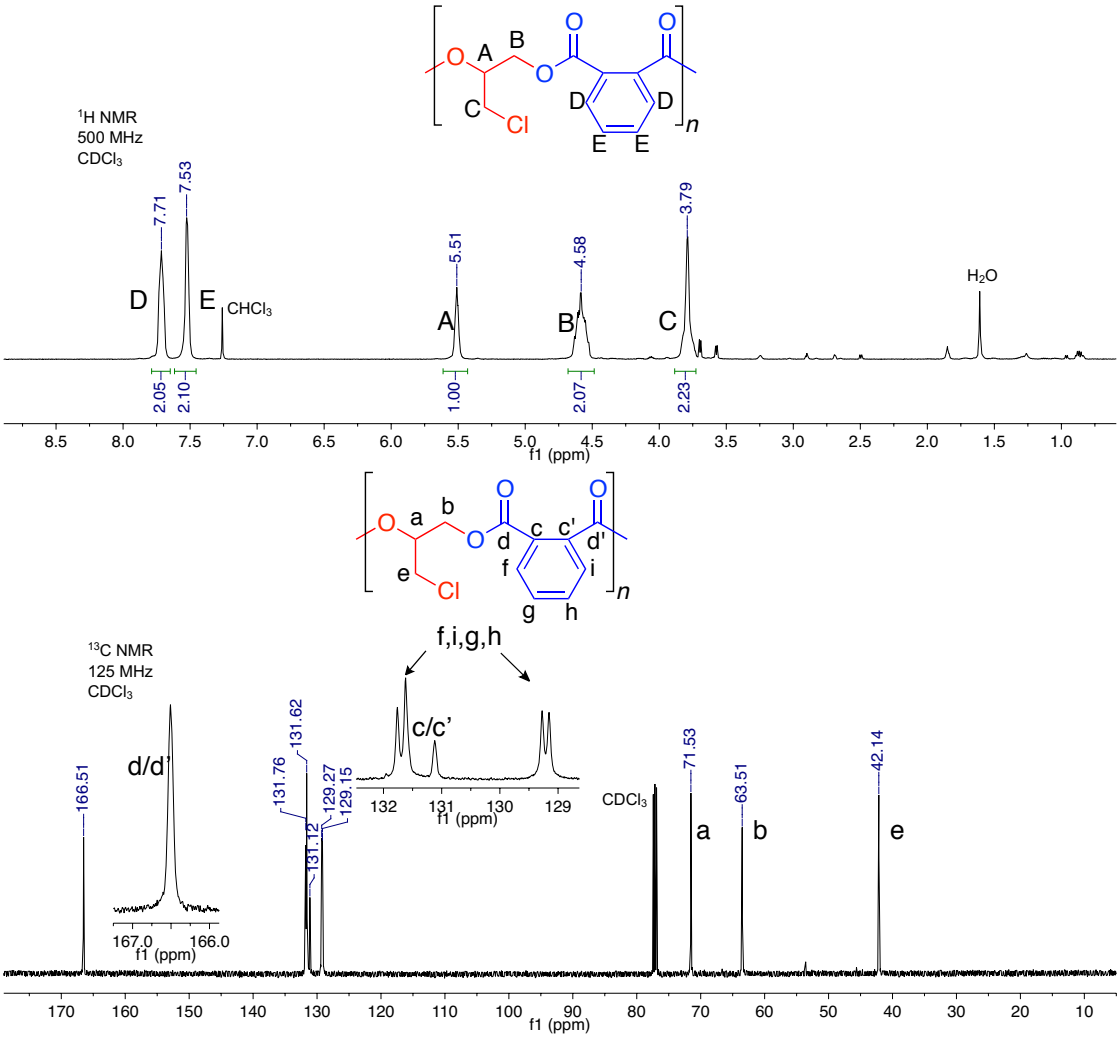


**Figure A2.20.** NMR spectra of poly(3-chloroprop-1-ene-*alt*-phthalate) in $CDCl_3$. Top: $^{1}$H NMR spectrum. Note: residual water (1.56 ppm) and peaks for end groups are present. Bottom: $^{13}$C NMR spectrum.

## 5. Full Explanation of the Regiochemistry Analysis in Figure 1

The copolymerization of maleic anhydride with terminal epoxides yields polyesters with three possible regioisomers (Figure A2.23).

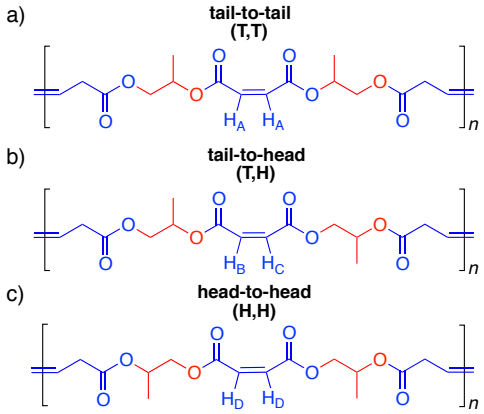


**Figure A2.21.** Possible regioisomers from the copolymerization of maleic anhydride with terminal epoxides: a) tail-to-tai b) tail-to-head c) head-to-head.

Each regioisomer of PPM has chemically distinct maleic anhydride units that produce different signals in the $^{1}$H NMR spectra. The symmetrical tail-to-tail (T,T) and head-to-head (H,H) isomers produce singlets at δ 6.23 ($H_A$) and 6.27 ($H_D$) ppm with corresponding carbons at δ 129.9 and 129.8 ppm, respectively. However, the unsymmetrical tail-to-head (T,H) arrangement produces overlapping leaning doublets at δ 6.24 ($H_B$) and 6.26 ($H_C$) ppm with carbon peaks at δ 129.2 and 130.4 ppm, respectively.

The distinct proton environments are useful indicators of regiochemistry but are complicated by overlap, obscuring definitive assessment (Figure A2.22). Our recent report details NMR assignments for all regioisomers of regioirregular PPM produced by (salcy)CrCl (Figure 2a). Notably, the alkene protons of PPM overlap in the $^{1}$H NMR spectrum to create a signal that is diagnostic of regiochemistry. In regioirregular

PPM, the two singlets from $H_A$ and $H_D$ overlap the outer peaks of the leaning doublets from $H_B$ and $H_C$, while the inner peaks of the leaning doublets overlap with each other (Figure A2.22a). Because of this overlap, in regioregular PPM, the outer peaks of the two leaning doublets from $H_B$ and $H_C$ make it difficult to confirm regioregular structure since it is difficult to rule out the presence of $H_A$ and $H_D$ (Figure A2.22b).

The alkene regioisomers are better visualized using bsgHSQC spectroscopy. Regioirregular maleate polyesters have four distinct proton environments: two singlets from tail-to-tail (T,T) and head-to-head (H,H) enchainments and two overlapping leaning doublets from tail-to-head (T,H) enchainments. The bsgHSQC spectrum of PPM produced by (salcy)$CoO_2CC_6F_5$ has two proton environments that correspond to exclusive T,H units, indicating perfect regiochemistry (Figure 2b). Therefore, to ensure the regioregularity of the polymers produced by **cat5** reported in Table 3.2, bsgHSQC was used to deconvolute the $^1$H NMR spectra.

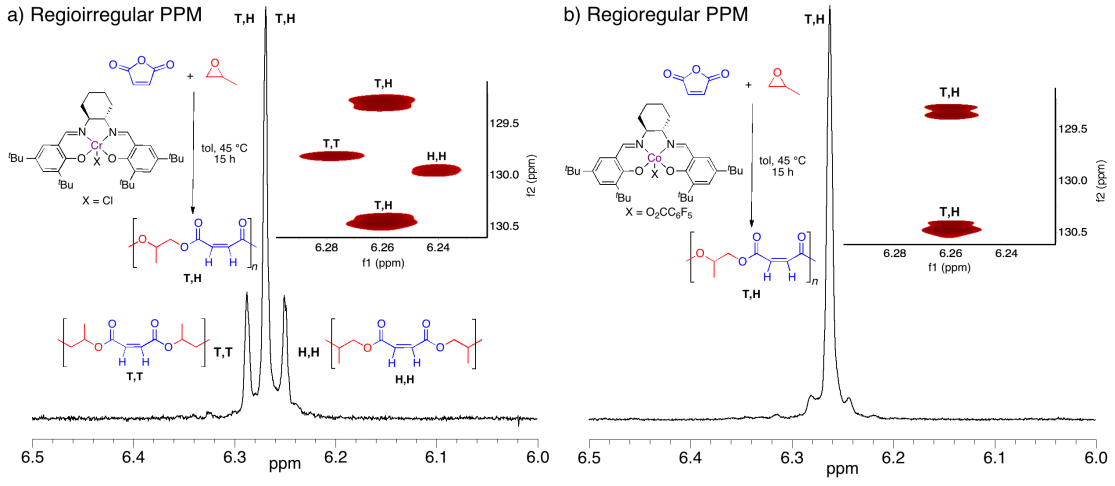


**Figure A2.22.** $^1$H NMR spectra of PPM: a) Regioirregular polyester produced by (salcy)CrCl b) Regioregular polyester produced by (salcy)$CoNO_3$.

### 5.1. bsgHSQC Spectral Analysis of Maleate Containing Polyesters

Poly(propylene maleate) (PPM) (Table 3.1)

Chemical shifts for the four possible regioisomers (Figure A2.23a) were used to analyze the bsgHSQC of the PPM produced with **cat5**. Figure A2.23b clearly demonstrates that there are two distinct proton environments for $H_B$ and $H_C$, signifying that this polymer contains only T,H arrangements. This observation agrees well with the $^1$H NMR spectrum that has one large peak with small side peaks attributed to the extremely close overlapping doublets.

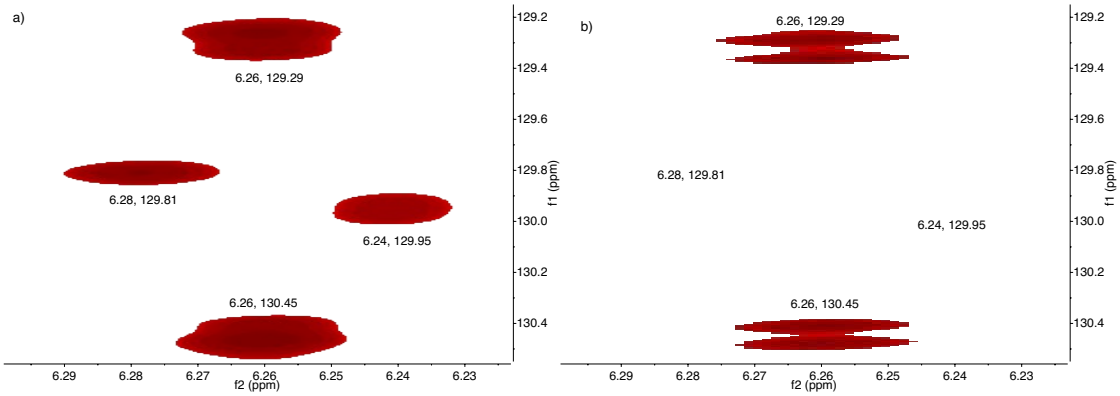


**Figure A2.23.** bsgHSQC spectrum of the alkene carbon/proton region of PPM: a) Regioirregular PPM produced by (salcy)CrCl b) Regioregular PPM produced by **cat5**.

To further confirm the regiochemistry of PPM, we used MNOVA software to extract slices corresponding to the $^1$H NMR spectrum of the individual signals in the bsgHSQC spectrum. The individual slices were overlaid to reconstitute the original $^1$H NMR signal (Figure A2.24b). In addition to the two apparent signals, the regions where H,H and T,T peaks would appear were probed. Using this technique, we can clearly detect that there are no signals corresponding to $H_A$ and $H_B$. The final overlaid spectrum matches the observed $^1$H NMR spectrum well.

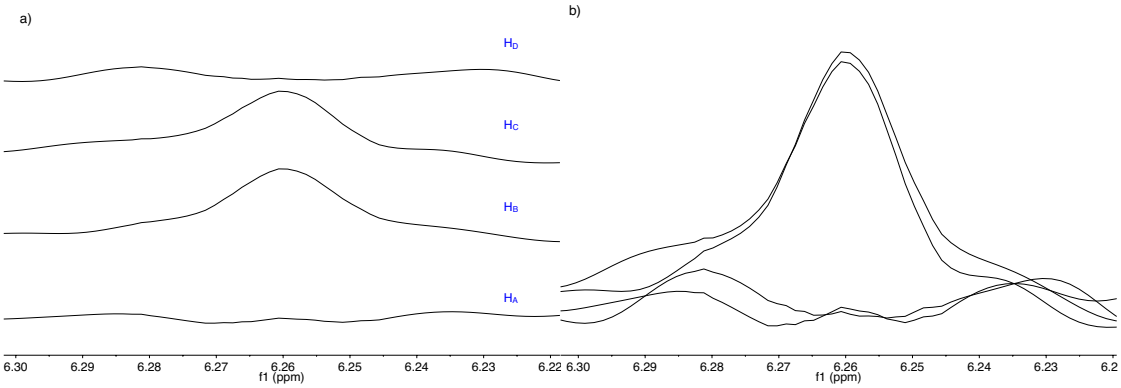


**Figure A2.24.** Extracted 1 dimensional slices from the indicated regions in the bsgHSQC of PPM representing the $^{1}$H NMR spectra of those regions: a) Stacked vertically b) Overlaid.

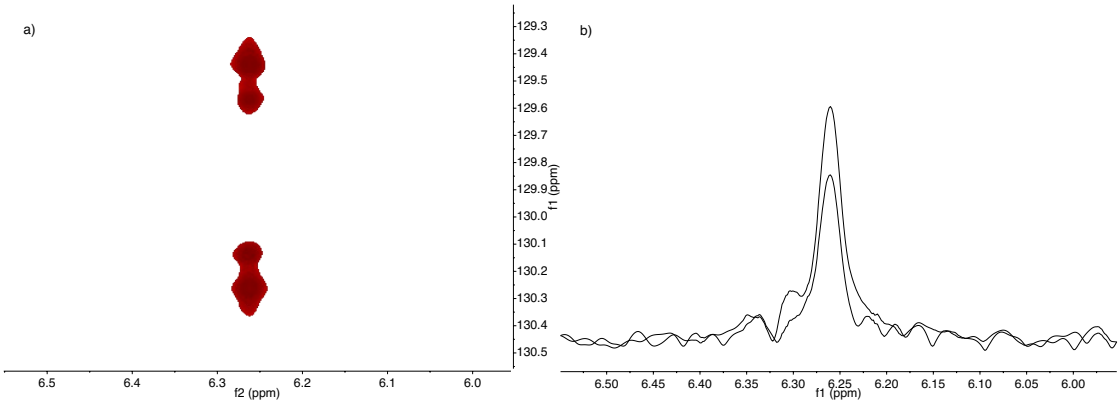


**Figure A2.25.** Poly(1-butene-*alt*-maleate), (Table 3.2, entry 2). a) bsgHSQC spectrum of the alkene proton/carbon region of the maleate monomer b) 1 dimensional slices extracted from each apparent bsgHSQC peak overlaid to reconstruct the original $^{1}$H NMR spectrum.

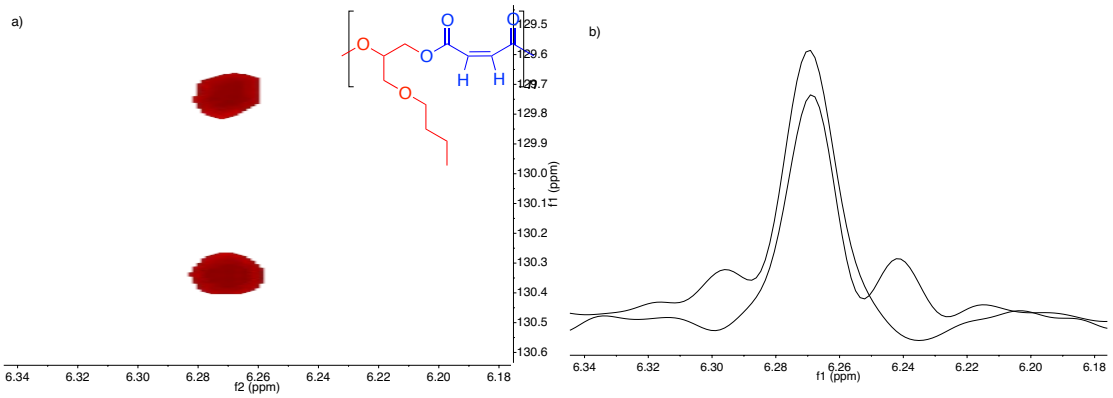


**Figure A2.26.** Poly([allyloxy]butane-*alt*-maleate), (Table 3.2, entry 3). a) bsgHSQC spectrum of the alkene proton/carbon region of the maleate monomer b) 1 dimensional slices extracted from each apparent bsgHSQC peak overlaid to reconstruct the original $^{1}$H NMR spectrum.

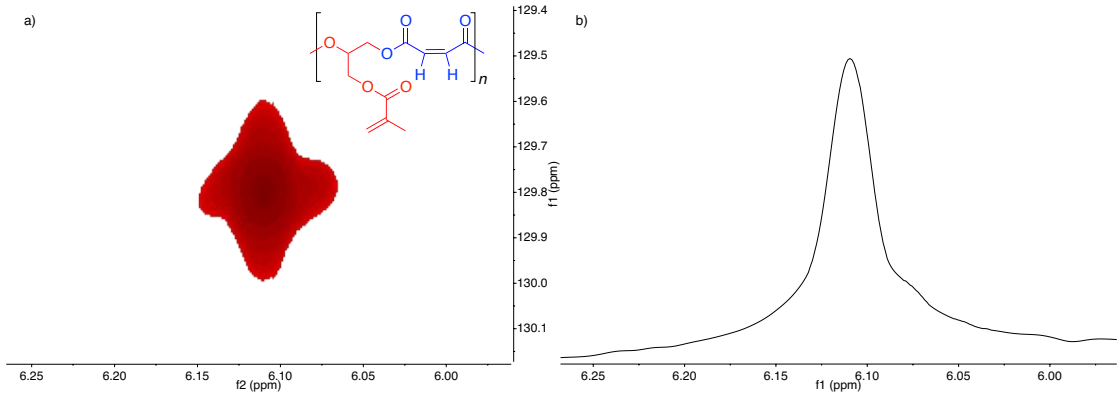


**Figure A2.27.** Poly([allyloxy]methacrylate-*alt*-maleate), (Table 3.2, entry 4). a) bsgHSQC spectrum of the alkene proton/carbon region of the maleate monomer b) 1 dimensional slice extracted from the bsgHSQC representing the $^{1}$H NMR spectrum of this peak.

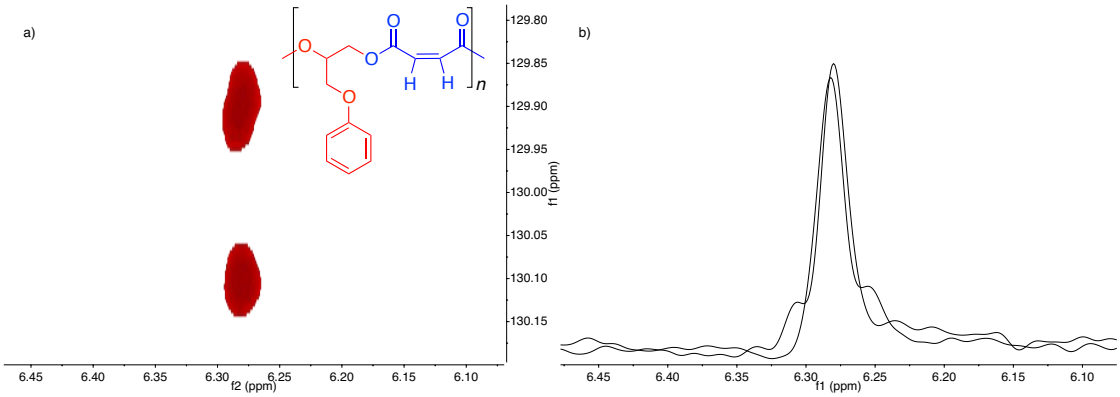


**Figure A2.28.** Poly([allyloxy]benzene-*alt*-maleate), (Table 3.2, entry 5). a) bsgHSQC spectrum of the alkene proton/carbon region of the maleate monomer b) 1 dimensional slices extracted from each apparent bsgHSQC peak overlaid to reconstruct the original $^{1}$H NMR spectrum.

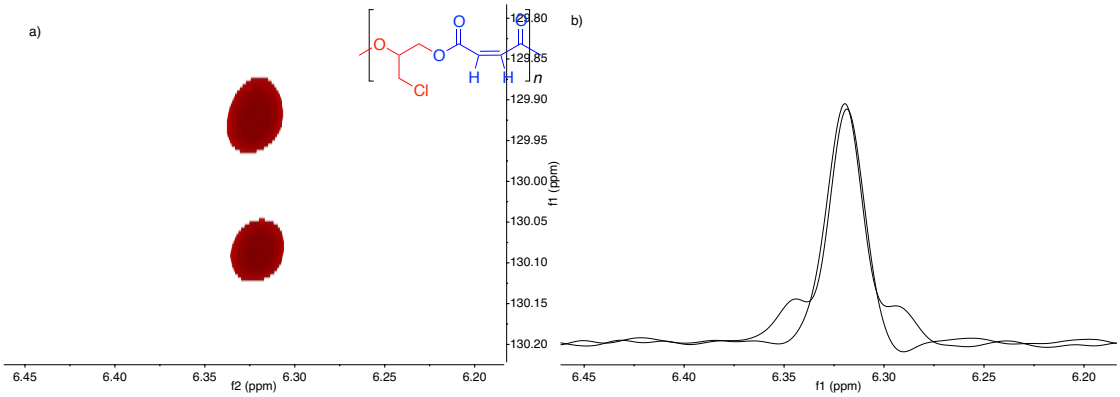


**Figure A2.29.** Poly(3-chloroprop-1-ene-*alt*-maleate), (Table 3.2, entry 6). a) bsgHSQC spectrum of the alkene proton/carbon region of the maleate monomer b) 1 dimensional slices extracted from each apparent bsgHSQC peak overlaid to reconstruct the original $^{1}$H NMR spectrum.

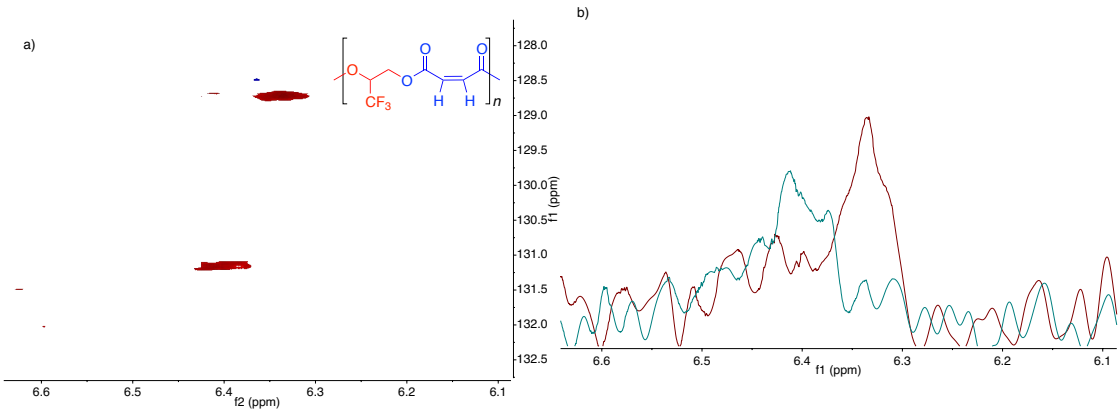


**Figure A2.30.** Poly(1,1,1-trifluoroprop-2,3-ene-*alt*-maleate), (Table 3.2, entry 7). a) bsgHSQC spectrum of the alkene proton/carbon region of the maleate monomer b) 1 dimensional slices extracted from each apparent bsgHSQC peak overlaid to reconstruct the original $^{1}$H NMR spectra. Note: due to the presence of fluorine splitting the detected peaks have very low signal and thus a lot of noticeable noise.

## 6. General Procedure for *in situ* $^{1}$H NMR Spectroscopy Studies

In the inert atmosphere of a nitrogen filled glovebox, 0.01 mmol of **cat2** or **cat 5**, [PPN][$NO_3$] (6.0 mg, 0.01 mmol) and maleic anhydride (98.0 mg, 1.0 mmol) (**2a**) were measured into a J-young tube. The solids were dissolved in 0.3 mL of $C_6D_6$ and the polymerization was initiated by addition of propylene oxide (0.14 mL, 2.0 mmol) (**1a**). The tube was sealed with a Teflon lined screw-cap, and incubated at 30 °C. NMRs were recorded on an INOVA 400 spectrometer with pulse angle of 45°, delay time of 2s, collected for 16 increments. MNOVA processing software was used to normalize all samples to the benzene internal standard for comparison across multiple spectra.

### 6.1. Analysis of *in situ* $^{1}$H NMR Spectra for the Copolymerization of 1a and 2a

To better understand the differences in activity observed for **cat2** and **cat5** in Figure 2, we used *in situ* $^{1}$H NMR experiments to monitor reaction progress over time.

We propose that the active catalyst in the epoxide/anhydride copolymerizations is a hexa-coordinate, low-spin (salcy)Co(III)$X_2$ where X is a propagating polymer chain or counteranion. Presumably, if the (salcy)$CoX_2$ is a cobaltate species, the associated cation from the [PPN][$NO_3$] cocatalyst will stabilize the anion. This species should be diamagnetic and visible by $^1$H NMR spectroscopy.

Figure A2.31 features the $^1$H NMR spectra recorded for polymerization mixtures with **cat2** (Figure A2.31a) and **cat5** (Figure A2.31b). Within the first 5 minutes of initiation, the polymerization mixture containing **cat2** was paramagnetic, concluded by the broad signals and the gradient shimming profiles on VNMRJ. The paramagnetic nature solution could not be monitored for polymerization progress. This result indicates that **cat2** became either a high-spin compound or was reduced to (salcy)Co(II) under these conditions. Cyclic voltammetry, discussed in section 7, implies that **cat2** is likely reduced to a (salcy)Co(II) species, accounting for the paramagnetism.

Conversely, Figure A2.31b follows the copolymerization of **1a**/**2a** through completion. Note that this reaction mixture was dilute to accommodate conditions required for NMR spectroscopy, which caused the polymerization to take longer than normal. The reaction containing **cat5** remained diamagnetic throughout the course of the polymerization and provided well-defined peaks that were analyzed for reaction progress. This result suggests that the active catalyst must be a hexa-coordinate, low-spin (salcy)Co(III) species, with strong axial donors. Based on molecular weights that are lower than theoretical, this supports the theory that multiple chains are initiated from one Co center.

Overall, these experiments make clear a stark difference in the copolymerization of **1a**/**2a** as catalyzed by **cat2** and **cat5**, which may account for the discrepancies in activity. Figure A2.31a suggested that a significant portion of **cat2** was immediately reduced to a (salcy)Co(II) species at the beginning of the copolymerization, which lowered the amount of active catalyst and the reaction rate. Conversely, Figure A2.31b demonstrates that **cat5** remained a stable hexa-coordinate active catalyst throughout the entire polymerization, and resulted in higher activity as demonstrated in Figure 3b.

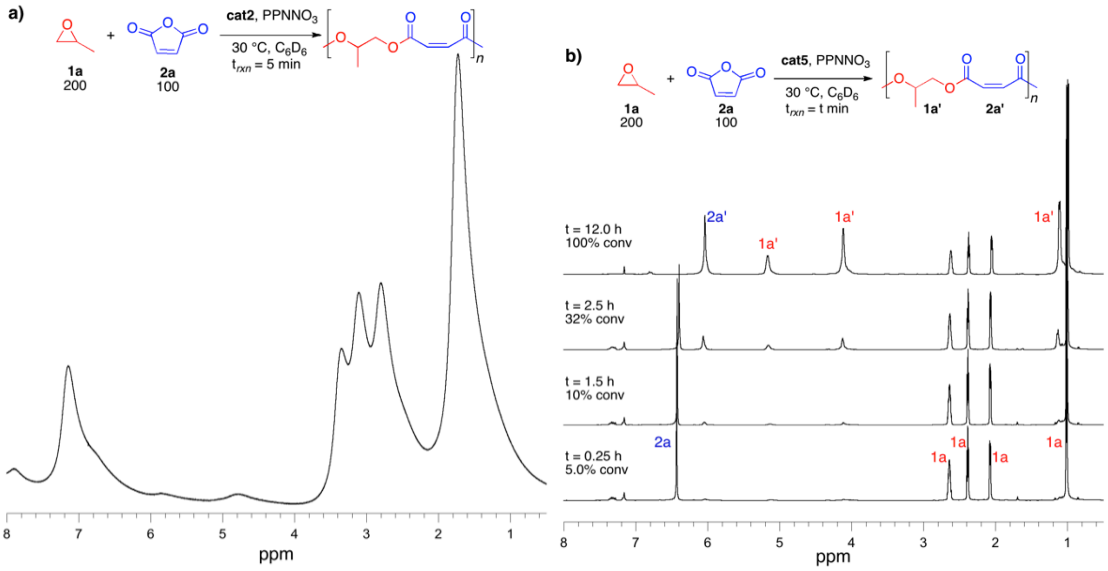


**Figure A2.31.** *In situ* $^{1}$H NMR reaction profiles following the copolymerization of propylene oxide with maleic anhydride over time catalyzed by a) **cat2** and b) **cat5**.

## 7. General Procedure for Cyclic Voltammetry Studies

Cyclic voltammetry was performed in a standard three-electrode cell under a blanket of argon in a 0.1 M solution of dry tetrabutyl ammonium perchlorate (TBAP) in dry-degassed acetonitrile (ACN) and referenced to a $Ag/AgNO_3$ redox couple with a Pt coil counter electrode (Figure A2.32). All scans reported were initiated from an oxidizing potential (1500 mV or 500 mV) and collected at a scan rate of 100 mV/s.

Controls were conducted at different scan rates and initiated from reductive potentials to ensure reproducible and reliable data. Reagents were prepared from the same stock of electrolyte and concentrations were carefully made as follows: 1.0 mM catalyst, 1.0 mM [PPN][$NO_3$], 0.1 M maleic anhydride (**2a**), and 0.2 M propylene oxide (**1a**). Each addition of reagent was the same volume (0.3 mL) to maintain consistent concentration changes. Note that polymerizations were conducted in excess epoxide, which acted as a coordinating solvent. Therefore these preliminary studies were conducted using the coordinating solvent acetonitrile, however, experiments that better mimic reaction conditions are being designed.

**Figure A2.32.** Standard three electrode cell used for cyclic voltammetry

### 7.1. Analysis of Cyclic Voltammograms of cat2 and cat5

To better understand the low activity and degradation of (salcy)CoX catalysts in the copolymerization of epoxides with cyclic anydrides, we considered literature studies of similar phenomena. Reduction of (salcy)Co(III)X catalysts to their (salcy)Co(II) analogues is well known in the context of ring-opening reactions of terminal epoxides.[7] Notably, Jacobsen et al. first described the formation of a brick red

solid, characteristic of insoluble (salcy)Co(II), associated with diminished activity of (salcy)CoOAc in the hydrolytic kinetic resolution (HKR) of epoxy ketones.[7a] This degradation was avoided by exposing the reaction to air, presumably reoxidizing the (salcy)Co(II) product and resuming catalysis. Our group optimized (salcy)Co(III)X processes for the copolymerization of epoxides with $CO_2$ under aerobic conditions with the goal of improving polyester molecular weights by excluding adventitious water from the atmosphere.[7c,d] Seeking alternative methods of stabilizing (salcy)Co(III)X, we discovered that addition of the ionic cocatalyst, [PPN][Cl], stabilized the active (salcy)Co(III)X species against reduction, and provided a system capable of producing polycarbonate under low pressures of $CO_2$ and aerobic conditions.

Recently, Lu et al. performed detailed mechanistic studies in the context of HKR to understand (salcy)CoOAc deactivation.[8] UV-vis and electrospray ionization mass spectrometry (ESI-MS) are used to monitor the HKR of propylene oxide by modified (salcy)CoOAc compounds with appended 1,5,7-triazabicyclo[4.4.0]dec-5-ene (TBD). These studies implicate a redox reaction between the (salcy)Co(III)X complexes and diols that forms the deactivated (salcy)Co(II) species and oxidized hydroxyl ketones. These results suggest a similar degradation pathway may be the culprit of low activity in copolymerization reactions involving epoxides with $CO_2$ or cyclic anhydrides. Therefore, to address these issues we studied the redox stability of (salcy)$CoNO_3$ complexes with different ligand electronics under simulated reaction conditions.

Non-innocent phenolate ligands in salen motifs are known to be electroactive and can influence the redox behavior of chelated metal centers, either by participating in

electron transfer reactions or by influencing the coordination chemistry of the metal.[9] Therefore, we thought it would be appropriate to compare the redox properties of **cat5**, which exhibited improved copolymerization activity and stability, with the commercially derived, less active and stable **cat2**. Cyclic voltammetry (CV) was used to measure and quantify the redox couples for Co(III)/Co(II). We anticipated different electrochemical profiles for **cat2** and **cat5** based on their ligand substitutions. Furthermore, we expected that the redox activity of **cat2** and **cat5** in the context of the copolymerization mixture of maleic anhydride (**2a**) with propylene oxide (**1a**) would lend insight to the extreme differences in activity observed between these systems.

Important variables that will be considered in this discussion include:

- $E_p^a$: the oxidation potential for the Co(II)/Co(III) transition. If the complex is in a solution that has a potential that is oxidizing (a more positive or anodic potential) with respect to $E_p^a$, the compound will exist as Co(III) near the electrode.
- $E_p^c$: the reduction potential for the Co(III)/Co(II) transition. If the complex is in a solution that has a potential that is reducing (a more negative or cathodic potential) with respect to $E_p^c$, the compound will exist as Co(II) near the electrode.
- $E_{1/2}$: the half-wave potential that defines the midpoint of the Co(III)/Co(II) redox couple. This value will determine the thermodynamic ratio of [Co(II)]/[Co(III)] that will exist in a solution at a given potential according to the Nernst equation.

- $\Delta E_p$: the potential difference between $E_p^a$ and $E_p^c$, the magnitude of which describes the redox kinetics of the system, i.e. a larger $\Delta E_p$ reflects slower redox kinetics. Increased $\Delta E_p$ can result from ligand exchanges or rearrangements associated with redox events, or from slow diffusion to/from electrodes.

The redox profiles of both (salcy)$CoNO_3$ complexes were collected for a sweep width of 1500.0 to -1500.0 mV. Both **cat2** and **cat5** exhibited one quasi-reversible cobalt centered redox couple near -100.0 mV, two reversible ligand centered transitions above 600.0 mV and a third subtle reversible ligand transition around 1200.0 mV (Figure A2.33). These curves were consistent with literature reports for salen type cobalt complexes, and demonstrate the electrochemical activity of the organic ligands.[9] Note that the CV curve of **cat5** (Figure A2.33b) exhibited higher resistance than **cat2** (Figure A2.33a), as seen by the broader peaks and increased sloping of the curve. This was either a result of poor electrode contact in the experimental setup or from low electrochemical activity of the complex. Background scans of the standard electrode suggested that the high resistance evident in Figure A2.37b was due to poor electrode contact which was improved upon addition of more solution and was not characteristic of **cat5**.

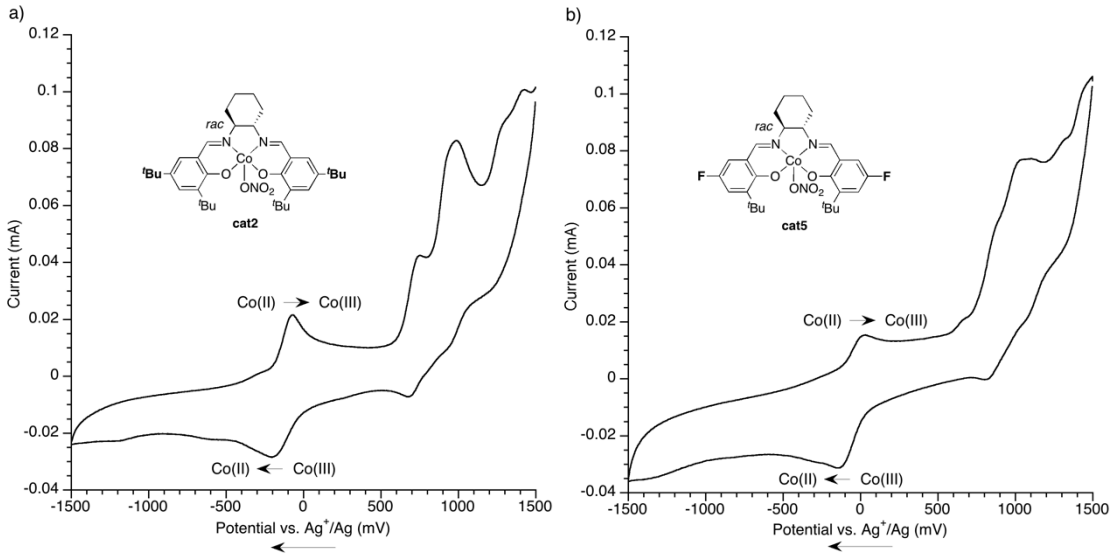


**Figure A2.33.** CV curves collected from 1500.0 to -1500.0 mV for 1.0 mM solutions of a) **cat2** and b) **cat5** in 0.1 M TBAP/ACN.

To better compare the redox activity of the metal centers, we cycled a sweep width between 500.0 to -500.0 mV, focused on the electroactive region for the Co(II) to Co(III) transition (Figure A2.34; Table A2.1, entry 1). The oxidation ($E_p^a$) and reduction ($E_p^c$) transitions for **cat2** occurred at lower potentials, -96.7 and -200.0 mV respectively (Figure A2.34a), than those for **cat5**, -56.6 and -153.3 mV (Figure A2.34b). This resulted in a more negative half-wave potential for **cat2** (-148.3 mV) compared to **cat5** (-105.0 mV), which correlated with the more electron rich cobalt center of **cat2**. The electron donating $^t$Bu groups in the 5 position of the salicylaldehyde moiety make the cobalt center of **cat2** an inherently more reducing compound. Note that the increased resistance of the **cat5** solution was again apparent in Figure A2.38b, but was improved in the next series of experiments.

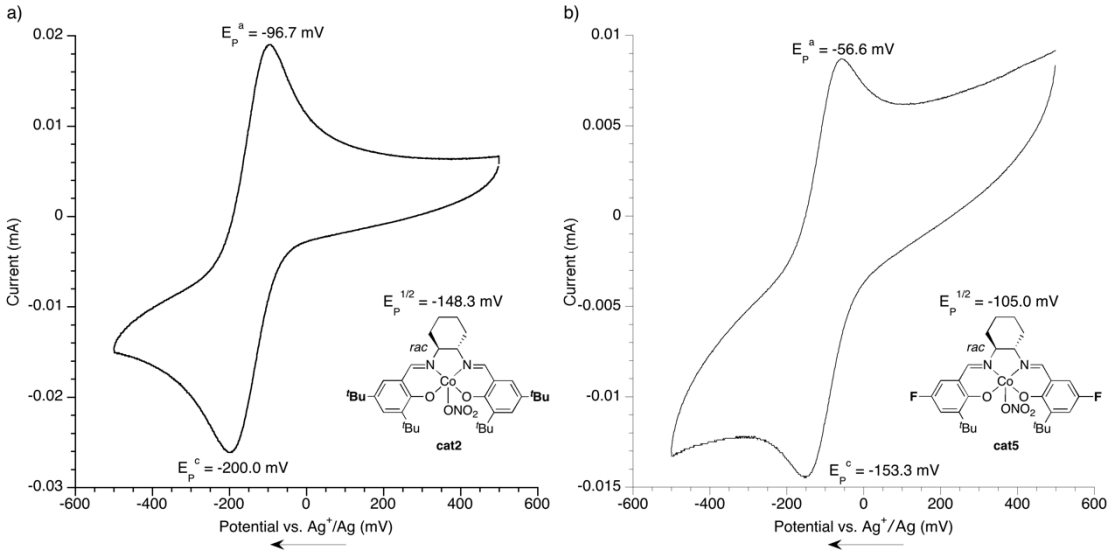


**Figure A2.34.** CV curves of the electroactive region for Co(II) to Co(III) for 1.0 mM solutions of a) **cat2** and b) **cat5** in 0.1 M TBAP/ACN.

### 7.2. Analysis of CV Curves of Cat2 and Cat5 after Addition of [PPN][$NO_3$]

Next we treated each catalyst with 1.0 molar equivalent of [PPN][$NO_3$] (Figure A2.39; Table A2.1, entry 2). Since axial ligands can influence the redox behavior of metal centers, we expected to see a change in the $E_p^a$ or $E_p^c$ of the complexes.[9] However, addition of [PPN][$NO_3$] to solutions of **cat2** and **cat5** resulted in very little change, visualized by overlaying the CV curves from before and after addition of [PPN][$NO_3$] (Figure A2.35). This suggests that coordination was either slow or too weak to significantly change the redox activity of the cobalt, however, it was also possible that the low concentrations and short time scale used in this study were not suitable to study the association between [PPN][$NO_3$] and (salcy)$CoNO_3$. Future studies will focus on better visualizing the redox implications of this association.

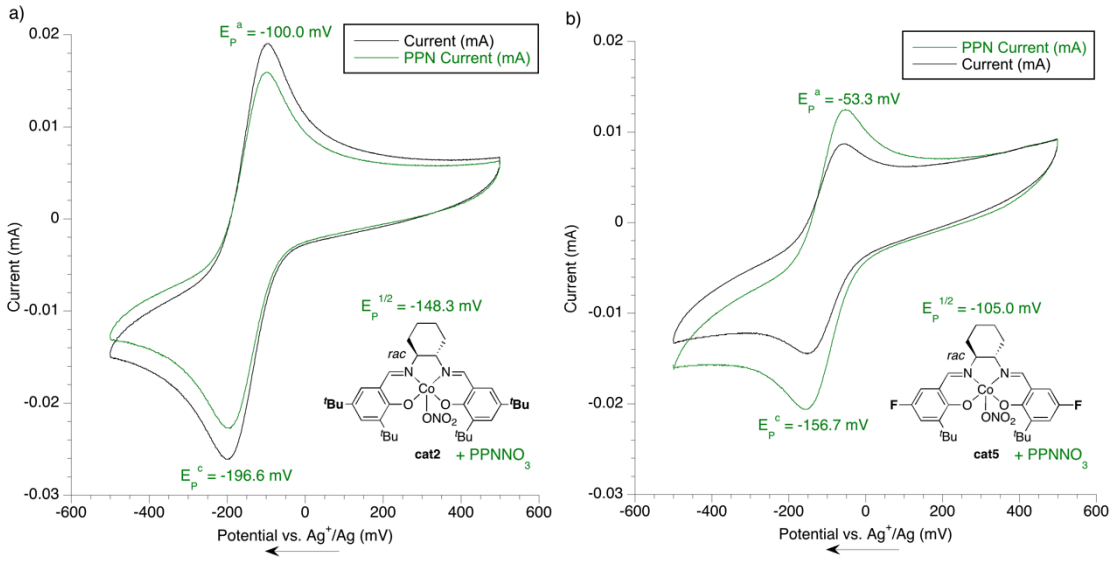


**Figure A2.35.** Overlaid CV curves of catalyst solutions alone (black) and in the presence of [PPN][$NO_3$] (green) for a) **cat2** and b) **cat5** in 0.1 M TBAP/ACN.

### 7.3. Analysis of CV Curves of Cat2/[PPN][$NO_3$] and Cat5/[PPN][$NO_3$] after Addition of 2a

Since these systems exhibited low activity in the presence of maleic anhydride (**2a**), we were interested in the impact of this monomer on their redox properties. **2a** (100 eq) was added to each solution of catalyst with [PPN][$NO_3$] to simulate normal polymerization conditions minus epoxide (Figure A2.36; Table A2.1, entry 3). The $\Delta E_p$ for **cat2** and **cat5** increased of as result of an increase in $E_p^a$ and decrease in $E_p^c$. The change in $\Delta E_p$ for **cat2** (96.6 to 110.0 mV) was smaller than the change for **cat5** (103.4 to 130.0 mV), consistent with better coordination of **2a** by the more Lewis acidic **cat5**. Overall, this change reflects slower electrode kinetics for both systems and a decrease in the electrochemical activity of the Co center. In the context of a polymerization, the slower redox kinetics would decrease the rate of cobalt transitions

between Co(II)/Co(III). Therefore, if a catalyst were to reduce, it would be very slow to reoxidize.

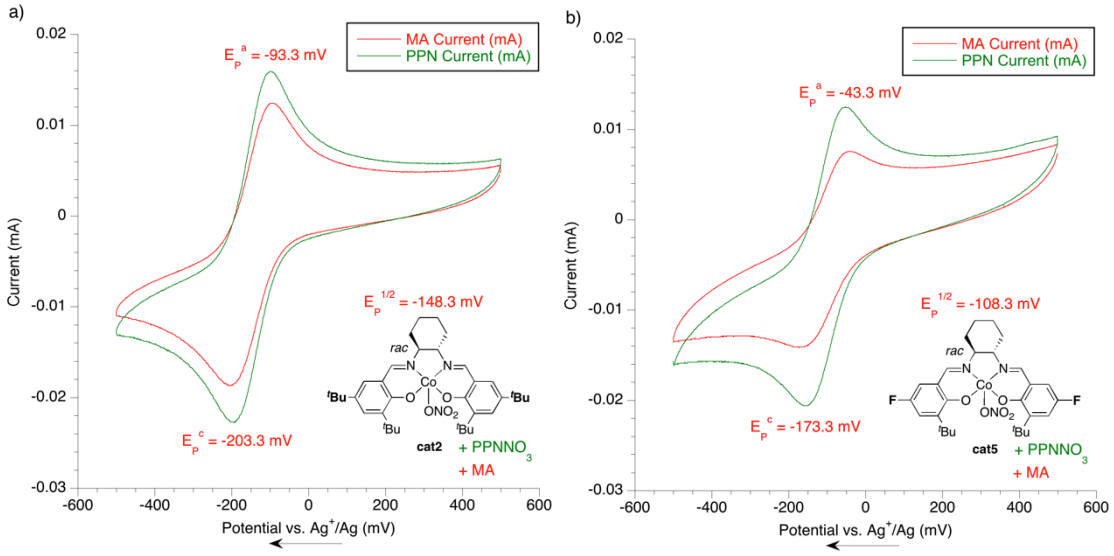


**Figure A2.36.** Overlaid CV curves of before (green) and after (red) addition of **2a** to solutions containing [PPN][$NO_3$] and a) **cat2** or b) **cat5** in 0.1 M TBAP/ACN.

### 7.4. Analysis of CV Curves after Addition of 1a to Solutions of Cat2/[PPN][$NO_3$]/2a and Cat5/[PPN][$NO_3$]/2a

Lastly, to reconstitute the complete polymerization system we added 200 equivalents of propylene oxide (**1a**) to each solution containing catalyst, [PPN][$NO_3$] and **2a** (Figure A2.41; Table A2.1, entry 4). Addition of **1a** changed both oxidation and reduction potentials for **cat2**; the $E_p^a$ shifted from -93.3 to -66.6 mV while $E_p^c$ shifted from -203.3 to -243.3 mV (Figure A2.41.a). This resulted in a significant increase in $\Delta E_p$ from 110.0 to 176.7 mV, indicating possible coordination of PO or a propagating species and slower redox kinetics. Additionally, the $E_{1/2}$ for **cat2** became more reductive, decreasing from -148.3 to -155.0 mV. Consistent with the changes seen for **cat2**, addition of **1a** to **cat5** resulted in an oxidative shift in the $E_p^a$ from -43.3 to -13.3 mV and a reductive shift in the $E_p^c$ from -173.3 to -226.7 mV (Figure

A2.41.b). The $\Delta E_p$ for **cat5** had a greater increase from 130.0 to 213.4 mV and the $E_{1/2}$ for **cat5** became more reductive, moving from -108.3 to -120.0 mV. Overall, the dramatic changes observed upon addition of **1a** to both systems indicated that the redox properties of the catalysts are heavily dependent on the composition of the reaction solution. These results also suggest that **1a** stimulates significant changes in the coordinated cobalt ligands.

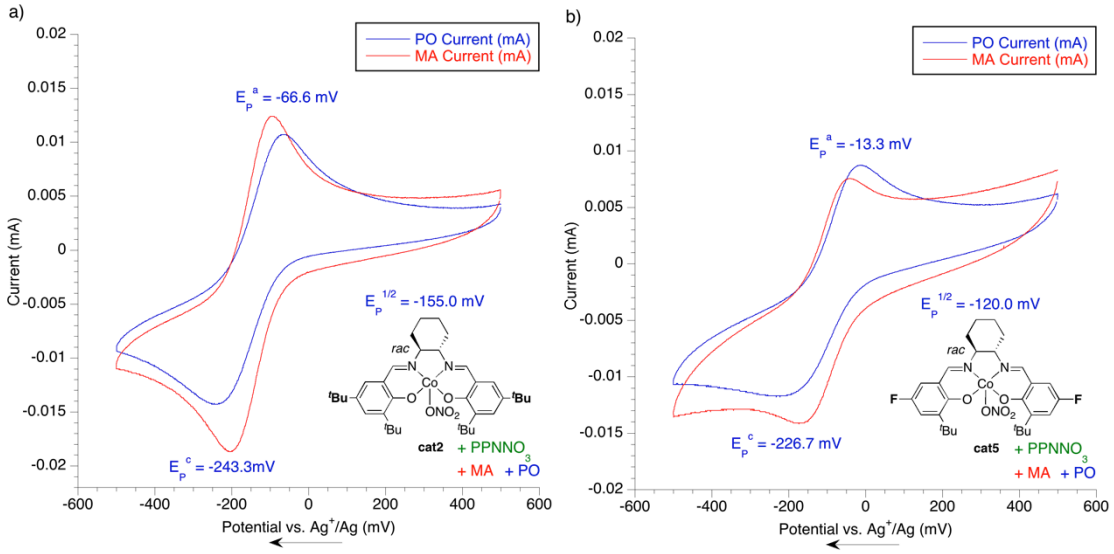


**Figure A2.37.** Overlaid CV curves from before (red) and after (blue) addition of **1a** to solutions containing [PPN][$NO_3$], **2a** and a) **cat2** or b) **cat5** in 0.1 M TBAP/ACN.

### 7.5. Summary of CV Curve Observations

**Table A2.1.** Summary of Co(II)/Co(III) redox couples for **cat2** and **cat5** after addition of copolymerization reagents

| entry | added reagent | $E_p^a$ (mV) | $E_p^c$ (mV) | $E_{1/2}$ (mV) | $\Delta E_p$ (mV) | added reagent | $E_p^a$ (mV) | $E_p^c$ (mV) | $E_{1/2}$ (mV) | $\Delta E$ (mV) |
|---|---|---|---|---|---|---|---|---|---|---|
| 1 | **cat2** | -96.7 | -200.0 | -148.3 | 103.3 | **cat5** | -56.6 | -153.3 | -105.0 | 96.7 |
| 2 | [PPN][$NO_3$] | -100.0 | -196.6 | -148.8 | 96.6 | [PPN][$NO_3$] | -53.3 | -156.7 | -105.0 | 103.4 |
| 3 | **2a** | -93.3 | -203.3 | -148.3 | 110.0 | **2a** | -43.3 | -173.3 | -108.3 | 130.0 |
| 4 | **1a** | -66.6 | -243.3 | -155.0 | 176.7 | **1a** | -13.3 | -226.7 | -120.0 | 213.4 |

Overall, the $E_{1/2}$ of **cat2** (-155.0 mV) was consistently at a more reducing potential than **cat5** (-120.0 mV), which is expected due to the increased electron donating ability of **cat2**'s ligand. The final parameter necessary to determine the significance of these values in the context of the polymerization is the representative resting potential in each environment. Therefore, open circuit potentials were measured for equilibrated reaction mixtures of **cat2** and **cat5**. The resting potential of the reaction mixture dictates the oxidation state and electrochemical stability of the (salcy)Co complex based on the individual $E_{1/2}$ values. If the resting potential is at an oxidizing voltage with respect to the $E_{1/2}$ of the Co(II)/Co(III) redox couple, then more Co(III) will be present. Conversely, a resting potential that is reducing with respect to the $E_{1/2}$ of the Co(II)/Co(III) redox couple will result in predominately Co(II) species.

The open circuit voltage of each polymerization system was measured after a 10-minute equilibration period to allow sufficient diffusion to/from the electrode. For **cat2**, after the initial 10-minutes of equilibration the resting potential was -88.0 mV, however, after 8 hours the solution continued to reduce and was measured at -98.0 mV. This potential was oxidative with respect to the $E_{1/2}$ of **cat2** (-155.5 mV), however, the continual decrease in voltage suggests a increasing concentration of Co(II). This was consistent with the slow tapering of activity seen for **cat2** in the copolymerization of **1a**/**2a** (Figure 3.3b). For **cat5** the resting potential of the solution stabilized at -23.5 mV. This voltage was also more oxidative with respect to the $E_{1/2}$ (-119 mV) of **cat5** under these conditions. In concert with the stability of the open circuit voltage, this data supports the improved stabilization of the Co(III) species

which correlates well with the robust, sustained activity of **cat5** in the copolymerization of **1a**/**2a** (Figure 3.3b).

Finally, the Nernst equation (eq. 1) was solved to calculate the relative ratios of Co(II) and Co(III) in each solution. For **cat2** and **cat5** we applied measured values of the open circuit potential for $E_p^{open}$ and calculated half-wave potentials ($E_p^{1/2}$) for the Co(II) to Co(III) redox couples in the context of the polymerization mixture. Constant variables were applied as follows: R as 8.314 J/mol•K, T as 298 K, n as 1 mole $e^-$, and F as 96,485 C•mol. Formally Q is the reaction quotient and describes the ratio of the activity coefficients of the redox active species ($a_{Co(II)}$ /$a_{Co(III)}$), however, under dilute conditions *a* approaches unity and thus this expression was assumed to represent relative concentrations ([Co(II)]/[Co(III)]) (eq. 5). Detailed calculations are included below.

$$E_p^{open} = E_p^{1/2} - (RT/nF)\ln Q \qquad \text{eq.1}$$

assume: (RT/nF) = 0.02378 C

| **cat2** | **cat5** | |
|---|---|---|
| -0.088V = -0.155V - (0.02378 C) • lnQ | -0.023V = -0.120V - (0.02378 C) • lnQ | eq.2 |
| 0.067V = -0.02378C • lnQ | 0.0965V = -0.02378C • lnQ | eq. 3 |
| -2.817 = lnQ | -4.058 = lnQ | eq. 4 |
| 0.0598 = Q = [Co(II)]/[Co(III)] | 0.0173 = Q = [Co(II)]/[Co(III)] | eq. 5 |
| [Co(III)] = [Co(II)] • 16.7 | [Co(III)] = [Co(II)] • 57.8 | eq. 6 |

The solutions to the Nernst equation revealed that **cat2** contained more reduced Co(II) species under polymerization conditions than **cat5**. Furthermore, solving for the decreased resting potential of -98.0 mV for **cat2** confirms the formation of more Co(II) as the ratio of Co(II):Co(III) increases from $5.98 \times 10^{-2}$ to $9.10 \times 10^{-2}$ indicating a

decrease from 17 times more Co(III) to only 10 times more. Conversely, **cat5** had a Co(II):Co(III) ratio of 0.023, indicating 58 times more Co(III) than Co(II).

Overall these studies revealed valuable information about the impact of ligand electronics on cobalt coordination and electrochemical properties in the context of the copolymerization of maleic anhydride (**2a**) with propylene oxide (**1a**). The electron withdrawing ligand of **cat5** increased the coordination of monomers as evidenced by significant changes in the CV curves of the Co(II)/Co(III) redox couple. Propylene oxide demonstrated the most drastic differences in redox couple changes for both **cat2** and **cat5**; however, this monomer was added in a greater concentration to simulate polymerization conditions. The electron donating ligand of **cat2** created an inherently more reducing metal center as demonstrated by the more negative $E_{1/2}$ potentials. Finally, in the context of the polymerization reaction mixture, the Nernst equation revealed that **cat2** contained a greater amount of Co(II) species in comparison to **cat5** and the continued resting potential decrease of **cat2** signifies the constant formation of more Co(II). Thus, the increased activity of **cat5** can be attributed to a number of factors including the greater amount of active Co(III) catalyst in solution, the better stability of Co(III) as indicated by the steady resting potential, and a more lewis acidic metal center that coordinates epoxide more strongly, allowing better activation for ring-opening.

Future studies will investigate competitive coordination of each monomer under equal concentrations to better gauge their individual affects on the Co(II)/Co(III) redox couple. Additionally, concentration dependent studies are necessary to better understand the issues associated with changing catalyst concentrations in the

copolymerization of **1a**/**2a**. Finally, redox studies of new ligands in the context of copolymerization conditions will provide direction for the discovery of new ligands better able to stabilize the active Co(III) catalysts against reduction.

## 8. Activity Screening of cat2-cat7 for ROC of Cyclic Anhydrides with Propylene Oxide

**Cat2-cat7** were screened with the representative copolymerization procedure for four different anhydrides with propylene oxide to gauge whether the impacts of ligand electronics on copolymerization rate were the same for different monomer combinations. Figure A2.42 summarizes the measured turn-over frequencies for each polymerization. Overall, **cat5** is the most active, producing the highest TOF for all anhydrides. In general, **cat7** is the slowest catalyst, likely due to the extreme electron withdrawing ligand that slows dissociation of propagating species from the Co metal center. Phthalic anhydride (**2d**) is the fastest copolymerization monomer while maleic anhydride (**2a**) is consistently the slowest.

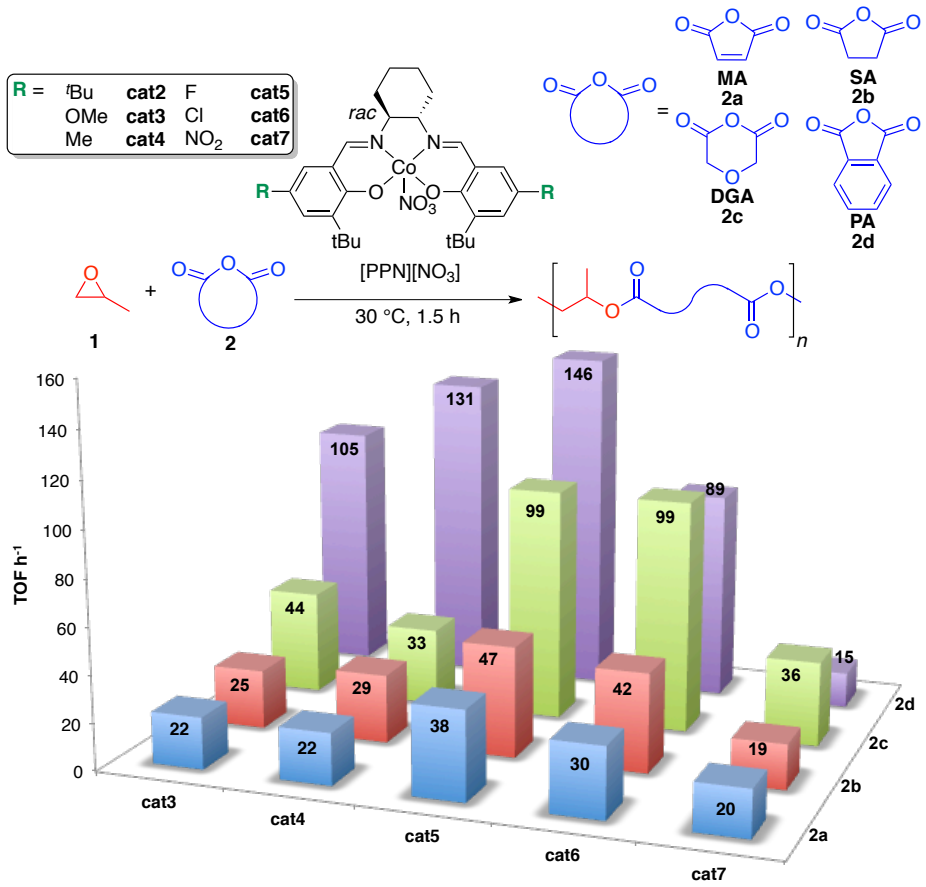


**Figure A2.38.** The impact of ligand electronics on catalyst activity for the copolymerization of different cyclic anhydrides with propylene oxide.

## REFERENCES


(1) Larrow, J. F.; Jacobsen, E. N. *J. Org. Chem.* **1994**, *59*, 1939.

(2) Binch, H,; Grootenhuis, P.; Hadida, R. S.; Zhou, J. (Vertex Pharmaceuticals Inc., US). Modulators of Cystic Fibrosis Transmembrane Conductance Regulator. US Patent W02008/14952A1, January 4, 2008.

(3) Kasai, S.; Kaku, T.; Kamaura, M. (Takeda Pharmaceutical, JP). Heterocyclic Compound. JP Patent EP 2202223, June 30, 2010.

(4) Sun, M.; Mu, Y.; Wu, Q.; Gao, W.; Ye, L. *New J. Chem.* **2010**, *34*, 2979-2992.

(5) Tokunaga, M.; Larrow, J. F.; Kakiuchi, F.; Jacobsen, E. N. *Science* **1997**, *277*, 936-938.

(6) Martinsen, A.; Songstad, J. *Acta Chem. Scand. A* **1977**, *31* 645-650.

(7) (a) Schaus, S. E.; Brandes, B. D.; Larrow, J. F.; Tokunaga, M.; Hansen, K. B.; Fould, A. E.; Furrow, M. E.; Jacobsen, E. N. *J. Am. Chem. Soc.* **2002**, *124*, 1307-1315. (b) Kim, G. J.; Park, D. W. *Catal. Today* **2000**, *63*, 537-547. (c) Qin, Z. Q.; Thomas, C. M.; Lee, S.; Coates, G. W. *Angew. Chem. Int. Ed.* **2003**, *42*, 5484-5487. (d) Cohen, C. T; Chu, T.; Coates, G. W. *J. Am. Chem. Soc.* **2005**, *127*, 10869-10878.

(8) Ren, W. M.; Wang, Y. M.; Zhang, R.; Jiang, J. Y.; Lu, X. B. *J. Org. Chem.* **2013**, *78*, 4801-4810.

(9) Selected papers that discuss these phenomena: (a) Kochem, A.; Kanso, H.; Baptiste, B.; Arora, H.; Philouze, C.; Jarjayes, O.; Vezin, H.; Luneau, D.; Orio, M.; Thomas, F. *Inorg. Chem.* **2012**, *51*, 10557-10571. (b) Kurahashi, T.; Fujii, H. *Inorg. Chem.* **2013**, *52*, 3903-3910. (c) Kochem, A.; Chiang, L.; Baptiste, B.; Philouze, C.; Leconte, N.; Jarjayes, O.; Storr, T.; Thomas, F. *Chem. Eur. J.* **2012**, *18*, 14590-14593. (d) Zhuang, X.; Oyaizu, K.; Niu, Y.; Koshika, K.; Chen, X.; Nishide, H. *Macromol. Chem. Phys.* **2010**, *211*, 669-676. (e) Thomas, F.; Arora, H.; Philouse, C.; Jarjayes, O. *Inorganic Chimica Acta* **2010**, *363*, 3122-3130. (f) Schenk, K. J.; Meghdadi, S.; Amirnasr, M.; Habibi, M. H.; Amiri, A.; Salehi, M.; Kashi, A. *Polyhedron* **2007**, *26*, 5448-5457. (g) Nishinaga, A.; Tajima, K.; Speiser, B.; Eichhorn, E.; Rieker, A.; Ohya-Nishiguchi, H.; Ishizu, K. *Chem. Lett.* **1991**, 1403-1407.

# CHAPTER FOUR

# COBALT SALEN CATALYST FOR THE LIVING COPOLYMERIZATION OF PHTHALIC ANHYDRIDE WITH TERMINAL EPOXIDES: EFFICIENT SYNTHESIS OF POLYESTER BLOCK COPOLYMERS AND ELASTOMERS

## 4.1 Abstract

Currently available catalysts for the copolymerization of epoxides with cyclic anhydrides control polyester compositions and microstructures but to date little control over molecular weight or polymer architecture has been reported. Herein, we describe a cobalt(III) catalyst system for the living copolymerization of phthalic anhydride with a variety of terminal epoxides that addresses these parameters. The polyesters formed are of high molecular weight (>50 kDa) and exhibit narrow molecular weight distributions (<1.2). This strategy directly accesses a variety of functionally diverse high molecular weight polyesters, as well as elastomeric multi-block copolymers.

## 4.2 Introduction

Thermoplastic elastomers such as polystyrene-*b*-polybutadiene-*b*-polystyrene (PS-PB-PS) or polystyrene-*b*-polyisoprene-*b*-polystyrene (PS-PI-PS) exemplify the broad utility of block copolymers as combinations of their parent homopolymers.[1] The success of these materials relies on covalently tethering macromolecules of different functionalities to prevent macrophase separation, thus transforming their bulk physical properties.[2] For example, PS-PB-PS and PS-PI-PS used in synthetic rubbers combine

the toughness of PS with the soft flexibility of PB or PI to create both strong and elastic thermoplastics.[1,3] Biodegradable block copolymers such as poly(lactide-*b*-ethylene oxide) (PLA-PEO) used in drug delivery applications provide amphiphilic character and tunable degradation rates.[2,4] The ability to customize the bulk properties of these block copolymers through variations in block size, sequence, and functionality, make them instrumental resources for advanced materials design.[3]

Polar thermoplastic elastomers valuable for applications requiring specific resistance or phylicity require design of both physical and chemical characteristics.[1,3] However, few living or controlled polymerizations can efficiently and consecutively enchain functionally diverse monomers with control over block sequence and size.[4] Examples of systems capable of forming multi-block polycarbonates *via* sequential addition include Nozaki's bi-functional N-N'-bissalicylidene(cyclohexadiimine)-cobalt(III) ((salcy)Co)[5] and our beta-diiminate-zinc(II) ((BDI)Zn)[6] catalysts. Using commodity materials, our group also applied (BDI)ZnOAc to the formation of poly(ester-*b*-carbonate) *via* a one-pot pre-rate determining terpolymerization of cyclohexene oxide, glutaric anhydride, and $CO_2$.[7] Still, substrate scope and sequence control limit the materials available from these processes. Herein, we expand the functionalities and architectures accessible for polar block copolymers *via* formation of high molecular weight polyesters from commodity feedstocks.

We recently reported a regioselective process for the synthesis of polyesters *via* the alternating copolymerization of epoxides with cyclic anhydrides.[8] Using *rac*-(salcy)$CoNO_3$/[PPN][$NO_3$], we identified **cat1** as the most active and stable catalyst (Scheme 4.1). This system is highly active for the copolymerization of phthalic

anhydride with terminal epoxides; however, in agreement with other reported polyester systems, molecular weight was limited by chain transfer events.[9] Using this complex as a starting point, we report an improved catalyst system that is capable of the living copolymerization of phthalic anhydride with a variety of terminal epoxides.

**Scheme 4.1.** Catalyst Synthesis: Route B is Modified Version of Route A

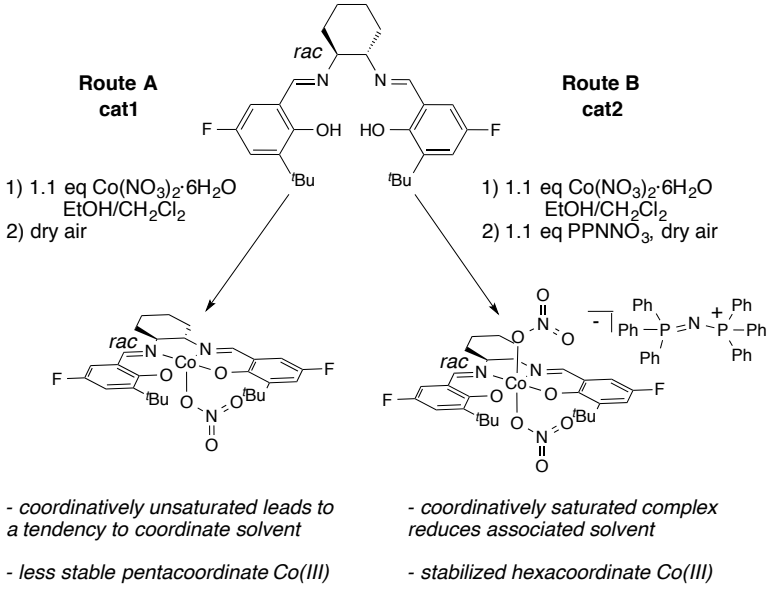


One requirement of a living polymerization is uniform initiation that provides for a narrow molecular weight distribution (PDI), and a linear increase of molecular weight ($M_n$) as a function of monomer conversion.[10] In the copolymerization of epoxides/cyclic anhydrides, initiation is proposed to operate *via* the nucleophilic ring-opening of an epoxide coordinated to the Co metal center, similar to epoxide/$CO_2$, and aided by the presence of an ionic cocatalyst. One model for improved initiation is to closely associate/tether ionic cocatalysts to the catalyst framework.[5,11,12] Another approach, explored by Darensbourg et al., is to prepare a catalyst/cocatalyst mixture *in situ* that is redissolved prior to initiation.[13] Seeking to test a simple synthetic analogue to this concept, we synthesized a [(salcy)$Co(NO_3)_2^-$][$PPN^+$] complex *via* a modified

metallation procedure that involves oxidation in the presence of the ionic [PPN][$NO_3$] salt to prepare [*rac*-(salcy)Co($NO_3$)$_2^-$][$PPN^+$] (Scheme 4.1, Route B).

Crystals of **cat2** were grown from a saturated solution of dichloromethane/methanol (Figure 4.1) and the structure was determined by X-ray crystallography. The salcy ligand of **cat2** was located in the plane of the cobalt center and two axial nitrates were bound in an $\eta^1$ mode. The crystal structure of **cat2** presumably represents the coordination complex formed by catalyst/[PPN][$NO_3$] and is a good model for the initiating species.

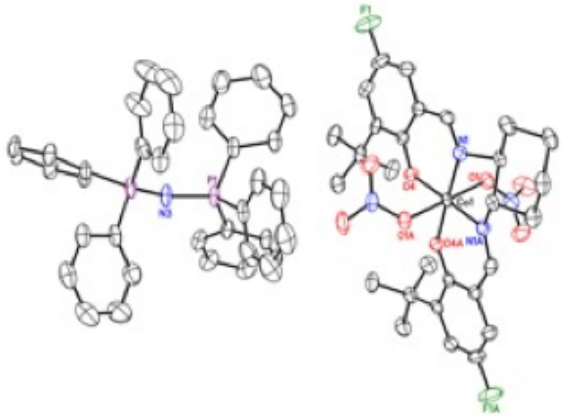

**Figure 4.1.** Crystal structure of one enantiomer of **cat2** isolated from a solution of $CH_2Cl_2$/MeOH with hydrogens eliminated for clarity; refined to >99% thermal ellipsoids of the X-ray structure.

**Cat1** and **cat2** were screened for the copolymerization of phthalic anhydride (**1**) with terminal epoxides (Table 4.1). All reactions formed perfectly alternating polyesters. **Cat1** was slower to copolymerize **1** with propylene oxide (**2a**), reaching only 55% conversion compared to 77% for **cat2** (entries 1 and 2). This difference may be due to the better solubility of **cat2** relative to **cat1**/[PPN][$NO_3$]. Both catalysts exhibited comparable activity for copolymerizations with the more polar epoxide, 1,1,1-trifluoropropan-2,3-ene oxide (**2b**) (entries 3 and 4). Overall, **cat1** and **cat2**

yielded polyesters of equivalent molecular weights, however, **cat2** consistently produced polyesters with more narrow PDIs, evident from GPC traces.[14]

**Table 4.1.** Copolymerization of Phthalic Anhydride/Epoxides Catalyzed by **cat1** and **cat2**[a]

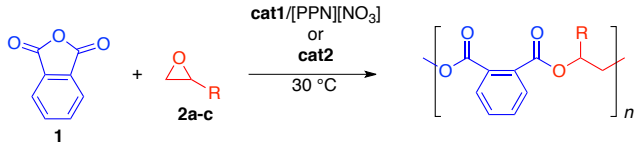


| entry | catalyst | R (epoxide) | time (h) | % conv.[b] | $M_n^{theo}$ (kDa)[c] | $M_n^{obs}$ (kDa)[d] | PDI[d] |
|---|---|---|---|---|---|---|---|
| 1 | **cat1** | $CH_3$ (**2a**) | 2.0 | 55 | 22.7 | 12.6 | 1.16 |
| 2 | **cat2** | $CH_3$ (**2a**) | 2.0 | 71 | 29.3 | 15.8 | 1.11 |
| 3 | **cat1** | $CF_3$ (**2b**) | 2.0 | 89 | 46.3 | 23.5 | 1.16 |
| 4 | **cat2** | $CF_3$ (**2b**) | 2.0 | 80 | 41.6 | 21.6 | 1.10 |

[a]General conditions: **1**:**2**:**cat1**/[PPN][$NO_3$] or **cat2** = 400:800:1. [b]Calculated using $^1$H NMR spectroscopy based on **1** as the limiting reagent. [c]Calculated assuming two initiators. [d]Measured with respect to polystyrene standards using gel-permeation chromatography eluted at 0.3 mL/min with THF at 30 °C.

**Cat2** was tested for its ability to produce high molecular weight polyesters with narrow PDIs using the copolymerization of phthalic anhydride (**1**) and propylene oxide (**2a**). $^1$H NMR spectroscopy was used to monitor the conversion of limiting reagent **1**.[14] The copolymerization rate slightly decreased after the mixture became viscous and the polymerization became diffusion limited. Gel-permeation chromatographs (GPC) of polyester samples at each time interval showed incremental increases with a consistently narrow peak shape.[14] A linear correlation between molecular weight and percent conversion was observed and PDI <1.12 was maintained through the course of the reaction, consistent with a living polymerization (Figure 4.2). Fast initiation was further supported through studies of initial rates at different

catalyst concentrations, showing a negligible initiation period at low catalyst concentrations (1.8 mM).[14]

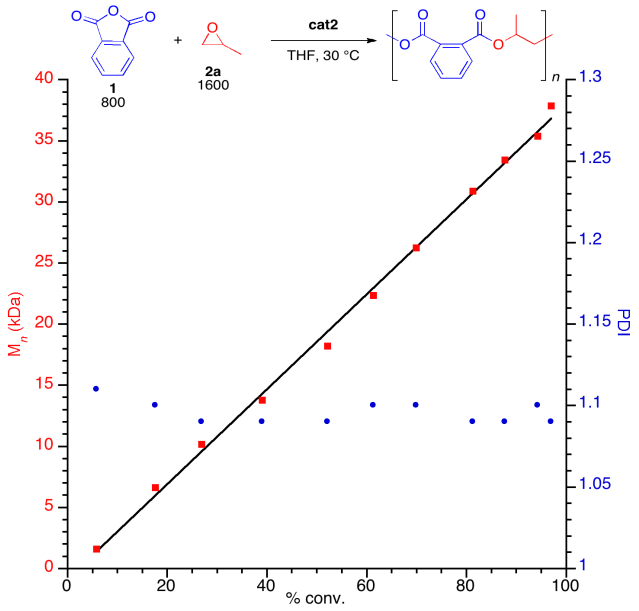


**Figure 4.2.** Plot of $M_n$ and PDI vs. conversion for the copolymerization of phthalic anhydride with propylene oxide catalyzed by **cat2**.

Next, **cat2** was tested for the living copolymerization of PA with a range of terminal epoxides (Table 4.2). High molecular weight polyesters (>50.0 kDa) with narrow PDIs (<1.19) were achieved for all combinations (entry 3). Propylene oxide produced the highest molecular weight polyester (79.0 kDa) with a narrow PDI (1.16) (entry 1) while 1,1,1-trifluoropropan-2,3-ene oxide (entry 2) yielded a convenient fluorinated analogue. Aliphatic epoxides of varying chain lengths were slower to polymerize but maintained perfectly alternating compositions. Notably a difference of 2 carbons per repeat unit between poly(1-butene-*alt*-phthalate) (40 °C, entry 3) and poly(1-hexene-*alt*-phthalate) (31 °C, entry 4) resulted in only an 9 °C decrease in the $T_g$ of comparable samples. Finally, dodecene oxide required higher heat (60 °C) to

form a miscible solution (entry 5). Poly(1,2-epoxydodecene-*alt*-phthalate) displayed a $T_g$ of -4 °C and was a clear, viscous syrup at room temperature.

**Table 4.2.** Living Copolymerization of Phthalic Anhydride/Terminal Epoxides Catalyzed by **cat2**[a]

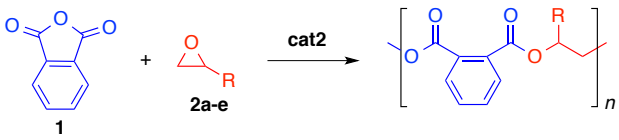


| entry | $R^1$ (epoxide) | time (h) | % conv.[b] | $M_n^{theo}$ (kDa)[c] | $M_n^{obs}$ (kDa)[d] | PDI[d] | $T_g$ (°C)[e] |
|---|---|---|---|---|---|---|---|
| 1 | Me (**2a**) | 17 | 96 | 198 | 78.8 | 1.16 | 63 |
| 2 | $CF_3$ (**2b**) | 13 | 75 | 195 | 66.6 | 1.12 | 59 |
| 3 | Et (**2c**) | 18 | 63 | 137 | 66.2 | 1.17 | 40 |
| 4 | $C_4H_9$ (**2d**) | 36 | 93 | 244 | 74.3 | 1.19 | 31 |
| 5[f] | $C_{10}H_{21}$ (**2e**) | 5.5 | 85 | 282 | 49.3 | 1.18 | -4 |

[a]General conditions: **1**:**2**:**cat2** = 2000:4000:1, $T_{rxn}$ = 30 °C. [b]Calculated based on **1** as the limiting reagent using $^1$H NMR spectroscopy. [c]Calculated assuming two initiators. [d]Measured with respect to polystyrene standards using gel-permeation chromatography eluted at 0.3 mL/min with THF at 30 °C. [e]Measured using differential scanning calorimetry, values reported from second heat. [f]Reaction performed at 60 °C.

Next, block copolymers were synthesized *via* the sequential addition of different epoxides with phthalic anhydride to active polymerizations.[14] To test whether tapering between blocks hindered microstructure formation, we screened chemically distinct monomers anticipated to microphase separate (Figure 4.3). **Cat2** was used to prepare high molecular weight (>40 kDa), narrow PDI (<1.2) samples of poly(propylene-*alt*-phthalate)-*b*-(1,2-epoxydodecene-*alt*-phthalate)-*b*-(propylene-*alt*-phthalate) (Figure 4.3a) and poly(1,1,1-trifluoropropan-2,3-ene-*alt*-phthalate)-*b*-(1,2-epoxydodecene-*alt*-phthalate)-*b*-(1,1,1-trifluoropropan-2,3-ene-*alt*-phthalate) (Figure 4.3b) with typical

compositions of thermoplastic elastomers. Differential scanning calorimetry (DSC) was used to evaluate microphase separation. Both triblock copolymers exhibited two $T_g$'s that were distinct to each block segment (Figure 4.4), confirming that our method was sufficient to create triblock copolymers able to microphase separate. Finally, an ABC triblock was formed by consecutive addition of three different epoxides to yield poly(propylene-*alt*-phthalate)-*b*-(1-butene-*alt*-phthalate)-*b*-(1,1,1-trifluoroprop-2,3-ene-*alt*-phthalate), demonstrating modular control of block sequence.[14]

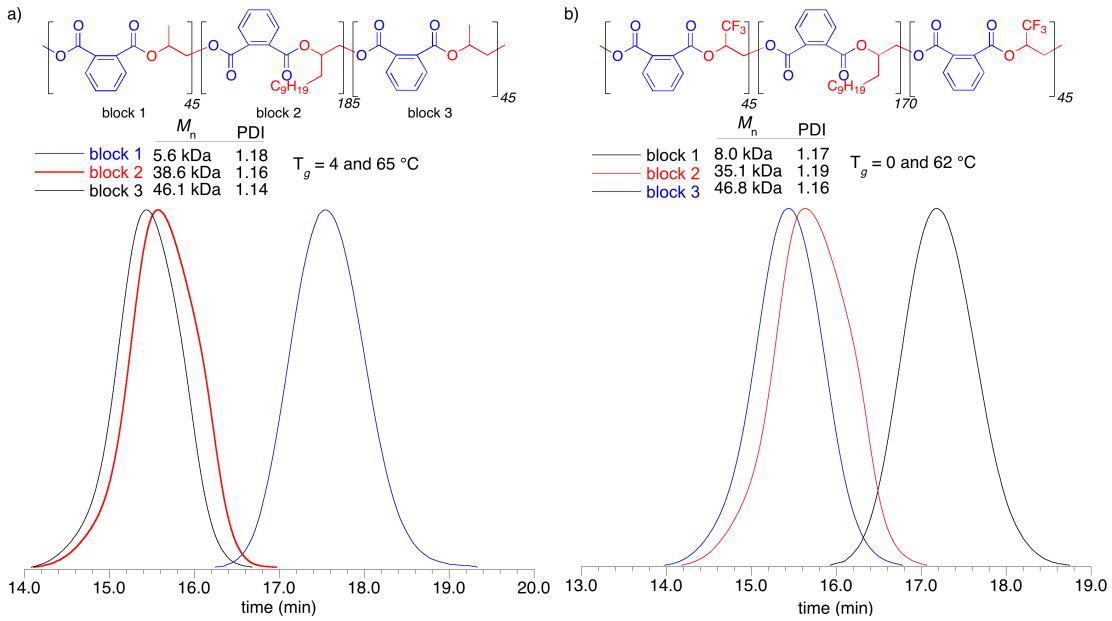


**Figure 4.3.** GPC traces, molecular weight and thermal data for: a) aliphatic poly(propylene-*alt*-phthalate)-*b*-(dodecene-*alt*-phthalate)-*b*-(propylene-*alt*-phthalate) b) fluorinated analogue poly(1,1,1-trifluoropropan-2,3-ene-*alt*-phthalate)-*b*-(dodecene-*alt*-phthalate)-*b*-(propylene-*alt*-phthalate)-*b*-(1,1,1-trifluoropropan-2,3-ene-*alt*-phthalate).

Herein we report a *rac*-(salcy)Co(III) based catalyst system capable of the living copolymerization of phthalic anhydride with terminal epoxides. High molecular weight polyesters (>50 kDa) with narrow PDIs (<1.2) under mild conditions are formed from commodity feedstocks. Sequential addition of diverse monomers yields

block copolymers that microphase separate. Block size, composition, and order can be tuned; easily accessing polyester based thermoplastic elastomers. Notably, aliphatic and fluorinated monomers are consecutively enchained in sequential blocks without side reactions or requiring a change of mechanism, providing a simple method for obtaining functionally diverse block copolymers. Further studies to optimize and diversify these systems to expand substrate scope and study the morphologies of these structures are currently underway.

REFERENCES

(1) Examples of methods and applications of these polymers include: (a) Schmidt, S. C.; Hillmyer, M. A. *Macromolecules* **1999**, *32*, 4794-4801. (b) Zalusky, A. S.; Olayo-Valles, R.; Taylor, C. J.; Hillmyer, M. A. *J. Am. Chem. Soc.* **2001**, *123*, 1519-1520. (c) Hillmyer, M. A.; Lodge, T. P. *J. Polym. Sci.: Part A: Polym. Chem.* **2002**, *40*, 1-8.

(2) Kumar, N.; Ravikumar, M. N. V.; Domb, A. J. *Advanced Drug Delivery Reviews* **2001**, *53*, 23-44.

(3) (a) Bates, F. S.; Hillmyer, M. A.; Lodge, T. P.; Bates, C. M.; Delaney, K. T.; Fredrickson, G. H. *Science* **2012**, *336*, 434-440. (b) Costello, C. A.; Schulz, D. N. 2000. Copolymers. Kirk-Othmer Encyclopedia of Chemical Technology (c) Holden, G. 2000. Thermoplastic Elastomers. Kirk-Othmer Encyclopedia of Chemical Technology.

(4) Dove, A. P. *Chem. Commun.* **2008**, 6446-6470.

(5) Nakano, K.; Kamada, T.; Nozaki, K. *Angew. Chem. Int. Ed.* **2006**, *45*, 7274-7277.

(6) Kim, J. G.; Cowman, C. D.; LaPointe, A. M.; Wiesner, U.; Coates, G. W. *Macromolecules* **2011**, *44*, 1110-1113.

(7) Jeske, R. C.; Rowley, J. M.; Coates, G. W. *Angew. Chem., Int. Ed.* **2008**, *47*, 6041-6044.

(8) DiCiccio, A. M.; Coates, G. W. Chapter Three/Manuscript in Preparation.

(9) (a) Jeske, R. C.; DiCiccio, A. M.; Coates, G. W. *J. Am. Chem. Soc.* **2007**, *129*, 11330-11331. (b) DiCiccio, A. M.; Coates, G. W. *J. Am. Chem. Soc.* **2011**, *133*, 10724-10727. (c) Huijser, S.; Nejad, E. H.; Sablong, R.; de Jong, C.; Koning, C. E.; Duchateau, R. *Macromolecules* **2011**, *44*, 1132. (d) Robert, C.; de Montigny, F.; Thomas, C. M. *Nat. Comm.* **2011**, *2*, 586-592. (e) Nejad, E. H.; van Melis, C. G. W.; Vermeer, T. J.; Koning, C. E.; Duchateau, R. *Macromolecules* **2012**, *45*, 1770-1776. (f) Darensbourg, D. J.; Poland, R. R.; Escobedo, C. *Macromolecules* **2012**, *45*, 2242-2248. (g) Nejad, E. H.; Paoniasari, A.; Koning, C. E.; Duchateau, R. *Polym. Chem.* **2012**, *3*, 1308-1313. (h) Liu, J.; Bao, Y.-Y.; Liu, Y.; Ren, W.-M.; Lu, X.-B. *Polym. Chem.* **2013**, *4*, 1439-1444. (i) Nejad, E. H.; Paoniasari, A.; van Melis, C. G. W.; Koning, C. E.; Duchateau, R. *Macromolecules* **2013**, *46*, 631-637. (j) Bernard, A.; Chatterjee, C.; Chisholm, M. H. *Polymer* **2013**, *54*, 2639-2646. (k) Harrold, N. D.; Li, Y.; Chisholm, M. H. *Macromolecules* **2013**, *46*, 692-698.

(10) Domski, G. J.; Rose, J. M.; Coates, G. W.; Bolig, A. D.; Brookhart, M. *Prog. Polym. Sci.* **2007** *32*, 30-92.

(11) Recent examples of highly active bifunctional catalysts include: (a) Noh, E. K.; Na, S. J.; S, S. ; Kim, S. W.; Lee, B. Y. *J. Am. Chem. Soc.* **2007**, *129*, 8082-8083. (b) Na, S. J.; S, S.; Cyriac, A.; Kim, B. E.; Yoo, J.; Kang, Y. K.; Han, S. J.; Lee, C.; Lee, B. Y. *Inorg. Chem.* **2009**, *48*, 10455-10465. (c) Ren, W.; Liu, Z.; Wen, Y.; Zhang, R.; Lu, X. B. *J. Am. Chem. Soc.* **2009**, *131*, 11509-11518. (d) Shen, Y. M.; Duan, W. L.; Shi, M.; *J. Org. Chem.* **2003**, *68*, 1559-1562.

(12) Several reviews and early examples of monometallic systems: (a) Kember, M. R.; Buchard, A.; Williams, C. K. *Chem. Comm.* **2010**, *47*, 141-163. (b) Darensbourg, D. J. *Chem. Rev.* **2007**, *107*, 2388-2410. (c) Coates, G. W.; Moore, D. R. *Angew. Chem. Int. Ed.* **2004**, *43*, 6618-6639. (d) Qin, Z. Q.; Thomas, C. M.; Lee, S.; Coates, G. W. *Angew. Chem. Int. Ed.* **2003**, *42*, 5484-5487. (e) Cohen, C. T.; Chu, T.; Coates, G. W. *J. Am. Chem. Soc.* **2005**, *127*, 10869-10878. (f) Cohen, C. T.; Coates, G. W. *J. Polym. Sci., Part A: Polym. Chem.* **2006**, *44*, 5182-5191.

(13) (a) Darensbourg, D. J.; Ulusoy, M.; Karroonirum, O.; Poland R. R.; Reibenspies, J. H.; Cetinkaya, B. *Macromolecules* **2009**, *42*, 6992-6998. (b) Darensbourg, D. J.; Mackiewicz, R. M.; Rodgers, J. M. *J. Am. Chem. Soc.* **2005**, *127*, 14026-14038.

(14) Please refer to Appendix three for further discussion and more detail.

APPENDIX THREE

# COBALT SALEN CATALYST FOR THE LIVING COPOLYMERIZATION OF PHTHALIC ANHYDRIDE WITH TERMINAL EPOXIDES: EFFICIENT SYNTHESIS OF POLYESTER BLOCK COPOLYMERS AND ELASTOMERS

**Contents**

### A3.1. General considerations

All manipulations of air and water sensitive compounds were performed under dry nitrogen using a Braun Labmaster Glovebox or standard Schlenk line techniques. NMR spectra were recorded on a Varian INOVA 400 ($^{1}$H, 400 MHz; $^{13}$C, 100 MHz; $^{19}$F 376 MHz), Varian INOVA 500 ($^{1}$H, 500 MHz; $^{13}$C, 125 MHz), or Varian INOVA 600 ($^{1}$H, 600 MHz; $^{13}$C, 150 MHz) spectrometer. $^{1}$H NMR spectra were referenced with residual non-deuterated solvent shifts ($CHCl_3$ = 7.26 ppm, or $C_5D_4HN$ = 7.22 ppm), $^{13}$C NMR spectra were referenced by solvent shifts ($CDCl_3$ = 77.16 ppm or $C_5D_5N$ = 123.87 ppm) and $^{19}$F NMR spectra were referenced to fluorobenzene added as an internal standard ($C_6H_5F$ = -131.15 ppm).

Gel permeation chromatography (GPC) analyses were conducted using an Agilent PL-GPC 50 integrated system, (2 x PLgel Mini-MIX C columns, 5 micron, 4.6 mmID) equipped with UV and refractive index detectors. The GPC columns were eluted at a rate of 0.3 mL/min with tetrahydrofuran at 30 °C and were calibrated relative to monodisperse polystyrene standards.

Differential scanning calorimetry of polymer samples was performed on a Mettler-Toledo Polymer DSC instrument equipped with a Julabo chiller and autosampler. Typical DSC experiments were made in crimped aluminum pans and experiments were conducted with a heating rate of 10 °C/min from -70 °C to +200 °C. Data was processed using StarE software.

HR/MS analysis was performed at Cornell University by direct-inject on a JEOL GCMate.

## A3.2. Materials

### 2.1. General Materials

$CaH_2$ pellets (90%) used for drying epoxides were purchased from Strem and used as received. Butylated hydroxytoluene (BHT) was purchased from Sigma Aldrich (>99% purity). [PPN]Cl was purchased from Sigma Aldrich (98% purity). Trifluoroacetic acid was purchased from Oakwood Products (99% purity). Hexamine (>99% purity) was purchased from Sigma Aldrich. HPLC grade dichloromethane used for metallation was purchased from Fisher Scientific and purified through a solvent purification system under inert atmosphere and degassed for 1 h prior to use. Ethanol used for metallation was purchased from Kroptect, stored over 3 Å sieves and degassed for 1 h prior to use. All NMR solvents were purchased from Cambridge Isotopes and stored over 3 Å molecular sieves. Fluorobenzene was purchased from Sigma Aldrich (99% purity) and used as received. All solvents were used as received unless otherwise noted. All other reagents were purchased from Aldrich, Alfa-Aesar, Acros, Fischer-Scientific or TCI and were used as received unless otherwise noted.

### 2.2. Polymerization Monomers

Propylene oxide (**2a**), 1-butene oxide (**2c**), 1,2-epoxyhexane (**2d**) and 1,2-epoxydodecane (**2e**) were purchased from either Sigma Aldrich or TCI, dried over $CaH_2$ for 3 days under inert atmosphere, vacuum transferred to a flame dried thick walled Schlenk adapted flask and stored in the glove box. 1,1,1-trifluoropropan-2,3-ene oxide (**2b**) was purchased from Oakwood Products, dried over $CaH_2$ for 3 days

under inert atmosphere, vacuum transferred to a flame dried thick walled Schlenk adapted flask and stored in the glove box.

Phthalic anhydride (**1**) (>99% purity**,** Sigma Aldrich) was boiled in $CHCl_3$ at 60 °C (10 g anhydride in 100 mL solvent) for 1 h followed by hot filtration to remove insoluble diacids. The organic filtrates were concentrated to white solids *via* roto-evaporation and washed with diethyl ether. The resulting white powder was collected, dried under vacuum for 12 h in the presence of drierite to remove residual moisture, and sublimed under reduced pressure (83 °C). The purified anhydride was collected under inert atmosphere and stored in the glovebox until use. The purity was confirmed by $^1H$ NMR in DMSO-$d_6$.

### 2.3. Catalyst Components

$Co(NO)_3$•$6H_2O$ (>99% purity) was purchased from Strem and stored in a dessicator until use. 4-fluorphenol was purchased from Oakwoods Chemicals and used as received.

### A3.3. Synthesis of Starting Materials

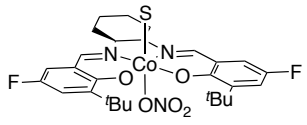


**cat1**

**Cat1.** The synthesis of **cat1** was performed according to literature/Chapter 3 **cat5**.

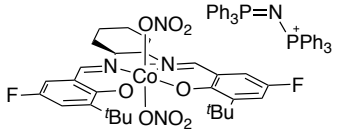


**cat2**

**Cat2.** A solution of *N,N'*-bis(3-*tert*-butyl-5-fluorosalicylidine)-1,2-cyclohexadiimine (0.30 g, 0.62 mmol), synthesized according to literature/Chapter 3 (**aldehyde5**), was made in dry, degassed dichloromethane under a flow of nitrogen. At the same time, $Co(NO_3)_2 \cdot 6H_2O$ (0.18 g, 0.68 mmol) was desiccated under vacuum at 60 °C while being masticated by a stir bar. Once the red solid became a light pink powder it was dissolved in a solution of dry, degassed ethanol. Next, the purple ethanol solution containing cobalt was cannulated into the yellow dichloromethane solution of ligand. Upon mixing, a deep red color formed. After stirring for 5 minutes, [PPN][$NO_3$] (0.42 g, 0.68 mmol) was added as a powder to the flask and the resulting mixture was stirred under dessicated air for 13 h (atmospheric air was allowed to diffuse through a tube filled with drierite into the reaction). After 13 h, the mixture was filtered through a fine frit, rinsed with dichloromethane until any green/brown residue was dissolved and rotovapped to dryness. The dark solid was suspended in pentane, sonnicated for 10 min and collected on a fine frit (80 % isolated yield average). Note that during HR/MS analysis, the cobaltate loses the nitrate counterions, thus only the (salcy)Co fragment is detected. This is typical of this kind of catalyst. HR/MS: expected: 527.19 g/mol found: 527.19 g/mol.

$^1$H NMR peaks corresponding to catalyst ligand (500 MHz, $C_5D_5N$): δ 8.66 (m, 2H); 7.50 (m, 2H); 7.31 (m, 2H); 3.90 (m, 2H); 3.02 (m, 2H); 2.09 (m, 2H); 1.76 (m, 2H); 1.47 (m, 18H); 1.43 (m, 2H). $^1$H NMR peaks corresponding to the PPN counterion: δ 7.63 (m, 18H); 7.45 (m, 12H). Note this compound is a salt and thus the integrations are not accurate for comparison between the compounds. $^{13}$C NMR peaks corresponding to catalyst ligand (125 MHz, $C_5D_5N$): δ 167.37; 167.35; 160.26;

154.22; 150.15; 145.85; 145.80; 122.16; 117.13; 116.96; 116.93; 116.87; 71.18; 36.15; 29.65; 24.82. $^{1}$C NMR peaks corresponding to the PPN counterion: δ 134.07; 132.63; 129.89; 127.98; 127.12. $^{19}$F NMR (376 MHz, $C_5D_5N$) referenced to $C_6H_5F$: δ -147.2 (m, 2F).

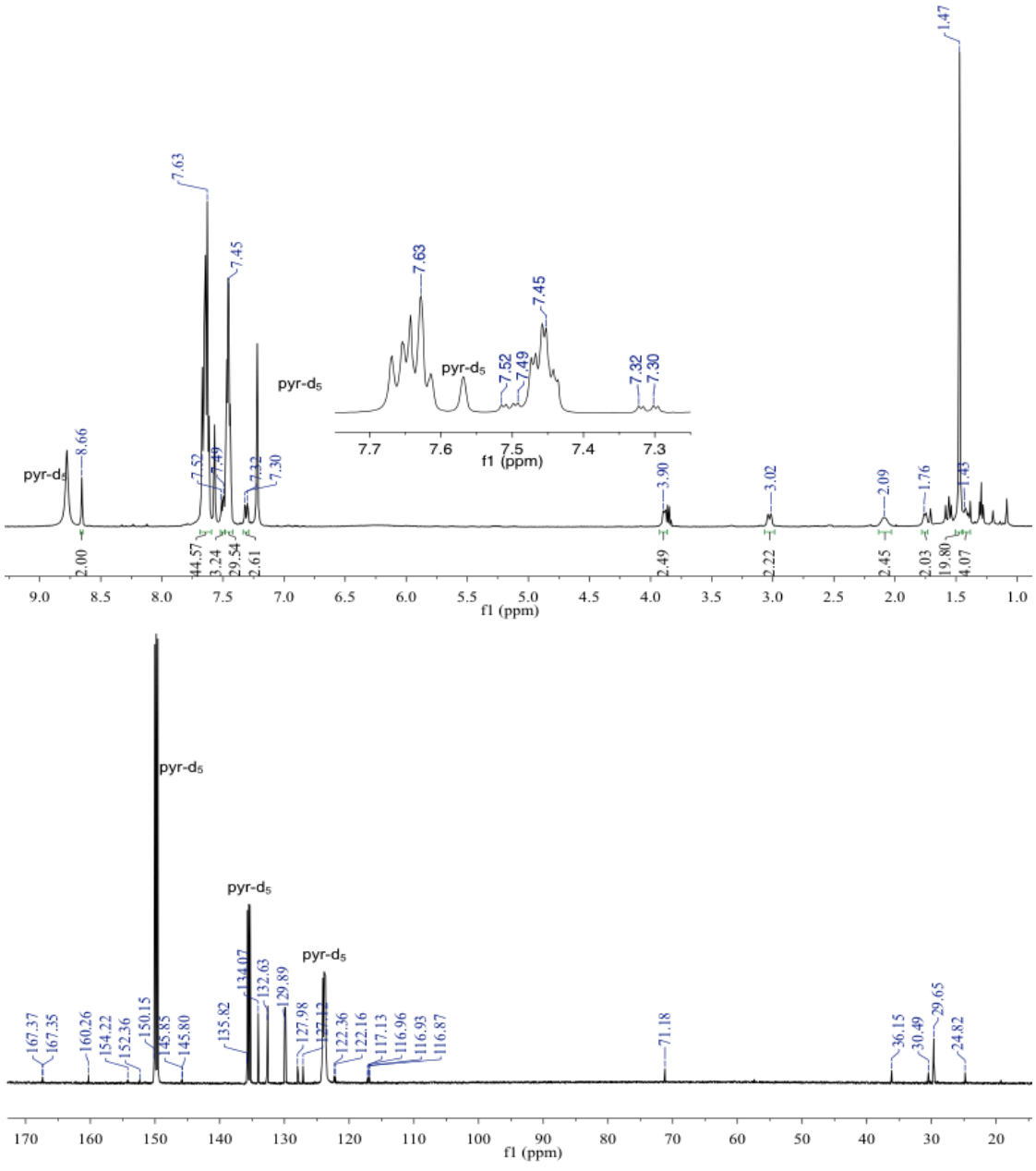

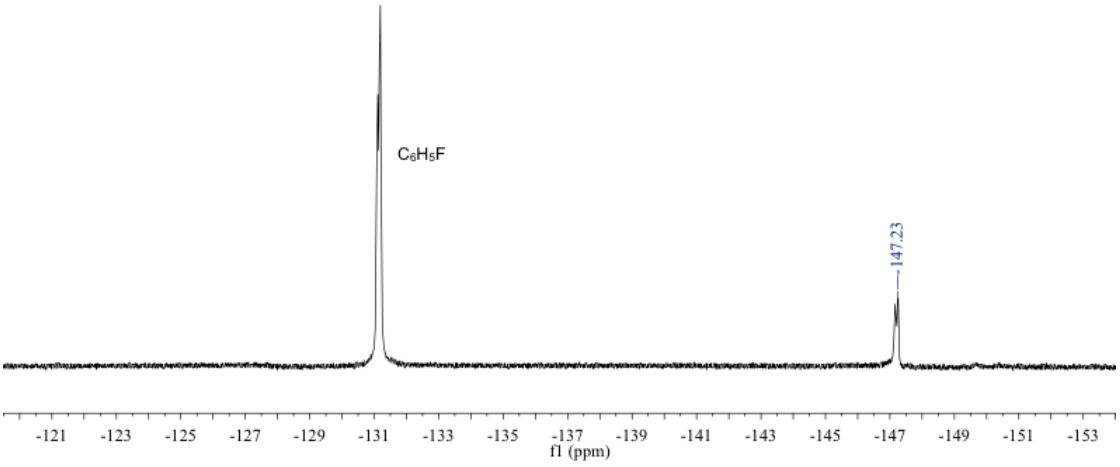


**Figure A3.1.** NMR spectra of **cat2** in pyridine-$d_5$. Top: $^{1}$H NMR spectrum. Middle: $^{13}$C NMR spectrum. Bottom: $^{19}$F NMR spectrum.

### A3.4. Representative Copolymerizations

#### 4.1. cat1 Catalyzed Copolymerization

**Poly(propylene phthalate)** (Table 4.1, entry 1). In a glovebox, **cat1** (3.0 mg, 5.0 μmol), [PPN][$NO_3$] (3.0 mg, 5.0 μmol) and phthalic anhydride (**1**) (0.30 g, 2.0 mmol) were placed in a flame dried 4.0 mL vial equipped with a Teflon coated stir bar. Propylene oxide (**2a**) (0.28 mL, 4.0 mmol) was added via syringe with care to wash all solids into the base of the vial. The vial was sealed with a Teflon lined cap, removed from the glovebox, and placed in an aluminum heat block preheated to the desired temperature (30 °C). After the reaction became viscous or anhydride was no longer visible, the vial was removed from the heat block. A small aliquot was removed for $^{1}$H NMR spectroscopy analysis to determine conversion. The viscous reaction mixture was dissolved in dichloromethane and precipitated into an excess of methanol or

hexanes. This process was repeated until all residual monomer was removed. After polymer washes, the material was collected and dried *in vacuo*.

### 4.2. cat2 Catalyzed Copolymerization

**Poly(propylene phthalate)** (Table 4.1, entry 2). In a glovebox, **cat2** (6.0 mg, 5.0 μmol) and phthalic anhydride (**1**) (0.30 g, 2.0 mmol) were placed in a flame dried 4.0 mL vial equipped with a Teflon coated stir bar. Propylene oxide (**2a**) (0.28 mL, 4.0 mmol) was added via syringe with care to wash all solids into the base of the vial. The vial was sealed with a Teflon lined cap, removed from the glovebox, and placed in an aluminum heat block preheated to the desired temperature (30 °C). After the reaction became viscous or anhydride was no longer visible, the vial was removed from the heat block. A small aliquot was removed for $^{1}$H NMR spectroscopy analysis to determine monomer conversion. The viscous reaction mixture was dissolved in dichloromethane and precipitated into an excess of methanol or hexanes. This process was repeated until all residual monomer was removed. After polymer washes, the material was collected and dried *in vacuo*.

### 4.3. Block Copolymerizations via Sequential Addition

**Representative triblock polymerization:** In a glovebox, **cat2** (6.0 mg, 5.0 μmol) and phthalic anhydride (**1**) (0.30 g, 2.0 mmol) were placed in a flame dried 4.0 mL vial equipped with a Teflon coated stir bar. Propylene oxide (**2a**) (0.28 mL, 4.0 mmol) was added via syringe with care to wash all solids into the base of the vial. The vial was sealed with a Teflon lined cap, removed from the glovebox, and placed in an

aluminum heat block preheated to the desired temperature (30 °C). After the reaction became viscous or anhydride was no longer visible, the vial was removed from the heat block. A small aliquot was removed for $^{1}$H NMR spectroscopy analysis to determine monomer conversion. The next block was initiated upon addition of more anhydride and epoxide, performed inside a nitrogen filled glovebox. If the solution was too viscous, THF or benzene was used to solubilize the polymer. The reaction flask was sealed and heated to the desired temperature for the next block. This procedure was repeated until the desired number of blocks was formed. The viscous reaction mixture was then dissolved in dichloromethane and precipitated into an excess of methanol or hexanes. This process was repeated until all residual monomer was removed. After polymer washes, the material was collected and dried *in vacuo*.

### A3.5. Gel-Permeation Chromatography Traces for Table 4.1

Overlaid GPC traces of polymers from Table 4.1.

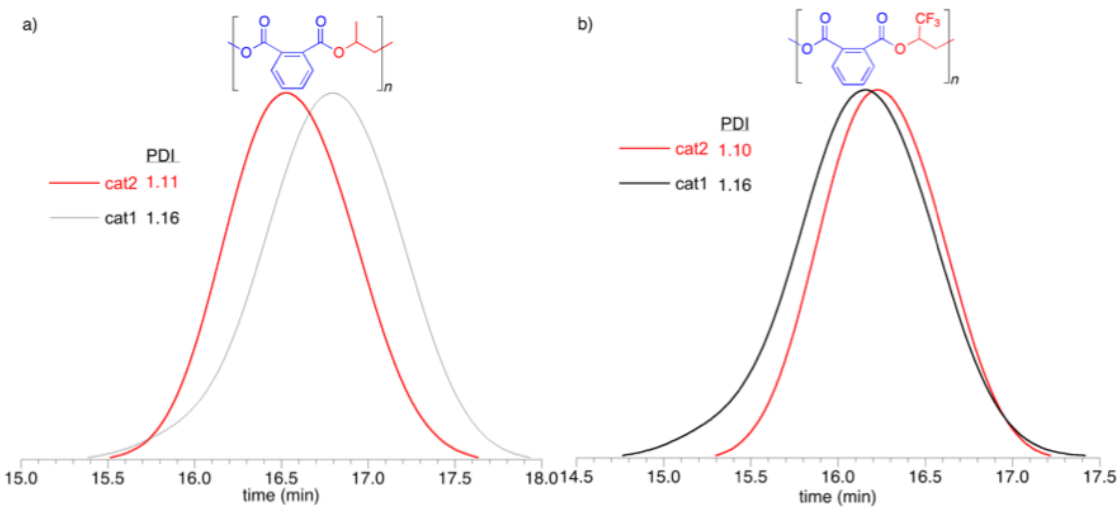


**Figure A3.2.** Overlaid gel-permeation chromatography traces for: a) poly(propylene-*alt*-phthalate) (entry 1 and 2) b) poly(1,1,1-trifluoropropan-2,3-ene oxide-*alt*-phthalate) (entry 3 and 4).

## A3.6. *In situ* Observations for the Living and Kinetic Studies of cat2

### 6.1. Experimental Procedure for Living Copolymerization

In a nitrogen filled glovebox, **cat2** (6.0 mg, 5.0 μmol) and phthalic anhydride (**1**) (0.60 g, 4.0 mmol) were placed in a flame dried 4.0 mL vial equipped with a Teflon coated stir bar. Propylene oxide (**2a**) (0.56 mL, 8.0 mmol) was added via syringe with care to wash all solids into the base of the vial. THF (0.20 mL) was added to reduce viscosity. The vial was sealed with a Teflon lined cap and stirred inside the glovebox ($T_{rxn}$ ~ 30 °C). Aliquots were removed periodically and dried under vacuum. The polymer samples were each dissolved in 0.50 mL of $C_6D_6$ for $^1H$ NMR analysis (Figure A3.3), then redried and redissolved in 2 mL of THF for GPC analysis (Figure A3.4). When the reaction was no longer able to stir, the viscous reaction mixture was removed from the glovebox, dissolved in dichloromethane, and precipitated into an excess of methanol. This process was repeated until all residual monomer was removed. After polymer washes, the material was collected and dried *in vacuo*.

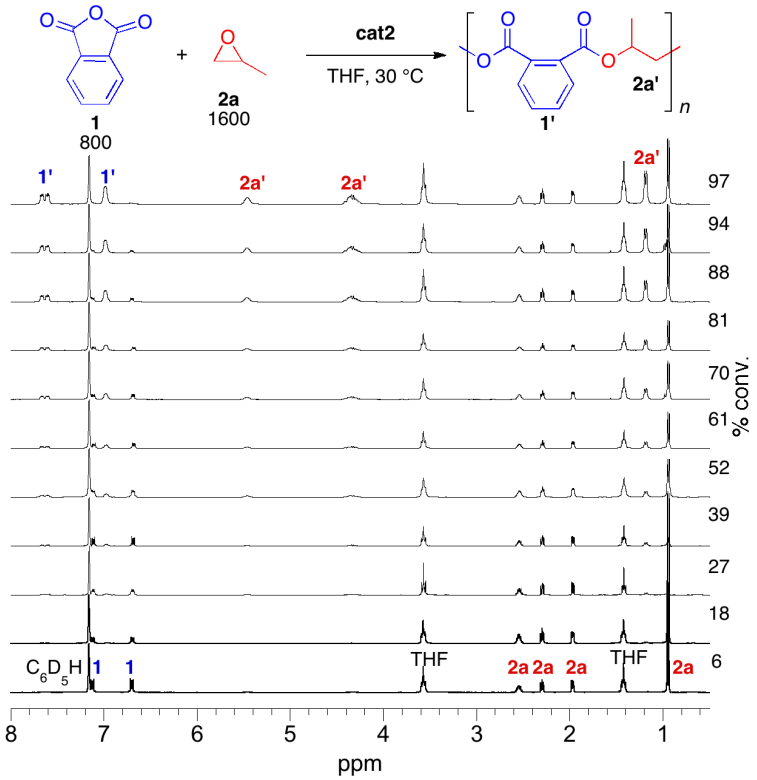


**Figure A3.3.** Overlaid $^{1}$H NMR spectra for the copolymerization of phthalic anhydride with propylene oxide catalyzed by **cat2**.

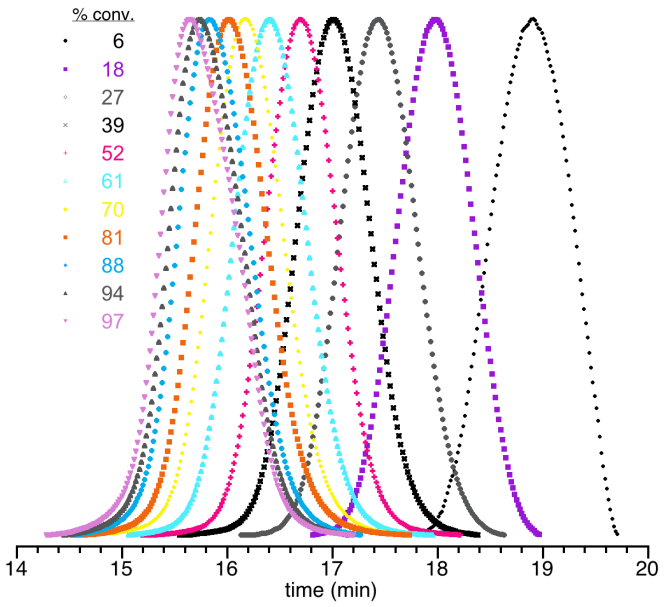


**Figure A3.4.** Overlaid GPC traces of poly(propylene-*alt*-phthalate) formed by **cat2**.

### 6.2. Representative Experimental Procedure for *in situ* NMR Evaluation

In a nitrogen filled glovebox, a stock solution of phthalic anhydride (0.30 g, 2.0 mmol), propylene oxide (0.56 mL, 8.0 mmol) and 2.2 mL of $C_6D_6$ was prepared and shaken until all anhydride was dissolved. Next, 2.5 μmol of **cat2** was dissolved in the appropriate amount of stock solution to make either a 1.8 mM, 3.6 mM or 7.1 mM reaction mixture. The solution was dispensed into an oven dried J-young tube and sealed with a Teflon lined cap. $^1$H NMR spectroscopy measurements were taken at intervals until the reaction was complete and care was taken to keep the reactions under inert atmosphere. Upon completion, all polymers were precipitated and isolated.

### 6.3. Analysis of $^1$H NMR Kinetics Studies

$^1$H NMR spectroscopy was used to calculate percent conversion from the time points collected in section A3.6.2. It should be noted that the conditions used for this experiment are more dilute than standard copolymerization conditions to accommodate for NMR solvent and poor solubility of phthalic anhydride. Figure A3.5 depicts the rates of each reaction and reflects a concentration dependence on **cat2**. No initiation period is observed except at low catalyst concentration (1.8 mM), however, it is negligibly small. Overall, this data supports the fast initiation for polymerization by **cat2**, even in dilute solutions.

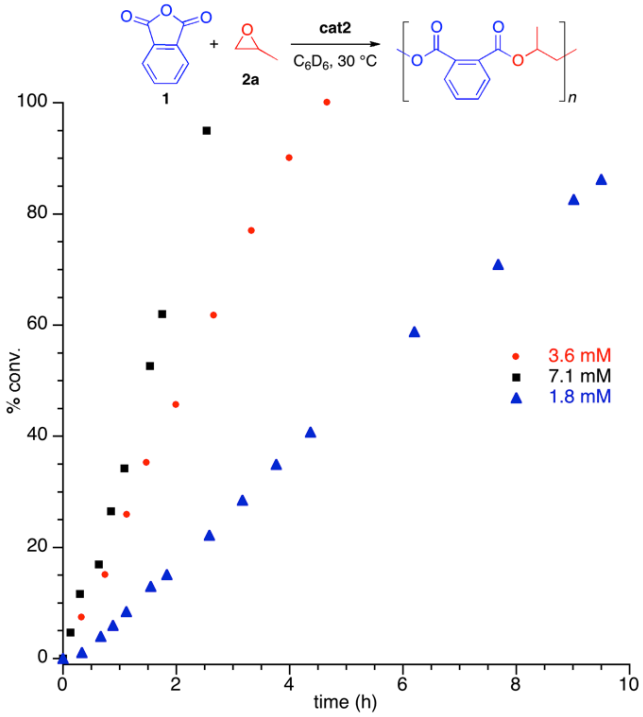


**Figure A3.5.** Percent conversion as calculated by $^{1}$H NMR spectroscopy vs. time for three different concentrations of **cat2** (1.8 mM).

## A3.10. NMR Spectra and Assignments for Reported Polyesters

**Poly(propylene-*alt*-phthalate)**, Table 4.2, entry 1. $^{1}$H NMR spectrum (500 MHz, $CDCl_3$): δ 7.71 (m, 1H); 7.66 (m, 1H); 7.48 (m, 2H); 5.42 (m, 1H); 4.38 (m, 2H); 1.36 (d, 3H, $J$ = 6.5 Hz). $^{13}$C NMR spectrum (125 MHz, $CDCl_3$): δ 166.9; 166.8; 132.3; 131.6; 131.4; 131.2; 129.1; 129.0; 69.7; 67.0; 16.5.

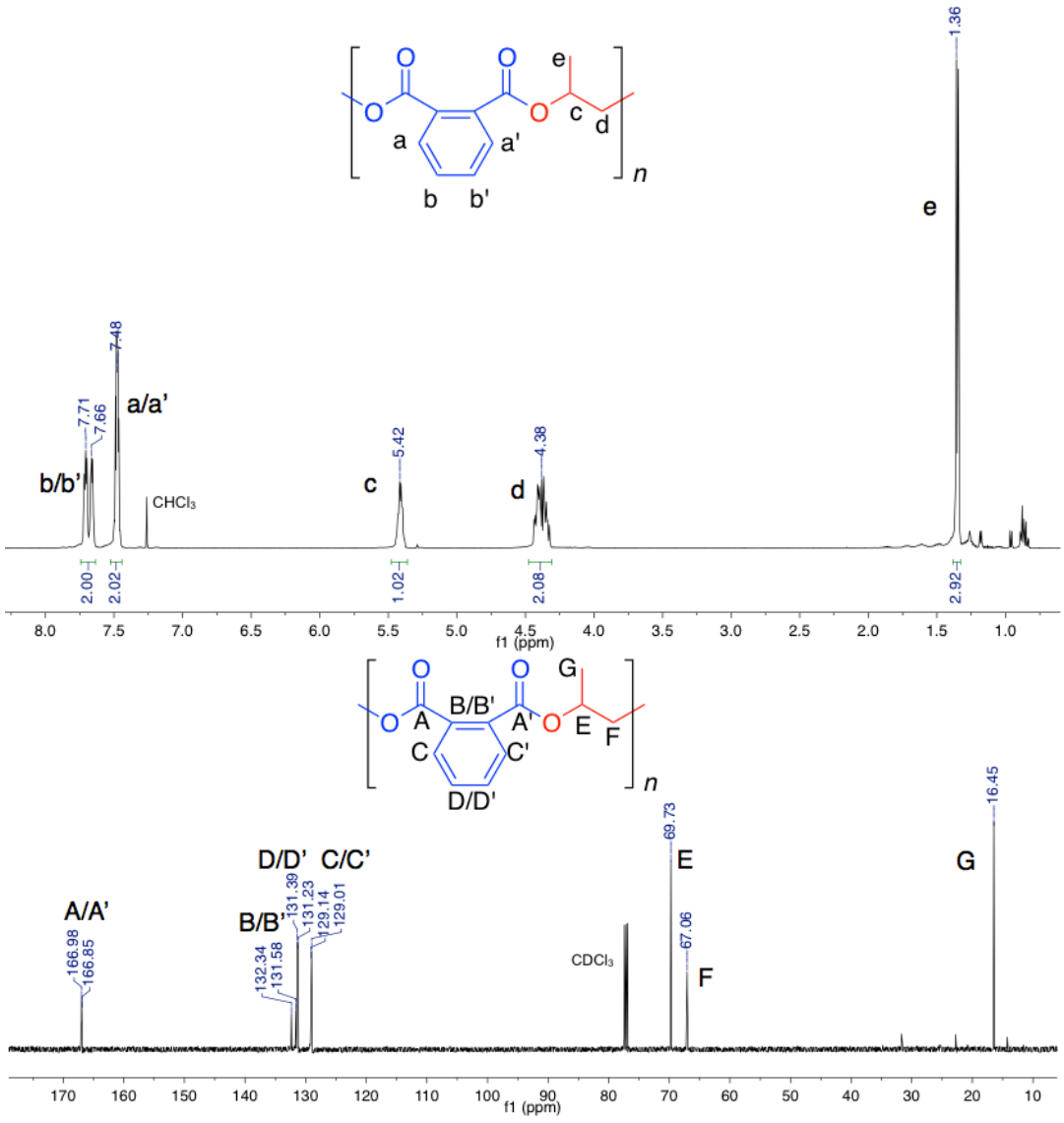


**Figure A3.6.** Poly(propylene-*alt*-phthalate) in $CDCl_3$. Top: $^{1}$H NMR spectrum. Bottom: $^{13}$C NMR spectrum.

**Poly(1,1,1-trifluoropropan-2,3-ene oxide-*alt*-phthalate)**, Table 4.2, entry 2. $^{1}$H NMR spectrum (500 MHz, $CDCl_3$): δ 7.75 (m, 1H); 7.67 (m, 1H); 7.52 (m, 2H); 5.80 (m, 1H); 4.71-4.54 (m, 2H). $^{13}$C NMR spectrum (125 MHz, $CDCl_3$): δ 166.0; 165.4; 132.0; 131.9; 130.9; 129.5; 129.3; 126.1-119.4 (q, $J$ = 281.5 Hz); 69.3-68.5 (m); 60.9 (m).

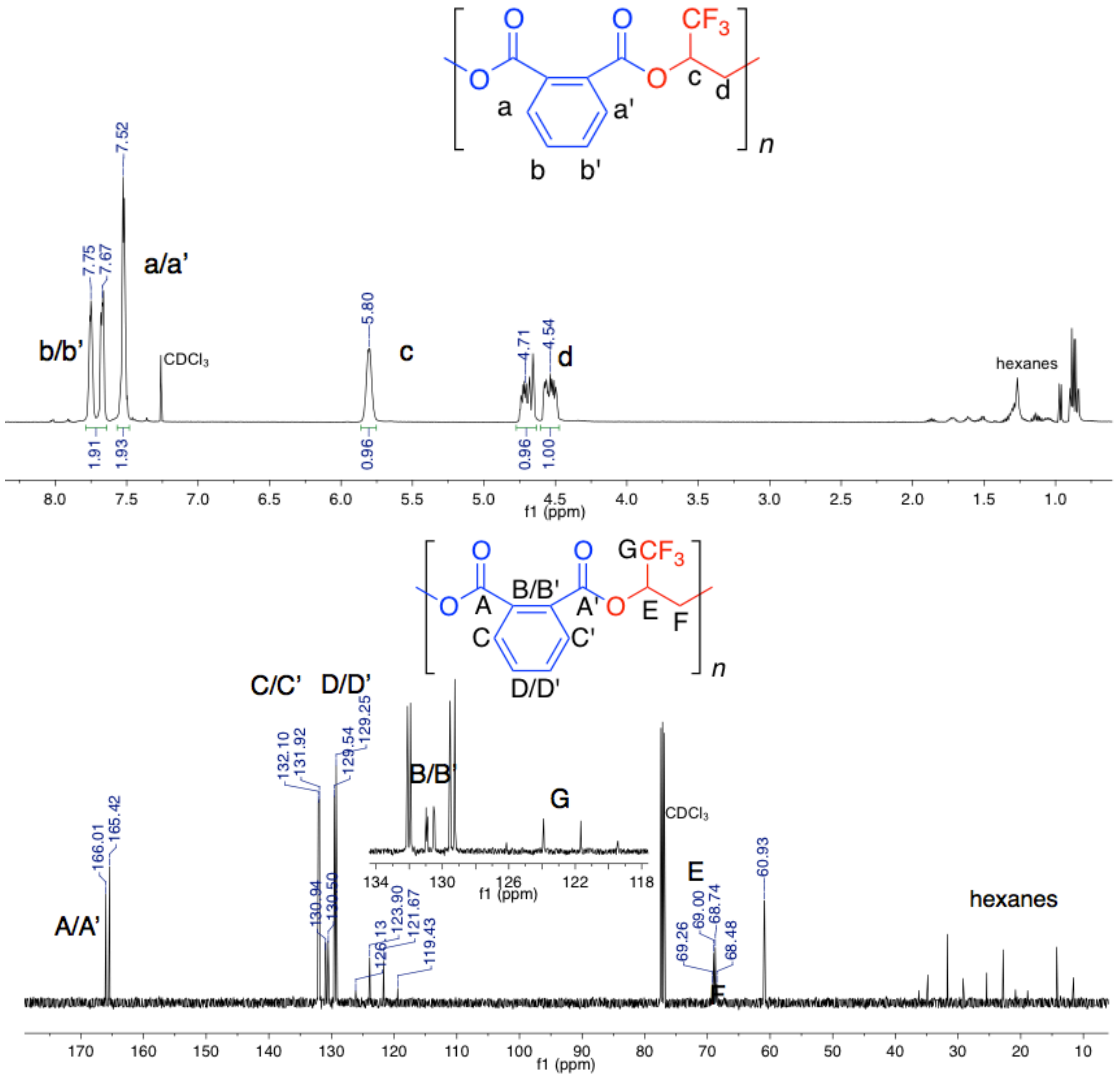


**Figure A3.7.** Poly(1,1,1-trifluoropropan-2,3-ene oxide-*alt*-phthalate) in $CDCl_3$. Top: $^{1}$H NMR spectrum. Bottom: $^{13}$C NMR spectrum.

**Poly(1-butene oxide-*alt*-phthalate)**, Table 4.2, entry 3. $^{1}$H NMR spectrum (500 MHz, $CDCl_3$): δ 7.70 (m, 2H); 7.47 (m, 2H); 5.30 (m, 1H); 4.50-4.39 (m, 2H); 1.75 (m, 2H); 0.97 (d, $J$ = 7.4 Hz, 3H). $^{13}$C NMR spectrum (125 MHz, $CDCl_3$): δ 167.02; 132.3; 131.7; 131.3; 129.0; 74.2; 65.6; 23.9; 9.6.

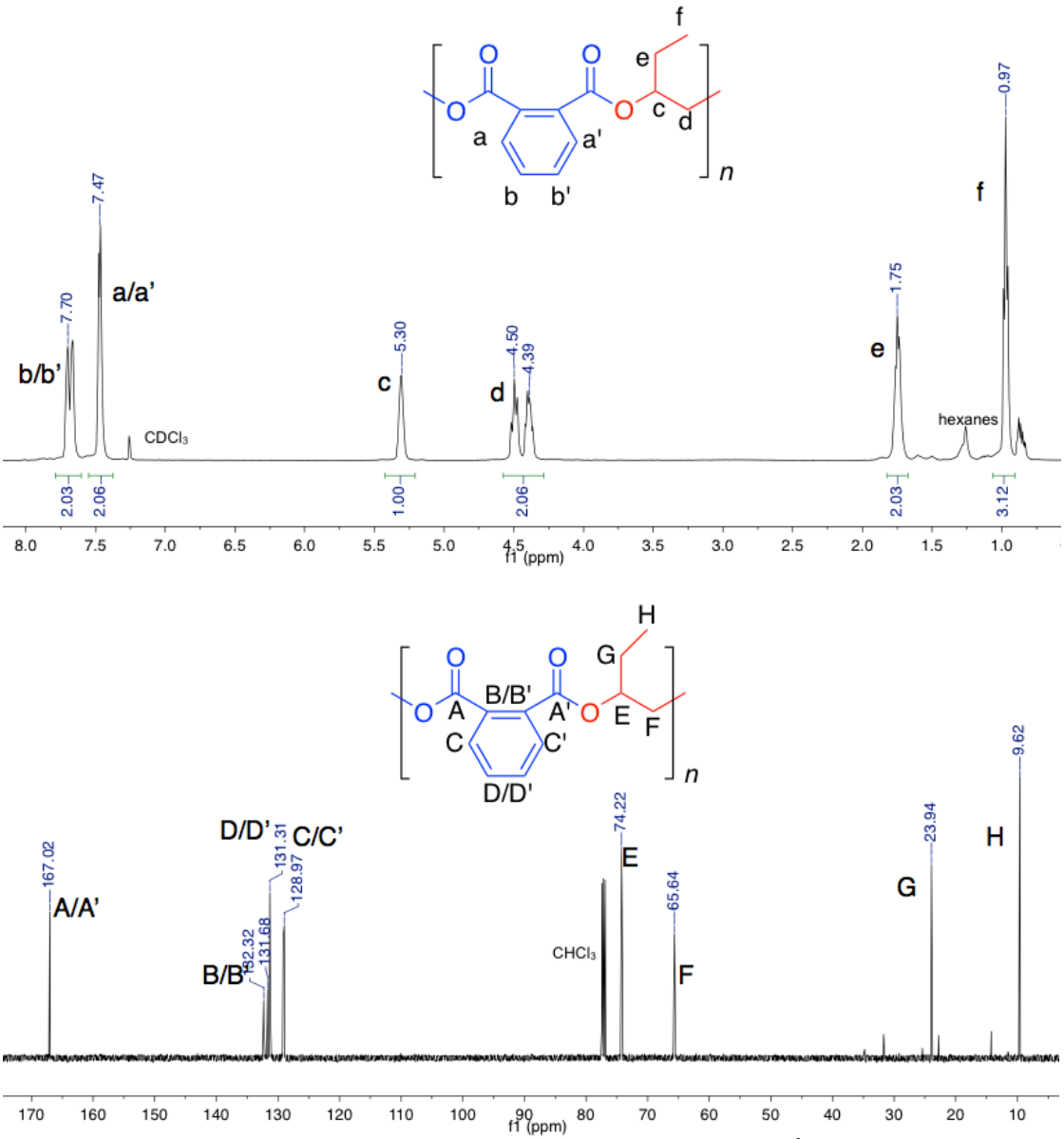


**Figure A3.8.** Poly(1-butene oxide-*alt*-phthalate) in $CDCl_3$. Top: $^{1}$H NMR spectrum. Bottom: $^{13}$C NMR spectrum.

**Poly(1,2-epoxyhexane-*alt*-phthalate)**, Table 4.2, entry 4. $^{1}$H NMR spectrum (500 MHz, $CDCl_3$): δ 7.71-7.67 (m, 2H); 7.47 (m, 2H); 5.39 (m, 1H); 4.52-4.37 (m, 2H); 1.73 (m, 2H); 1.34 (m, 4H); 0.87 (t, $J$ = 7.0 Hz, 3H). $^{13}$C NMR spectrum (125 MHz, $CDCl_3$): δ 167.0; 132.4; 131.7; 131.3; 131.2; 129.2; 128.9; 73.1; 66.0; 30.5; 27.3; 22.6; 14.0.

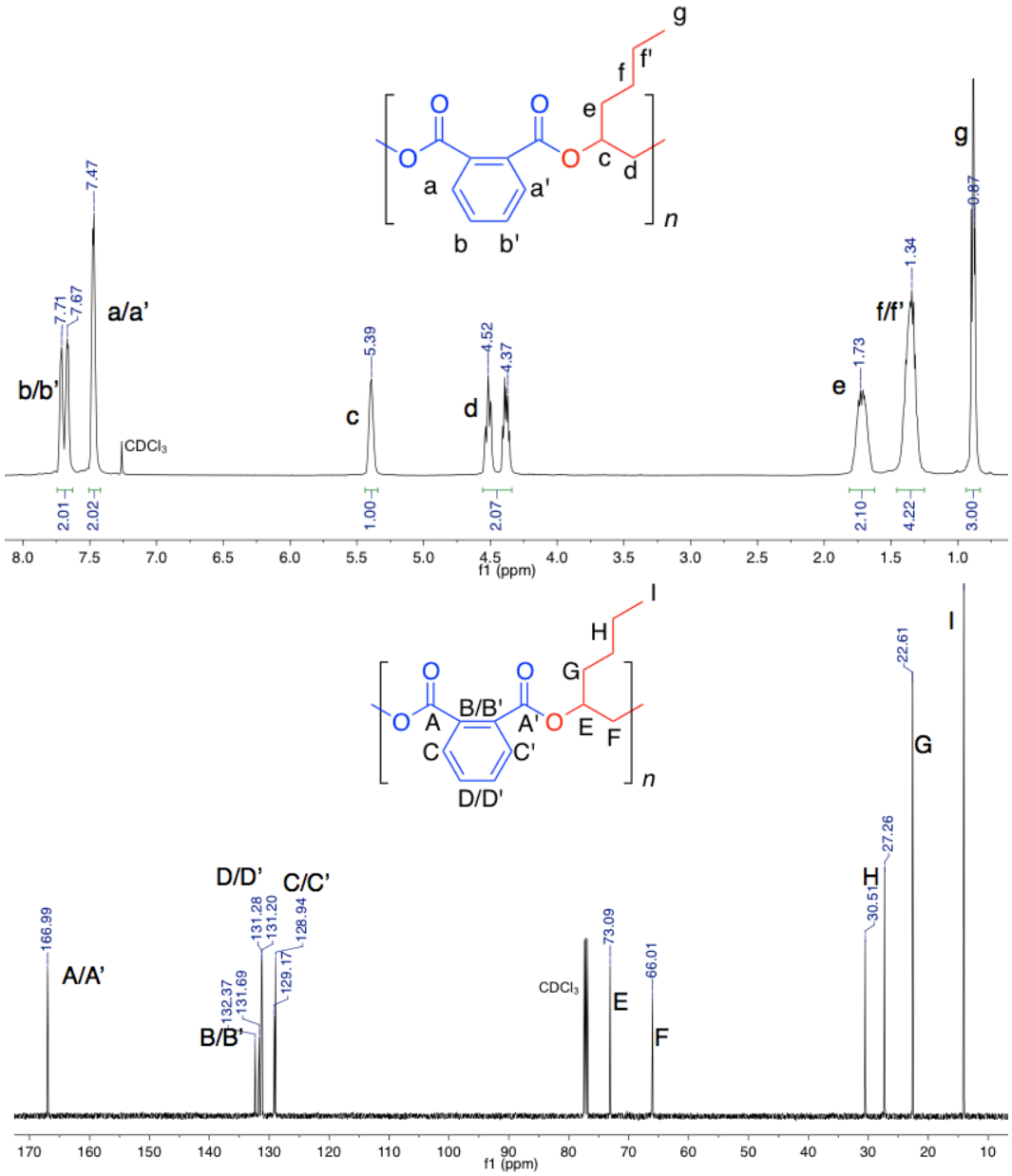


**Figure A3.9.** Poly(1,2-epoxyhexane-*alt*-phthalate) in $CDCl_3$. Top: $^{1}$H NMR spectrum. Bottom: $^{13}$C NMR spectrum.

**Poly(1,2-epoxydodecane-*alt*-phthalate)**, Table 4.2, entry 5. $^{1}$H NMR spectrum (500 MHz, $CDCl_3$): δ 7.72 (m, 1H); 7.66 (m, 1H); 7.47 (m, 2H); 5.41 (m, 1H); 4.54-4.37 (m, 2H); 1.73 (m, 2H); 1.42 (m, 2H); 1.24 (m, 14H); 0.87 (t, $J$ = 6.7 Hz, 3H). $^{13}$C NMR spectrum (125 MHz, $CDCl_3$): δ 167.0; 166.9; 132.4; 131.7; 131.3; 131.2; 129.2; 128.4; 73.1; 66.1; 32.0; 30.9; 29.8; 29.6; 29.5; 25.2; 22.8; 14.2.

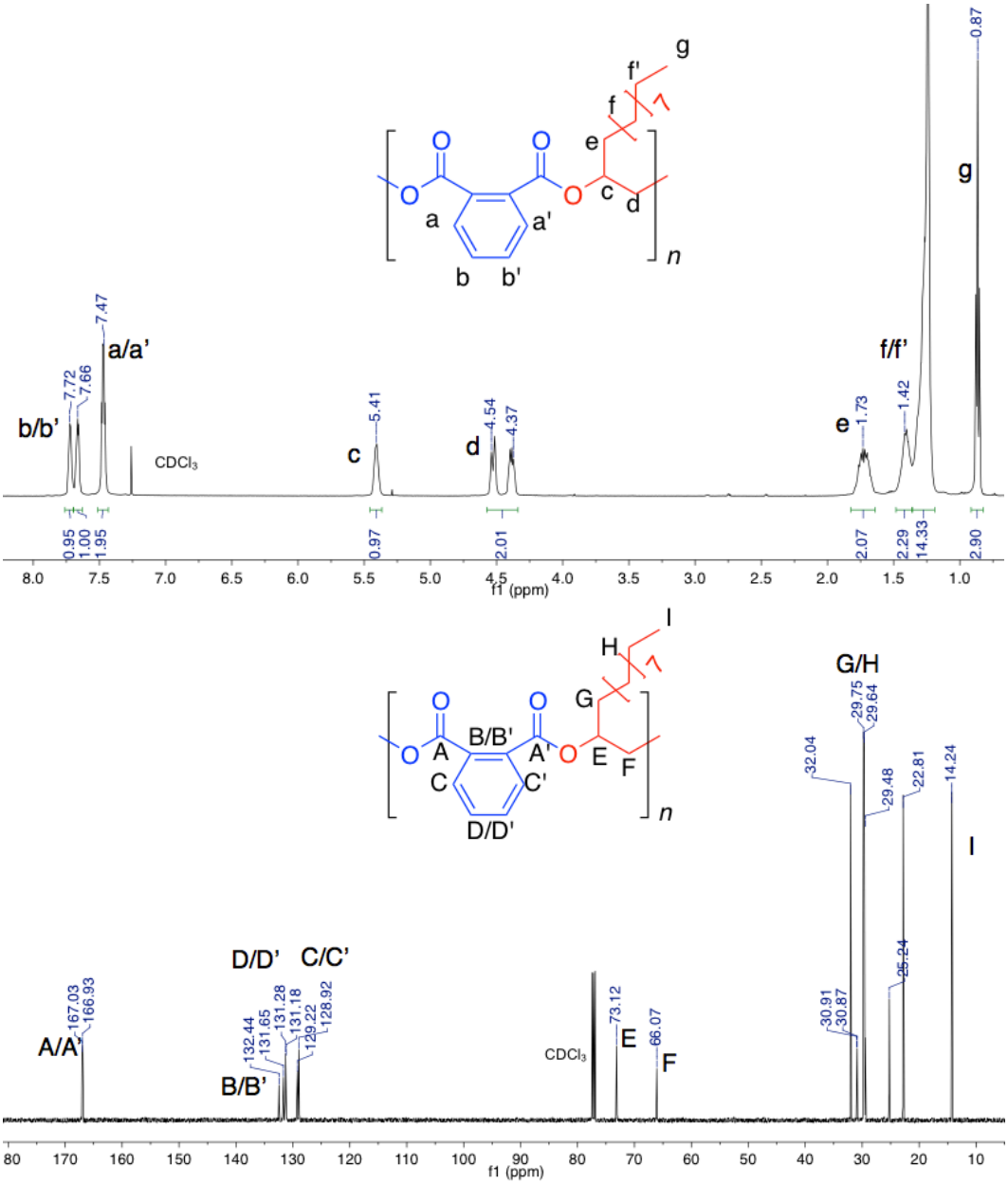


**Figure A3.10.** Poly(1,2-epoxydodecane-alt-phthalate) in $CDCl_3$. Top: $^{1}$H NMR spectrum. Bottom: $^{13}$C NMR spectrum.

## A3.9. DSC Thermograms for Reported Polyesters

**Poly(propylene-*alt*-phthalate)**, Table 4.2, entry 1.

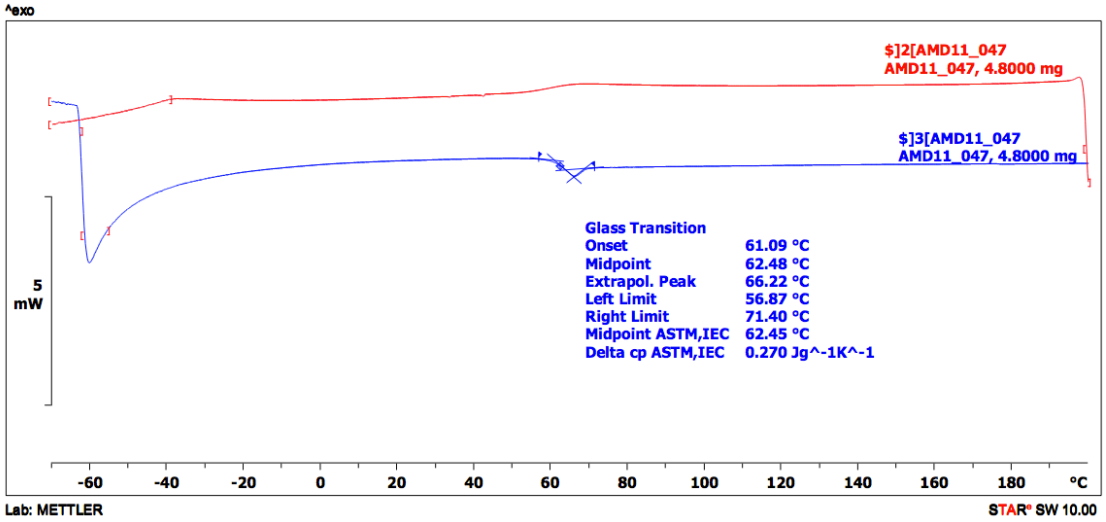


**Figure A3.11.** DSC thermogram for poly(propylene-*alt*-phthalate), Table 4.2, entry 1.

**Poly(1,1,1-trifluoropropan-2,3-ene oxide-*alt*-phthalate)**, Table 4.2, entry 2.

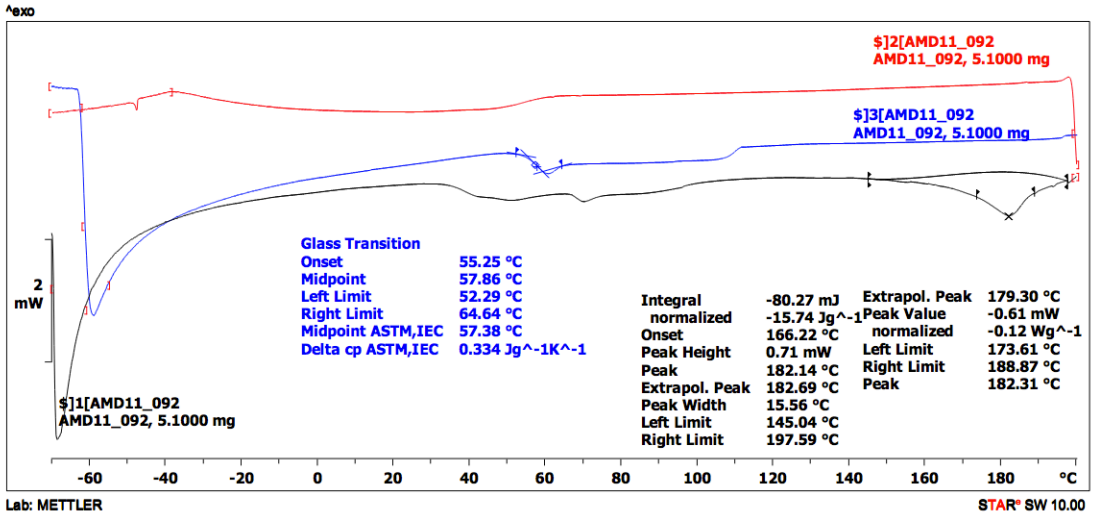


**Figure A3.12.** DSC thermogram for poly(1,1,1-trifluoropropan-2,3-ene oxide-*alt*-phthalate), Table 4.2, entry 2. Note the detected endotherm at 182 °C is a potential melting point.

**Poly(1-butene oxide-*alt*-phthalate)**, Table 4.2, entry 3.

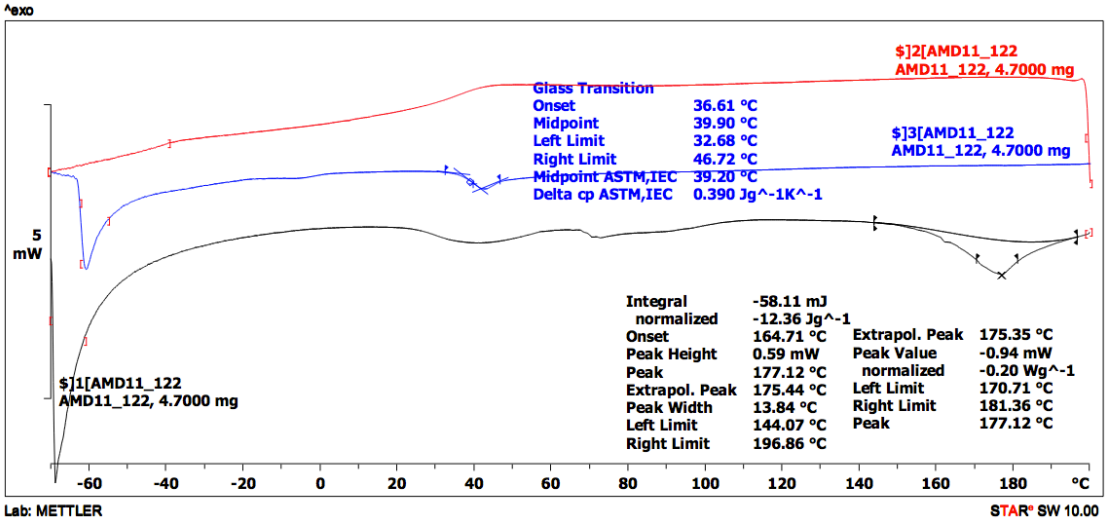


**Figure A3.13.** DSC thermogram for poly(1-butene oxide-*alt*-phthalate), Table 4.2, entry 3. Note the endotherm at 177 °C is considered a potential melting point.

**Poly(1,2-epoxyhexane-*alt*-phthalate)**, Table 4.2, entry 4.

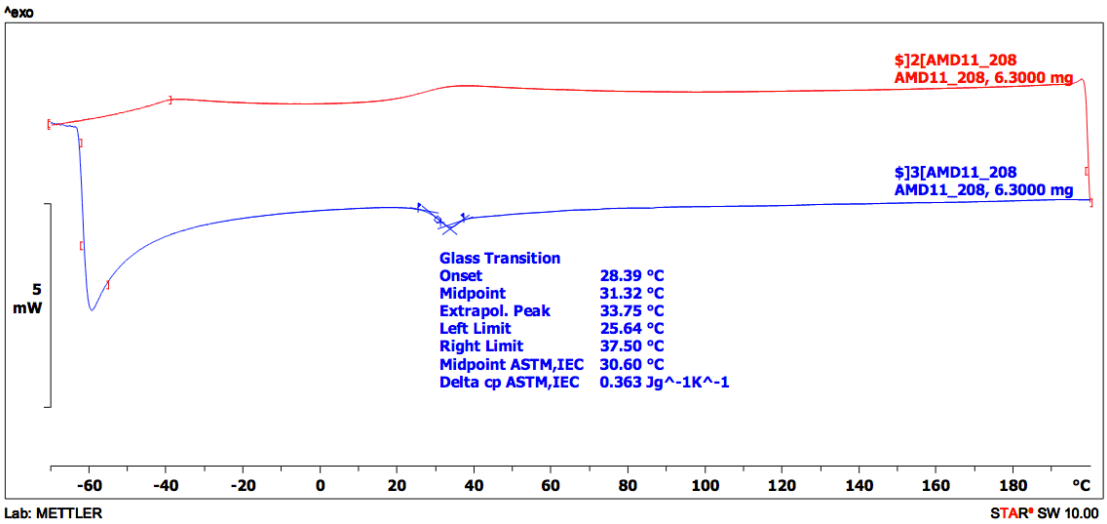


**Figure A3.14.** DSC thermogram for poly(1,2-epoxyhexane-*alt*-phthalate), Table 4.2, entry 4.

**Poly(1,2-epoxydodecane-*alt*-phthalate)**, Table 4.2, entry 5.

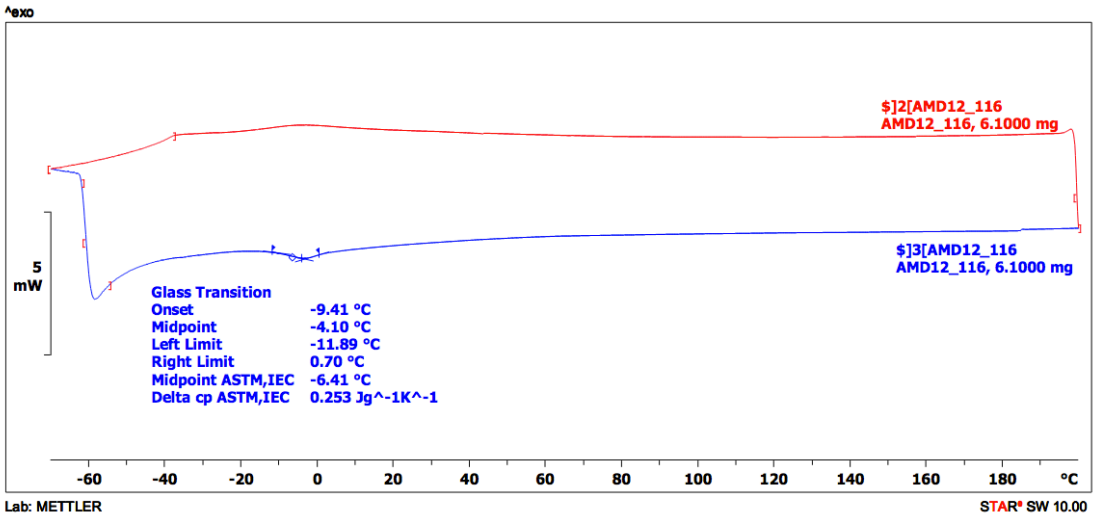


**Figure A3.15.** DSC thermogram for poly(1,2-epoxydecane-*alt*-phthalate), Table 4.2, entry 5.

## A3.10. *In situ* $^1$H NMR Observation of Poly(propylene-*alt*-phthalate)-*b*-(1-butene-*alt*-phthalate) Growth using Vacuum Between Blocks

### 10.1. Experimental Procedure

In a nitrogen filled glovebox, approximately 3.0 mg of **cat2** (2.5 μmol), 0.15 g of phthalic anhydride (1.0 mmol), 0.14 mL of propylene oxide (2.3 mmol), and 0.40 mL of $C_6D_6$ were measured into an oven dried J-Young tube and sealed with a Teflon lined cap. The tube was removed from the glovebox and stored in an oil bath at 30 °C, and manually agitated periodically. After 9 h, $^1$H NMR spectroscopy was used to analyze the reaction mixture to assess conversion and the tube was placed under vacuum for 13 h to remove excess epoxide. The following day, the solid mixture was resuspended in 0.4 mL of $C_6D_6$, analyzed using NMR spectroscopy, and 0.15 g of phthalic anhydride (1.0 mmol) and 0.17 mL of 1-butene oxide (2.3 mmol) were added. The tube was sealed, removed from the glovebox, stored in an oil bath at 30 °C, and

manually agitated periodically. After 16 h, $^1$H NMR spectroscopy was used to analyze the reaction mixture to assess conversion and the tube was placed under vacuum for 5 h to remove excess epoxide. Finally, the mixture was resuspended in 0.40 mL of $C_6D_6$, measured by $^1$H NMR spectroscopy, and precipitated. GPC was used for molecular weight analysis.

### 10.2. Analysis of *in situ* $^1$H NMR Block Copolymer Formation using Vacuum

To form perfect block copolymers and avoid tapering, either complete conversion of all monomer or removal of excess monomer is required. However, the synthesis of copolymers able to phase separate is not dependent on perfect block formation and some tapering may be tolerated. Therefore, two approaches were tested for the synthesis of block copolymers.

Since the identity of different blocks depends on the epoxide subunit and our standard procedure utilizes excess epoxide, we first tested whether **cat2** retained activity after removal of excess epoxide under vacuum. **cat2** was used to copolymerize phthalic anhydride (**1**) with propylene oxide (**2a**) in a J-Young tube sealed with a Teflon lined cap. The first block of poly(propylene-*alt*-phthalate) was terminated upon 90% conversion of **1** and 60% conversion of **2a** (Figure A3.16a). The reaction was placed under vacuum for 13 h (overnight) to ensure complete removal of excess epoxide, confirmed by redissolving the mixture in $C_6D_6$ and checking for the presence of epoxide by $^1$H NMR spectroscopy (Figure A3.16b). Next, the poly(propylene-*alt*-phthalate)-**cat2** chain was used to initiate the copolymerization of **1** with 1-butene oxide (**2c**) (Figure A3.16c). The reaction proceeded to 44% conversion of **2c** before

becoming diffusion limited. Excess epoxide was removed under vacuum and the isolated polymer was analyzed for composition. The diblock copolymer was assigned as: poly(propylene-*alt*-phthalate)$_{180}$-*b*-(1-butene-*alt*-phthalate)$_{120}$. The conversion of the limiting reagent **1** was used to calculate values for *n* and *m*, which assume two initiators. GPC analysis of the isolated polymer indicated an $M_n$ of 26.5 kDa with a PDI of 1.24.

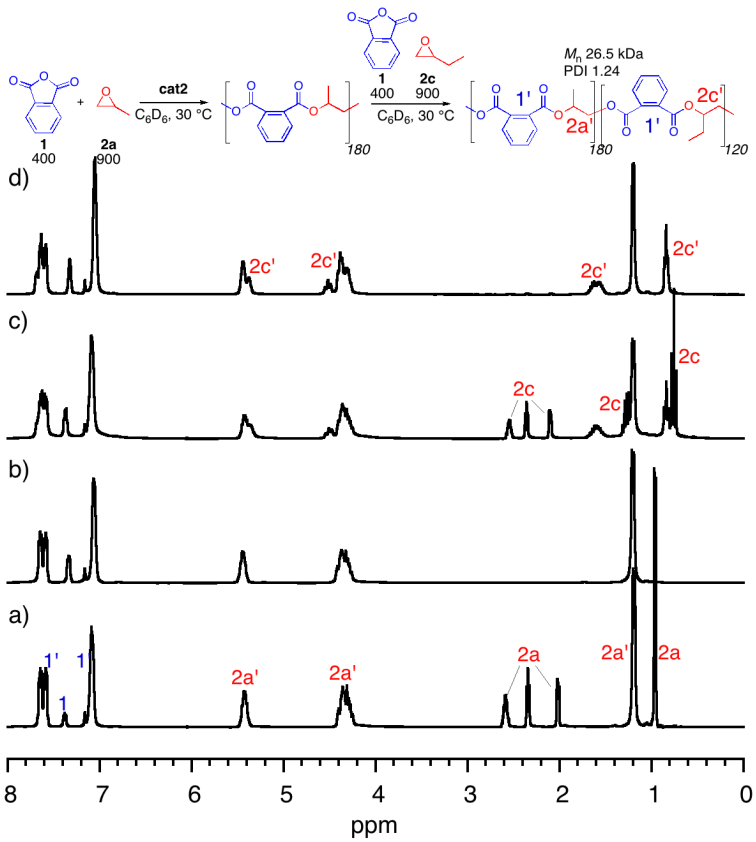


**Figure A3.16.** $^1$H NMR spectra of the diblock copolymer formed by **cat2**. a) Reaction mixture of propylene oxide and phthalic anhydride before evacuation. b) Evacuated poly(propylene-*alt*-phthalate) formed as block 1. c) Reaction mixture of 1-butene oxide and phthalic anhydride initiated from the polymer isolated in part b. d) The isolated diblock-copolymer of poly(propylene-*alt*-phthalate)-*b*-(1-butene-*alt*-phthalate).

### 10.3. NMR Analysis of poly(propylene-*alt*-phthalate)-*b*-(1-butene-*alt*-phthalate)

The $^1$H NMR spectrum (500 MHz, $CDCl_3$) includes notations for which block the protons belong to using the letter notations indicated in the spectrum: δ 7.63 (m, 2H, a); 7.32 (m, 2H, a'); 7.05 (m, 2H, a and a'); 5.44 (m, 1H, c); 5.28 (m, 1H, c'); 4.52 (m, 1H, d'); 4.38 (m, 1H, d); 4.31 (m, 1H, d'); 1.59 (m, 2H, f'); 1.19 (d, $J$ = 5.6 Hz, 3H, e); 0.84 (t, $J$ = 7.3 Hz, 3H, g').

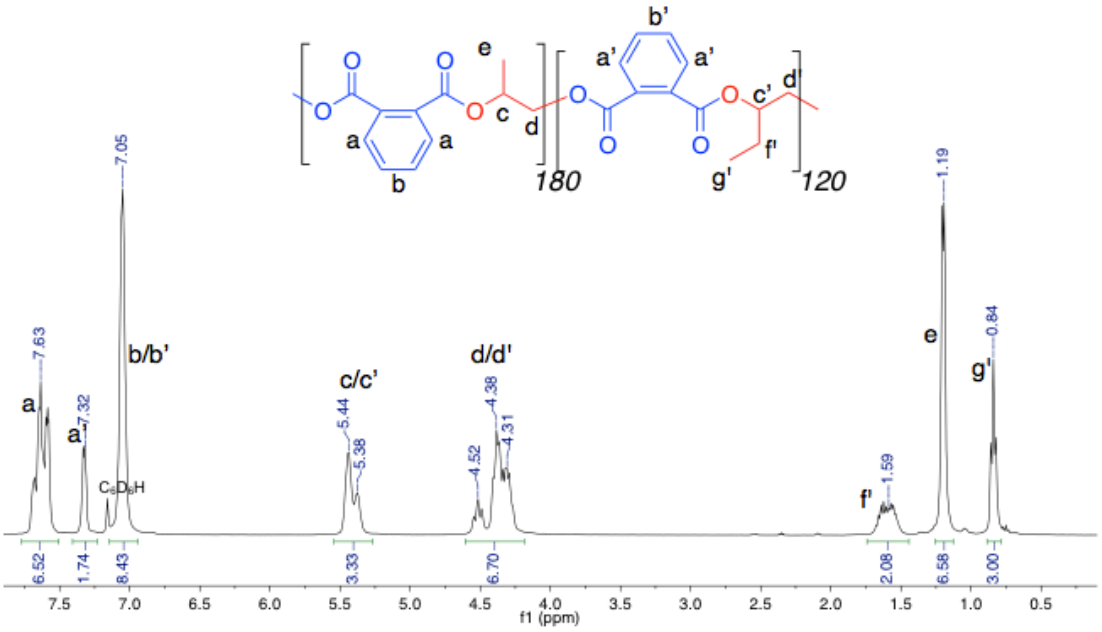


**Figure A3.17.** $^1$H NMR of poly(propylene-*alt*-phthalate)-*b*-(1-butene-*alt*-phthalate) in $C_6D_6$.

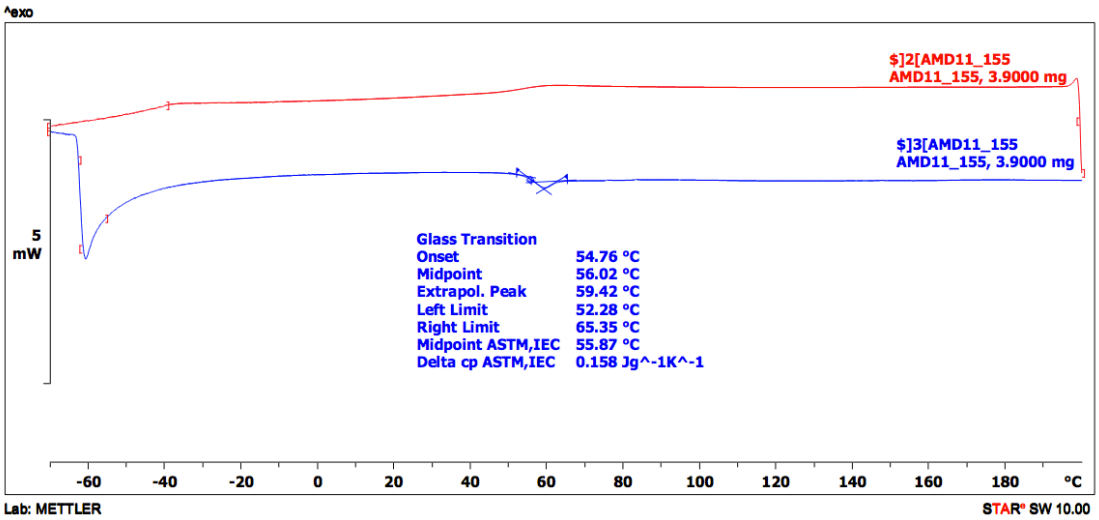


**Figure A3.18.** DSC thermogram of poly(propylene-*alt*-phthalate)-*b*-(1-butene-*alt*-phthalate).

## A3.11. Sequential Addition for Construction of Triblock Copolymers -No Vacuum

### 11.1. Representative Experimental Procedure

In the inert atmosphere of a nitrogen filled glovebox, **cat2** (6.0 mg, 5.0 μmol) and phthalic anhydride (0.11 g, 0.75 mmol) were dispensed into an oven dried vial containing a teflon coated stir bar. Propylene oxide (34 μL, 0.50 mmol) and benzene (0.10 mL) was used to dissolve the solids. The reaction was placed in an aluminum stir block and heated to 20 °C. Periodic aliquots were removed and conversion was measured by $^{1}$H NMR spectroscopy. When the solution became too viscous to continue stirring and conversion was no longer increasing, the mixture was dissolved with 0.20 mL of benzene and the second block was initiated by addition of phthalic anhydride (0.30 mg, 2.0 mmol) and 1,2-epoxydodecane (0.22 mL, 2.0 mmol). The mixture was stirred at 60 °C and periodic aliquots were checked for conversion by $^{1}$H

NMR spectroscopy. Once the solution became too viscous to stir, an additional 0.20 mL of benzene and more phthalic anhydride (0.10 g, 0.60 mmol) were added to encourage complete epoxide consumption. Once the reaction stopped stirring and the consumption of 1,2-epoxydodecane was greater than 90%, the final block was initiated by addition of phthalic anhydride (0.10 g, 0.75 mmol), propylene oxide (34 μL, 0.50 mmol) and benzene (0.20 mL). The third block was stirred at 40 °C to aid in solubility. Note: addition of excess anhydride must be done in small quantities.

### 11.2. Synthetic Details and Analysis of ABA Triblock Construction

**Poly(propylene-*alt*-phthalate)-*b*-(1,2-epoxydodecane-*alt*-phthalate)-*b*-(propylene-*alt*-phthalate)** (AMD12_219). Block ratios are based on the final composition of the polymer and are assigned according to $[block1]_n$:$[block2]_m$:$[block3]_p$. The conversion of the limiting reagent **1** for the first block was used to calculate values for *n*, *m*, and *p*, which assume two initiators.

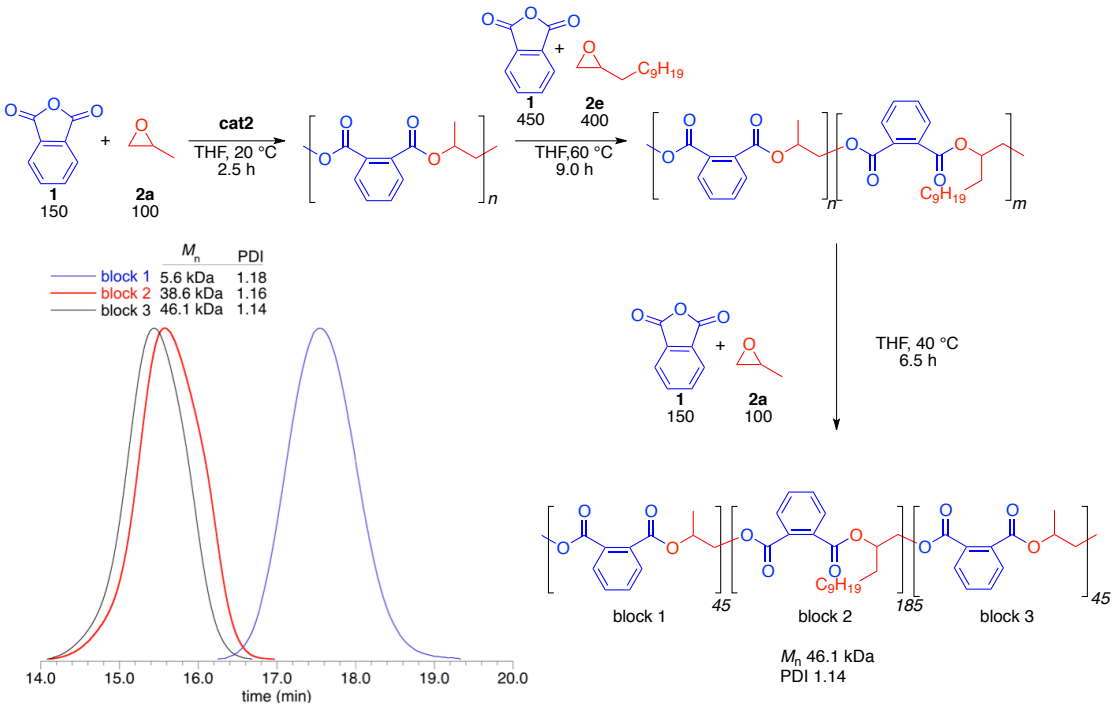


**Figure A3.19.** Synthesis and GPC analysis of poly(propylene-*alt*-phthalate)-*b*-(1,2-epoxydodecane-*alt*-phthalate)-*b*-(propylene-*alt*-phthalate)

For specific assignments please refer to the corresponding homopolymer segments above. 1H NMR spectrum (C6D6, 400 MHz) includes notations for which block the protons belong to using the letter notations indicated in the spectrum: δ 7.81-7.60 (m, 2H); 6.99 (m, 2H); 5.62 (m, 1H); 5.47 (m, 1H); 4.64-4.46 (m, 2H); 4.35 (m, 2H); 1.76 (m, 1H); 1.62 (m, 1H); 1.42 (m, 2H); 1.30 (m, 14H); 1.19 (d, J = 6.1 Hz, 3H); 0.94 (t, J = 6.1 Hz, 3H). 13C NMR (CDCl3, 125 MHz): δ 167.03; 166.99; 166.93; 166.85; 132.44; 132.35; 131.65; 131.59; 131.39; 131.28; 131.23; 131.18; 129.21; 129.15; 129.02; 128.92; 73.12; 69.74; 67.07; 66.07; 32.03; 30.91; 29.75; 29.64; 29.47; 25.24; 22.81; 16.46; 14.24.

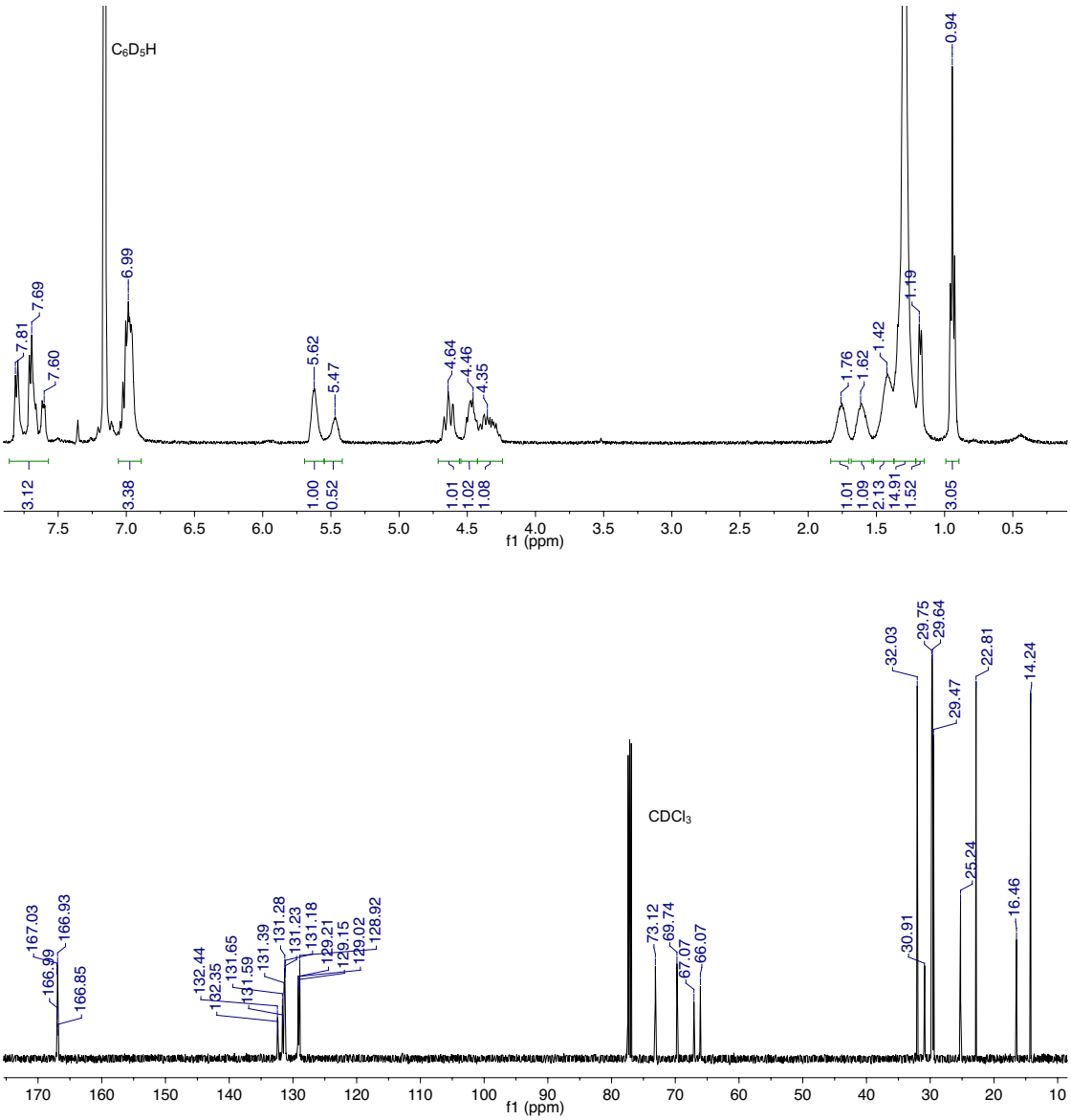


**Figure A3.20.** NMR analysis of poly(propylene-*alt*-phthalate)-*b*-(1,2-epoxydodecane-*alt*-phthalate)-*b*-(propylene-*alt*-phthalate). Top: $^{1}H$ NMR spectrum in $C_6D_6$. Bottom: $^{13}C$ NMR spectrum in $CDCl_3$.

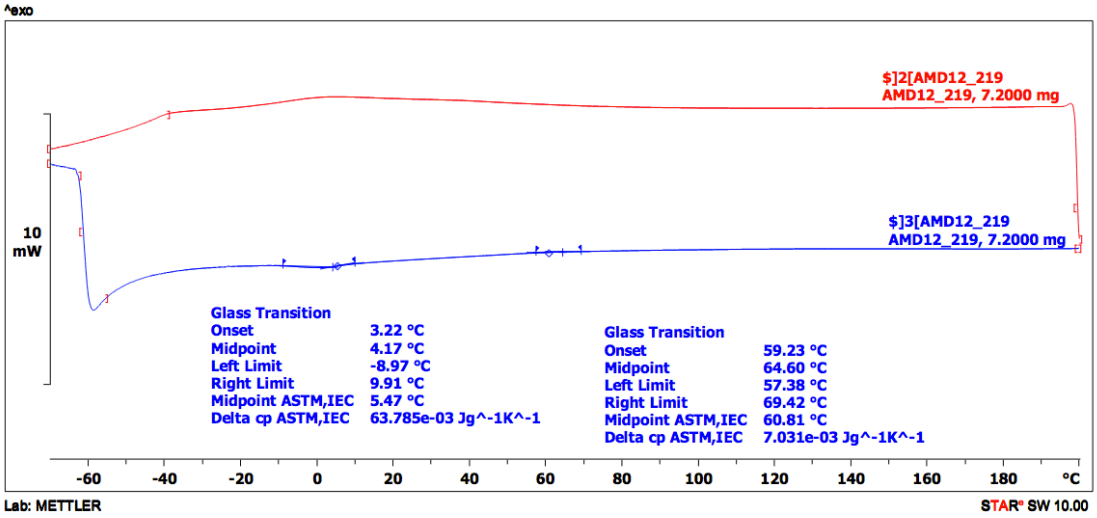


**Figure A3.21.** DSC curve of poly(propylene-*alt*-phthalate)-*b*-(1,2-epoxydodecane-*alt*-phthalate)-*b*-(propylene-*alt*-phthalate)

**Poly(1,1,1-trifluoropropan-2,3-ene-*alt*-phthalate)-*b*-(1,2-epoxydodecane-*alt*-phthalate)-b-(1,1,1-trifluoropropan-2,3-ene-*alt*-phthalate)** (AMD12_220). Block ratios are based on the final composition of the polymer and are assigned according to $[block1]_n$:$[block2]_m$:$[block3]_p$. The conversion of the limiting reagent **1** was used to calculate values for *n*, *m*, and *p*, which assume two initiators.

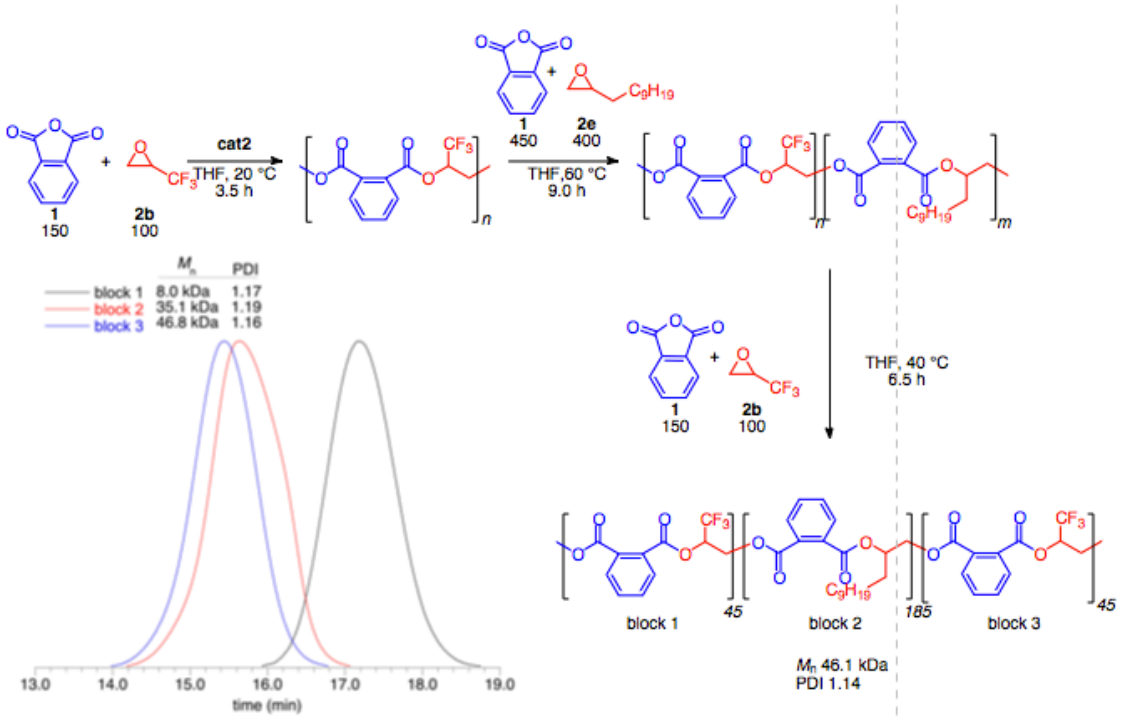


**Figure A3.22.** Synthesis and GPC analysis of poly(1,1,1-trifluoroprop-2,3-ene-*alt*-phthalate)-*b*-(1,2-epoxydodecane-*alt*-phthalate)-*b*-(1,1,1-trifluoroprop-2,3-ene-*alt*-phthalate)

For specific assignments please refer to the homopolymer analogues above. $^{1}$H NMR spectrum ($CDCl_3$, 500 MHz): δ 7.75 (m, 2H); 7.67 (m, 2H); 7.52 (m, 2H); 7.48 (m, 2H); 5.81 (m, 1H), 5.41 (m, 1H), 4.72-4.39 (m, 4H), 1.72 (m, 2H), 1.40 (m, 2H), 1.24 (m, 12H), 0.87 (t, $J$ = 7.0 Hz, 3H). $^{13}$C NMR spectrum ($CDCl_3$, 126 MHz): δ 167.04; 166.94; 166.02; 165.40; 132.44; 132.09; 131.90; 131.66; 131.29; 131.18; 130.93; 130.49; 129.52; 129.23; 128.93; 126.12-119.41 (q, $J$ = 281.0 Hz); 73.13; 69.25-68.46 (m); 66.06; 60.92; 32.04; 30.91; 29.76; 29.65; 29.48; 25.24; 22.81; 14.24.

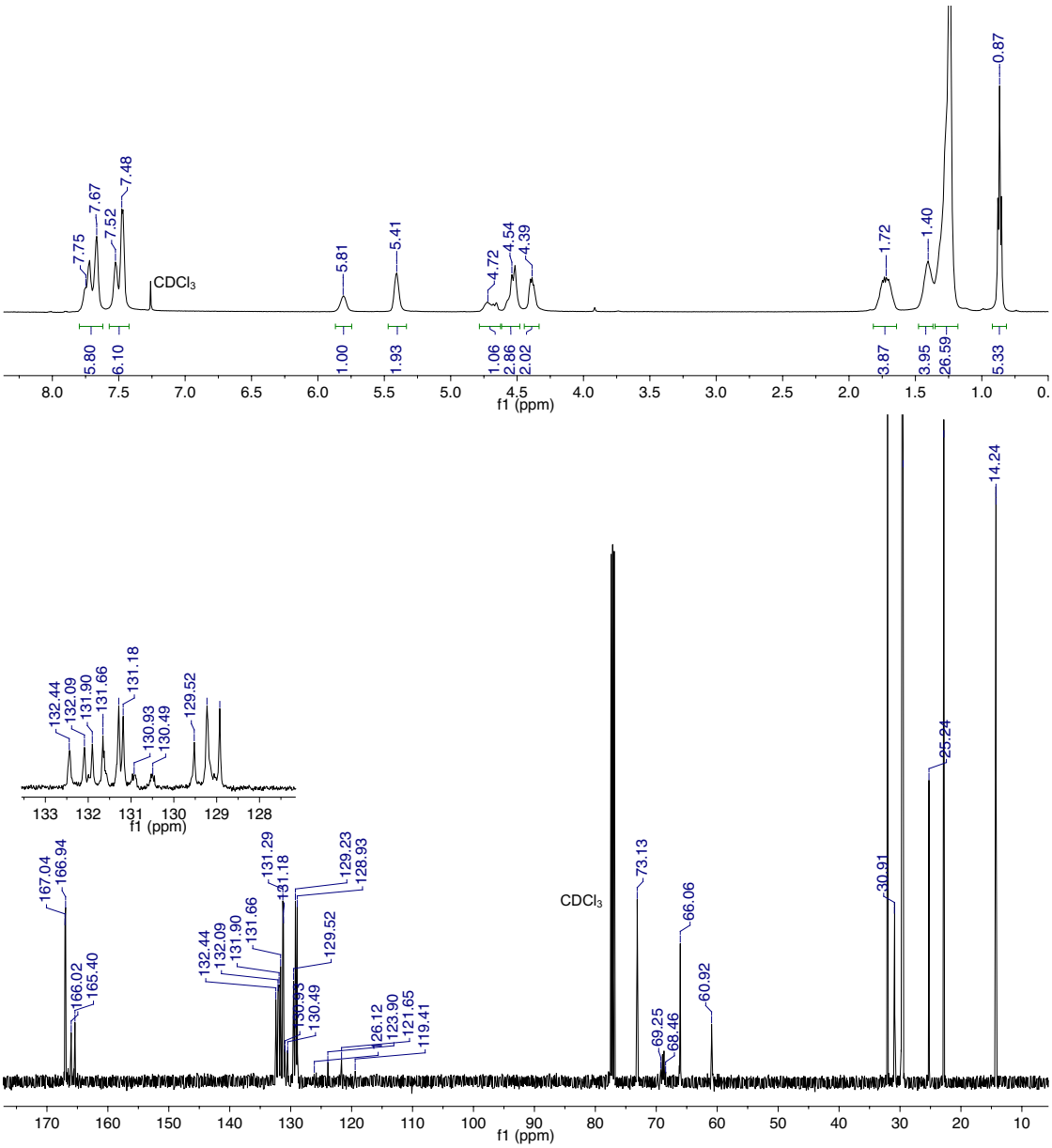


**Figure A3.23.** NMR analysis of poly(1,1,1-trifluoropropan-2,3-ene-*alt*-phthalate)-*b*-(1,2-epoxydodecane-*alt*-phthalate)-*b*-(1,1,1-trifluoropropan-2,3-ene-*alt*-phthalate) in $CDCl_3$. Top: $^{1}H$ NMR spectrum. Bottom: $^{13}C$ NMR spectrum.

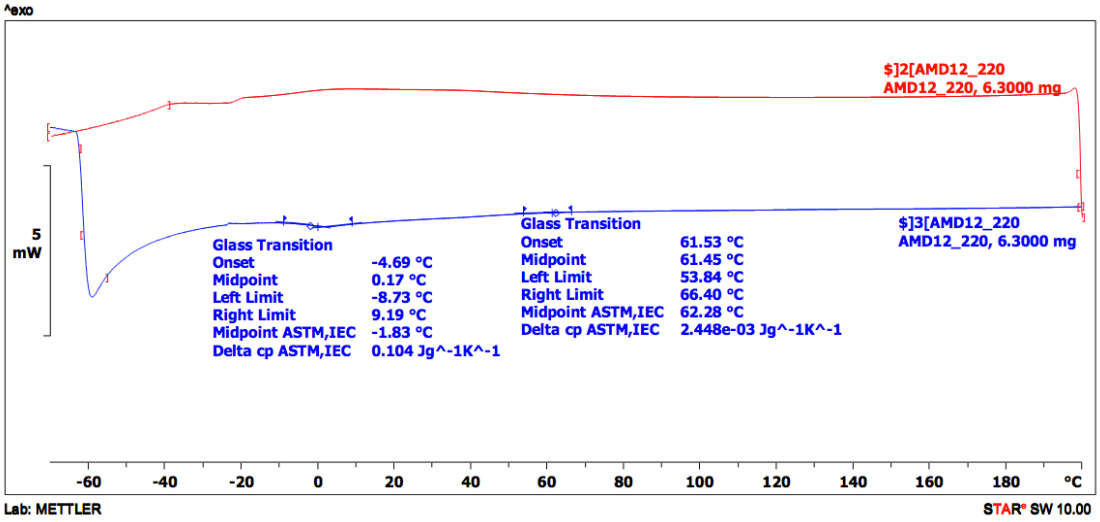


**Figure A3.24.** DSC curve of poly(1,1,1-trifluoroprop-2,3-ene-*alt*-phthalate)-*b*-(1,2-epoxydodecane-*alt*-phthalate)-*b*-(1,1,1-trifluoroprop-2,3-ene-*alt*-phthalate)

**Poly(propylene-*alt*-phthalate)-*b*-(1-butene-*alt*-phthalate)-*b*-(1,1,1-trifluoroprop-2,3-ene-*alt*-phthalate)** (AMD12_221). Block ratios are based on the final composition of the polymer and are assigned according to $[\text{block1}]_n$:$[\text{block2}]_m$:$[\text{block3}]_p$. The conversion of the limiting reagent **1** was used to calculate values for *n*, *m*, and *p*, which assume two initiators.

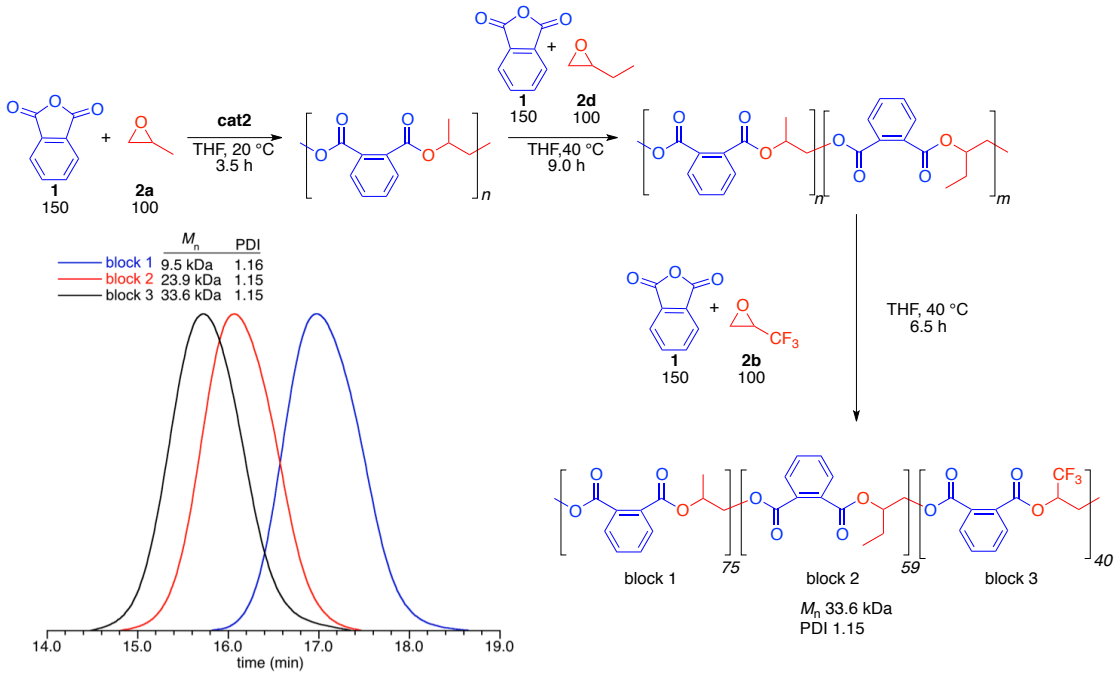


**Figure A3.25.** Synthesis and GPC analysis of poly(propylene-*alt*-phthalate)-*b*-(1-butene-*alt*-phthalate)-*b*-(1,1,1-trifluoropropan-2,3-ene-*alt*-phthalate).

For specific assignments please refer to the homopolymer analogues above. $^{1}$H NMR spectrum ($CDCl_3$, 500 MHz): δ 7.75 (m, 2H); 7.71 (m, 2H); 7.67 (m, 2H); 7.52 (m, 2H); 7.47 (m, 2H); 5.80 (m, 1H); 5.42 (m, 1H); 5.31 (m, 1H); 4.74-4.35 (m, 6H); 1.75 (m, 2H); 1.36 (d, $J$ = 6.4 Hz, 3H); 0.98 (t, $J$ = 7.0 Hz, 3H). $^{13}$C NMR (CDCl3, 126 MHz): δ 167.02; 166.84; 166.01; 165.39; 132.32; 132.08; 131.90; 131.68; 131.58; 131.55; 131.39; 131.32; 131.23; 130.95; 130.49; 129.51; 129.23; 129.14; 129.02; 128.97; 126.12-119.41 (q, $J$ = 284.5 Hz); 74.22; 69.73; 69.27; 68.37; 67.07; 65.63; 60.90; 23.95; 16.45; 9.62.

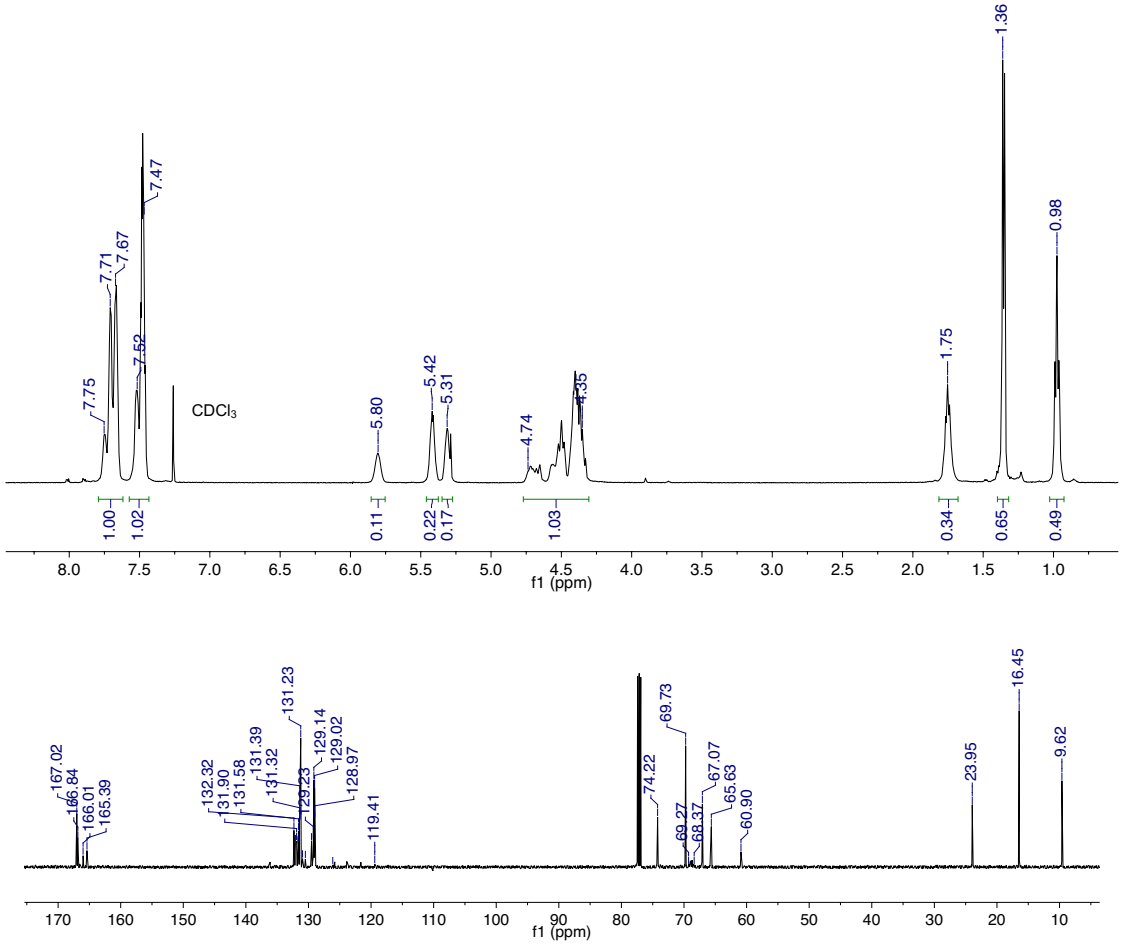


**Figure A3.26.** Spectra for poly(propylene-*alt*-phthalate)-*b*-(1-butene-*alt*-phthalate)-*b*-(1,1,1-trifluoropropan-2,3-ene-*alt*-phthalate) in $CDCl_3$. Top: $^{1}H$ NMR spectrum. Bottom: $^{13}C$ NMR spectrum.

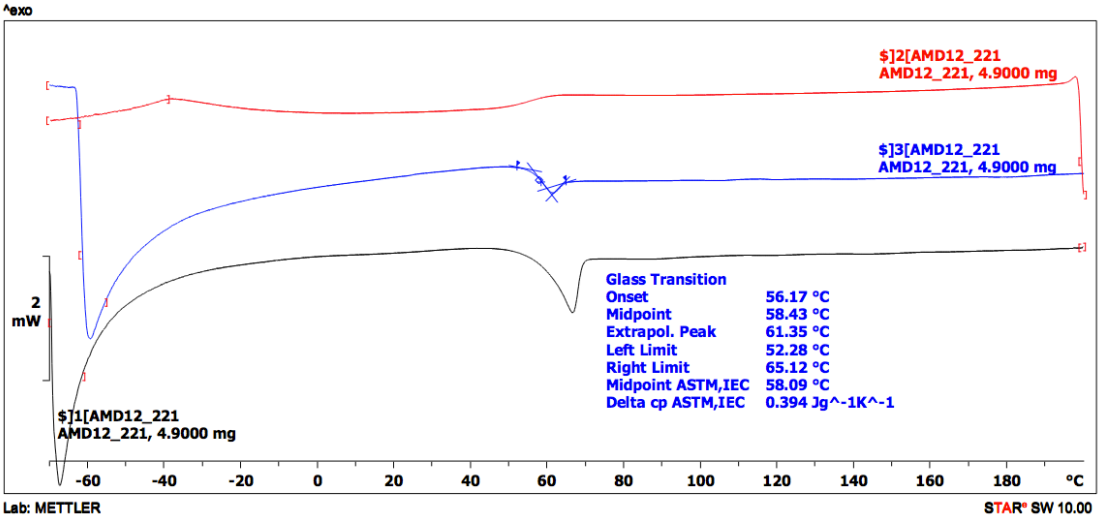


**Figure A3.27.** DSC curve of poly(propylene-*alt*-phthalate)-*b*-(1-butene-*alt*-phthalate)-*b*-(1,1,1-trifluoroprop-2,3-ene-*alt*-phthalate)

### A3.12. SLS Analysis of Polyesters

Static light scattering was performed on the high molecular weight polyesters reported in Table 4.2 to gain perspective of their absolute molecular weight. Due to the sensitivity of this measurement, a dn/dc must be calculated for each polymer and is reported in the table. More rigorous analysis is underway to accurately determine dn/dc via titration as variations in this value were seen for difference GPC runs. The reported values are polymers with relatively close dn/dc values.

**Table A3.1 Absolute Molecular Weights for Polyesters from Table 4.2 Measured by Static Light Scattering**

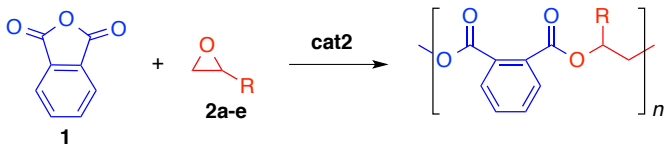


| entry | $R^1$ (epoxide) | $M_n^{theo}$ (kDa) | $M_n^{obs}$ (kDa) | PDI | dn/dc |
|---|---|---|---|---|---|
| 1 | Me (**2a**) | 198 | 132.4 | 1.09 | 0.075 |
| 2 | $CF_3$ (**2b**) | 195 | 74.0 | 1.08 | 0.061 |
| 4 | Et (**2c**) | 137 | 119.1 | 1.11 | 0.062 |
| 5 | $C_4H_9$ (**2d**) | 244 | 67.4 | 1.13 | 0.114 |
| 6[f] | $C_{10}H_{21}$ (**2e**) | 282 | 74.3 | 1.09 | 0.070 |

## A3.12. Crystallography Structures and Data Tables

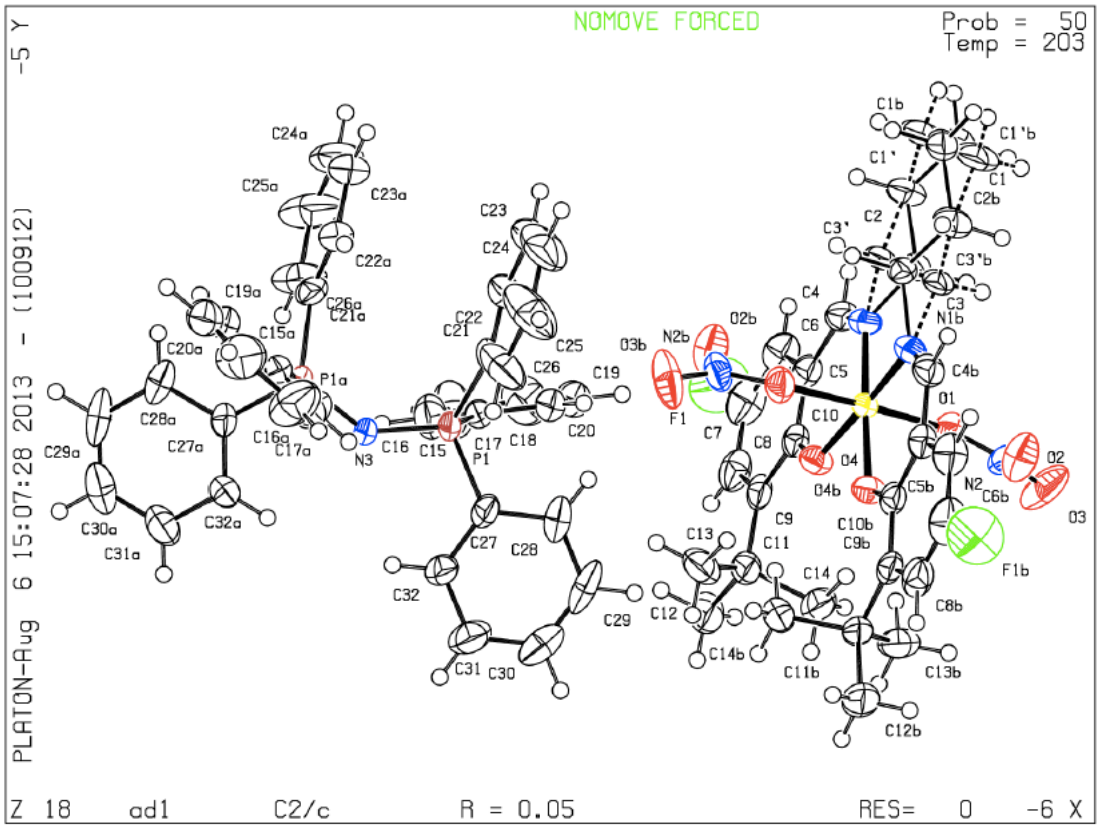


**Figure A3.28.** Ellipsoid plot for crystal structure of **cat2**.

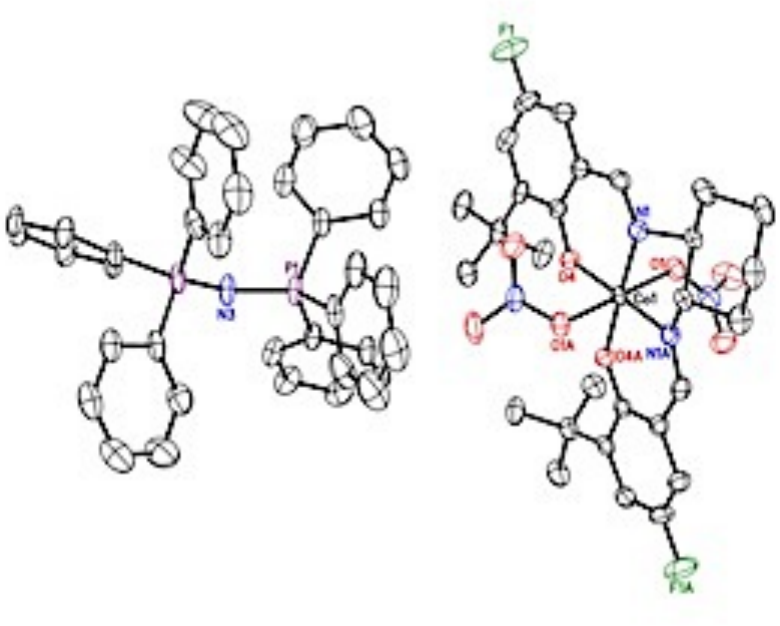

**Figure A3.29.** ORTEP drawing for crystal structure of **cat 2.**

**Table A3.2.** Crystal data and structure refinement for **cat2.**

| | |
|---|---|
| Identification code | ad1 |
| Empirical formula | C64 H64 Co F2 N5 O8 P2 |
| Formula weight | 1190.07 |
| Temperature | 203(2) K |
| Wavelength | 0.71073 Å |
| Crystal system | Monoclinic |
| Space group | C2/c |
| Unit cell dimensions | a = 17.5918(11) Å a= 90°. |
| | b = 27.6019(18) Å b= 112.172(2)°. |
| | c = 13.1145(9) Å g = 90°. |
| Volume | 5897.1(7) Å3 |
| Z | 4 |
| Density (calculated) | 1.340 Mg/m3 |
| Absorption coefficient | 0.412 mm-1 |
| F(000) | 2488 |
| Crystal size | 0.40 x 0.10 x 0.03 mm3 |
| Theta range for data collection | 1.45 to 25.08°. |
| Index ranges | -20<=h<=12, -32<=k<=32, -15<=l<=15 |
| Reflections collected | 20408 |
| Independent reflections | 5237 [R(int) = 0.0351] |
| Completeness to theta = 25.08° | 99.6 % |

Absorption correction Semi-empirical from equivalents
Max. and min. transmission 0.9898 and 0.8527
Refinement method Full-matrix least-squares on F2
Data / restraints / parameters 5237 / 0 / 393
Goodness-of-fit on F2 1.195
Final R indices [I>2sigma(I)] R1 = 0.0487, wR2 = 0.1355
R indices (all data) R1 = 0.0707, wR2 = 0.1564
Largest diff. peak and hole 0.458 and -0.539 e.Å-3

**Table A3.3.** Atomic coordinates ( x 104) and equivalent isotropic displacement parameters (Å2x 103) for **cat2**. U(eq) is defined as one third of the trace of the orthogonalized Uij tensor.

| | x | y | z | U(eq) |
|---|---|---|---|---|
| Co(1) | 5000 | 9462(1) | 2500 | 27(1) |
| F(1) | 2296(2) | 9069(1) | -2738(2) | 101(1) |
| O(1) | 5778(1) | 9451(1) | 1785(2) | 44(1) |
| O(2) | 6915(2) | 9478(1) | 3219(2) | 65(1) |
| O(3) | 6911(2) | 9263(1) | 1650(3) | 79(1) |
| N(1) | 4503(2) | 9964(1) | 1491(2) | 37(1) |
| O(4) | 4466(1) | 8964(1) | 1513(2) | 36(1) |
| N(2) | 6549(2) | 9390(1) | 2242(3) | 47(1) |
| C(1) | 4949(8) | 11340(3) | 1901(11) | 51(3) |
| C(3) | 4935(7) | 10442(2) | 1888(6) | 33(2) |
| C(1') | 4588(13) | 11330(4) | 2069(15) | 67(4) |
| C(3') | 4571(9) | 10433(3) | 2079(9) | 42(3) |
| C(2) | 4453(2) | 10883(1) | 1315(3) | 52(1) |
| C(4) | 4025(2) | 9908(1) | 478(3) | 40(1) |
| C(5) | 3735(2) | 9456(1) | -56(3) | 37(1) |
| C(6) | 3166(2) | 9476(1) | -1159(3) | 49(1) |
| C(7) | 2859(2) | 9059(2) | -1676(3) | 59(1) |
| C(8) | 3083(2) | 8613(2) | -1190(3) | 51(1) |
| C(9) | 3634(2) | 8570(1) | -122(3) | 39(1) |
| C(10) | 3965(2) | 9003(1) | 484(3) | 34(1) |
| C(11) | 3868(2) | 8070(1) | 407(3) | 46(1) |
| C(12) | 3434(2) | 7662(1) | -385(4) | 64(1) |
| C(13) | 3626(3) | 8032(1) | 1406(3) | 57(1) |
| C(14) | 4796(2) | 7998(1) | 733(4) | 61(1) |
| P(1) | 834(1) | 8470(1) | 2487(1) | 45(1) |
| N(3) | 0 | 8263(1) | 2500 | 48(1) |
| C(15) | 787(2) | 8551(1) | 1105(3) | 46(1) |
| C(16) | 111(3) | 8396(2) | 221(4) | 68(1) |
| C(17) | 84(3) | 8443(2) | -829(5) | 88(2) |

| | | | | |
|---|---|---|---|---|
| C(18) | 744(4) | 8644(2) | -1014(5) | 86(2) |
| C(19) | 1428(3) | 8789(2) | -140(4) | 67(1) |
| C(20) | 1447(2) | 8749(1) | 918(4) | 55(1) |
| C(21) | 1167(2) | 9037(1) | 3186(4) | 53(1) |
| C(22) | 973(2) | 9467(1) | 2624(5) | 66(1) |
| C(23) | 1187(3) | 9903(2) | 3192(6) | 82(2) |
| C(24) | 1600(4) | 9905(2) | 4313(6) | 93(2) |
| C(25) | 1801(4) | 9484(2) | 4872(5) | 103(2) |
| C(26) | 1583(4) | 9046(2) | 4320(5) | 82(2) |
| C(27) | 1614(2) | 8021(1) | 3105(3) | 46(1) |
| C(28) | 2436(2) | 8127(2) | 3360(4) | 65(1) |
| C(29) | 3018(2) | 7758(2) | 3713(4) | 77(2) |
| C(30) | 2788(3) | 7296(2) | 3831(4) | 71(1) |
| C(31) | 1987(2) | 7190(2) | 3605(4) | 66(1) |
| C(32) | 1394(2) | 7552(1) | 3233(3) | 53(1) |

**Table A3.4.** Bond lengths [Å] and angles [°] for **cat2**.

| | |
|---|---|
| Co(1)-O(4) | 1.879(2) |
| Co(1)-O(4)#1 | 1.879(2) |
| Co(1)-N(1)#1 | 1.886(3) |
| Co(1)-N(1) | 1.887(3) |
| Co(1)-O(1) | 1.929(2) |
| Co(1)-O(1)#1 | 1.929(2) |
| F(1)-C(7) | 1.372(4) |
| O(1)-N(2) | 1.271(4) |
| O(2)-N(2) | 1.221(4) |
| O(3)-N(2) | 1.227(4) |
| N(1)-C(4) | 1.286(4) |
| N(1)-C(3') | 1.488(9) |
| N(1)-C(3) | 1.515(8) |
| O(4)-C(10) | 1.308(4) |
| C(1)-C(1)#1 | 1.51(3) |
| C(1)-C(2) | 1.560(11) |
| C(3)-C(2) | 1.511(8) |
| C(3)-C(3)#1 | 1.534(19) |
| C(1')-C(1')#1 | 1.46(4) |
| C(1')-C(2) | 1.542(15) |
| C(3')-C(3')#1 | 1.50(2) |
| C(3')-C(2) | 1.560(10) |
| C(4)-C(5) | 1.429(5) |
| C(5)-C(6) | 1.415(5) |
| C(5)-C(10) | 1.418(4) |
| C(6)-C(7) | 1.343(5) |

| | |
|---|---|
| C(7)-C(8) | 1.374(6) |
| C(8)-C(9) | 1.375(5) |
| C(9)-C(10) | 1.431(4) |
| C(9)-C(11) | 1.529(5) |
| C(11)-C(13) | 1.526(5) |
| C(11)-C(12) | 1.528(5) |
| C(11)-C(14) | 1.537(5) |
| P(1)-N(3) | 1.5814(15) |
| P(1)-C(21) | 1.796(4) |
| P(1)-C(15) | 1.797(4) |
| P(1)-C(27) | 1.798(4) |
| N(3)-P(1)#2 | 1.5814(15) |
| C(15)-C(16) | 1.378(6) |
| C(15)-C(20) | 1.386(5) |
| C(16)-C(17) | 1.366(7) |
| C(17)-C(18) | 1.386(7) |
| C(18)-C(19) | 1.371(7) |
| C(19)-C(20) | 1.379(6) |
| C(21)-C(22) | 1.372(6) |
| C(21)-C(26) | 1.388(6) |
| C(22)-C(23) | 1.391(6) |
| C(23)-C(24) | 1.372(8) |
| C(24)-C(25) | 1.350(8) |
| C(25)-C(26) | 1.386(6) |
| C(27)-C(32) | 1.378(5) |
| C(27)-C(28) | 1.387(5) |
| C(28)-C(29) | 1.393(6) |
| C(29)-C(30) | 1.363(7) |
| C(30)-C(31) | 1.359(6) |
| C(31)-C(32) | 1.394(5) |

| | |
|---|---|
| O(4)-Co(1)-O(4)#1 | 85.97(13) |
| O(4)-Co(1)-N(1)#1 | 177.54(11) |
| O(4)#1-Co(1)-N(1)#1 | 94.29(10) |
| O(4)-Co(1)-N(1) | 94.29(10) |
| O(4)#1-Co(1)-N(1) | 177.54(11) |
| N(1)#1-Co(1)-N(1) | 85.55(16) |
| O(4)-Co(1)-O(1) | 85.20(10) |
| O(4)#1-Co(1)-O(1) | 93.53(10) |
| N(1)#1-Co(1)-O(1) | 97.22(11) |
| N(1)-Co(1)-O(1) | 84.05(11) |
| O(4)-Co(1)-O(1)#1 | 93.53(10) |
| O(4)#1-Co(1)-O(1)#1 | 85.20(10) |
| N(1)#1-Co(1)-O(1)#1 | 84.06(11) |
| N(1)-Co(1)-O(1)#1 | 97.22(11) |

| | |
|---|---|
| O(1)-Co(1)-O(1)#1 | 178.27(14) |
| N(2)-O(1)-Co(1) | 126.9(2) |
| C(4)-N(1)-C(3') | 122.2(4) |
| C(4)-N(1)-C(3) | 120.4(4) |
| C(3')-N(1)-C(3) | 29.8(4) |
| C(4)-N(1)-Co(1) | 125.9(2) |
| C(3')-N(1)-Co(1) | 110.5(4) |
| C(3)-N(1)-Co(1) | 111.1(3) |
| C(10)-O(4)-Co(1) | 128.16(19) |
| O(2)-N(2)-O(3) | 121.8(3) |
| O(2)-N(2)-O(1) | 121.0(3) |
| O(3)-N(2)-O(1) | 117.2(3) |
| C(1)#1-C(1)-C(2) | 109.7(8) |
| C(2)-C(3)-N(1) | 114.6(6) |
| C(2)-C(3)-C(3)#1 | 110.7(8) |
| N(1)-C(3)-C(3)#1 | 102.5(7) |
| C(1')#1-C(1')-C(2) | 111.3(14) |
| N(1)-C(3')-C(3')#1 | 104.1(9) |
| N(1)-C(3')-C(2) | 113.3(8) |
| C(3')#1-C(3')-C(2) | 109.0(11) |
| C(3)-C(2)-C(1') | 113.8(6) |
| C(3)-C(2)-C(3') | 29.0(3) |
| C(1')-C(2)-C(3') | 106.0(8) |
| C(3)-C(2)-C(1) | 107.5(6) |
| C(1')-C(2)-C(1) | 27.8(5) |
| C(3')-C(2)-C(1) | 114.4(6) |
| N(1)-C(4)-C(5) | 125.7(3) |
| C(6)-C(5)-C(10) | 120.3(3) |
| C(6)-C(5)-C(4) | 116.7(3) |
| C(10)-C(5)-C(4) | 123.0(3) |
| C(7)-C(6)-C(5) | 118.4(3) |
| C(6)-C(7)-F(1) | 119.6(4) |
| C(6)-C(7)-C(8) | 123.0(3) |
| F(1)-C(7)-C(8) | 117.4(4) |
| C(7)-C(8)-C(9) | 121.2(3) |
| C(8)-C(9)-C(10) | 118.4(3) |
| C(8)-C(9)-C(11) | 120.4(3) |
| C(10)-C(9)-C(11) | 121.2(3) |
| O(4)-C(10)-C(5) | 122.8(3) |
| O(4)-C(10)-C(9) | 118.6(3) |
| C(5)-C(10)-C(9) | 118.7(3) |
| C(13)-C(11)-C(12) | 107.7(3) |
| C(13)-C(11)-C(9) | 109.7(3) |
| C(12)-C(11)-C(9) | 112.2(3) |
| C(13)-C(11)-C(14) | 111.3(3) |

| | |
|---|---|
| C(12)-C(11)-C(14) | 107.4(3) |
| C(9)-C(11)-C(14) | 108.5(3) |
| N(3)-P(1)-C(21) | 115.73(16) |
| N(3)-P(1)-C(15) | 111.49(12) |
| C(21)-P(1)-C(15) | 106.77(18) |
| N(3)-P(1)-C(27) | 107.41(16) |
| C(21)-P(1)-C(27) | 108.91(18) |
| C(15)-P(1)-C(27) | 106.12(17) |
| P(1)#2-N(3)-P(1) | 137.6(3) |
| C(16)-C(15)-C(20) | 119.2(4) |
| C(16)-C(15)-P(1) | 120.4(3) |
| C(20)-C(15)-P(1) | 120.3(3) |
| C(17)-C(16)-C(15) | 120.6(4) |
| C(16)-C(17)-C(18) | 120.1(5) |
| C(19)-C(18)-C(17) | 119.9(5) |
| C(18)-C(19)-C(20) | 119.8(4) |
| C(19)-C(20)-C(15) | 120.3(4) |
| C(22)-C(21)-C(26) | 118.9(4) |
| C(22)-C(21)-P(1) | 120.9(4) |
| C(26)-C(21)-P(1) | 120.1(3) |
| C(21)-C(22)-C(23) | 120.0(5) |
| C(24)-C(23)-C(22) | 120.2(5) |
| C(25)-C(24)-C(23) | 120.2(5) |
| C(24)-C(25)-C(26) | 120.2(6) |
| C(25)-C(26)-C(21) | 120.4(5) |
| C(32)-C(27)-C(28) | 118.9(3) |
| C(32)-C(27)-P(1) | 120.0(3) |
| C(28)-C(27)-P(1) | 120.8(3) |
| C(27)-C(28)-C(29) | 119.7(4) |
| C(30)-C(29)-C(28) | 120.6(4) |
| C(31)-C(30)-C(29) | 120.3(4) |
| C(30)-C(31)-C(32) | 119.9(4) |
| C(27)-C(32)-C(31) | 120.6(4) |

Symmetry transformations used to generate equivalent atoms:
#1 -x+1,y,-z+1/2  #2 -x,y,-z+1/2

**Table A3.5.** Anisotropic displacement parameters (Å2x 103) for **cat2**. The anisotropic displacement factor exponent takes the form: -2p2[ h2 a*2U11 + ... + 2 h k a* b* U12 ]

| | U11 | U22 | U33 | U23 | U13 | U12 |
|---|---|---|---|---|---|---|
| Co(1) | 28(1) | 21(1) | 35(1) | 0 | 15(1) | 0 |
| F(1) | 91(2) | 120(2) | 51(2) | -14(1) | -20(1) | 7(2) |
| O(1) | 40(1) | 44(1) | 55(1) | 6(1) | 27(1) | 6(1) |
| O(2) | 40(1) | 95(2) | 59(2) | 3(2) | 17(1) | 5(1) |
| O(3) | 73(2) | 104(2) | 81(2) | 22(2) | 53(2) | 48(2) |
| N(1) | 39(2) | 25(1) | 44(2) | 1(1) | 14(1) | 3(1) |
| O(4) | 40(1) | 27(1) | 37(1) | -2(1) | 10(1) | -2(1) |
| N(2) | 44(2) | 44(2) | 61(2) | 18(1) | 29(2) | 19(1) |
| C(1) | 49(6) | 30(4) | 86(9) | 14(4) | 40(6) | 5(4) |
| C(3) | 38(5) | 26(3) | 42(5) | -1(3) | 24(4) | -3(3) |
| C(1') | 90(12) | 20(4) | 107(12) | 7(5) | 55(10) | 2(6) |
| C(3') | 53(7) | 18(4) | 72(7) | 8(3) | 42(6) | 3(4) |
| C(2) | 63(2) | 27(2) | 70(3) | 13(2) | 29(2) | 5(2) |
| C(4) | 41(2) | 36(2) | 44(2) | 10(1) | 17(2) | 6(1) |
| C(5) | 32(2) | 43(2) | 39(2) | 2(1) | 17(1) | 3(1) |
| C(6) | 45(2) | 63(2) | 39(2) | 7(2) | 15(2) | 7(2) |
| C(7) | 42(2) | 88(3) | 36(2) | -12(2) | 3(2) | 1(2) |
| C(8) | 34(2) | 65(3) | 52(2) | -23(2) | 15(2) | -5(2) |
| C(9) | 27(2) | 45(2) | 49(2) | -16(2) | 20(2) | -6(1) |
| C(10) | 28(2) | 42(2) | 36(2) | -5(1) | 17(1) | -1(1) |
| C(11) | 35(2) | 36(2) | 69(2) | -20(2) | 21(2) | -8(1) |
| C(12) | 51(2) | 53(2) | 89(3) | -33(2) | 28(2) | -16(2) |
| C(13) | 65(2) | 37(2) | 72(3) | -6(2) | 30(2) | -14(2) |
| C(14) | 38(2) | 42(2) | 97(3) | -17(2) | 19(2) | 3(2) |
| P(1) | 30(1) | 28(1) | 88(1) | -9(1) | 35(1) | -5(1) |
| N(3) | 29(2) | 26(2) | 98(3) | 0 | 35(2) | 0 |
| C(15) | 39(2) | 27(2) | 84(3) | -8(2) | 37(2) | -2(1) |
| C(16) | 53(2) | 64(3) | 96(3) | -25(2) | 38(2) | -19(2) |
| C(17) | 82(3) | 102(4) | 86(4) | -32(3) | 38(3) | -36(3) |
| C(18) | 107(4) | 81(4) | 94(4) | -20(3) | 65(4) | -17(3) |
| C(19) | 68(3) | 46(2) | 110(4) | -2(2) | 62(3) | 0(2) |
| C(20) | 43(2) | 39(2) | 92(3) | 0(2) | 38(2) | 0(2) |
| C(21) | 50(2) | 37(2) | 94(3) | -17(2) | 51(2) | -15(2) |
| C(22) | 51(2) | 36(2) | 120(4) | -12(2) | 42(2) | -8(2) |
| C(23) | 73(3) | 36(2) | 150(5) | -15(3) | 55(3) | -11(2) |
| C(24) | 123(5) | 50(3) | 136(5) | -40(3) | 82(4) | -37(3) |
| C(25) | 164(6) | 69(4) | 108(4) | -41(3) | 86(4) | -57(4) |
| C(26) | 123(4) | 49(3) | 102(4) | -21(2) | 75(4) | -35(3) |
| C(27) | 31(2) | 43(2) | 70(2) | -11(2) | 27(2) | 0(2) |

| | | | | | | |
|---|---|---|---|---|---|---|
| C(28) | 33(2) | 80(3) | 89(3) | 0(2) | 31(2) | -6(2) |
| C(29) | 27(2) | 125(5) | 82(3) | 7(3) | 27(2) | 16(2) |
| C(30) | 53(2) | 83(3) | 76(3) | -4(2) | 24(2) | 30(2) |
| C(31) | 53(2) | 50(2) | 88(3) | -12(2) | 20(2) | 15(2) |
| C(32) | 37(2) | 36(2) | 85(3) | -14(2) | 21(2) | 2(2) |

**Table A3.6.** Hydrogen coordinates ( x 104) and isotropic displacement parameters (Å2x 10 3) for **cat2**.

| | x | y | z | U(eq) |
|---|---|---|---|---|
| H(1A) | 5489 | 11338 | 1846 | 61 |
| H(1B) | 4658 | 11633 | 1540 | 61 |
| H(3A) | 5474 | 10440 | 1812 | 39 |
| H(1'A) | 4512 | 11625 | 1626 | 80 |
| H(1'B) | 4179 | 11331 | 2409 | 80 |
| H(3'A) | 4172 | 10443 | 2447 | 51 |
| H(2B) | 3911 | 10883 | 1364 | 62 |
| H(2C) | 4378 | 10882 | 536 | 62 |
| H(4A) | 3850 | 10190 | 51 | 48 |
| H(6A) | 3007 | 9775 | -1520 | 59 |
| H(8A) | 2856 | 8332 | -1596 | 61 |
| H(12A) | | 2845 | 7706 | -638 | 96 |
| H(12B) | | 3582 | 7353 | -9 | 96 |
| H(12C) | | 3600 | 7666 | -1011 | 96 |
| H(13A) | | 3917 | 8277 | 1943 | 85 |
| H(13B) | | 3768 | 7713 | 1734 | 85 |
| H(13C) | | 3039 | 8083 | 1177 | 85 |
| H(14A) | | 4926 | 8003 | 77 | 92 |
| H(14B) | | 4958 | 7689 | 1104 | 92 |
| H(14C) | | 5090 | 8257 | 1224 | 92 |
| H(16A) | | -335 | 8256 | 342 | 81 |
| H(17A) | | -382 | 8340 | -1427 | 106 |
| H(18A) | | 722 | 8680 | -1737 | 104 |
| H(19A) | | 1882 | 8916 | -262 | 80 |
| H(20A) | | 1911 | 8856 | 1515 | 66 |
| H(22A) | | 695 | 9467 | 1855 | 79 |
| H(23A) | | 1048 | 10198 | 2807 | 99 |
| H(24A) | | 1743 | 10201 | 4693 | 111 |
| H(25A) | | 2090 | 9487 | 5639 | 124 |
| H(26A) | | 1718 | 8753 | 4716 | 99 |
| H(28A) | | 2600 | 8445 | 3294 | 78 |
| H(29A) | | 3574 | 7828 | 3873 | 92 |

| | | | | |
|---|---|---|---|---|
| H(30A) | 3186 | 7050 | 4069 | 85 |
| H(31A) | 1832 | 6872 | 3699 | 79 |
| H(32A) | 840 | 7477 | 3068 | 64 |

CHAPTER FIVE

# CHIRAL CATALYSTS FOR THE COPOLYMERIZATION OF COMMODITY EPOXIDES AND CYCLIC ANHYDRIDES TO FORM SEMI-CRYSTALLINE POLYESTERS

## 5.1 Abstract

The advent of systems capable of performing the alternating copolymerization of epoxides with cyclic anhydrides has enabled the formation of polyesters with diverse compositions, controlled regiochemistry, and regulated molecular weight. However, to date, no stereoselective methods have been reported. Herein, two processes are discussed for the synthesis of semi-crystalline polyesters *via* the ring-opening copolymerization of epoxides with cyclic anhydrides. The regioselective copolymerization of (*S*)-propylene oxide with maleic and phthalic anhydrides yields semi-crystalline polyesters from enantiopure starting material. Conversely, a chiral catalyst able to perform stereoselective copolymerizations of racemic propylene oxide produces comparable semi-crystalline polyesters from racemic starting materials. Finally, several different terminal epoxides can be stereoselectively copolymerized with maleic and phthalic anhydrides to yield functionally diverse semi-crystalline materials. This is the first example of systems capable of forming semi-crystalline polyesters *via* copolymerization of commodity epoxides and cyclic anhydrides.

## 5.2 Introduction

The semi-crystalline properties of polyethylene (PE) and isotactic polypropylene (iPP) contribute to their importance as the most widely utilized commodity polymers.[1,2] Semi-crystallinity provides the strength, stiffness, and thermal properties required by most applications and processing methods. Recent advances in the synthesis of PE and iPP enable the preparation of tailored polyolefins with precise control over stereo- and regiochemistry, molecular weight, and block sequences.[3] However, a remaining limitation for polyolefins is the difficulty of incorporating polar monomers that are necessary for new engineering applications.[4] Alternatives designed to compliment these high value, durable thermoplastics must be competitive with their low cost, facile synthesis, and superior physical performance.[5]

Polyesters are promising as a new class of semi-crystalline polymer because they can be prepared from inexpensive commodity materials that offer diverse compositions and often environmental compatibility.[6,7] Poly(ethylene terephthalate) (PET) closely follows PE and iPP in industrial significance but is derived from fossil fuels, and difficult to degrade (Scheme 5.1a).[8] D- or L-poly(lactide) (PLA) and poly(hydroxybutyrate) (PHB) are bio-derived, degradable semi-crystalline polyesters; however, their thermal properties are unsuitable for many applications and they offer little functional diversity (Scheme 5.1b).[9] Furthermore, the polymerization strategies used to synthesize PET, PLA, or PHB precludes production of precise materials and the ability to tune thermal properties, hindering their commercial significance.[10]

**Scheme 5.1** Polymerization Routes for the Synthesis of Polyesters: a) Step-Growth Condensation Copolymerization b) Chain-Growth Ring-Opening Polymerization c) Chain-Growth Ring-Opening Copolymerization

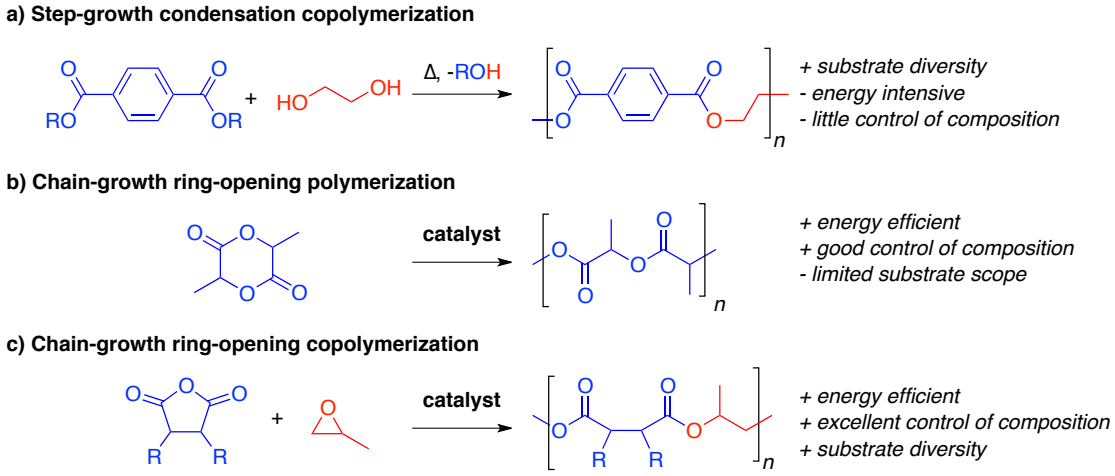


Recent advances in polyester catalysis have enabled the synthesis of diverse polyesters through the controlled chain-growth ring-opening alternating copolymerization (ROAC) of epoxides and cyclic anhydrides.[11] This approach combines the main advantages of step-growth condensation and chain-growth ring-opening polymerization into a diverse, economical, and efficient process (Scheme 5.1c).[6,7] Different monomer combinations impact polyester thermal properties and blocks are readily assembled. Furthermore, molecular weights are controlled using living or immortal conditions, the latter route generating end-functionalized polyesters. Thus, this method is a powerful tool for constructing polymer blends with tunable thermal properties or creating functionally diverse polyol precursors with controlled sequence and structure.

Despite the major advantages of ROAC, this method has not been reported for the formation of semi-crystalline polyesters. Many commercially available cyclic

anhydrides are symmetric; therefore processes that perform asymmetric epoxide ring-opening are of interest for the creation of stereoregular polyesters *via* ROAC. [12] N,N'-bis(salicylidene)cyclohexanediimine (salcy) complexes are well known to effect regioselective epoxide ring-opening and in ROAC, cobalt complexes are found to be more selective than chromium (Scheme 5.2). [13] Since neither systems have been explored for their stereoselectivity, we began by evaluating the stereoselectivity of (salcy)-Co(III) and (salcy)Cr(III) catalysts for the ROAC of propylene oxide with maleic and phthalic anhydrides.

**Scheme 5.2.** Regiochemistry of Epoxide Ring-Opening

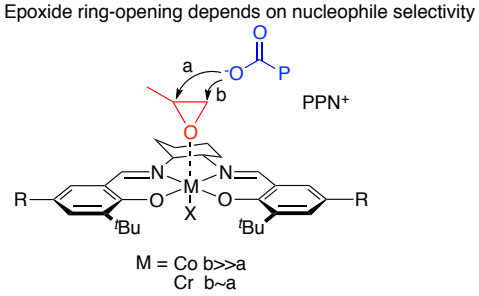


## 5.3 Results and Discussion

Two approaches were studied to achieve semi-crystalline polyesters. The regioselective copolymerization of enantiopure epoxides by a racemic catalyst transfers the inherent monomer stereochemistry to a stereo-regular polyester (Scheme 5.3, Route A). Alternatively, the kinetic resolution of racemic epoxides by a chiral catalyst creates polyesters with stereochemistry that reflects catalyst enantioselectivity ($k_{rel}$) (Scheme 5.3, Route B). Synthetically simpler, Route A relies on enantiopure epoxides and racemic catalysts that are often commercially available or easy to synthesize; however, this method is not viable on an industrial scale. Economically

viable, Route B has the potential to form two valuable products if catalyst activity and selectively ($k_{rel}$) is high enough to efficiently perform kinetic resolution during copolymerization.

**Scheme 5.3.** Polymerization Routes for Stereo-enriched Polyesters: Route A) Regioselective Copolymerization Route B) Kinetic Resolution Copolymerization

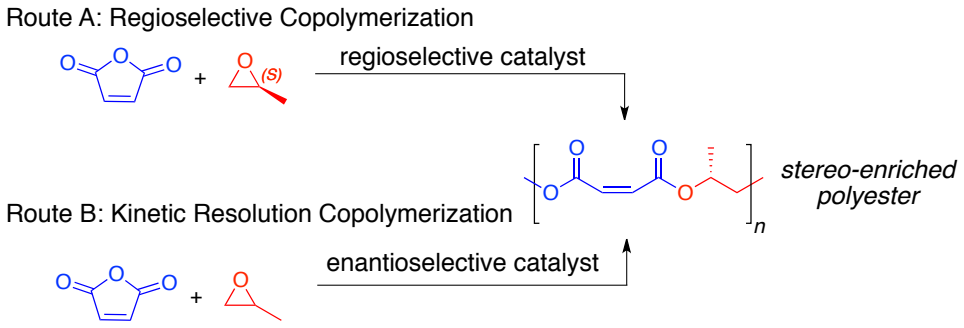


## 5.4 Semi-crystalline Polyesters from Enantiopure Epoxides

We first focused on the formation of stereo-enriched polyester using regioselective copolymerization methods described in Route A from Scheme 5.3. Enantiopure (*S*)-propylene oxide (**(*S*)-2a**) was copolymerized with maleic (**1a**) and phthalic (**1b**) anhydrides using *rac*-(salcy)$CoNO_3$ (***rac*-cat1**) and *rac*-(salcy)CrCl (***rac*-cat2**) (Table5.1). Both catalysts produced alternating semi-crystalline polyesters for each monomer combination. $^1$H NMR spectroscopy (Figure A4.3a) was used to confirm the regioregularity of the poly(propylene maleate) (PPM) produced by ***rac*-cat1** (entry 1) which exhibited a higher melting point (134 °C). The same analysis (Figure A4.3b) established that PPM produced by ***rac*-cat2** (entry 2) was regioirregular, in agreement with its lower melting point (93 °C). Poly(propylene phthalate) (PPP) produced by ***rac*-cat1** and ***rac*-cat2** exhibited comparable thermal properties (entries 3 and 4). Minor regioerrors were detected in the $^{13}$C NMR spectrum of PPP produced by ***rac*-**

**cat2** (Figure A4.4). Overall, polyesters produced by ***rac*-cat1** (entries 1 and 3) had higher melting points ($T_m$) than those produced by ***rac*-cat2** (entries 2 and 4). Notably, semi-crystallinity does not depend on perfect regiochemistry for these polyesters. Finally, static light scattering was used to measure the molecular weights of the semi-crystalline polyesters and confirmed that they were larger than the reported relative sizes (Table A4.1). This underestimation of size is attributed to reduced hydronamic radius of the semi-crystalline polyesters in solution.

**Table 5.1.** Copolymerization of (*S*)-Propylene Oxide with Maleic or Phthalic Anhydride[a]

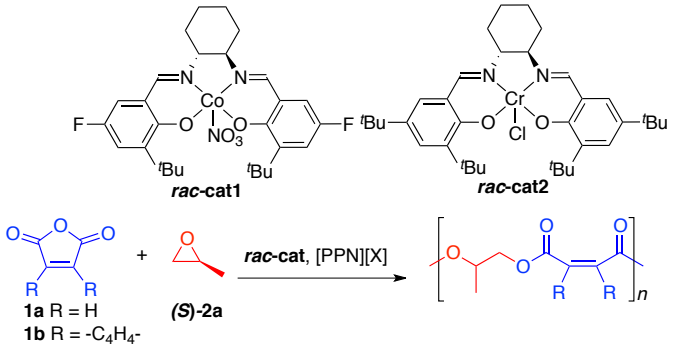


| entry | *rac*-cat | [X] | 1 | time (h) | temp (°C) | % conv.[d] | $M_n$ (kDa)[e] | PDI[e] | $T_g$ (°C)[f] | $T_m$ (°C)[g] |
|---|---|---|---|---|---|---|---|---|---|---|
| 1[b] | **cat1** | $NO_3$ | **1a** | 1.0 | 30 | 66 | 2.1 | 1.17 | 19 | 134 |
| 2[b] | **cat2** | n/a | **1a** | 4.0 | 45 | 95 | 7.0 | 1.31 | 21 | 93 |
| 3[c] | **cat1** | $NO_3$ | **1b** | 1.0 | 30 | 48 | 6.1 | 1.16 | 55 | 150 |
| 4[c] | **cat2** | Cl | **1b** | 3.0 | 45 | 40 | 8.2 | 1.26 | 59 | 147 |

[a]Corresponding SLS data is found in Appendix Four. [b]General conditions: **1**:**2**:**cat**:[PPN][X] = 100:200:1:1. [c]General conditions: **1**:**2**:**cat**:[PPN][X] = 400:800:1:1. [d]Calculated using $^1$H NMR spectroscopy of the crude reaction mixture based on **1** as the limiting reagent. [e]Measured relative to polystyrene standards using GPC eluted at 0.3 mL/min with THF at 30 °C. [f]Measured using DSC, second heat values. [g]Measured using DSC, first heat values due to slow crystallization of polyesters.[14]

Next, to address Route B, enantiopure **(*R*,*R*)-cat1** and **(*R*,*R*)-cat2** were tested for the copolymerization of racemic propylene oxide (***rac*-2a**) with maleic (**1a**) and

phthalic (**1b**) anhydrides (Table 4.2). The thermal properties of the polymers and enantiomeric excess of the epoxides were measured to gauge catalyst selectivity. Only PPM produced by **(*R,R*)-cat1** exhibited a melting transition ($T_m$ 102 °C), although the apparent selectivity of this process ($k_{rel}$ 1.4) was low (entry 1). **(*R,R*)-cat1** was more selective ($k_{rel}$ 4.0) for the copolymerization of phthalic anhydride with *rac*-propylene oxide (entry 3), despite no evidence of semi-crystallinity for the PPP product. Overall, **(*R,R*)-cat1** was more enantioselective than **(*R,R*)-cat2** for comparable reactions (entries 1-2 and entries 3-4). This difference was attributed to the regioirregularity of Cr complexes for this transformation; therefore Co derivatives were explored further.

**Table 5.2.** Chiral Catalysts Evaluated for Enantioselective Copolymerizations of Racemic Propylene Oxide with Maleic or Phthalic Anhydride

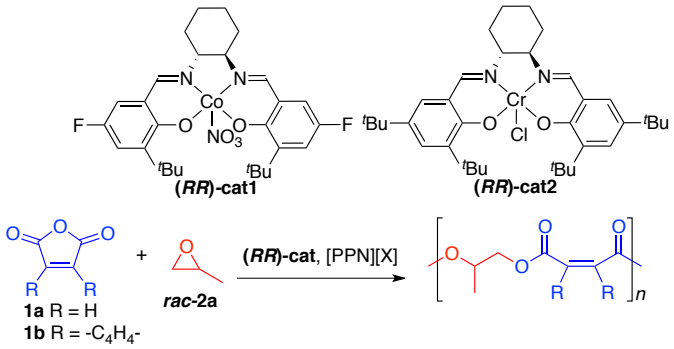


| entry | (*R,R*)-cat | [X] | 1 | time (h) | temp (°C) | % conv.[c] | $M_n$ (kDa)[d] | PDI[d] | $T_g$ (°C)[e] | $T_m$ (°C)[f] | $k_{rel}$[g] |
|---|---|---|---|---|---|---|---|---|---|---|---|
| 1[a] | **cat1** | $NO_3$ | **1a** | 2.2 | 30 | 86 | 3.4 | 1.36 | 23 | 102 | 1.4 |
| 2[a] | **cat2** | n/a | **1a** | 3.0 | 45 | 64 | 5.4 | 1.26 | 21 | n/a | 1.2 |
| 3[b] | **cat1** | $NO_3$ | **1b** | 1.5 | 30 | 86 | 8.1 | 1.20 | 61 | n/a | 4.1 |
| 4[b] | **cat2** | Cl | **1b** | 3.5 | 45 | 60 | 8.9 | 1.27 | 48 | n/a | 2.0 |

[a]General conditions: **1**:**2**:**cat**:[PPN][X] = 100:200:1:1. [b]General conditions: **1**:**2**:**cat**:[PPN][X] = 400:800:1:1. [c]Calculated using $^1$H NMR spectroscopy of the crude reaction mixture based on **1** as the limiting reagent. [d]Measured relative to polystyrene standards using GPC eluted at 0.3 mL/min with THF at 30 °C. [e]Measured using DSC, second heat values. [f]Measured using DSC, first heat values. [g]Calculated based on % conv. of **2a**; the full equation is detailed in Appendix 4.7.

Arguably the most successful example of asymmetric epoxide ring-opening is hydrolytic kinetic resolution (HKR).[12] Mechanistic analyses suggest that two catalysts interact in a fixed fashion determined by ligand conformations that create a chiral environment for epoxide ring-opening.[15] The efficiency of such an arrangement is exemplified by the high activity and selectivity for epoxide homopolymerization by the bimetallic (salen)cobalt catalyst presented by our group.[16] However, no enantioselectivity was observed for the copolymerization of epoxides with cyclic anhydrides using this bimetallic polymerization process.[17] Therefore, we chose to explore variations to the monometallic salcy ligand framework that might influence the selectivity of the carboxylate during epoxide ring-opening.

Initial studies evaluated the steric environment imparted by $R^1$. Adjustments to this position give rise to good selectivity in reactions such as asymmetric carbonylation[18] and the enantioselective copolymerization of epoxides/$CO_2$.[19] Four catalysts with different $R^1$ substitutions were screened for the ROAC of *rac*-propylene oxide (***rac*-2a**) with maleic (**1a**) and phthalic (**1b**) anhydrides (Table 5.3). **Cat3**, with a small methyl group in the $R^1$ position, was less active and selective than the *tert*-butyl analogue (**(*R*,*R*)-cat1**), and produced amorphous PPM (entry 1) and PPP (entry 5). The increased steric bulk of **cat4** and **cat5** imparted by a mesityl and napthyl substituent in $R^1$, respectively, also produced less active and selective catalysts. **Cat4** was more active than **cat5** for ROAC with maleic anhydride (entries 2 and 3), however, $^1$H NMR analysis suggested regioirregular products. For ROAC with phthalic anhydride, **cat5** (entry 7) was more active than **cat4** (entry 6), although both catalysts were significantly slower than their less bulky counterparts. Lastly, **cat6** with

a fluorinated aryl was highly active and selective for both copolymerizations and yielded semi-crystalline PPM ($T_m$ 117 °C) (entry 4) and PPP ($T_m$ 130 °C) (entry 8). These ligand variations indicated that a bulky ortho substitutent was required for selectivity; however, both activity and selectivity were very sensitive to the identity of the substituent.

**Table 5.3.** Chiral Ligands Tested for Enantioselective Copolymerization of Racemic Propylene Oxide with Maleic (**1a**) or Phthalic (**1b**) Anhydride

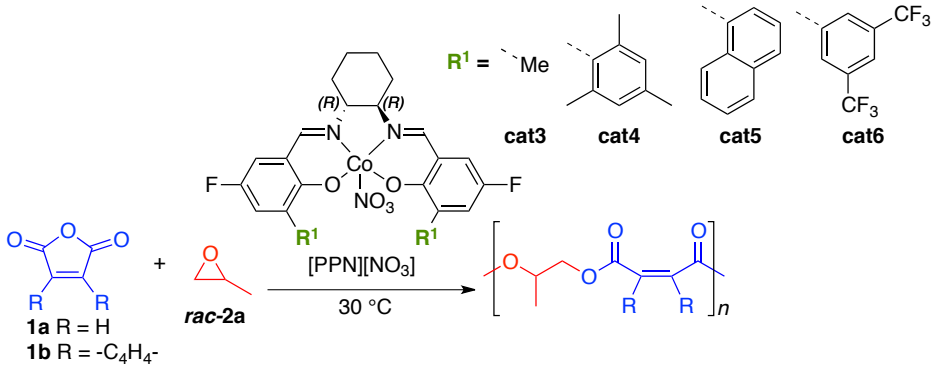


| entry | catalyst | 1 | time (h) | % conv.[c] | $M_n^{theo}$ (kDa)[c] | $M_n^{obs}$ (kDa)[d] | PDI[d] | $T_g$ (°C)[e] | $T_m$ (°C)[f] |
|---|---|---|---|---|---|---|---|---|---|
| 1[a] | **cat3** | **1a** | 18.0 | 41 | 3.2 | <1.0 | - | 20 | n.o.[g] |
| 2[a] | **cat4** | **1a** | 18.0 | 11 | 0.9 | <1.0 | - | n.a.[h] | n.a. |
| 3[a] | **cat5** | **1a** | 18.0 | 5 | 0.4 | <1.0 | - | n.a. | n.a. |
| 4[a] | **cat6** | **1a** | 2.5 | 94 | 7.3 | 3.0 | 1.23 | 18 | 117 |
| 5[b] | **cat3** | **1b** | 4.0 | 87 | 35.8 | 16.7 | 1.17 | 52 | n.o. |
| 6[b] | **cat4** | **1b** | 50.0 | 49 | 20.2 | 5.7 | 1.19 | 57 | 68 |
| 7[b] | **cat5** | **1b** | 30.0 | 59 | 24.3 | 12.5 | 1.18 | 62 | n.o. |
| 8[b] | **cat6** | **1b** | 3.0 | 50 | 20.6 | 7.1 | 1.16 | 60 | 130 |

[a]General conditions: **1**:**2**:**cat**:[PPN][$NO_3$] = 100:200:1:1. [b]General conditions: **1**:**2**:**cat**:[PPN][$NO_3$] = 400:800:1:1. [c]Calculated using $^1$H NMR spectroscopy of the crude reaction mixture based on **1** as the limiting reagent. [d]Measured relative to polystyrene standards using GPC eluted at 0.3 mL/min with THF at 30 °C. [e]Measured using DSC, second heat values. [f]Measured using DSC, first heat values. [g]Not observed. [h]Not applicable.

In the copolymerization of epoxides/$CO_2$, a rate enhancement is seen for polymerizations using a chiral catalyst with the preferred epoxide.[20] Therefore, **cat6** was tested for the copolymerization of (*S*)-propylene oxide with maleic (**1a**) and phthalic (**1b**) anhydride (Table 5.4, entries 1 and 2). A clear rate enhancement was observed for the formation of PPM (entry 1 vs. 3). The polymerization of PPP produced polymer with a high percent crystallinity that caused the reaction to solidify before an accurate rate was measured (entry 2 vs. 4). These results support the high preference of **cat6** for (*S*)-propylene oxide. The $k_{rel}$ of **cat6** for both copolymerizations was also enhanced compared to **(*R,R*)-cat1** (entries 3 and 4). Therefore, variations to the sterics of position $R^1$ impart enhanced selectivity to the copolymerization of propylene oxide with maleic and phthalic anhydride.

**Table 5.4.** Thermal Properties and $k_{rel}$ Values for Polymerization Processes using **cat6**

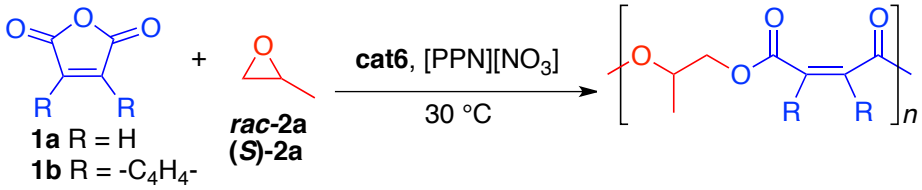


| entry | 1 | 2 | time (h) | % conv.[c] | TOF ($h^{-1}$) | $M_n$ (kDa)[d] | PDI[d] | $T_g$ (°C)[e] | $T_m$ (°C)[f] | $k_{rel}$[g] |
|---|---|---|---|---|---|---|---|---|---|---|
| 1[a] | **1a** | **(*S*)-2a** | 1.0 | 91 | 91 | 1.7 | 1.15 | 16 | 141 | n.a.[h] |
| 2[b] | **1b** | **(*S*)-2a** | 2.0 | 28 | 56 | 4.0 | 1.18 | 51 | 150 | n.a. |
| 3[a] | **1a** | ***rac*-2a** | 2.0 | 52 | 26 | 2.6 | 1.26 | 15 | 119 | 5.0 |
| 4[b] | **1b** | ***rac*-2a** | 2.0 | 38 | 70 | 3.2 | 1.24 | 54 | 108 | 5.6 |

[a]General conditions: **1**:**2**:**cat**:[PPN][X] = 100:200:1:1. [b]General conditions: **1**:**2**:**cat**:[PPN][X] = 400:800:1:1. [c]Calculated using $^1$H NMR spectroscopy of the crude reaction mixture based on **1** as the limiting reagent. [d]Measured relative to polystyrene standards using GPC eluted at 0.3 mL/min with THF at 30 °C. [e]Measured using DSC, second heat values. [f]Measured using DSC, first heat values. [g]Calculated based on % conv. of **2a** determined relative to conversion of **1** and the enantiomeric excess of residual **2a** based on GC analysis. [h]Not applicable.

Finally, **cat6** was tested for the ROAC of maleic (**1a**) and phthalic (**1b**) anhydride with other terminal epoxides. Table 5.5 summarizes the semi-crystalline polyesters that were formed from this process, although other epoxides were active and their polyesters are detailed in Table A4.2. The fluorinated analogue of propylene oxide, 1,1,1-trifluoropropan-2,3-ene oxide (**2b**) produced semi-crystalline polyesters with both maleic (entry 1) and phthalic (entry 2) anhydrides. Although the thermal properties of these fluorinated analogues are not drastically different from their aliphatic counterparts, specific chemical attributes make them valuable engineering precursors.[21] The addition of one carbon in 1-butene oxide (**2c**) also formed semi-crystalline polyester with phthalic anhydride (entry 3), showing a lower $T_g$ and higher $T_m$ (39 and 130 °C) than the propylene oxide analogue (54 and 108 °C).

**Table 5.5.** Enantioselective ROAC of Terminal Epoxides with maleic or phthalic Anhydride

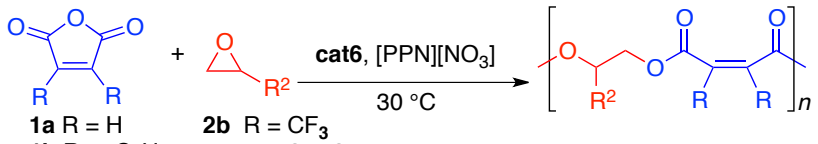


| entry | 1 | 2 | time (h) | % conv.[c] | $M_n$ (kDa)[d] | PDI[d] | $T_g$ (°C)[e] | $T_m$ (°C)[f] |
|---|---|---|---|---|---|---|---|---|
| 1[a] | **1a** | **2b** | 20 | 100 | 12.2 | 1.44 | 18 | 115 |
| 2[b] | **1b** | **2b** | 6.5 | 45 | 10.1 | 1.20 | 61 | 103 |
| 3[b] | **1b** | **2b** | 4.5 | 24 | 4.7 | 1.22 | 39 | 130 |

[a]General conditions: **1**:**2**:**cat**:[PPN][$NO_3$] = 200:400:1:1. [b]General conditions: **1**:**2**:**cat**:[PPN][$NO_3$] = 400:800:1:1. [c]Calculated using $^1$H NMR spectroscopy of the crude reaction mixture based on **1** as the limiting reagent. [d]Measured relative to polystyrene standards using GPC eluted at 0.3 mL/min with THF at 30 °C. [e]Measured using DSC, second heat values. [f]Measured using DSC, first heat values.

## 5.5 Conclusions

In summary, two new processes are described for the synthesis of semi-crystalline and stereo-enriched polyesters. The differing regioselectivities of *rac*-(salcy)$CoNO_3$ (**cat1**) and *rac*-(salcy)CrCl (**cat2**) for the ROAC of enantiopure (*S*)-propylene oxide with maleic and phthalic anhydrides offers the opportunity to form polyesters with tailored thermal properties ($T_g$, $T_m$, and percent crystallinity). In a separate process, the enantioselective copolymerization of racemic epoxides by (*R,R*)-(salcy)$CoNO_3$ catalyst (**cat6**) with maleic and phthalic anhydrides is used to prepare five new semi-crystalline polyesters from racemic starting materials. This process results in enantio-enriched starting materials and products, both of which are valuable synthetic precursors. Future work will focus on improving enantioselectivity through ligand modifications and optimization of reaction conditions. All of the processes presented are compatible with immortal polymerization conditions, enabling preparation of semi-crystalline polyester diols with controlled molecular weight. These precursors are valuable for powder coatings,[6] polyurethanes,[22] biomedical,[9,10a] and engineering applications.[5,6,10]

## REFERENCES


(1) (a) Leiz, J. R.; Asua, J. M. 2002. Copolymers. Kirk-Othmer Encyclopedia of Chemical Technology. (b) Kissin, Y. V. 2005. Olefin Polymers, Introduction. Kirk-Othmer Encyclopedia of Chemical Technology.

(2) (a) Rosen, S. L. 2000. Polymers. Kirk-Othmer Encyclopedia of Chemical Technology. (b) Deplace, F.; Wang, Z.; Lynd, N. A.; Hotta, A.; Rose, J. M.; Hustad, P. D.; Ian, J.; Ohtaki, H.; Coates, G. W.; Shimizu, F.; Hirokane, K.; Yamada, F.; Shin, Y.-W.; Rong, L.; Zhu, J.; Toki, S.; Hsiao, B. S.; Fredrickson, G. H.; Kramer, E. J. *J. Polym. Sci., Part B: Polym. Phys.* **2010**, *49*, 1428-1437.

(3) (a) Coates, G. W. *Chem. Rev.* **2000**, *100*, 1223-1252. (b) Resconi, L.; Cavallo, L.; Fait, A.; Piemontesi, F. *Chem. Rev.* **2000**, *100*, 1253-1345. (c) Domski, G. J.; Rose, J. M.; Coates, G. W.; Bolig, A. D.; Brookhart, M. *Prog. Polym. Sci.* **2007**, *32*, 30-92. (d) Anderson-Wile, Amelia M.; Edson, Joseph B.; Coates, Geoffrey W. Living Alkene Polymerization for Polyolefin Architectures. In *Complex Macromolecular Architectures*; Hadjichristidis, N., Ed.; John Wiley & Sons: Singapore, Singapore, 2011; pp. 267-316. (e) Coates, G. W.; Hustad, P. D.; Reinartz, S. *Angew. Chem. Int. Ed.* **2002**, *41*, 2236-2257.

(4) (a) Boffa, L. S.; Novak, B. M. *Chem. Rev.* **2000**, *100*, 1479-1493. (b) Chung, T. C. M. Functionalization of Polyolefins; Academic Press, London, 2002. (c) Nakamura, A.; Ito, S.; Nozaki, K. *Chem. Rev.* **2009**, *109*, 5215-5244.

(5) a) Gross, R. A.; Kalra, B. *Science* **2002**, *297*, 803-807. b) Harracksingh, R. Bioplastics surge towards commercialization. *ICIS Chem. Bus.* [Online] June 29, 2012. (accessed Sept 1, 2013). c) Philp, J. C.; Bartsev, A.; Ritchie, R. J.; Baucher, M. A.; Guy, K. *New Biotechnol.* **2012**, http://dx.doi.org/10.1016/j.nbt.2012.11.021. d) Ribeiro, I.; Peças, P.; Henriques, E. *Materials and Design* **2013**, *51*, 300-308. (e) Bioplastics Market Update. *Compounding World* [Online] June 20, 2012. (accessed Aug 30, 2013).

(6) (a) Nava, H. 2004. Polyesters, Unsaturated. Kirk-Othmer Encyclopedia of Chemical Technology. (b) East, A. J. 2006. Polyesters, Thermoplastic. Kirk-Othmer Encyclopedia of Chemical Technology.

(7) (a) Jeske, R. C.; Coates, G. W. Homogenous Catalyst Design for the Synthesis of Aliphatic Polycarbonates and Polyesters. In *Handbook of Green Chemistry;* Crabtree, R. H., Ed.; Wiley-VCH: Weinheim, Germany, 2009; Vol. 1, pp 343-373. (b) Kamber, N. E.; Jeong, W.; Waymouth, R. M.; Pratt, R. C.; Lohnmeijer, B. G. G.; Hedrick, J. L. *Chem. Rev*. **2007**, *107*, 5813-5840. (c) Stanford, M. J.; Dove, A. P. *Chem. Soc. Rev.* **2010**, *39*, 486-494. (d) Dijkstra, P. J.; Du, H.; Feijen, J. *Polym. Chem.* **2011**, *2*, 520-527.

(8) Webb, H. K.; Arnott, J.; Crawford, R. J.; Ivanova, E. P. *Polymers* **2013**, *5*, 1-18.

(9) (a) Tsui, A.; Wright, Z. C.; Frank, C. W. *Annu. Rev. Chem. Biomol. Eng.* **2013**, *4*, 143-170. (b) Jérôme, C.; Lecomte, P. *Adv. Drug Delivery Rev.* **2008**, *60*, 1056-1076.

(10) (a) Dove, A. P. *Chem. Commun.* **2008**, 6446. (b) Sepe, M. PBT & PET Polyester in *Plastics Technology* [Online] posted Oct. 2012. www.ptonline.com/columns/pbt-and-pet-polyester-the-difference-crystallinity-makes (accessed Sept 20, 2013).

(11) (a) Jeske, R. C.; DiCiccio, A. M.; Coates, G. W. *J. Am. Chem. Soc.* **2007**, *129*, 11330-11331. (b) Jeske, R. C.; Rowley, J. M.; Coates, G. W. *Angew. Chem., Int. Ed.* **2008**, *47*, 6041-6044. (c) DiCiccio, A. M.; Coates, G. W. *J. Am. Chem. Soc.* **2011**, *133*, 10724-10727. (d) Huijser, S.; Nejad, E. H.; Sablong, R.; de Jong, C.; Koning, C. E.; Duchateau, R. *Macromolecules* **2011**, *44*, 1132. (e) Robert, C.; de Montigny, F.; Thomas, C. M. *Nat. Comm.* **2011**, *2*, 586-592. (f) Nejad, E. H.; van Melis, C. G. W.; Vermeer, T. J.; Koning, C. E.; Duchateau, R. *Macromolecules* **2012**, *45*, 1770-1776. (g) Darensbourg, D. J.; Poland, R. R.; Escobedo, C. *Macromolecules* **2012**, *45*, 2242-2248. (h) Nejad, E. H.; Paoniasari, A.; Koning, C. E.; Duchateau, R. *Polym. Chem.* **2012**, *3*, 1308-1313. (i) Liu, J.; Bao, Y.-Y.; Liu, Y.; Ren, W.-M.; Lu, X.-B. *Polym. Chem.* **2013**, *4*, 1439-1444. (j) Nejad, E. H.; Paoniasari, A.; van Melis, C. G. W.; Koning, C. E.; Duchateau, R. *Macromolecules* **2013**, *46*, 631-637. (k) Bernard, A.; Chatterjee, C.; Chisholm, M. H. *Polymer* **2013**, *54*, 2639-2646. (l) Harrold, N. D.; Li, Y.; Chisholm, M. H. *Macromolecules* **2013**, *46*, 692-698.

(12) For a review on this topic please see: Jacobsen, E. N. *Acc. Chem. Res.* **2000**, *33*, 421-431.

(13) DiCiccio, A. M.; Longo, J. L; Coates, G. C. Manuscript in preparation, refer to Chapter Three.

(14) Please refer to Appendix Four for further discussion.

(15) (a) Kemper, S.; Hrobárik, P.; Kaupp, M.; Schlörer, N. *J. Am. Chem. Soc.* **2009**, *131*, 4172-4173. (b) Ford, D. D.; Nielsen, L. P. C.; Zuend, S. J.; Jacobsen, E. N. *J. Am. Chem. Soc.* **2013**, *135*, 15595-15608.

(16) (a) Hirahata, W.; Thomas, R. M.; Lobkovsky, E. B.; Coates, G. W. *J. Am. Chem. Soc.* **2008**, *130*, 17658-17659. (b) Thomas, R. M.; Widger, P. C. B.; Ahmed, S. M.; Jeske, R. C.; Hirahata, W.; Lobkovsky, E. B.; Coates, G. W. *J. Am. Chem. Soc.* **2010**, *132*, 16520-16525. (c) Widger, P. C. B.; Ahmed, S. M.; Hirahata, W.; Thomas, R. M.; Lobkovsky, E. B.; Coates, G. W. *Chem. Commun.* **2010**, *46*, 2935-2937.

(17) Preliminary unpublished results- please refer to Ian Childers for more details.

(18) Mulzer, M.; Whiting, B. T.; Coates, G. W. *J. Am. Chem. Soc.* **2013**, *135*, 10930-10933.

(19) (a) Lu, X. B.; Ren, W. M.; Wu, G. P. *Acc. Chem. Res.* **2012**, *45*, 1721-1735. (b) Ren, W. M.; Wu, G. P.; Lin, F.; Jiang, J. Y.; Liu, C.; Luo, Y.; Lu, X. B. *Chem. Sci.* **2012**, *3*, 2094. (c) Li, B.; Wu, G. P.; Ren, W. M.; Wang, Y. M.; Rao, D. Y.; Lu, X. B. *J. Polym. Sci. Part A: Polym. Chem.* **2008**, *46*, 6102-6113. (d) Lu, X. B.; Shi, L.; Wang, Y. M.; Zhang, R.; Zhang, Y. J.; Peng, X. J.; Zhang, Z. C.; Li, B. *J. Am. Chem. Soc.* **2006**, *128*, 1664-1674.

(20) For an example please refer to: Cohen, C. T.; Chu, T.; Coates, G. W. *J. Am. Chem. Soc.* **2005**, *127*, 10869-10878.

(21) (a) Schmidt, S. C.; Hillmyer, M. A. *Macromolecules* **1999**, *32*, 4794-4801. (b) Zalusky, A. S.; Olayo-Valles, R.; Taylor, C. J.; Hillmyer, M. A. *J. Am. Chem. Soc.* **2001**, *123*, 1519-1520. (c) Hillmyer, M. A.; Lodge, T. P. *J. Polym. Sci.: Part A: Polym. Chem.* **2002**, *40*, 1-8.

(22) (a) Engels, H. W.; Pirkl, H. G; Albers, R.; Albach, R. W.; Krause, J. K.; Hoffmann, A.; Casselmann, H.; Dormish, J. *Angew. Chem. Int. Ed.* **2013**, *52*, 9422-9441. (b) Sonnenschien, M. F.; Lysenko, Z.; Brune, D. A.; Wendt, B. L.; Schrock, A. K. *Polymer* **2005**, *46*, 10158.

APPENDIX 4

# CHIRAL CATALYSTS FOR THE COPOLYMERIZATION OF COMMODITY EPOXIDES AND CYCLIC ANHYDRIDES TO FORM SEMI-CRYSTALLINE POLYESTERS

**Contents**

### A4.1. General Considerations

All manipulations of air and water sensitive compounds were performed under dry nitrogen using a Braun Labmaster Glovebox or standard Schlenk line techniques. NMR spectra were recorded on a Mercury 300 ($^{1}$H, 300 MHz), Varian INOVA 400 ($^{1}$H, 400 MHz; $^{13}$C, 100 MHz; $^{19}$F 376 MHz), Varian INOVA 500 ($^{1}$H, 500 MHz; $^{13}$C, 125 MHz), or Varian INOVA 600 ($^{1}$H, 600 MHz; $^{13}$C, 150 MHz) spectrometer. $^{1}$H NMR spectra were referenced with residual non-deuterated solvent shifts ($CHCl_3$ = 7.26 ppm or $C_5D_4HN$ = 7.22 ppm), $^{13}$C NMR spectra were referenced by solvent shifts ($CDCl_3$ = 77.16 ppm or $C_5D_5N$ = 123.87 ppm) and $^{19}$F NMR spectra were referenced to fluorobenzene added as an internal standard ($C_6H_5F$ = -131.15 ppm).

Gel permeation chromatography (GPC) analyses were conducted using an Agilent PL-GPC 50 integrated system, (2 x PLgel Mini-MIX C columns, 5 micron, 4.6 mmID) equipped with UV and refractive index detectors. The GPC columns were eluted at a rate of 0.3 mL/min with tetrahydrofuran at 30 °C and were calibrated relative to monodisperse polystyrene standards.

Differential scanning calorimetry of polymer samples was performed on a Mettler-Toledo Polymer DSC instrument equipped with a Julabo chiller and autosampler. Typical DSC experiments were made in crimped aluminum pans and experiments were conducted with a heating rate of 10 °C/min from -70 °C to +200 °C. Data was processed using StarE software.

Gas chromatography analyses were performed on a Hewlett Packard 6890 gas chromatograph (GC) equipped with a Chiraldex α-cyclodextrin trifluoroacetyl column and a flame detector. Helium (Airgas, UHP grade) was used as a carrier gas.

HR/MS analysis was performed at Cornell University.

## A4.2. Materials

### 2.1. General materials

All reagents were used as received unless otherwise noted. $CaH_2$ pellets (90%) used for drying epoxides were purchased from Strem. Butylated hydroxytoluene (BHT) was purchased from Sigma Aldrich (>99% purity). [PPN][Cl] was purchased from Sigma Aldrich (98% purity). Trifluoroacetic acid was purchased from Oakwood Products (99% purity). Hexamine (>99% purity) was purchased from Sigma Aldrich. HPLC grade dichloromethane used for metallation was purchased from Fisher Scientific and purified through a solvent purification system under inert atmosphere and degassed for 1 h prior to use. Ethanol used for metallation was purchased from Kroptec, stored over 3 Å sieves and degassed for 1 h prior to use. All NMR solvents were purchased from Cambridge Isotopes and stored over 3 Å molecular sieves. Fluorobenzene was purchased from Sigma Aldrich (99% purity). All other reagents were purchased from Aldrich, Alfa-Aesar, Acros, Fischer-Scientific or TCI and were used as received unless otherwise noted.

### 2.2. Polymerization Monomers

Both *rac*- and (*S*)- propylene oxide (**2a**), and 1-butene oxide (**2b**) were purchased from Sigma Aldrich, dried over $CaH_2$ for 3 days under inert atmosphere, vacuum transferred to a flame dried thick walled Schlenk adapted flask and stored in the glove box. 1,1,1-trifluoropropan-2,3-ene oxide (**2c**) was purchased from Oakwood Products,

dried over $CaH_2$ for 3 days under inert atmosphere, vacuum transferred to a flame dried thick walled Schlenk adapted flask and stored in the glove box.

Maleic anhydride (**1a**) (>99% purity, Bartek) was stored under inert atmosphere and sublimed before use. Phthalic anhydride (**1b**) (>99% purity**,** Sigma Aldrich) was boiled in $CHCl_3$ at 60 °C (10 g anhydride in 100 mL solvent) for 1 h followed by hot filtration to remove insoluble diacids. The organic filtrate was concentrated to a white solid via roto-evaporation and washed with diethyl ether. The resulting white powder was collected, dried under vacuum for 12 h in the presence of drierite to remove residual moisture, and sublimed under reduced pressure (83 °C). The purified anhydride was collected under inert atmosphere and stored in the glovebox until use. The purity of all anhydrides was confirmed by $^1$H NMR in DMSO-$d_6$.

**2.3. Catalyst Components**

$Co(NO)_3$•$6H_2O$ (>99% purity) was purchased from Strem and stored in a dessicator until use. Anhydrous $CrCl_2$ (>98% purity) was purchased from Strem and stored in a nitrogen filled glovebox until use.

**A4.3. Synthesis of Starting Materials**

3,5-di-*tert*-butylsalicylaldehyde was purchased from Combi-Blocks and used as received.

3-*tert*-butyl-5-fluorosalicylaldehyde was synthesized according to literature/Chapter 3.

**3.1. General procedure A: Formylation of bromophenols**

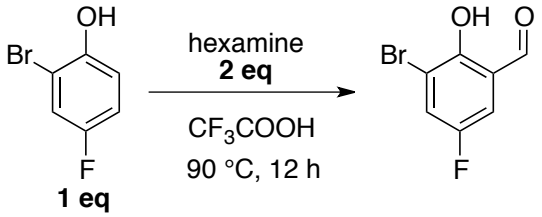


A modified Duff formylation procedure was used as described in Chapter 3 and reported for the formylation of all bromophenols.

The appropriate bromophenol and 2 equivalents of hexamine were dissolved in trifluoroacetic acid (TFA) and refluxed at 90 °C overnight (13 h). The mixture turned a yellow/orange color. After 13 h, the mixture was allowed to cool. For a reaction stirred with 40 mL of TFA, 60 mL of $dH_2O$ and 30 mL of 50% $H_2SO_4$ were added and the solution was stirred for another 3 h. In some cases, a precipitate formed immediately. The resulting mixture was extracted into ethyl acetate, washed with 2 M HCl and water, dried over $Na_2SO_4$ and concentrated. If necessary, the products were purified using column chromatography (typically 20% EtOAc/hex). Bromo-salicylaldehydes generated by this method were obtained in >60% yield.

### 3.2. General Procedure B: Suzuki coupling onto bromo-salicylaldehydes

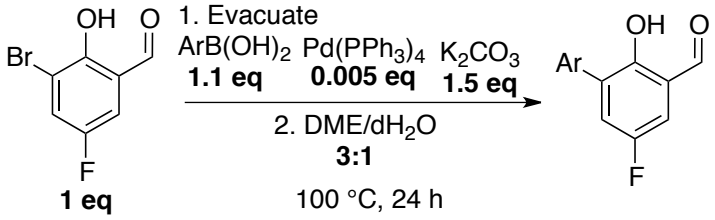


The appropriate bromo-salicyladehyde (1 eq) was placed in a round bottom with the appropriate boronic acid derivative (1.1 eq), $Pd(PPh_3)_4$ (0.05 eq) and $K_2CO_3$ (1.5 eq). The flask was equipped with a reflux column, evacuated 3 times and refilled with inert

atmosphere. The solids were dissolved in a 3:1 mixture of rigorously degassed dimethoxyethane and water, placed under a constant atmosphere of nitrogen and refluxed at 100 °C for 24 h. The next day, the mixture was either a bright yellow or orange color with some black precipitate. After 24 h, the solution was cooled to room temperature and the organics were extracted into diethyl ether, washed with brine and saturated ammonium chloride, dried over $Na_2SO_4$ and concentrated to give a powder. If necessary, the products were purified using column chromatography (20% DCM/hex). The salicylaldehydes generated by this method were obtained in ~50% yield.

### 3.3. General Procedure C: *N,N'*-bis(3-R-5-F-salicylidine)-1,2-cyclohexadiimine formation

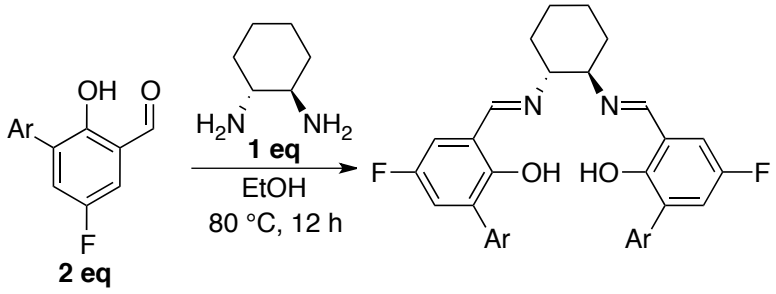


The appropriate salicylaldehyde (2 eq) was dissolved in a solution of ethanol and heated to 80 °C. Cyclohexanediamine (1 eq) was added via syringe causing a color change to bright yellow, and the mixture was refluxed at 80 °C for 12 h. The ligand was extracted into dichloromethane (DCM) and washed with saturated ammonium chloride and brine. The DCM mixture was dried over sodium sulfate and concentrated

to yield a powder. All ligands generated by this method were obtained in >80 % isolated yield.

### 3.4. General Procedure D: Enantiopure N,N'-bis(3-R-5-F-salicylidine)-1,2-cyclohexadiimine formation

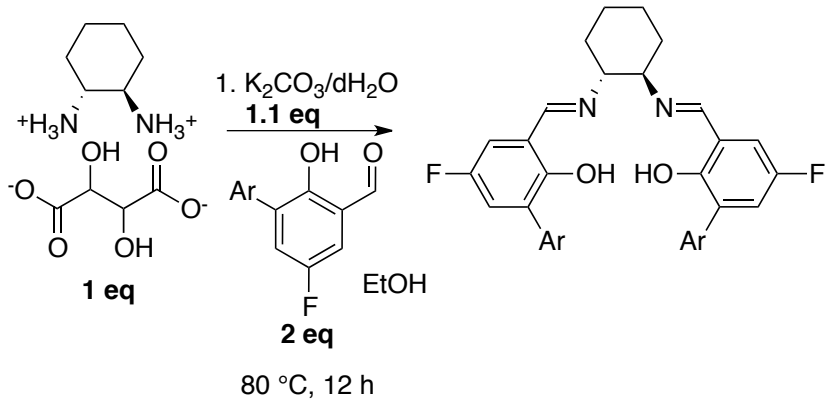


The tartrate salt of *R,R*-trans cyclohexane diamine (1 eq) and $K_2CO_3$ (1.1 eq) was dissolved in $dH_2O$. A solution of the appropriate salicylaldehyde in ethanol was added quickly and the resulting mixture was refluxed at 80 °C for 12 h. The ligand was extracted into dichloromethane (DCM) and washed with saturated ammonium chloride and brine. The DCM mixture was dried over sodium sulfate and concentrated to yield a powder. All ligands generated by this method were obtained in >80 % isolated yield.

### 3.5. General Procedure E: Metallation

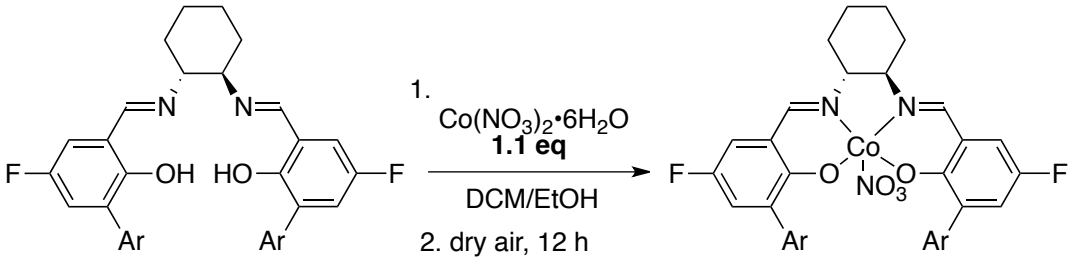


The appropriate ligand was measured into a Schlenk adapted round bottom and evacuated. A solution of the ligand was made in dry, degassed dichloromethane. 1.1 equivalents of $Co(NO)_3$•$6H_2O$ (99% purity Strem, 0.17 mg, 0.60 mmol) was desiccated in a flame dried Schlenk flask under vacuum at 60 °C while being crushed by a stir bar. When the red crystals turned to light pink powder, a solution was made in dry, degassed ethanol. The purple solution was slowly added to a stirring solution of the yellow/brown salcy ligand in dichloromethane, which turned red upon mixing. The red solution was allowed to stir for 1 h and then was opened to air that was diffused through a tube filled with desiccant to allow oxidation. After 12 h, the solution was filtered and solvent was removed under vacuum. The resulting powder was rinsed rigorously with pentane until the filtrate was clear, collected, and further dried under vacuum. All catalysts formed using this method were isolated in >70% yield.

### A4.4. Representative Copolymerization Procedure

#### 4.1. Enantiopure Epoxide

In a glovebox, catalyst (0.01 mmol), [PPN][$NO_3$] (6.0 mg, 0.01 mmol) and maleic anhydride (**1a**) (98.0 mg, 1.0 mmol) were placed in a flame dried 4.0 mL vial equipped with a Teflon coated stir bar. (*S*)-Propylene oxide ((***S*)-2a**) (0.14 mL, 2.0

mmol) was added via syringe with care to wash all solids into the base of the vial. The vial was sealed with a Teflon lined cap, removed from the glovebox, and placed in an aluminum heat block preheated to the desired temperature (30 °C). After the reaction solidified, the vial was removed from the heat block, and the polymer was dissolved in dichloromethane. A small aliquot was removed and analyzed for conversion with $^{1}$H NMR spectroscopy. The dissolved mixture was then precipitated into an excess of hexanes. If a powder precipitated (instead of a goo), it was dissolved again in dichloromethane and precipitated into methanol to remove excess [PPN] salts. For small amounts of polymer, a centrifuge was used to concentrate the solids. This process was repeated until all residual monomer, catalyst, and cocatalyst were removed. After polymer washes, the material was collected and dried *in vacuo*.

### 4.2. Racemic Epoxide

In a glovebox, catalyst (0.01 mmol) and [PPN][$NO_3$] (6.0 mg, 0.01 mmol) were placed in a flame dried 4.0 mL vial equipped with a Teflon coated stir bar. The vial was tared and maleic anhydride (**1a**) (98.0 mg, 1.0 mmol) was added. The vial was massed and an accurate number for the amount of maleic anhydride was recorded. The vial containing the solids was subsequently tared and closed with a puncturable Teflon lined cap. *rac*-Propylene oxide (***rac*-2a**) (0.14 mL, 2.0 mmol) was added via syringe to the open vial with care to wash all solids into the base. The vial was sealed with the puncturable Teflon lined cap, massed to record an accurate amount of ***rac*-2a** and removed from the glovebox. The vial was placed in an aluminum heat block preheated to the desired temperature (30 °C). After the reaction solidified, the vial was removed

from the heat block, and excess epoxide was collected via vacuum transfer using the set-up pictured below (Figure A4.1) The polymer was dissolved in dichloromethane, and a small aliquot was removed for $^{1}$H NMR spectroscopy analysis to determine conversion of **1**. The dissolved mixture was then precipitated into an excess of hexanes. If a powder precipitated, it was dissolved again in dichloromethane and precipitated into methanol to remove excess [PPN] salts. For small amounts of polymer, a centrifuge was used to concentrate the solids. This process was repeated until all residual monomer, catalyst, and cocatalyst was removed. After polymer washes, the material was collected and dried *in vacuo*. The collected propylene oxide was diluted in THF and analyzed using gas chromatography to measure % enantiomeric excess.

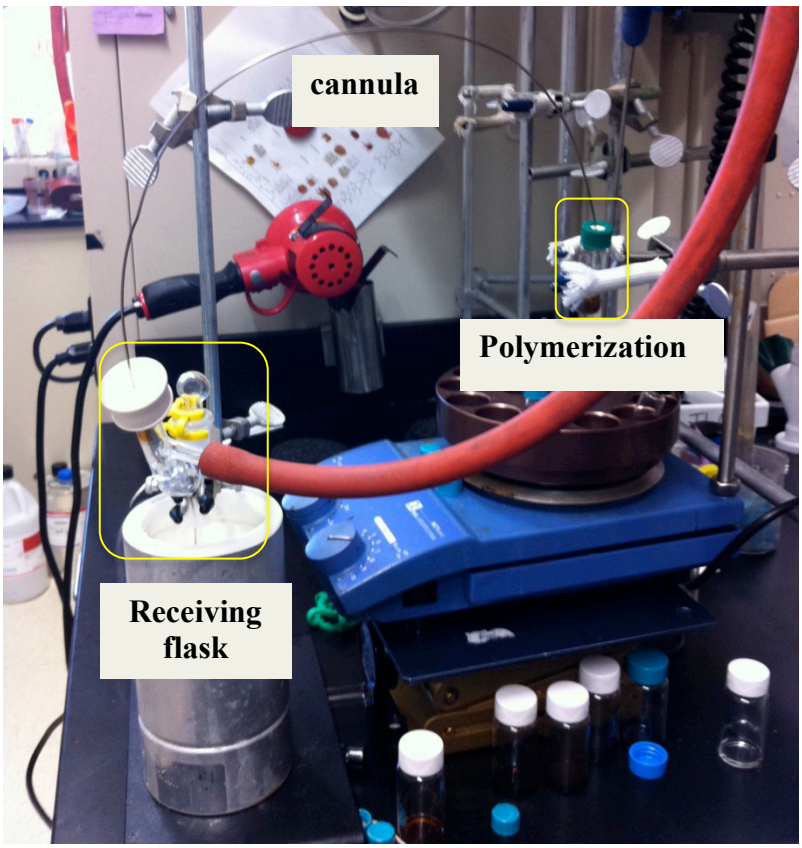


**Figure A4.1.** Picture of the vacuum transfer method used to collect excess epoxide from enantioselective polymerizations.

## A4.5. Investigation and Discussion of Regiochemistry and Semi-crystallinity

### 5.1. Poly(propylene maleate)

The impact of regiochemistry on semi-crystallinity was studied by screening regioregular *rac*-(salcy)$CoNO_3$ (***rac*-cat1**) and regioirregular *rac*-(salcy)CrCl (***rac*-cat2**) systems for the copolymerization of *s*-propylene oxide (***s*-2a**) with maleic (**1a**) and phthalic (**1b**) anhydride (Table 5.1). In all cases, semi-crystalline polyester was obtained as determined by the presence of a melting point in the DSC thermograms (Figure A4.2 and Figure A4.4).

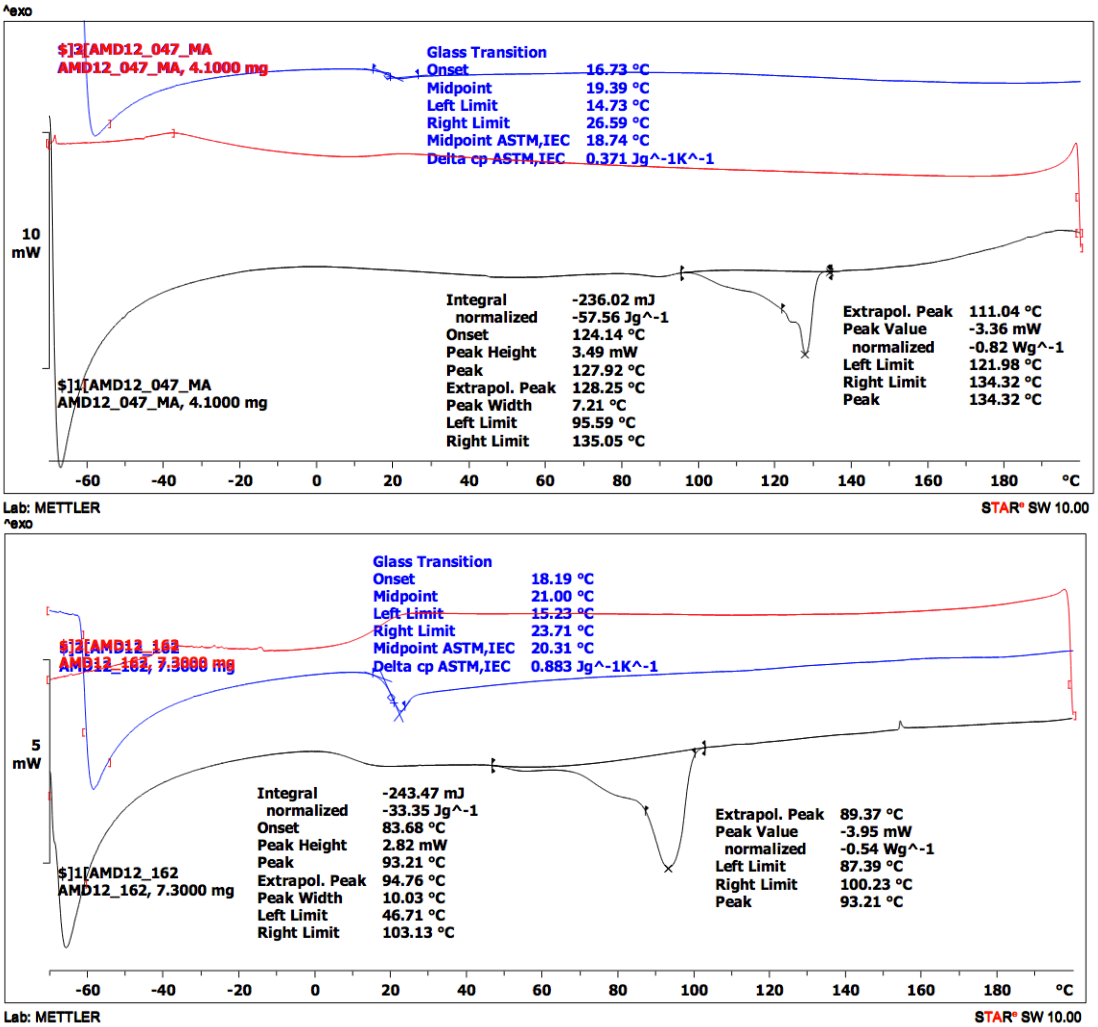


**Figure A4.2.** DSC thermograms of poly(propylene maleate), a) polyester produced by ***rac*-cat1** b) polyester produced by ***rac*-cat2**.

A 40 °C difference in the melting point was observed for poly(propylene maleate) (PPM) samples from ***rac*-cat1** (134 °C) and ***rac*-cat2** (93 °C) (Figure A4.2). The enthalpy of melting was also larger for the PPM produced by ***rac*-cat1** (-58 J/g) than ***rac*-cat2** (-33 J/g). These results suggested that ***rac*-cat1** formed polyester with a higher percent of crystalline domains. The $T_g$ of these polyesters showed the opposite trend, lower for ***rac*-cat1** (19 °C) than ***rac*-cat2** (21 °C). A larger window between $T_g$ and $T_m$ is valuable for industrial processing.[1]

$^1$H NMR spectroscopy was used to correlate the thermal properties with regiochemistry. The alkene region of the $^1$H NMR spectra of the poly(propylene maleate) (PPM) was analyzed for indications of regiochemistry. The high crystallinity of PPM produced by ***rac*-cat1** caused it to be minimally soluble in chloroform at room temperature, contributing to the broad signal in the $^1$H NMR spectrum (Figure A4.3a); however, the polyester was confirmed to be perfectly regioregular by $^{13}$C and HSQC NMR spectra. Conversely, PPM produced by ***rac*-cat2** was readily soluble in chloroform at room temperature and the $^1$H NMR spectrum (Figure A4.3b) showed regioirregularities as indicated by the H,H and T,T signals apparent in the alkene region. These data indicate that perfect stereoregularity is not a prerequisite for semi-crystallinity in PPM and that the thermal properties of this polymer can be adjusted by tuning the regiochemistry of the product.

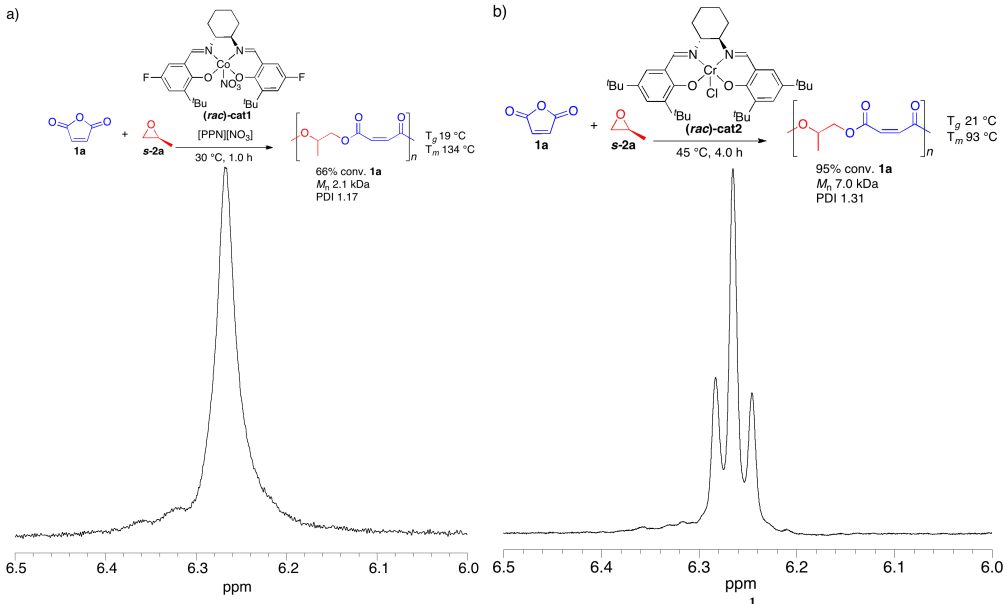


**Figure A4.3.** Regiochemical analysis of PPM as indicated by $^1$H NMR spectroscopy of the alkene proton region for each catalyst product: a) ***rac*-cat1** and b) ***rac*-cat2**.

## 5.2. Poly(propylene phthalate)

The same analysis was performed for the poly(propylene phthalate) (PPP) produced by ***rac*-cat1** and ***rac*-cat2** except that NMR analysis of regiochemistry focused on regioerrors evident from the carbonyl carbons.

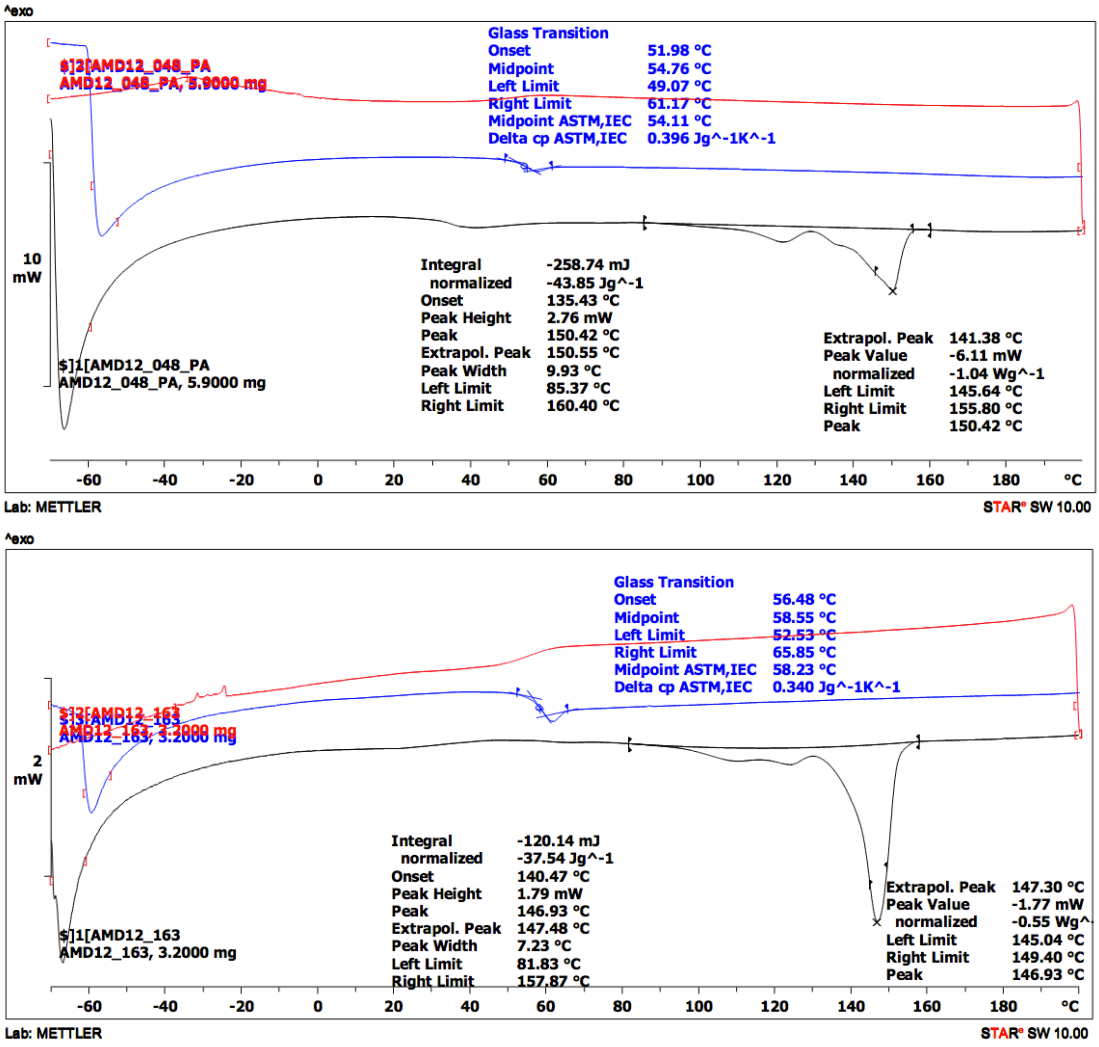


**Figure A4.4.** DSC thermograms of poly(propylene phthalate): a) polyester produced by ***rac*-cat1** b) polyester produced by ***rac*-cat2**.

The DSC thermograms of PPP produced by ***rac*-cat1** and ***rac*-cat2** were strikingly similar, with very close $T_m$s and $T_g$s: (**cat1**: 150 and 55 °; **cat2**: 147 and 56 °C)

(Figure A4.4). However, the enthalpy of melting was different, and suggested a higher percent crystallinity in the PPP produced by ***rac*-cat1** (-44 J/g) than ***rac*-cat2** (-38 J/g).

$^{13}$C NMR spectroscopy of PPP was used to analyze the carbonyl signals for regioerrors. Baseline peaks around 166.7 and 167.1 ppm in Figure A4.5b suggested the presence of H,H and T,T regioerrors for PPP from ***rac*-cat2** that were not apparent in the PPP from ***rac*-cat1** (Figure A4.5a). Additional baseline peaks were also apparent for other regions of the $^{13}$C NMR spectrum of ***rac*-cat2** that were not apparent for ***rac*-cat1**, suggesting a difference between these polyesters.

While these attributes were subtle, they present indicators of slight variations in the regiochemistry of the polyesters. It appeared that *rac*-(salcy)CrCl was more regioregular for copolymerizations involving phthalic anhydride than those with maleic anhydride. Quantification of regioselectivity for each catalyst using polymer degradation are underway.

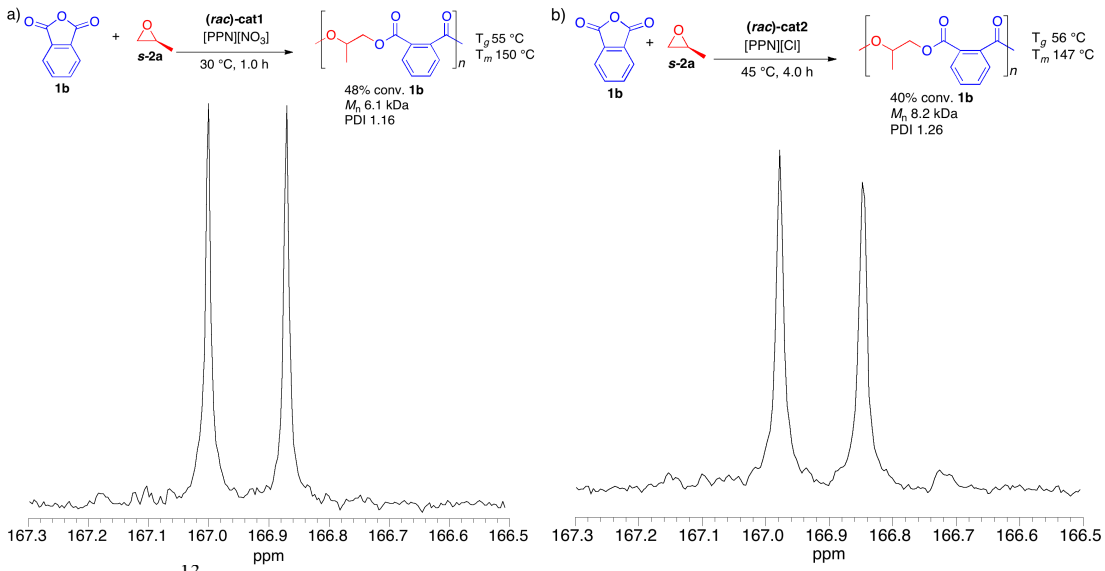


**Figure A4.5.** $^{13}$C NMR spectra of the carbonyl regions for PPP produced by a) ***rac*-cat1** and b) ***rac*-cat2**.

Ultimately, for both polyester systems, it was found that perfect stereoregularity was not required for semi-crystalline properties. This is similar to well-studied systems such as polypropylene, where the ability to control polymer composition and tune melting points is advantageous for creating custom materials for specific applications.[2]

**A4.6. Investigation and Discussion of Polyester Crystallization Rate**

The crystallization of polyesters is complex due to the slow rate, thermal sensitivity, and multiple polymorphs associated with this process.[1, 3] Industrial methods have been designed to take advantage of this feature for polyesters such as PET and PLA,[1] however, this phenomena generally limits commercial application of polyesters. Significant research efforts invested in controlling these processes are a field of their own.[3]

In this report, only melting points from first heats are reported because the slow crystallization rate from the melt, characteristic of many types of polyesters,[4] precludes detection of a melting point on second heat using our standard DSC method. Therefore, the melting points in this publication reflect crystallization from solution. To ensure that the thermal history of all samples were consistent all polymers were precipitated according to the same procedure and dried under vacuum at 45 °C before thermal analysis. Additionally, several control experiments were performed to ensure that melting points were reproducible. Future work will focus on enhancing the semi-crystalline character of these systems using annealing, additives, and temperature gradient crystallization techniques.

**6.1. Multiple DSCs of the Same Sample**

To test that the measured melting point was not an artifact of sample preparation, repeated DSC measurements were analyzed for different pans of the same sample of poly(propylene phthalate). Figure A4.6 shows the similarity of the DSC thermograms measured for two pans of the same sample. The same glass and melting transitions and peak shapes were measured within +/- 0.5 °C. The reproducibility of these transitions confirms that the observed melting point is not an artifact of sample preparation.

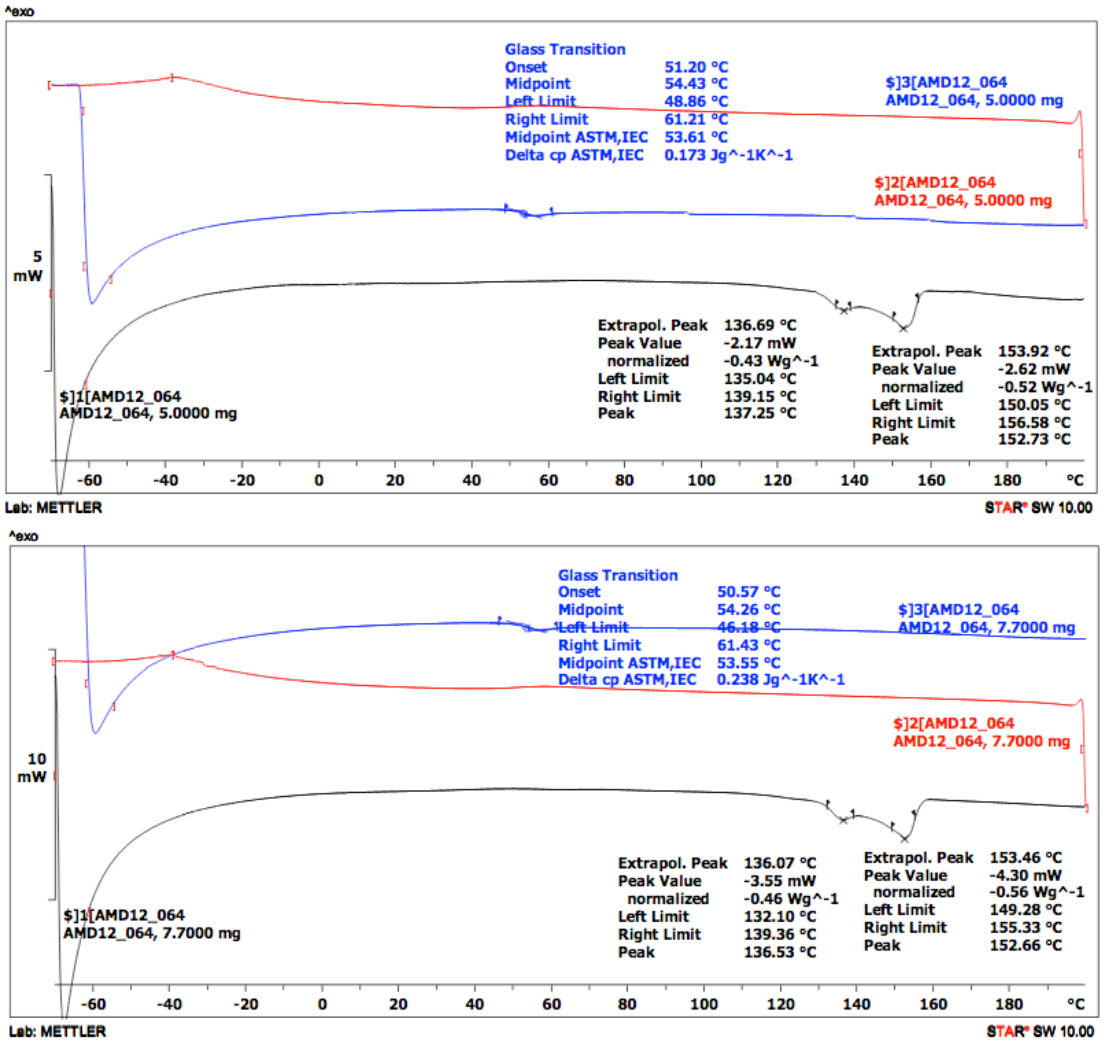


**Figure A4.6.** Repeat DSC measurements for two different pans made from the same polymer sample.

### 6.2. Analysis of Crystallization from the Melt vs Solution

The multiple endotherms corresponding to melting transitions reflect the different polymorphs that PPM and PPP adopt during crystallization, an attribute common to polyesters.[3d,5] These polymorphs vary between samples, however, we were curious if they were characteristic to an individual sample. To test the reproducibility of the polymorph formations, a sample of poly(propylene phthalate) was analyzed by DSC, melted, re-precipitated, and analyzed again.

The first DSC of the PPP sample originally precipitated from solution shows an irreversible melting transition indicative of two polymorphs and a reversible glass transition that becomes stronger after the first heat (Figure A4.7 top). The PPP was incubated at 160 °C, above the melting temperature, and the cloudy polymer changed to a translucent goo that became a hard glass upon cooling. Another DSC measurement was performed on the quickly cooled sample of PPP. After being melted and quickly cooled, PPP did not recrystallize and instead a stronger $T_g$ with a relaxation was measured (Figure A4.7 middle). Finally, the PPP sample was dissolved in dichloromethane, precipitated into methanol according to the original precipitation procedure, dried at 45 °C and reanalyzed. The second precipitation resulted in a polymer with three very distinct polymorphs (Figure A4.7 bottom). For clarity, the integrations of these peaks are not included on the thermogram but all three are -50 J/g or larger, indicating a higher percent crystallinity in this second precipitation.

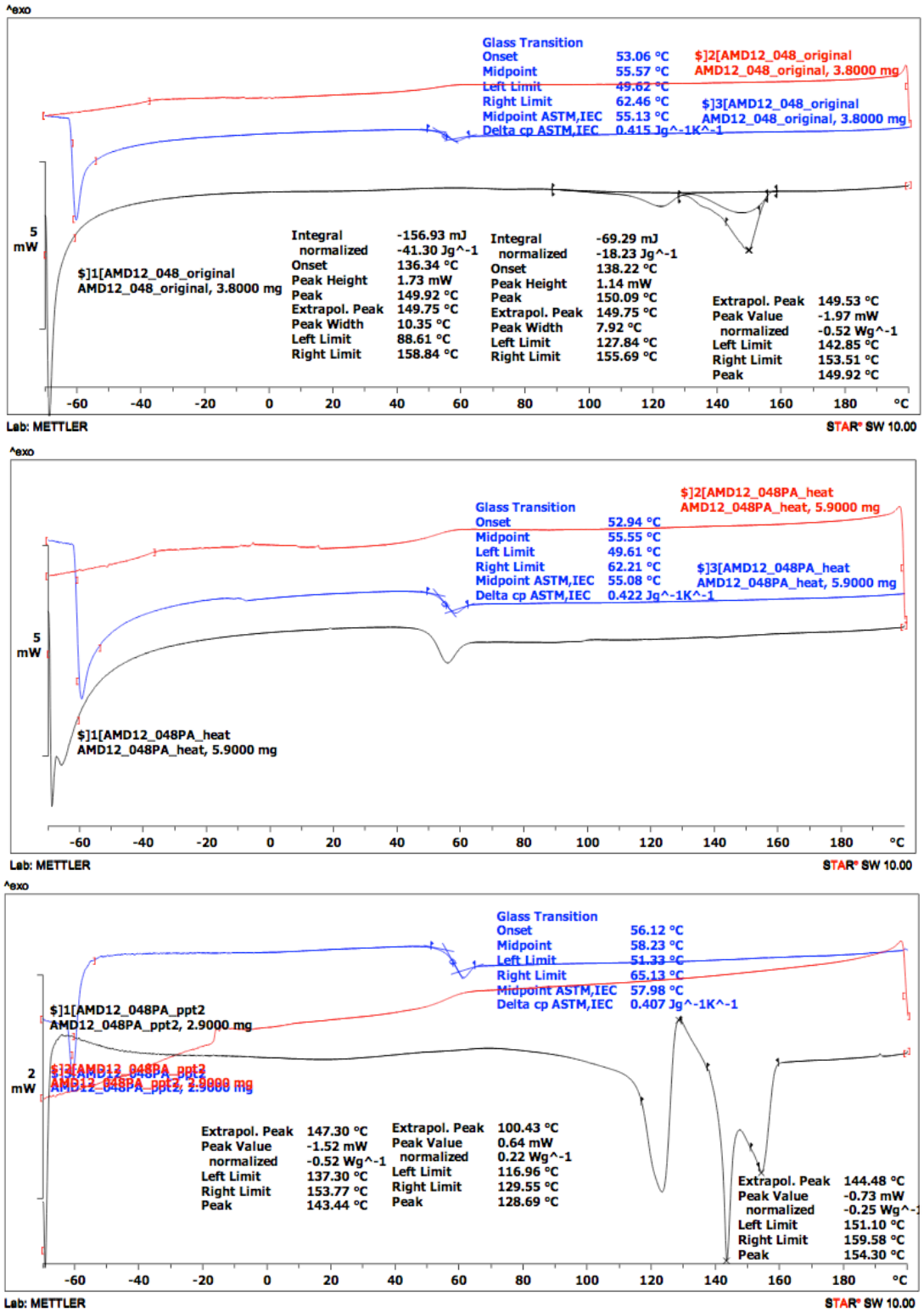


**Figure A4.7.** DSC thermograms of poly(propylene phthalate). Top: original PPP crystallized from solution. Middle: melted and quickly cooled. PPP Bottom: re-precipitated PPP using the same precipitation procedure at the first crystallization.

This analysis confirmed that the polyesters crystallized more quickly from solution and the polymorphs were not inherent to the sample, but related to the sample history. Further studies on precipitation rate, annealing, crystallization from the melt, and processing methods to create reproducible melting behavior are underway.

### A4.7. SLS Data for Table 5.1

Semi-crystallinity presumably impacts the apparent hydrodynamic radius and behavior of a polymer in solution. Therefore, to gain a better perspective of the actual molecular weight of these polyesters, size exclusion chromatography analyzed with static light scattering (SLS) was performed for the polyesters from Table 5.1. The molecular weight data are summarized below.

In all cases, the molecular weight measured by SLS was larger than the relative molecular weights originally measured. The most significant difference was seen for PPM (entries 1 and 2), both polyesters were double in size when analyzed by SLS. This confirms that the stereochemistry causes changes in the solution dynamics of the polymers, accounting for discrepancies in molecular weight measurements. The actual molecular weights are higher than what has been reported by relative methods. These results are preliminary and more rigorous analyses that accurately calculate for dn/dc differences are being pursued.

**Table A4.1.** A summary of SLS measurements for polyesters from Table 5.1

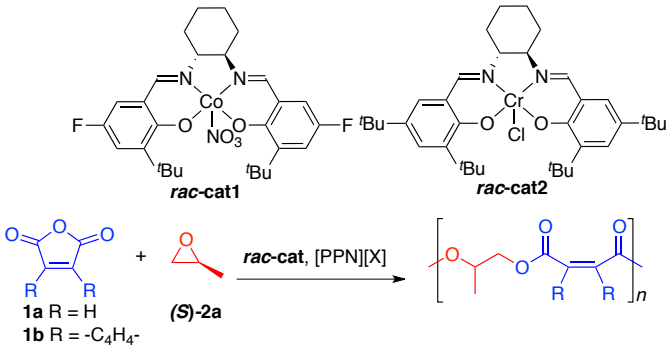


| entry | *rac*-cat | [X] | 1 | $M_n$ (kDa) | PDI |
|---|---|---|---|---|---|
| 1 | **cat1** | $NO_3$ | **1a** | 5.1 | 1.10 |
| 2 | **cat2** | n/a | **1a** | 16.4 | 1.13 |
| 3 | **cat1** | $NO_3$ | **1b** | 8.6 | 1.09 |
| 4 | **cat2** | Cl | **1b** | 10.7 | 1.16 |

### A4.8. Summary of other epoxides screened for copolymerization with maleic (1a) and phthalic (1b) anhydride using cat6

**Cat6** was tested for the copolymerization of a variety of terminal epoxides with maleic (**1a**) and phthalic (**1b**) anhydride (Table A4.2). Maleic anhydride was active for copolymerization with epichlorohydrin (**2d**) (entry 1) and phenyl glycidyl ether (**2e**) (entry 2). Both polyesters have higher $T_g$'s than their stereo-random analogues, suggesting enantio-enrichment. Phthalic anhydride was also active with epichlorohydrin (**2d**) (entry 3) and phenyl glycidyl ether (**2e**) (entry 4) and produced amorphous polyesters with $T_g$'s comparable to poly(propylene phthalate). Longer chain epoxides such as butyl glycidyl ether (**2f**) (entry 5) and 1-hexene oxide (**2g**) (entry 6) yielded polyesters with lower $T_g$'s (9 and 29 °C). While these polymers do not display semi-crystallinity, the selectivity of the polymerizations may still be high and work to measure $k_{rel}$s is underway.

**Table A4.2.** Amorphous polyesters from the enantioselective copolymerization of terminal epoxides (**2b-c**) with maleic (**1a**) and phthalic (**1b**) anhydride using **cat6**

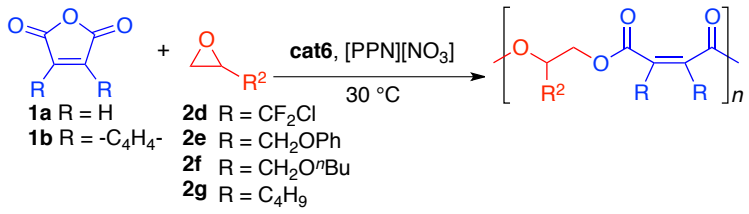


| entry | 1 | 2 | time (h) | % conv.[c] | $M_n$ (kDa)[d] | PDI[d] | $T_g$ (°C)[e] | $T_m$ (°C)[f] |
|---|---|---|---|---|---|---|---|---|
| 1[a] | **1a** | **2d** | 3.0 | 73 | 6.3 | 1.19 | 32 | n.o. |
| 2[a] | **1a** | **2e** | 5.5 | 75 | 7.3 | 1.20 | 39 | n.o. |
| 3[b] | **1b** | **2d** | 12.0 | 45 | 17.1 | 1.17 | 67 | n.o. |
| 4[b] | **1b** | **2e** | 7.0 | 95 | 8.5 | 1.20 | 60 | n.o. |
| 5[b] | **1b** | **2f** | 13.0 | 87 | 10.9 | 1.21 | 9 | n.o. |
| 6[b] | **1b** | **2g** | 13.0 | 53 | 12.6 | 1.16 | 29 | n.o. |

[a]General conditions: **1**:**2**:**cat**:[PPN][$NO_3$] = 200:400:1:1. [b]General conditions: **1**:**2**:**cat**:[PPN][$NO_3$] = 400:800:1:1. [c]Calculated using $^1$H NMR spectroscopy of the crude reaction mixture based on **1** as the limiting reagent. [d]Measured relative to polystyrene standards using GPC eluted at 0.3 mL/min with THF at 30 °C. [e]Measured using DSC, second heat values. [f]Measured using DSC, first heat values.

### A4.9. Calculation of $k_{rel}$

Equation A4.1 was used to calculate $k_{rel}$. The variables used were calculated as follows: c is the percent conversion of **2a** which was calculated based on the conversion of **1** and the ratios of monomers measured during reaction preparation as described section A4.4.1. ee is the percent enantiomeric excess that was calculated based on GC analysis according to equation 4.2.

$$k_{rel} = \frac{k_{fast}}{k_{slow}} = \frac{\ln[(1-c)(1-ee)]}{\ln[(1-c)(1+ee)]} \qquad \text{eq. 4.1}$$

$$\%\ ee = \frac{[(S)\text{-}\mathbf{2a}] - [(R)\text{-}\mathbf{2a}]}{[(S)\text{-}\mathbf{2a}] + [(R)\text{-}\mathbf{2a}]} \qquad \text{eq. 4.2}$$

REFERENCES

(1) (a) Dove, A. P. *Chem. Commun.* **2008**, 6446. (b) Sepe, M. PBT & PET Polyester in *Plastics Technology* [Online] posted Oct. 2012. www.ptonline.com/columns/pbt-and-pet-polyester-the-difference-crystallinity-makes (accessed Sept 20, 2013).

(2) (a) Copolymers. *Kirk-Othmer Encyclopedia of Chemical Technology* [Online]; Wiley & Sons, Posted October 18, 2002. DOI: 10.1002/0471238961.0315161503151920.a01.pub2 (accessed June 15, 2013). (b) Olefin Polymers, Introduction. *Kirk-Othmer Encyclopedia of Chemical Technology* [Online]; Wiley & Sons, Posted March 18, 2005. DOI: 10.1002/0471238961.0914201811091919.a01.pub2 (accessed June 15, 2013). (c) Coates, G. W. *Chem. Rev.* **2000**, *100*, 1223. (d) Resconi, L.; Cavallo, L.; Fait, A.; Piemontesi, F. *Chem. Rev.* **2000**, *100*, 1253. (e) Domski, G. J.; Rose, J. M.; Coates, G. W.; Bolig, A. D.; Brookhart, M. *Prog. Polym. Sci.* **2007**, *32*, 30. (f) Arriola, D. J.; Carnahan, E. M.; Hustad, P. D.; Kuhlman, R. L.; Wenzel, T. T. *Science* **2006**, *312*, 714.

(3) Some papers that discuss this dynamic include: (a) Yasuniwa, M.; Iura, K.; Dan, Y. *Polymer* **2007**, *48*, 5398. (b) Kattan, M.; Dargent, E.; Grenet, J. *J. Thermal Analysis and Calorimetry* **2004**, *76*, 379. (c) Kattan, M.; Dargent, E.; Grenet, J. *Polymer* **2002**, *43*, 1399. (d) Wang, Y.; Mano, J. F. *Euro. Polym. J.* **2005**, *41*, 2335. (e) Arnoult, M.; Dargent, E.; Mano, J. F. *Polymer* **2007**, *48*, 1012. (f) Gao, H.; Vadlamudi, M.; Alamo, R. G.; Hu, W. *Macromolecules* **2013**, doi: 10.1021/ma400842h (g) Alve, N. M.; Mano, J. F.; Balaguer, E.; Meseguer Dueñas, J. M.; Gómez Ribelles, J. L. *Polymer* **2002**, *43*, 4111. (h) Mano, J. F.; Gómez Ribelles, J. L.; Alves, N. M.; Salmerón Sanchez, M. *Polymer* **2005**, *46*, 8258. (i) Seguela, R. *J. Macromolecular Sci. Part C: Polym. Reviews* **2005**, *45*, 263. (j) Xu, H.; Teng, C.; Yu, M. *Polymer* **2006**, *47*, 3922.

(4) Examples that report polyesters that crystallize slowly from the melt: (a) Wu, J.; Eduar, P.; Thiyagarajan, S.; Jasinka-Walc, L.; Rozanski, A.; Guerra, C. F.; Noordover, B. A. J.; van Haveren, J.; van Es, D. S.; Koning, C. E. *Macromolecules* **2012**, *45*, 5069.

(5) (a) Lebarbé, T.; Maisonneuve, L.; Nguyen, T. H. N.; Gadenne, B.; Alfos, C.; Cramail, H. *Polym. Chem.* **2012**, *3*, 2842. (b) He, Y.; Fan, Z.; Hu, Y.; Wu, T.; Wei, J.; Li, S. *Euro. Polym. J.* **2007**, *43*, 4431.

CHAPTER SIX

# MECHANISM INISGHTS TO THE ALTERNATING RING-OPENING COPOLYMERIZATION OF EPOXIDES WITH CYCLIC ANHYDRIDES

## 6.1 Abstract

In the past decade, many systems have been developed capable of performing the alternating ring-opening copolymerization of epoxides with cyclic anhydrides. Despite this progress, few studies have directly addressed the mechanisms of these systems and none have made comparisons. Herein, mechanism data is summarized for two polyester catalyst systems and comparisons are discussed.

## 6.2 (BDI)ZnOAc ROC of epoxides with cyclic anhdyrides

Note: catalyst labels for the (BDI)Zn complexes are a continuation from Chapter 1

In 2007, our group reported a (BDI)ZnOAc (beta-diiminate zinc acetate) complex (**2a**) to catalyze the ring-opening copolymerization (ROC) of epoxides and cyclic anhydrides (Figure 6.1a).[1] A variety of (BDI)ZnOAc complexes are highly active for the polymerization of lactide as well as for the copolymerization of epoxides/$CO_2$. Thus, this framework was selected as a promising candidate to catalyze the copolymerization of epoxides/cyclic anhydrides to form polyesters. This summary will propose a mechanism for polyester formation based on mechanistic implications of single insertion studies in conjunction with information from epoxide/$CO_2$ copolymerizations.

Initial trials revealed that the most active epoxide/$CO_2$ copolymerization catalyst (**2b**) is unstable under the conditions employed for the ROC of epoxides/cyclic anhydrides. The crystal structure of a representative degradation product[2] isolated from a copolymerization mixture corroborates literature reports that the BDI ligand is reactive towards electrophiles.[3] The proposed degradation initiates when the methine carbon of the BDI backbone ring-opens an anhydride (Figure 6.1b). However, replacing the methine proton with an electron withdrawing cyano group sufficiently deters degradation and allows **2a** to catalyze the ROC of epoxides/cyclic anhydrides (Figure 6.1a).[4]

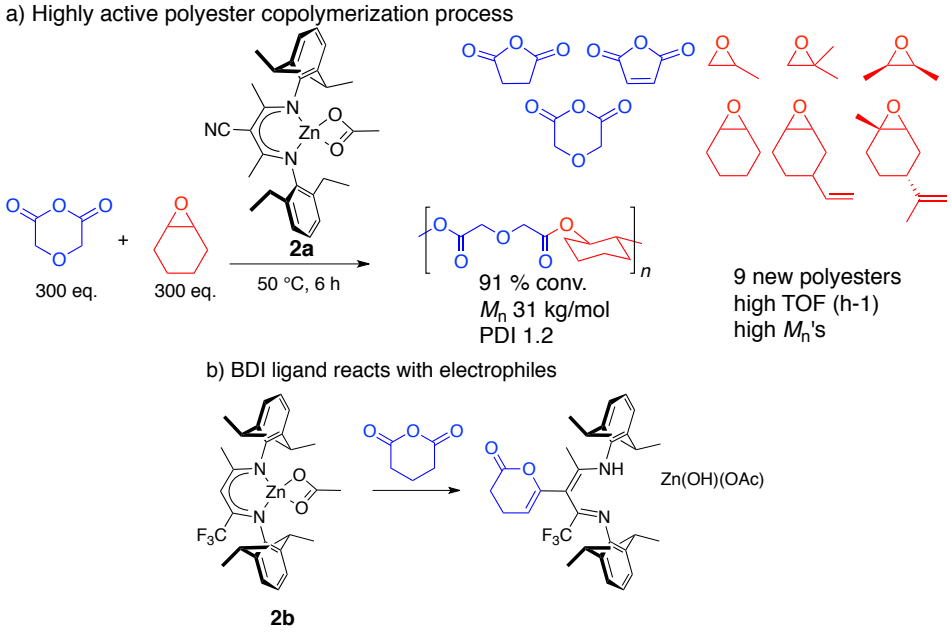


**Figure 6.1.** The methine substituent of (BDI)ZnOAc catalysts determines stability in the presence of cyclic anhydrides as demonstrated by a) the stability of cyano substituted **2a** compared to b) the degradation of proton substituted **2b**.

Catalyst **2a** has a high turn-over frequency (TOF) for the copolymerization of diglycolic anhydride (DGA) and cyclohexane oxide (CHO), consuming up to 50 monomers per hour (**Figure 6.1**a). While observed molecular weights are lower than the theoretical, high molecular weight polyesters (up to 55.0 kDa) with narrow PDIs (1.2)

are obtained. Preliminary mechanistic studies suggest that **2a** operates through a monomer/dimer equilibrium similar to **2b** in polycarbonate polymerizations (**Figure 6.2**).[5]

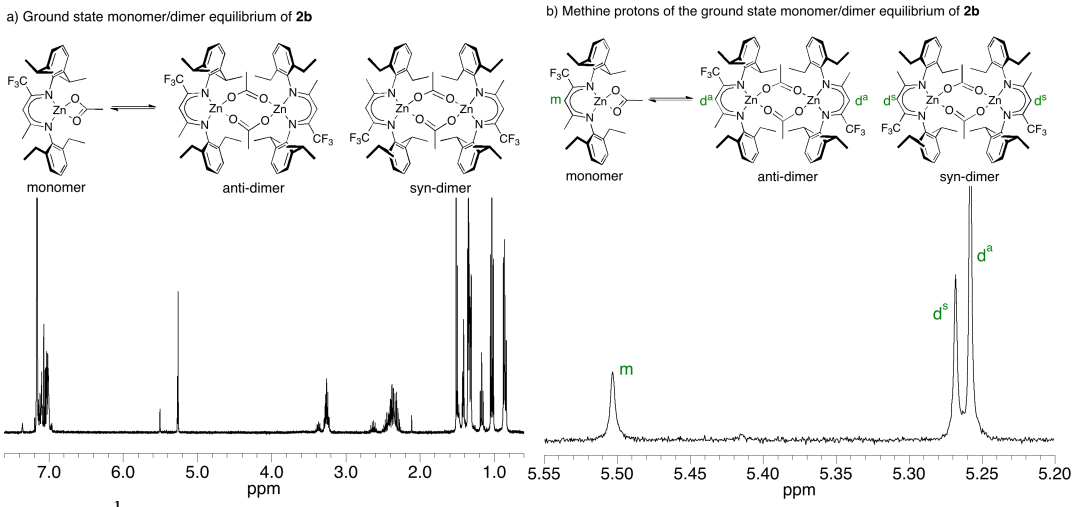


**Figure 6.2.** $^{1}$H NMR spectra of the ground state of 18 mM (BDI)ZnOAc in $C_6D_6$ at 30 °C. a) The entire ligand region shows there are multiple isomers and b) a close-up of the diagnostic methine proton region identifies monomer (m), anti-dimer ($d^a$) and syn-dimer ($d^s$) isomers.

The poor solubility of **2a** caused by the cyano substituent precludes unambiguous assignment of solution state catalyst isomers in NMR spectra. Therefore, **2b** was chosen for NMR spectroscopy studies to probe the role of each isomer during single insertion events. Under stoichiometric conditions at room temperature, **2b** is stable in the presence of cyclic anhydrides and provides a sufficient model for exploring putative propagating intermediates in the copolymerization of epoxides/cyclic anhydrides. $^{1}$H and $^{19}$F NMR spectra of the methine proton and $CF_3$ fluorines on **2b** indicate a distribution of one monomer and two dimers in equilibrium. Figure 6.2b identifies the proton signals for the monomer (m), syn-dimer ($d^s$), and anti-dimer ($d^a$) isomers. Changes in temperature perturb the equilibrium such that the ratio of monomer:dimer

increases at high temperatures and decreases at low temperatures. At room temperature the ratios are approximately: [m]:[$d^s$]:[$d^a$] = [0.3]:[0.6]:[1.0].

Consistent with the proposed mechanism for epoxide/$CO_2$ copolymerization, (BDI)Zn-carboxylates react with epoxides (Figure 6.3)[1e] and (BDI)Zn-alkoxides react with anhydrides (discussed in Figure 6.5). Figure 6.3a shows the distinct changes in the $^1$H NMR signals of the BDI methine proton as **2b** reacts with a molecule of CHO. The monomer/dimer isomers gradually disappear and a fourth peak attributed to the epoxide-inserted product ($p^E$) appears (Figure 6.3a). Figure 6.3b shows that the same changes are evident in the $^{19}$F NMR spectra. The epoxide-inserted species is assumed to be monomeric because the signal for $p^E$ appears in the monomer region of both spectra and does not show structural isomers characteristic of a dimer. This is in contrast to the dimeric crystal structure reported by our group of **2a** with a single inserted CHO.[1e] It is not uncommon, however, for solid state structures to differ from reactive intermediates. Additionally, preliminary mechanistic work from polycarbonate systems indicate an order of activity between 1 and 2 for the Zn catalysts, suggesting that these two species are in equilibrium and both participate in polymerization.

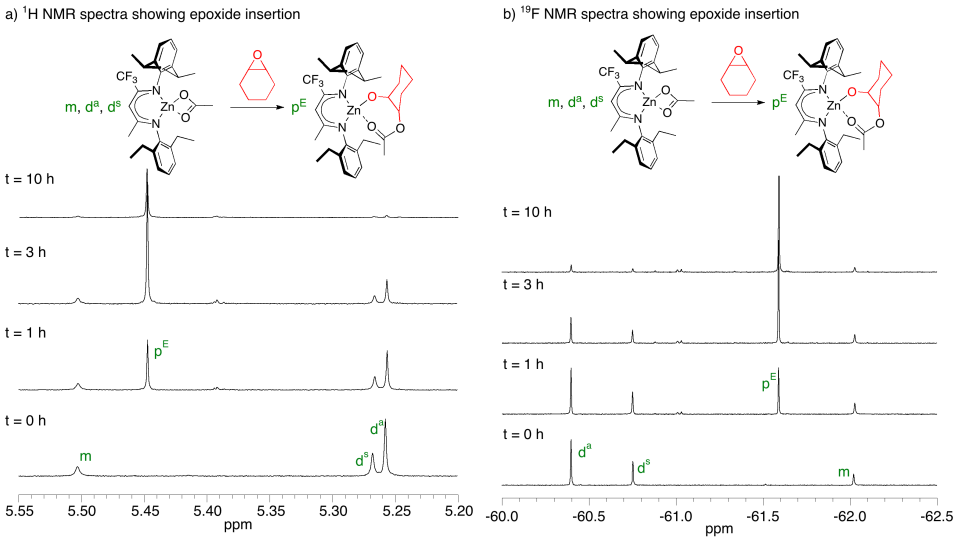


**Figure 6.3.** Reaction progress of **2c** with two equivalents of CHO over time monitored by changes in the a) methine protons and b) $CF_3$ fluorines of **2c**.

Initial changes are not detected in the ratio of unreacted monomer:dimer isomers during CHO insertion. After 10 hours, the ratio equilibrates to: [m]:[d$^{s}$]:[d$^{a}$] = [0.9]:[0.6]:[1.0], reflecting an increase in the relative ratio of monomer. At this point, the major species in solution is the epoxide-inserted product, which was proposed to be a reversible insertion product in the polycarbonate polymerization mechanism. The implications of the equilibrium ratio changes are thus far unclear and the fast $k_{eq}$ prevents the determination of the rates and order of reactivity for each isomer (Scheme 6.1; monomer ($k_m$), anti-dimer ($k_{da}$), syn-dimer ($k_{ds}$)). The design of new polyester processes to obtain high molecular products requires insight to the role of each isomer during polymerization. Lee et al. reports a series of bimetallic zinc complexes able to operate at low catalyst loadings for the production of high molecular weight poly(cyclohexene carbonate).[6] This precedent is encouraging for the development of bimetallic zinc complexes for polyester synthesis. Temperature studies that influence the ground state equilibrium coupled with insertion studies of the epoxide might provide insight to the active species for epoxide insertion and should be considered.

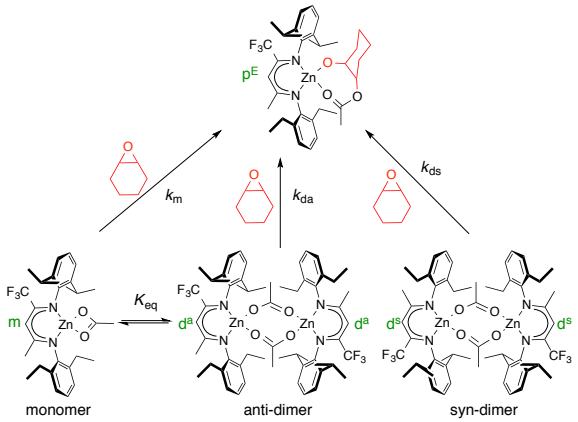


**Scheme 6.1**. The ground state isomers of **2b** rapidly equilibrate ($k_{eq}$) during CHO insertion, preventing measurement of $k_m$, $k_{da}$ and $k_{ds}$.

In agreement with proposed polycarbonate mechanisms, the slow reaction of **2b** with CHO suggests that epoxide ring-opening is the rate determining step (Figure 6.4).[1] The thermodynamic barrier of creating a more basic alkoxide from a less basic carboxylate defines the energy requirements of this step and the nucleophilic attack of the carboxylate on the epoxide defines the rate. Anhydride ring-opening is thermodynamically favored because of the creation of a less basic carboxylate from a more basic alkoxide and occurs quickly because of the rapid attack of the strongly nucleophilic propagating alkoxide on the electrophilic anhydride.

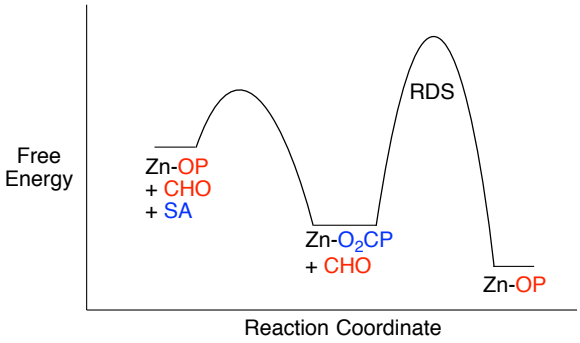


**Figure 6.4.** The thermodynamic barrier of forming a more basic alkoxide from a carboxylate defines the RDS of (BDI)ZnOAc copolymerization of epoxides/cyclic anhydrides, P = polymer chain.

The (BDI)Zn-alkoxide complex of **2b**/CHO inserts 1 equivalent of succinic anhydride (SA) in less than 5 minutes (Figure 6.5). Figure 6.5 shows the rapid change

that occurs upon addition of SA and the transformation of $p^E$ to the multiple isomers of anhydride-inserted product assigned as $p^A$. The anhydride-inserted product appears in both the monomeric and dimeric regions of the spectra and discrete identification remains illusive. The flexibility of the inserted anhydride likely adopts many conformers, attributing to the broad NMR signals and making this intermediate difficult to define. Note that after 20 hours, the extra equivalent of CHO inserts to resume a (BDI)Zn-alkoxide species.

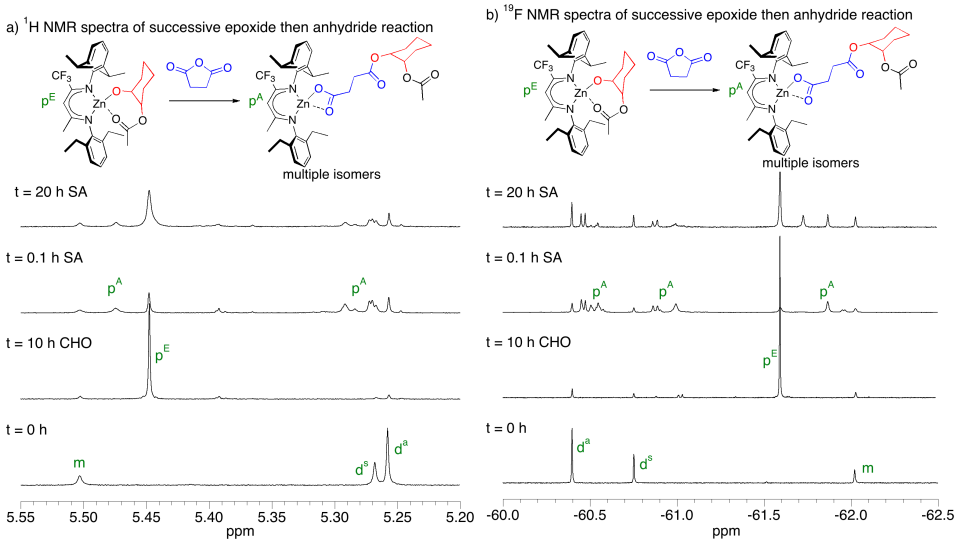


**Figure 6.5.** Reaction of **2b** with one equivalent of SA followed by insertion of excess epoxide as monitored by changes in the a) methine protons and b) $CF_3$ fluorines of **2c**.

Presuming copolymerization involves dynamic association/disassociation of dimeric and monomeric species, exchange of propagating chains likely occurs between catalytic species. This may explain the regioirregular epoxide enchainment and account for molecular weight discrepancies that cause $M_n^{theo} > M_n^{obs}$.[4] A bimetallic system that restricts exchange with multiple partners may prevent chain transfer and orient the propagating species for directional enchainment, thus resolving these issues.

Another consideration when designing polymerization processes is the steric constraints of the dimer intermediate, which likely limits the substrate scope to

anhydrides that are flexible and compact such as SA and DGA. For example, the ROC of the rigid and bulky phthalic anhydride (PA) using **2a** does not yield polyester (Figure 6.6a), and stoichiometric NMR studies with **2b** do not show evidence of anhydride ring-opening (note: catalyst degradation is also not observed).[7] Finally, a distinction should be noted concerning the copolymerization of maleic anhydride (MA) with limonene oxide (LO) catalyzed by **2a** (Figure 6.6b). Different from other copolymerizations, this reaction mixture turns a light green color and is slower than copolymerizations with DGA and SA. Copolymerizations catalyzed by **2a** or **2b** of MA with PO or CHO produce polymers containing mostly polyether linkages. Furthermore, if THF is used as a solvent, a terpolymer is formed with the sequence: -(PO-THF-PO-MA)-. These observations suggest that an unexpected catalytic species is generated in systems containing **2a** or **2b** with MA.

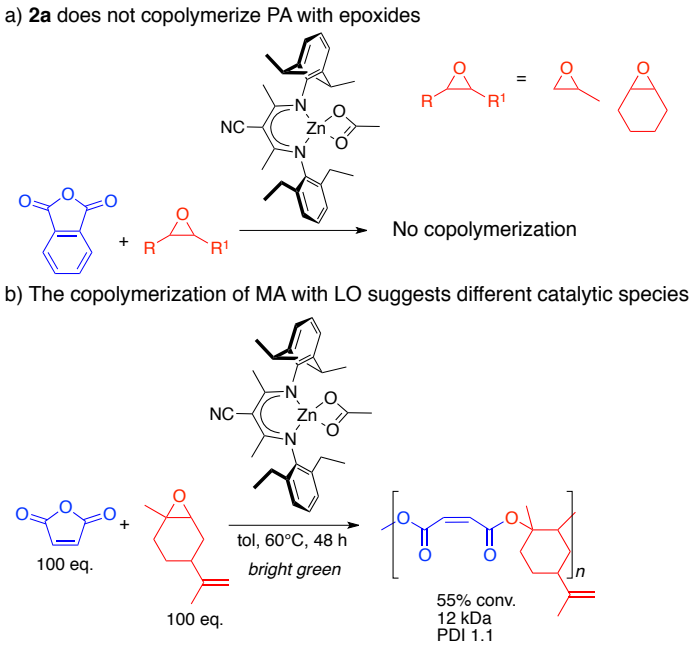


**Figure 6.6.** Copolymerizations of **2a** with rigid and bulky anhydrides such as a) PA result in no polymer formation or b) MA results in a bright green mixture that produces polyester only with LO as the epoxide comonomer.

In 2009 our group exploited the versatility of this process in a one-pot terpolymerization to produce a poly(ester-*block*-carbonate).[8] In the presence of cyclic anhydride, $CO_2$, and excess epoxide, **2a** first copolymerizes epoxide/cyclic anhydride into a polyester block followed by epoxide/$CO_2$ into a polycarbonate block (Figure 6.7). This is an elegant example of a product-determining step that occurs before the rate-determining step.

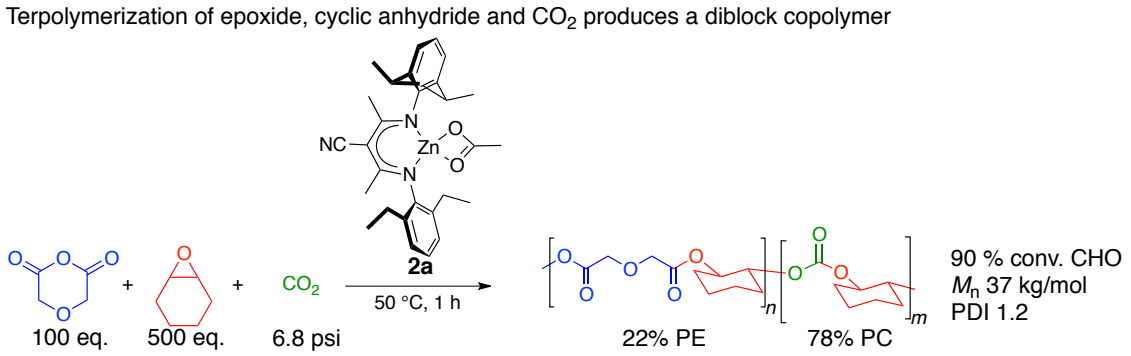


**Figure 6.7.** The terpolymerization of epoxide, anhydride, and $CO_2$ using **2b** produces a poly(ester-*block*-carbonate) diblock.

Interestingly, the rate-determining step (epoxide ring-opening) for polyester formation is slower than for polycarbonate formation (Figure 6.8, $k_1>>k_3$), despite the faster product-determining step that selects for polyester (Figure 6.8, $k_4>>k_2$). Rate differences for epoxide reactions can be attributed to the greater nucleophilicity of the propagating carboxylate compared to that of the carbonate species. Insight from mechanistic investigations, solid-state structures, and NMR spectroscopy suggest that both processes operate through structurally analogous intermediates, allowing direct comparison of the rate-determining steps. The greater nucleophilicity of the propagating carboxylate results in $k_1>k_3$ and a faster rate of polycarbonate polymerization (Figure 6.8).

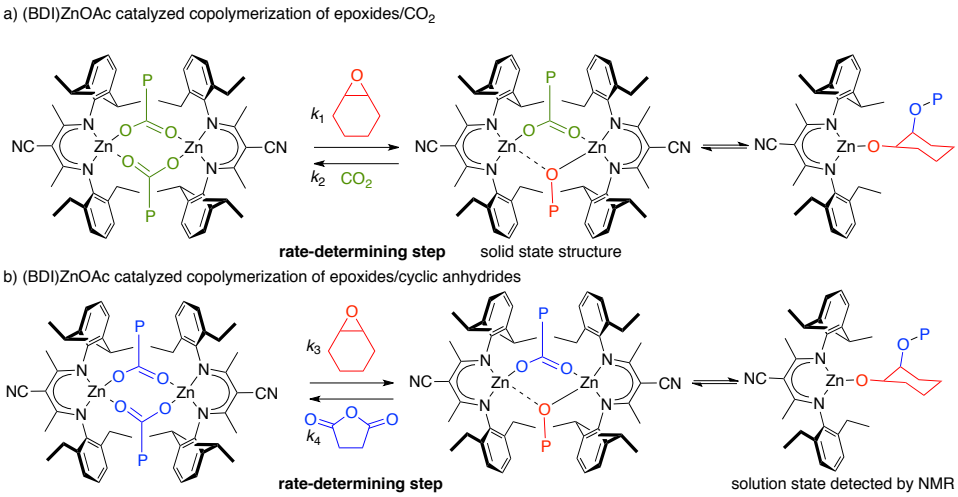


**Figure 6.8.** Similar mechanisms are proposed for the (BDI)ZnOAc catalyzed copolymerization of a) epoxides/$CO_2$ and b) epoxides/cyclic anhydrides.

Rate differences for anhydride and $CO_2$ insertion are attributed to the quicker ring-opening of the more electrophilic anhydride ($k_4$), selecting for polyester formation before polycarbonate. The irreversible insertion of anhydride and $CO_2$ allows the polymerization rates of the individual blocks to remain unaffected by the presence of the competing monomer. However, at increased $CO_2$ pressures, $k_2$ competes with $k_4$ to form random block copolymers.

## 6.2. (Salcy)$CoNO_3$ catalyzed ROC of epoxides with cyclic anhydrides

Our group recently reported the development of highly active (salcy)$CoNO_3$ catalysts for the ring-opening copolymerization of epoxides and cyclic anhydrides (Figure 6.9). (Salcy)MX catalysts are well known to catalyze copolymerizations of epoxides/$CO_2$ and epoxides/cyclic anhydrides as well as for the asymmetric ring-opening of epoxides. Thus, this framework seemed appropriate for the development of regioregular polyester polymerization catalysts. This summary analyzes mechanistic

implications interpreted by measuring changes in copolymerization rate associated with variations of the electronics and structure of catalyst and monomers.

Preliminary results indicated that (salcy)CoX complexes catalyze the regioregular copolymerization of epoxides and cyclic anhydrides but suffered from low activity Figure 6.6.9a

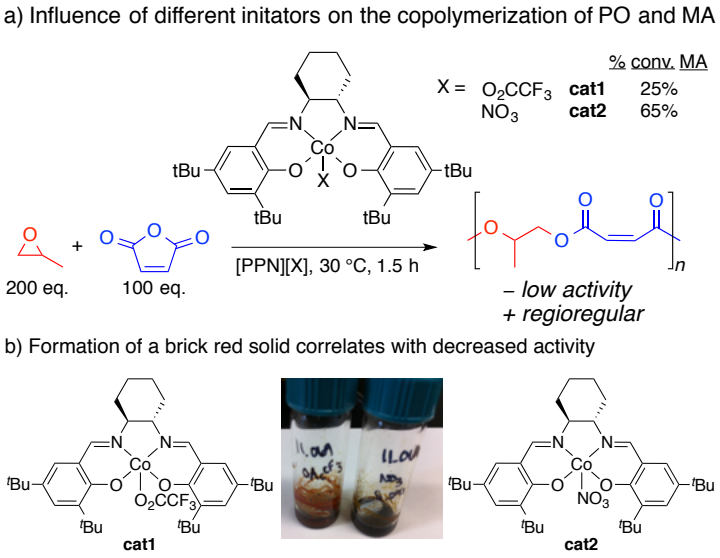


**Figure 6.9.** Different initiators influence a) copolymerization activity and b) apparent rate of catalyst degradation.

Visual indication of catalyst reduction during the copolymerization of MA/PO implicates catalyst instability as an explanation of low activity (Figure 6.9b). Shortly after combining reagents, the reaction mixture turns a dark ink color with a ring of brick red solid. Time-lapse aliquots of the reaction mixture correlate this transformation with decreased polymerization rate. Different initiators were screened for the copolymerization of MA/PO and all resulted in formation of a brick red solid, however, **cat2** achieved highest conversion (Figure 6.9a) and produced noticeably less degradation product (Figure 6.9b), suggesting a more robust system. An important distinction about **cat2** is the *in situ* metallation and oxidation procedure used for

synthesis compared to the two pot procedure used for **cat1** and most other (salcy)CoX complexes.

The formation of a brick red solid associated with decreased activity is documented in several other systems.[9] For example, Jacobsen et al. reports a similar observation for the hydrolytic kinetic resolution (HKR) of epoxy-ketones; note that activity is restored if the reaction is run under oxidizing conditions open to atmosphere.[9a] Xiao-Bing Lu and coworkers recently used ESI-MS and UV-vis to confirm that reduction of Co(III) to Co(II) produces the brick red solid that is associated with diminished HKR activity.[10] Lu isolated α-hydroxy ketones from these reaction mixtures, which suggests that diols formed in the course of the HKR are oxidized to α-hydroxy ketones.

A similar redox cycle likely contributes to formation of the brick red solid degradation product observed during copolymerizations. The influence of ligand electronics on the (salcy)$CoNO_3$ catalyzed copolymerization of MA/PO was evaluated by measuring TOF and observing reduction product (Figure 6.6.10). In general, electron-withdrawing ligands had higher turn-over frequencies (TOF $h^{-1}$) and less degradation. The increased TOF may reflect a faster rate-determining step or a higher ratio of active catalysts. The decrease in activity of the electron-donating ligands is presumably due to catalyst degradation. Conversely, the decrease in activity for the strongly electron-withdrawing ligands is likely due to changes in the lability of the propagating chain coordinated to the Lewis acidic Co center.

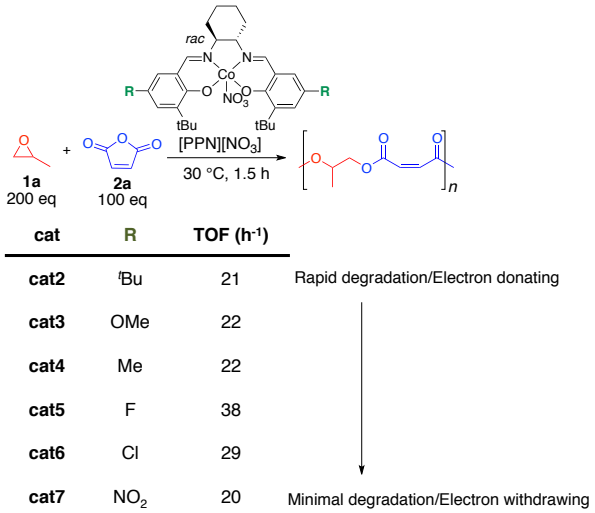


**Figure 6.10.** Ligand electronics impact the polymerization rate of (salcy)$CoNO_3$ catalysts as well as the formation of degradation product.

Cyclic voltammetry (CV) and NMR spectroscopy were used to directly study the redox stability of (salcy)Co(III)$NO_3$ catalysts during copolymerization (Figure 6.6.11a). Two catalysts with different ligand electronics were compared; the electron-donating **cat2** and electron-withdrawing **cat5**. CV was used to measure the potentials for the Co(III) to Co(II) redox couple in copolymerization mixtures of **cat2** and **cat5**. Calculations with the Nernst equation indicated a larger ratio of Co(III):Co(II) species in the reaction mixture of **cat5** compared to that using **cat2** (?). CV measurements also demonstrated that **cat5** is redox stable while **cat2** experiences a continual decrease in potential, indicating increased Co(II) formation (Figure 6.11b). Thus, the decreased activity of **cat2** can be attributed to the degradation of the active Co(III) catalyst to Co(II). In agreement with Jacobsen and coworkers, performing these reactions in an oxidizing environment improves the activity of **cat2**.

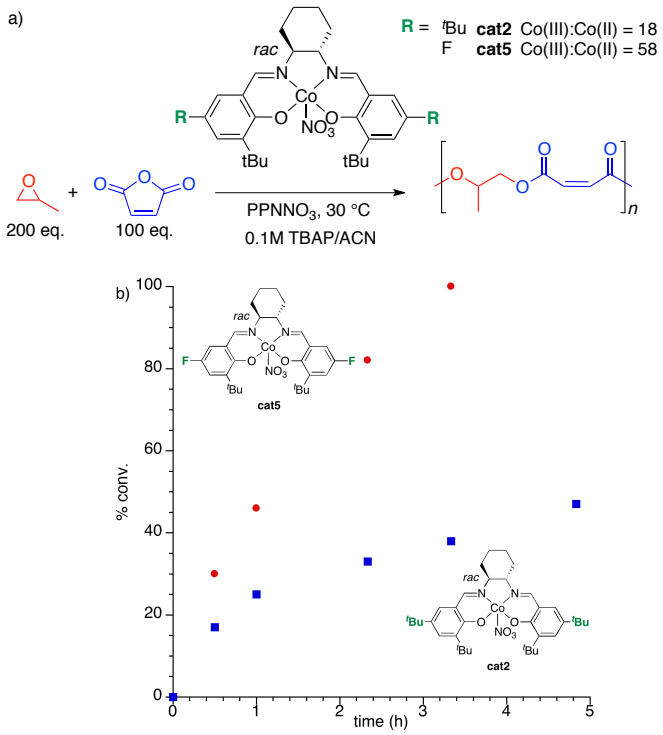


**Figure 6.11.** Electron withdrawing ligands result in a) a higher ratio of stable Co(III) and b) a more active copolymerization process.

The original design of salicylidene based ligands were intended to mimic the active site of galactose oxidase. This enzyme uses a radical pathway that involves a local tyrosine residue associated with a Cu(II) metal center for oxidation of substrates such as alcohols.[11] This pathway is reminiscent of the degradation products found by the groups of Xiao-Bing Lu and Jacobsen, suggesting that salen ligands may mimic the tyrosine residues in redox processes and it would be prudent to reconsider the mechanisms of galactose oxidase when proposing degradation pathways. Recent studies are beginning to uncover the non-innocent nature of salicylidene moieties and will provide insight for tuning catalyst activity and stability.[12]

It is important to note that low molecular weight polyesters are a persistent issue for these systems, although certain anhydrides consistently are capable of being polymerized with higher molecular weights. Inevitable protic impurities serve as chain

transfer agents that limit molecular weights. Processes are needed that can attenuate the rates of propagation ($k_P$) and chain transfer ($k_{CT}$) such that $k_{CT}$ becomes negligible.

Copolymerizations containing phthalic anhydride (PA) do not form any observable degradation product, regardless of ligand electronics, and consistently produce polymers with higher molecular weights (Figure 6.12). Without degradation to consider, the impacts of ligand electronics can be directly studied. Increased Lewis-acidic Co centers bearing electron-withdrawing ligands stimulate a faster reaction. The extremely electron-withdrawing ligand of **cat7** decreases TOF, likely because the increased Lewis acidity hinders dissociation of the propagating alkoxide. This trend is consistent for all copolymerizations catalyzed by **cat7**. Copolymerizations with diglycolic anhydride (DGA) experience low levels of degradation maintaining high TOFs while reactions containing maleic (MA) and succinic anhydride (SA) undergo rapid degradation and have low TOFs. Overall, the ligand electronics of **cat5** provides the Co with the ideal balance of enhanced Lewis-acidity and electrochemical stability for all monomers.

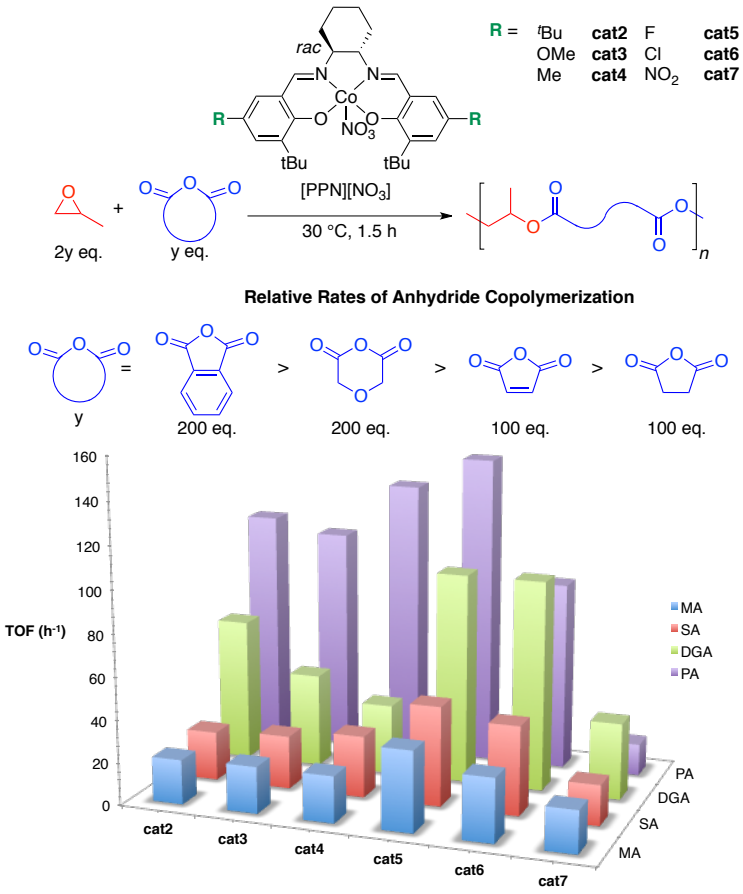


**Figure 6.12.** The impact of ligand electronics on copolymerization activity as measured by turn-over frequency (TOF) at 1.5 hours is different for each anhydride.

More detailed studies comparing the electrochemical nature of **cat5** in various copolymerization conditions are necessary at lower catalyst loading where degradation persists as an issue. In particular, decreased catalyst loading for polymerizations containing MA or SA undergo rapid degradation that severely limits obtainable molecular weights. The reducing environment created by these monomers should be quantified and variations of temperature, solvent, and additives should be probed. Studies should also be performed for PA as a comparison.

Anhydride competition experiments were performed to gauge if degradation occurs for copolymerizations containing combinations of PA and either MA, SA, or DGA. Visible signs of degradation were not apparent for any reaction containing PA.

Surprisingly, the relative rates of anhydride ring-opening do not correspond to the relative rates of copolymerization and are: DGA > MA > PA > SA. This series roughly correlates to the predicted ring-strain of the anhydrides[refs] as well as the strength of the conjugate bases predicted by the $pK_a$s of the diacids. More strained anhydrides that produce the weakest conjugate bases were opened more quickly. This information indicateted that catalyst degradation must not be associated with the rate of anhydride ring-opening since PA exhibits the least degradation but is ring-opened more slowly than MA or DGA.

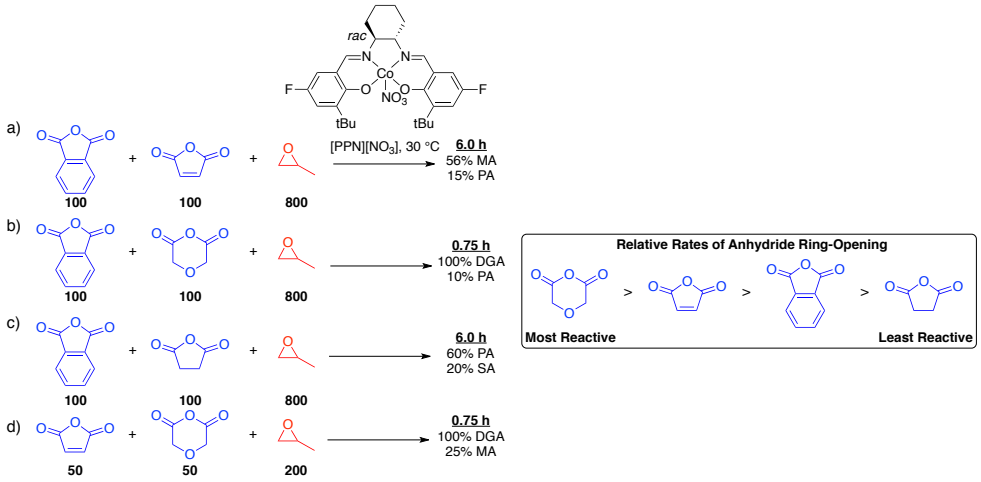


**Figure 6.13.** Competition experiments between anhydrides reveals insight to preference for anhydride ring-opening.

These results confirmed epoxide ring-opening as the rate determining step because copolymerizations containing PA exhibit the highest rate, yet PA is not ring-opened most quickly. The increased activity of PA copolymerizations must result from the more nucleophilic phthalate group rapidly ring-opening a coordinated epoxide. Processes able to enhance the nucleophilicity of other anhydrides should be considered in the pursuit of high molecular weight polyesters .

The impact of epoxide electronics on copolymerization and degradation rates paralleled the trends observed for ligand electronics (Figure 6.14). In general, the more

electron-withdrawing substituents resulted in faster polymerization rates, less degradation, and higher molecular weights. The most electron-poor epoxide exhibited a slight decrease in rate. This may be caused by a change in the rate-determining step and reflecting reduced dissociation rates from the Co center or decreased alkoxide nucleophilicity. Overall, the more electron-poor epoxides were better electrophiles for nucleophilic ring-opening by the propagating carboxylate, thus supporting epoxide ring-opening as the rate-determining step. These results also suggested that less nucleophilic alkoxides lead to less degradation and undergo fewer chain transfer events to form higher molecular weight polyesters.

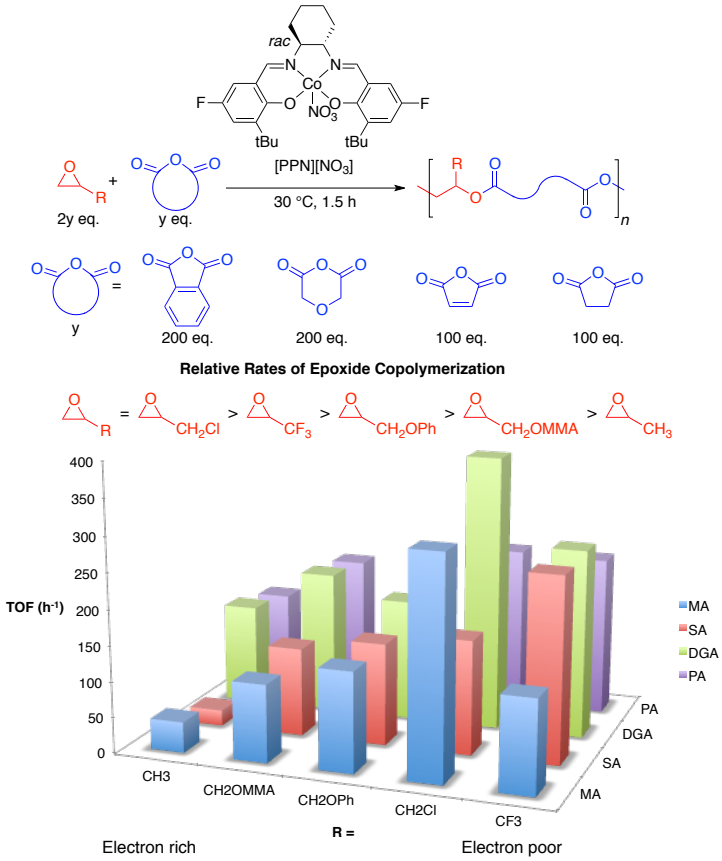


**Figure 6.14.** Electron-poor epoxides have higher copolymerization rates and less degradation.

Scheme 6.2 describes a proposed mechanism for the copolymerization of epoxides and cyclic anhydrides based on literature reports on related systems [13] and this discussion. In agreement with the copolymerization of epoxides/$CO_2$, epoxide ring-opening is proposed as the rate-determining step (Scheme 6.2c). In processes with terminal epoxides, this step also determines the regiochemistry of epoxide enchainment. Most anhydrides studied for this process are symmetrical, thus the regiochemistry of anhydride insertion is not discussed.

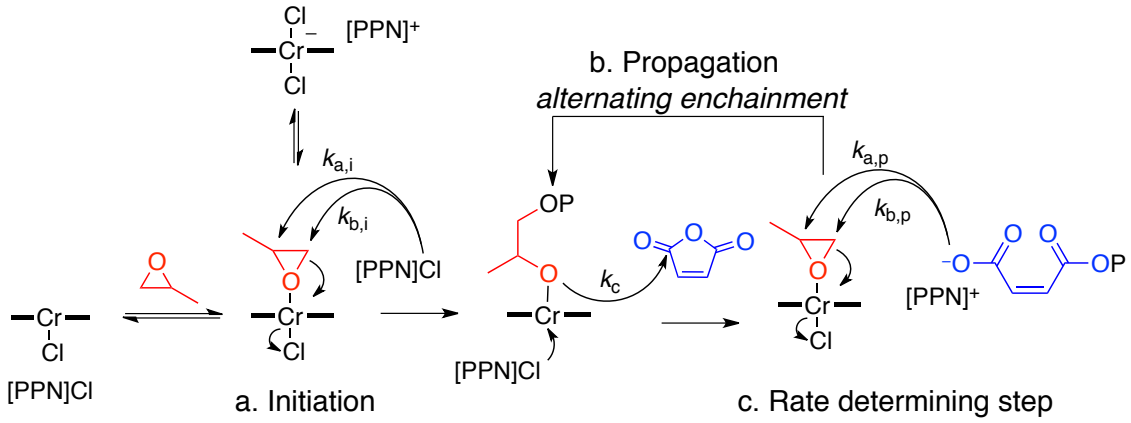


a. *Initiation*: ring-opening of coordinated epoxide
b. *Propagation*: alternating enchainment of anhydride and epoxide
c. *Rate-determining step*: carboxylate attack on coordinated epoxide

**Scheme 6.2.** Proposed mechanism for the (salcy)$CoNO_3$/[PPN][$NO_3$] catalyzed copolymerization of epoxides with cyclic anhydrides, P = polymer chain.

Electron with-drawing ligands generally increase catalyst activity, presumably by enhancing the Lewis acidity of (salcy)$CoNO_3$ complexes and increasing copolymerization rates. This affect may be the result of higher propagation rates ($k_p$) than termination ($k_T$) and chain-transfer rates ($k_{CT}$) created by increasing the rate of epoxide ring-opening in the rate-determining step or by stabilizing the Co(III) oxidation state of the catalyst against reduction. Co metal centers prefer $k_b >> k_a$ and produce regioregular polyesters based on NMR analysis.

The rates of anhydride ring-opening ($k_c$) do not correspond to rate of copolymerization, which agrees with epoxide ring-opening as the rate determining step. Additionally, this suggests that the identity of the propagating carboxylate impacts the rate-determining step and perhaps degradation reactions. More nucleophilic carboxylates likely enhance $k_P$ (=$k_b$) >> $k_T$ and $k_{CT}$.

Finally, the electronics of the epoxide directly impact the rate-determining step such that more electron-poor epoxides are better electrophiles and enhance copolymerization rate. Additionally, reactions containing more electron-poor epoxides exhibit reduced degradation and higher molecular weights. It is possible that degradation is decreased because the rate-determining step is increased, thus increasing the rate of propagation above the rate of termination or chain transfer. Conversely, it is possible that more nucleophilic/basic alkoxides participate in degradation or chain transfer and thus, the less nucleophilic/basic epoxides are less effective for these side-reactions.

Some considerations for the design of improved polyester processes include: more nucleophilic carboxylates increase $k_P/k_T$ or $k_P/k_{CT}$; for less nucleophilic carboxylates $k_T$ and $k_{CT}$ compete with $k_P$. For electron-poor epoxides, it is possible that $k_P/k_T$ and $k_P/k_{CT}$ increase because $k_P$ increased. Conversely, more nucleophilic/basic alkoxides may directly participate in degradation or chain transfer or less nucleophilic/basic alkoxides may be inefficient for these side-reactions.

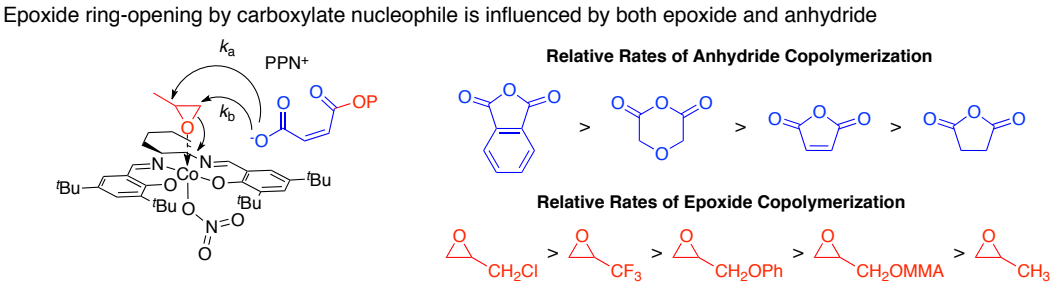


**Figure 6.15.** Many factors are unresolved in explaining the rate-determining epoxide ring-opening step in the copolymerization of epoxides/cyclic anhydrides.

REFERENCES

(1) a) Cheng, M.; Moore, D. R.; Reczek, J. J.; Chamberlain, B. M.; Lobkovsky, E. B.; Coates, G. W. *J. Am. Chem. Soc.* **2001**, *123*, 8738. b) Allen, S. D.; Moore, D. R.; Lobkovsky, E. B.; Coates, G. W. *J. Am. Chem. Soc.* **2002**, *124*, 14284. c) Moore, D. R.; Cheng, M.; Lobkovsky, E. B.; Coates, G. W. *Angew. Chem. Int. Ed.* **2002**, *41*, 2599. d) Allen, S. D.; Moore, D. R.; Lobkovsky, E. B.; Coates, G. W. *J. Org. Chem.* **2003**, *683*, 137. e) Moore, D. R.; Cheng, M.; Lobkovsky, E. B.; Coates, G. W. *J. Am. Chem. Soc.* **2003**, *125*, 11911.

(2) Jeske, R. C. Ph.D. Thesis, Cornell University, June 2009.

(3) a) Radzewich, C. E.; Coles, M. P.; Jordan, R. F.; *J. Am. Chem. Soc.* **1998**, *120*, 9384. b) Yokota, S.; Tachi, Y.; Itoh, S. *Inorg. Chem.* **2002**, *41*, 1342. c) Carey, D. T.; Cope-Eatough, E. K.; Vilaplana-Mafé, E.; Mair, F. S.; Pritchard, R. G.; Warren, J. E.; Woods, R. J. *Dalton Trans.* **2003**, 1083. d) Basuli, F.; Huffman, J. C.; Mindiola, D. J. *Inorg. Chem.* **2003**, *42*, 8003.

(4) Jeske, R. C.; DiCiccio, A. M.; Coates, G. W. *J. Am. Chem. Soc.* **2007**, *129*, 11330.

(5) Unpublished results.

(6) a) Lee, B. Y; Kwon, H. Y.; Lee, S. Y.; Na, S. J.; Hari, S. I.; Yun, H. S.; Lee, H.; Park, Y. W. *J. Am. Chem. Soc.* **2005**, *127*, 3031. b) Bok, T.; Yuri, H.; Lee, B. Y. *Inorg. Chem.* **2006**, *45*, 4228.

(7) Unpublished results.

(8) Jeske, R. C.; Rowley, J. M.; Coates, G. W. *Angew. Chem. Int. Ed.* **2008**, *47*, 6041.

(9) a) Schaus, S. E.; Brandes, B. D.; Larrow, J. F.; Tokunaga, M.; Hansen, K. B.; Fould, A. E.; Furrow, M. E.; Jacobsen, E. N. *J. Am. Chem. Soc.* **2002**, *124*, 1307. b) Kim, G. J.; Park, D. W. *Catal. Today* **2000**, *63*, 537. c) Qin, Z. Q.; Thomas, C. M.; Lee, S.; Coates, G. W. *Angew. Chem. Int. Ed.* **2003**, *42*, 5484. d) Cohen, C. T; Chu, T.; Coates, G. W. *J. Am. Chem. Soc.* **2005**, *127*, 10869.

(10) Ren, W. M.; Wang, Y. M.; Zhang, R.; Jiang, J. Y.; Lu, X. B. *J. Org. Chem.* **2013**, *78*, 4801.

(11) (a) Whittaker, M. M.; Whittaker, J. W. *J. Biol. Chem.* **1988**, *263*, 6074. (b) Babcock, G. T.; El-Deeb, M. K.; Sandusky, P. O.; Whittaker, M. M.; Whittaker, J. W. *J. Am. Chem. Soc.* **1992**, *114*, 3121. (c) McGlashen, M. L.; Eads, D. D.; Spiro, T. G.; Whittaker, J. W. *J. Phys. Chem*. **1995**, *99*, 4918. (d) Whittaker, M. M.; Ekberg, C. A.; Peterson, J.; Sendova, M. S.; Day, E. P.; Whittaker, J. W. *J. Mol. Catal. B: Enzym.* **2000**, *8*, 3.

(12) Selected papers that discuss these phenomena: a) Kochem, A.; Kanso, H.; Baptiste, B.; Arora, H.; Philouze, C.; Jarjayes, O.; Vezin, H.; Luneau, D.; Orio, M.; Thomas, F. *Inorg. Chem.* **2012**, *51*, 10557. b) Nishinaga, A.; Tajima, K.; Speiser, B.; Eichhorn, E.; Rieker, A.; Ohya-Nishiguchi, H.; Ishizu, K. *Chem. Lett.* **1991**, 1403. c) Zhuang, X.; Oyaizu, K.; Niu, Y.; Koshika, K.; Chen, X.; Nishide, H. *Macromol. Chem. Phys.* **2010**, *211*, 669. d) Schenk, K. J.; Meghdadi, S.; Amirnasr, M.; Habibi, M. H.; Amiri, A.; Salehi, M.; Kashi, A. *Polyhedron* **2007**, *26*, 5448.

(13) a) DiCiccio, A. M.; Coates, G. W. *J. Am. Chem. Soc.* **2011**, *133*, 10724. b) Huijser, S.; Nejad, E. H.; Sablong, R.; de Jong, C.; Koning, C. E.; Duchateau, R. *Macromolecules* **2011**, *44*, 1132. c) Robert, C.; de Montigny, F.; Thomas, C. M. *Nat. Comm.* **2011**, *2*, 586. d) Tang, T.; Oshimura, M.; Yamada, S.; Takasu, A.; Yang, X.; Cai, Q. *J. Polym. Sci. Part A: Polym. Chem.* **2012**, *50*, 3171. e) Nejad, E. H.; van Melis, C. G. W.; Vermeer, T. J.; Koning, C. E.; Duchateau, R. *Macromolecules* **2012**, *45*, 1770. f) Darensbourg, D. J.; Poland, R. R.; Escobedo, C. *Macromolecules* **2012**, *45*, 2242. g) Nejad, E. H.; Paoniasari, A.; Koning, C. E.; Duchateau, R. *Polym. Chem.* **2012**, *3*, 1308. h) Liu, J.; Bao, Y.-Y.; Liu, Y.; Ren, W.-M.; Lu, X.-B. *Polym. Chem.* **2013**, *4*, 1439. i) Nejad, E. H.; Paoniasari, A.; van Melis, C. G. W.; Koning, C. E.; Duchateau, R. *Macromolecules* **2013**, *46*, 631. j) Bernard, A.; Chatterjee, C.; Chisholm, M. H. *Polymer* **2013**, *54*, 2639. k) Harrold, N. D.; Li, Y.; Chisholm, M. H. *Macromolecules* **2013**, *46*, 692.